DESIGN OF RF FRONTEND AND ANTENNA FOR SATELLITE COMMUNICATIONS

by

İsmail Şişman

Submitted to Graduate School of Natural and Applied Sciences
in Partial Fulfillment of the Requirements
for the Degree of Doctor of Philosophy in
Electrical and Electronics Engineering

Yeditepe University
2023

DESIGN OF RF FRONTEND AND ANTENNA FOR SATELLITE COMMUNICATIONS

APPROVED BY:

Prof. Dr. Duygun Erol Barkana ……………………………
(Thesis Supervisor)
(Yeditepe University)

Prof. Dr. Sezer Gören Uğurdağ ……………………………
(Yeditepe University)

Assoc. Prof. Dr. Engin Maşazade ……………………………
(Marmara University)

Prof. Dr. Şahabettin Taha İmeci ……………………………
(Fatih Sultan Mehmet University)

Assist. Prof. Dr. İpek Baz ……………………………
(Yeditepe University)

DATE OF APPROVAL: …./…./20…

I hereby declare that this thesis is my own work and that all information in this thesis has been obtained and presented in accordance with academic rules and ethical conduct. I have fully cited and referenced all material and results as required by these rules and conduct, and this thesis study does not contain any plagiarism. If any material used in the thesis requires copyright, the necessary permissions have been obtained. No material from this thesis has been used for the award of another degree.
I accept all kinds of legal liability that may arise in case contrary to these situations.

Name, Last name İsmail Şişman…...………..……

Signature …...……………….………………………..

ACKNOWLEDGEMENTS

I would like to express my gratitude to Prof. Dr. Duygun Erol Barkana for my appreciated acts, which have lighted my path via the mentored with her knowledge, education, and experiences up to now, as I completed my Ph.D. thesis.

I am also grateful to the PROFEN Group organization for providing me with all the hardware support I need to conduct this investigation.

I am grateful to Instructor Tugba Haykir Ergin, my beloved professor, who has always provided me with advice and encouragement as I worked on my thesis,

It is a pleasure to thank my respected professor Prof. Dr. Korkut Yeğin, who raised my consciousness throughout my doctorate studies while also helping me to become more technically proficient.

I would like to thank my very dear wife Zeynep Şişman, who has never left my side with her unwavering support and belief in me at every moment of my life, and my dear son Ali Uras Şişman, who was born and gave us the world during my thesis. Finally, I would like to thank all my family and friends with my deep and sincere gratitude.

I wish this study to be beneficial and guide every engineer studying, to all engineer candidates who have always made progress and are learning their mission.

ABSTRACT

DESIGN OF RF FRONTEND AND ANTENNA FOR SATELLITE COMMUNICATIONS

Satellite communication is an indispensable technology due to its wide range of applications and usage scenarios. Frequent bands such as S, C, X, Ku, and Ka are typically preferred in the design of ground stations for satellite communication. This dissertation aims to design an antenna with circular polarization in the X-band frequency range, a low-noise amplifier with high gain, and a frequency downconverter with low image rejection. Ground station designs require large-scale reflective antenna systems based on the usage scenario and the G/T value. In this design, subsystems including an X-band feed antenna capable of generating the tracking signal from an electromagnetic perspective for a ground station with a diameter of 7.3 meters, a low-noise amplifier with high gain that minimally alters the noise value of the received signal, and a frequency downconverter that downconverts the high-frequency signal to the IF frequency band without compromising signal quality were designed. The X-band feed antenna consists of a septum polarizer, a quadruple tracking antenna, and a corrugated antenna. The feed antenna achieves a gain above 19.3 dBi with a variation of ±0.3 dB across the band. The impedance match (S11) is less than -15 dB. First, the septum polarizer structure was designed. A corrugated antenna structure was created and combined with the septum polarizer structure to increase antenna gain. Once the desired antenna aperture was achieved, a quadruple antenna structure with tracking capability and suitable dimensions was added to the system. Another subsystem in the ground station system is the low-noise amplifier, which is designed with four stages. The first two stages were designed using transistors to ensure low noise performance. In comparison, the final two stages were designed using amplifiers to achieve both gain and the desired output P1dB value. The low-noise amplifier has a gain exceeding 50 dB, a noise value below 0.7 dB, and input and output impedance match below -15 dB. The subsequent subsystem in the system is the frequency downconverter unit. The frequency downconverter was designed using a single-conversion superheterodyne architecture. The RF signal received at the X-band frequency is designed to provide an IF signal output with a center frequency of 720 MHz and a bandwidth of 400 MHz. In conclusion, the developed subsystem structures are suitable for use in ground stations.

ÖZET

UYDU HABERLEŞMESİ İÇİN ANTEN VE RF ÖN UÇ DEVRE TASARIMI

Uydu haberleşme iletişimi, sunduğu geniş kullanım senaryoları nedeniyle vazgeçilmez bir teknolojidir ve bu iletişimde çok çeşitli çalışma frekans bantları kullanılır. Uydu ile haberleşmede yer istasyonları tasarımında genellikle S, C, X, Ku, Ka gibi frekans bantları tercih edilir. Bu tez çalışmasında X-bant frekans bandında, dairesel polarizasyona sahip bir anten, yüksek kazanç değerine sahip düşük gürültülü yükselteç ve düşük görüntü bastırma değerine sahip frekans aşağı çevirici tasarımı yapılması amaçlanmıştır. Yer istasyonu tasarımları, kullanım durumu ve G/T değerine göre büyük çaplı yansıtıcı anten sistemine ihtiyaç duyar. Bu tasarımda 7.3 m çapa sahip bir yer istasyonu için elektromanyetik açıdan takip sinyalini oluşturabilecek özellikte X-bant besleme anteni, alınacak sinyalin gürültü değerini çok az değiştirip yüksek kazanca sahip düşük gürültülü yükseltece ve yüksek frekansa sahip sinyali IF frekans bandına, sinyal kalitesini bozmadan düşürecek frekans aşağı çevirici alt sistemleri tasarlanmıştır. X-bant besleme anteni, septum polarizör, dörtlü takip anteni ve oluklu antenden oluşmaktadır. Besleme anteni kazancı bant boyunca ±0.3 dB değişimle 19.3 dBi'nin üzerindedir. Empedans uyumu S11 -15 dB den azdır. İlk olarak septum polarizör yapısı tasarlanmıştır. Anten kazancını artırmak için oluklu anten yapısı oluşturularak septum polarizör yapısı ile birleştirilmiştir. İstenen anten açıklığı sağlandığında takip özelliğine sahip uygun ölçülerde dörtlü anten yapısı sisteme eklenmiştir. X-Bant besleme anten CNC de Alüminyum malzemeden parçalar halinde üretililip alodin kaplama yapılmıştır. Yer istasyonu sisteminde diğer alt birim olan düşük gürültü yükselteç 4 katlı olarak tasarlanmıştır. İlk iki katında transistor kullanılarak tasarımı yapılmıştır ve düşük gürültü değeri bu şekilde garanti altına alınmış olup son iki katında ise yükselteç kullanılarak hem kazancı hem de çıkış P1dB değerinin sağlanması hedeflenmiştir. Düşük gürültülü yükseltecin kazancı 50 dB'nin üzeri, gürültü değeri 0.7 dB'nin altında ve giriş ve çıkış empedans uyumu -15 dB den azdır. Sistemde düşük gürültülü yükselteçten sonraki alt sistem ise frekans aşağı çevirici birimidir. Frekans aşağı çeviricide tek çevrimi superheterodyne yapısı kullanılarak tasarım yapılmıştır. X-bant frekansında gelen RF sinyali, 720 MHz merkez frekansında 400 MHz bant genişliğine sahip IF sinyal çıkışı veren bir tasarıma sahiptir. Sonuç olarak, geliştirilen alt sistem yapıları yer istasyonlarında kullanılmaya uygundur.

TABLE OF CONTENTS

LIST OF FIGURES

LIST OF TABLES

LIST OF SYMBOLS/ABBREVIATIONS

AR	Axial ratio
AWR	Advancing the wireless revolution
AZ	Azimuthal error
CMOS	Complementary metal oxide semiconductor
CST	Computer simulation technology
dB	Decibel
DC	Direct current
E	Electric field
EM	Electromagnetic
EIRP	Effective isotropic radiated power
EL	Elevation error
ENR	Excess noise ratio
EoC	End of call
FOM	Figure of merit
f/D	Antenna focus point-to-diameter ratio
GaAs	Gallium arsenide
GaN	Gallium nitride
GEO	Geostationary earth orbit
G/T	Antenna gain to noise temperature
H	Magnetic field
HBT	Heterojunction bipolar junction
HEMT	High electron mobility transistor
Hz	Hertz
IF	Intermediate frequency
ITU	International telecom union
LDO	Low drop out
LEO	Low earth orbit
LHCP	Left-hand circular polarization
LNA	Low noise amplifier
LO	Local oscillator
MEO	Medium earth orbit

MMIC	Monolithic microwave integrated circuit
OIP3	Third order intercept point
P1dB	1 dB compression point
pHEMT	Pseudomorphic high electron mobility transistor
PLL	Phase-locked loop
RF	Radio frequency
RHCP	Right-hand circular polarization
SCIR1	Input stability circles
SCIR2	Output stability circles
SiGe	Silicon-germanium
SLL	Side lobe level
SMA	Sub-miniature a
T/R	Transmitter/Receiver
TE	Transverse electric
TCXO	Temperature compensated crystal oscillator
TM	Transverse magnetic
TT&C	Telemetry, tracking & command
VCO	Voltage-controlled oscillator
VCTCXO	Voltage controlled temperature compensated crystal oscillator
VSWR	Voltage standing wave ratio
XP	Cross-polarization

β	Propagation constant
κ	Wavenumber
κ_c	Cut-off wavenumber
f	Frequency
λ	Wavelength
γ	Gama
c	Speed of light
Γ	Reflection coefficient

1. INTRODUCTION

1.1. PROBLEM STATEMENT

In satellite communication, different orbits are preferred for specific applications[1]. Satellites in circular orbits are classified as geosynchronous Earth orbits (GEO), medium Earth orbits (MEO), and low Earth orbits (LEO), with the main difference being in the altitude above the Earth's surface. This further affects the satellite's velocity and the orbital period in the appropriate orbit[1,2].

LEO is a region of space located between 400 and 2000 km above the Earth's surface. One of the most significant advantages of LEO is its proximity to the Earth, which makes it ideal for a wide range of applications, including Earth observation and satellite communications. Additionally, LEO is an attractive option for satellite communication as it offers low latency and high bandwidth, making it ideal for applications such as internet connectivity and video streaming. In the range of the LEO, the lower altitude range is restricted by the Earth's atmosphere, which has almost no air, preventing the satellite from reducing speed and experiencing the drag necessary to stay in orbit. The inner Van Allen belt limits the higher altitude range, a region of space radiation that can have undesirable effects on a satellite's payload and platform, making it unsuitable for LEO satellite accommodation [1,2].

Figure 1.1 depicts the standard architecture of a satellite communication system comprising three segments: ground, space, and control [3,4]. The space segment includes a constellation of one or more active and backup satellites. Each satellite comprises a platform and payload, including transmitting and receiving antennas and electronics necessary to receive and transmit radio signals. The satellite's payload performs two main functions: amplifying received signals for retransmission to the ground station and frequency conversion. The ground station is equipped with appropriate equipment for communicating with the satellite. The control segment comprises ground facilities that monitor and manage the satellites, known as Tracking, Telemetry, and Command. (TT&C)[3].

A satellite ground station is an essential component of any satellite communications network, serving as an intermediary for communication between the satellite and various users. Its primary function is to ensure reliable transmission and reception of information to/from the satellite while maintaining optimal signal quality at the destination. To achieve this, the ground station must establish communication with the satellite and provide telemetry, tracking, and command services for managing and controlling LEO satellite constellations. During a typical pass that lasts only a few minutes, the ground station's reflector antenna must precisely track the satellite's movement to maximize communication capacity.

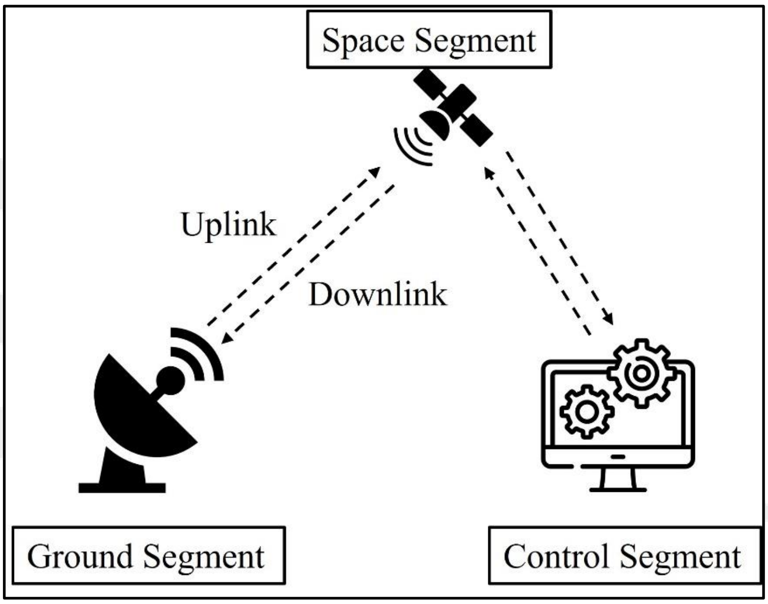

Figure 1.1. The scheme of a satellite communication system

The complexity and size of ground stations vary depending on their intended applications. Tracking antennas are commonly employed in LEO stations to utilize the satellite's total capacity, which requires high accuracy in following the satellite's trajectory. To ensure high-quality communication, the ground station's design and construction must consider environmental factors such as rain effects, antenna isolation for uplink and downlink, intermodulation interference, and analysis of the contact time duration under low elevation angles. As satellite services often share frequency bands with terrestrial services, the International Telecommunication Union (ITU) has set constraints on the transmitted effective isotropic radiated power (EIRP) from satellites to enable coexistence. This constraint affects the ground station's design and necessitates trade-offs for optimising the signal design concept. The efficiency of a ground station can be gauged through its Figure of Merit (FOM), which can be obtained by dividing the receiving antenna gain by the system noise temperature (G/Ts). A higher FOM indicates greater sensitivity of the ground station.

Specific components such as antennas, low noise amplifier (LNA), converters, and safety systems can be considered a single unit in a ground station system. The ground station antenna must possess high signal gain and directivity due to significant signal attenuation at RF (radio frequency) to transmit and receive satellite signals efficiently. Parabolic reflector antennas are commonly used in ground stations as they can offer high gain and desired side lobe levels. Tracking antennas are used in LEO ground stations, which require an antenna mount such as an azimuth-elevation mount to control the azimuth and elevation angles. The power control electronics are responsible for driving the antenna tracking motors. The control computer precomputes the antenna pointing angle coordinates based on the satellite's orbital parameters for a satellite pass, which are then uploaded to the antenna control processor. The power electronics module commands the antenna to align with the satellite in angular alignment. The antenna's position is frequently updated for mission-required accuracy.

In satellite systems, an LNA is the system’s first part after the ground station antenna since the signal received from the satellite experiences further losses. Therefore, amplifying these weak signals becomes an essential issue. An LNA should have a high gain to amplify weak signals from the satellite while maintaining a low noise figure to minimise additional noise introduced in the amplification process. The weak signals at the downlink from the satellite are received by the parabolic antenna and then amplified by LNA.

The frequency downconverters used in LEO ground station systems play a critical role in converting high-frequency signals received from the satellite into an intermediate frequency (IF) for further processing. The downconverter should have several key characteristics to ensure efficient and reliable operation. Firstly, the downconverter should have a high conversion gain to minimise signal loss during the frequency conversion process. Additionally, it should have a wide dynamic range to accommodate variations in signal strength and avoid overloading. The downconverter should also have a low noise figure to minimise the additional noise introduced during frequency conversion.

1.2. AIM OF THE DISSERTATION

The dissertation focuses on the design and performance analysis of a ground station antenna, LNA, and frequency down-converter subsystem specifically intended for LEO ground stations. The main objective of this dissertation is to develop subsystems that exhibit good performance in terms of gain, cross-pol, VSWR, noise figure, image rejection, spurious level compared to other ground station system architectures that have been proposed and fabricated to date. The developed subsystems aim to be easy to fabricate, manufacture, and integrate, utilizing new technologies, using consistent with the numerical results obtained for the antenna, LNA, and frequency down-converter subsystems' performance.

In this dissertation, an antenna, an LNA, and frequency down-converter subsystems with satellite tracking capabilities are designed for use in LEO satellite ground station tracking systems. The developed subsystems are expected to exhibit high performance such as directivity and G/T, be straightforward to fabricate and integrate and offer compatibility with X-Band. This dissertation also aims to develop a reliable, high-performance ground station subsystem in X-Band that can effectively transmit instantaneous images from LEO satellites to ground stations while being easy to implement and integrate. This is because we want to receive all the data from the satellite without losing it. Since the development of such a ground station is essential to enhance the efficiency and accuracy of satellite imaging, enabling better data collection and analysis.

1.3. RESEARCH CONTRIBUTION OF THE DISSERTATION

In recent years, there has been an increasing interest in the research of systems that facilitate the instantaneous transmission of images from any location worldwide to ground stations using LEO satellites in satellite communication systems because of the growing demand for real-time and high-resolution satellite imagery across various sectors such as military, agriculture, climate monitoring or urban planning. Since the availability of instant and accurate satellite imagery can provide valuable information for decision-making processes, which is crucial in many industries and government agencies.

This dissertation aims to develop antenna, LNA, and frequency down-converter subsystems capable of meeting the high data rate requirements of the images to be received from LEO satellites and transmitted to the ground station and the user in the desired frequency band. The subsystems developed in this dissertation can be integrated into all ground stations capable of tracking LEO satellites in the X- Band and offer ease of integration.

In the design of the feed antenna, it has been studied to achieve better RF characteristics than those listed below:

- 1:1.5 VSWR
- -20 dB port isolation
- 53.8 dB gain at 8250 MHz with parabolic reflector
- -25 dB cross polarization (XP)
- -15 dB side lobe level (SLL)

Also, the G/T of the feed antenna experiences 1.5 dB increase with placing on the Cassegrain reflector.

The proposed study has set certain minimum boundaries for the design of the LNA, which have been further improved to enhance the performance of the LNA, thereby making it a noticable addition to the existing literature:

- 1:1.5 VSWR
- 50 dB gain
- maximum 0.7 noise figure
- 10 dBm P1dB

The designed frequency down converter in this dissertation adheres to folllowing requirements, making it a noteworthy contribution to the existing literature on this subject.

- 1:1.5 VSWR
- 10 dBm P1dB
- maximum 20 dB noise figure
- -60 dBc/Hz phase noise at 1 KHz
- 50 dB image rejection

- -50 dBm LO Leakage

Consequently, the proposed study presents a novel antenna, low-noise amplifier (LNA), and frequency down-converter subsystems that are highly efficient, compact, and cost-effective for ground station systems that operate within the 8-8.5 GHz frequency range. This research contribution is specifically intended to address the gaps in the existing literature on high-performance subsystems designed for this frequency range.

1.4. OUTLINE OF THE DISSERTATION

The outline of the dissertation can be separated into three main categories. In Chapter 1, a brief explanation of satellite and satellite communication is introduced. Then, it is described for satellite orbits. Moreover, LEO and its properties, LEO satellite system segments such as space, ground, and control are presented.

Chapter 2 presents a comprehensive literature review of LEO ground station components. Different designs of satellite communication antennas, X-band satellite communication antennas, X-band LNAs, and X-band frequency down converters are introduced. In Chapter 3, the design details of the feed antenna, X-band LNA, and X-band frequency down are presented. The experimental setup and the experiments used to measure RF characteristics of feed antenna, LNA and frequency down converter are demonstrated in Chapter 4. For the feed antenna, VSWR, return loss, insertion loss, gain and directivity are measured. Then, sum and difference pattern of the feed antenna is obtained after placing on the Cassegrain reflector. Also, the measurement of the LNA and down converter is realized with gain, noise figure, P1dB, image rejection, and input and output reflections measurements. The discussion about the experimental results is given in Chapter 5. Chapter 6 concludes the work and a possible future work directions are presented in Chapter 7.

2. LITERATURE REVIEW

A satellite is an object in space that orbits or circles around a larger object [1]. There are two types of satellites: natural and artificial. The moon is an example of a natural satellite because it orbits around the Earth, while the International Space Station can be described as an artificial satellite. There are many natural satellites in the solar system, with almost every planet having at least one moon. However, artificial satellites only became a reality in the mid-20th century.

Satellites play a crucial role in global telecommunication systems, facilitating the transmission of significant multimedia traffic[1]. Communication satellites have been a cornerstone of the worldwide communication network for approximately 60 years. In satellite communication, the essential resources are orbits and RF spectrum. The orbit is the path a satellite follows in space, and frequency allocations are determined by international agreements and managed by international organizations.

Due to some well-recognized benefits, satellites are used extensively for various communication applications, including communication, navigation, weather forecasting, scientific research, and national security[1,2]. These derive from the introductory essential physics of the system, the most important of which is that a satellite can see a substantial amount of geography at one time. Several advantages are interrelated, while others will become more important as the technology and applications evolve [1].

Satellites offer numerous advantages, including wireless communication and location independence. Any user within the satellite's coverage area can utilise it, provided they are within the range of an appropriate Earth station. A well-designed service establishes an effective radio link between the user and the satellite. In addition, satellites offer extensive area coverage, which is not restricted by provincial, national, or continental boundaries, and can serve any region within its sight.

Satellite communication antennas, down converters, and LNAs are essential components of modern communication systems that operate in the X-Band frequency range[1-3]. A wide range of research has been conducted on designing, developing, and optimising these components to enhance the performance of satellite communication systems. In particular, the design of X-Band antennas has been extensively studied, with various types of antennas being proposed, including microstrip patch antennas, phased array antennas, and horn antennas. Similarly, the design and implementation of X-band down converters and LNAs have been widely investigated to achieve low noise figures, high linearity, and a wide dynamic range. Various techniques have been proposed, such as inductive source degeneration, body floating, and composite right/left-handed transmission lines, to enhance the performance of X-band LNAs. Overall, these components are crucial in developing high-performance satellite communication systems, and the research in this area continues to advance as new technologies and applications emerge.

Satellite communication monopulse tracking feeds are widely used in satellite tracking systems to improve the pointing accuracy of satellite antennas. Much research has been conducted on these tracking feeds' design, optimisation, and performance analysis. Monopulse tracking feeds are designed to receive signals from a satellite and generate a differential signal that provides information about the direction and angle of the satellite. These feeds can achieve high tracking accuracy and maintain a stable lock on the satellite, even with environmental factors such as rain and wind. Various types of monopulse tracking feeds have been proposed in the literature, including the dual-reflector monopulse feed, the corrugated feed, and the planar monopulse feed. Each of these feed types has its advantages and disadvantages, and the choice of feed depends on the specific application and requirements. Overall, the research in this area has contributed significantly to developing high-accuracy satellite tracking systems, and further advancements are expected as new technologies and applications emerge.

In satellite communications, wide varieties of antennas and frequency bands are preferred depending on the application[4]. Reflector antennas have been used as satellite ground stations for a long history [4]. Typically, corrugated horn antennas have been used as feeders for reflectors antennas deployed in communications, radar, and remote sensing, where stable radiation characteristics and low side lobe level are mandatory requirements [4]. Various corrugated horn designs with different corrugation profiles are proposed in (5,6). Also, the choke horn [7–9] or dielectric rods [10–12] are good reflector feed alternatives. In addition to typical feed structures, phased array antennas are considered attractive candidates for future satellite ground stations [13]. The architecture of the phased array antennas is discussed in [14,15]. Also, Ka-band phased antenna [16], phased antenna design for TT&C [17], and other configurations are discussed in [16–19]. Moreover, multi-beam antennas can be an alternative solution for LEO ground stations. A Ku/Ka-band multi-beam antenna is presented in [20].

In the feed structure of the ground station, a monopulse structure also can be added to the system. Therefore, it can track remote sensing satellites within the communication. Different frequency bands are chosen for the monopulse structure. W-band monopulse [21], Ka-band [22,23]Ku band [24], and S-band [25] structures are shown.

A dual (S/X) band ground station antenna is presented in [26,27] when it is focused on the X-band applications. Different methods are chosen to obtain the requirements [26,27]. Also, in [28], X-band isoflux choke horn antenna is used to achieve high image data rate transmission from LEO satellites. The design of the X-Ka band multimode monopulse feed for LEO satellite tracking is also reported in [29]. In [30], a compact isoflux X-band payload telemetry antenna with simultaneous dual circular polarization for LEO satellite applications. Also, a simultaneous S and X-band feed system for the LEO satellite tracking reflector antenna is shown in [31]

An LNA, a frequency down converter, and the feed antenna are also essential parts of the LEO satellite system. LEO satellites receive signals from the earth's surface using antennas. These signals are often weak and need to be amplified to be helpful. However, the amplification process can introduce noise into the signal, reducing the quality of the received signal. To overcome these issues, an LNA becomes a part of the system. LNAs are designed to amplify weak signals with minimal noise. They are commonly used in the receiver chain of LEO satellites to amplify signals received from the earth's surface. LNAs are designed to have a low noise figure, which measures the amount of noise added to the signal during amplification. The lower the noise figure, the better the LNA amplifies weak signals with minimal noise.

In [32], a 9.7-12 GHz monolithic microwave integrated circuit LNA has been designed and fabricated. In [33], a design of single-stage broadband LNA based upon 0.15 um GaN HEMT (gallium nitride high electron mobility transistors) technology in the frequency range of 8-12 GHz. In [34], an LNA for X and K band operations is designed 0.18 um SiGe HBT (silicon germanium heterojunction bipolar transistor) technology and proposed a noise match optimization optimisation method concerning base inductance in SiGe LNA design with large transistors. Also, an X-band monolithic three-stage LNA employing series feedback has demonstrated a 1.8 dB noise figure with a 30 dB gain [35]. In [36], two different LNA are described in terms of operating frequency range from 8-10 GHz to 10-12 GHz. In [37], a novel linearised LNA for X-band applications with plat power gain, low noise performance, and enhanced linearity is proposed. In [38], an LNA is designed using standard 0.18 um complementary metal oxide semiconductor technology (CMOS) for X-band satellite receiver applications. A two-stage common source configuration with a transformer matching network is chosen to obtain low noise and compact size. In [39], an X and Ku band LNA with quad flat no-leads packaging for the satellite communication application is proposed. The LNA can support the reception of dual horizontally and vertically polarized signals. In [40], a reconfigurable S and X-band GaN cascade LNA monolithic microwave integrated circuit (MMIC) is presented. The LNA is based on a 0.15 um GaN HEMT technology and utilizes GaN field effect transistor (FET) switches to tune the frequency range. A low-power X-band SiGe HBT LNA for near-space radar applications is also described in [41,42].

The frequency down converter is a critical component in the LEO satellite system. It converts the high-frequency signals received by satellites into lower-frequency signals that can be quickly processed, and transmitted. The frequency down converter is typically located in the receiver chain of the satellite after LNA. Also, it allows the system to operate over a wide range of frequencies. LEO satellites receive signals ranging from a few MHz to several GHz. However, the receiver chain of the satellite is typically designed to operate at a specific frequency range. The frequency down converter allows the satellite to receive signals at any frequency within its operating range and convert them to the appropriate frequency for processing.

[43] introduces a design of an X-band down converter module based on microwave hybrid integrated. Also, in [44], an X-band down converter for the data acquisition system of a satellite ground station is analysed and designed. Another X-band frequency down converter is developed in [45] for the front-end T/R module. In [46], a low current GaAs (Gallium Arsenide) monolithic image rejection downconverter for X-band broadcast satellite

applications is proposed. Furthermore, a down converter design with low noise figure, excellent image rejection, and high gain is described in [47].

2.1 FEED ANTENNA

The design and realisation of a dual-polarized composite monopulse tracking feed covering the S-band (2-2.3 GHz) and X-band feed (7.8-8.5 GHz) are described [26]. X-band feed is a five-element monopulse feed consisting of a corrugated horn that is the sum element surrounded by four circular septum polarizers that serve as tracking features. S-band feed is a four-element monopulse feed with a square dielectric array arranged in 2 × 2 configurations. The illumination efficiency of the proposed composite feed, positioned in the same Cassegrain plane, is above 90% for both bands. The realised antenna system achieves the expected/targeted G/T of 32 dB/K. The suggested feed antenna is cost-effective and efficient, a simple design approach that is small and suitable for use as a reflector ground station. It meets industry standards.

In [27], the design of a tracking radar system utilising a four-horn monopulse feed includes a pyramidal horn and a circular aperture parabolic reflector made of conductive material. This minimises any errors in tracking angles. The numerical evaluation assumes a nominal frequency of 10 GHz and a focal length-to-distance ratio of unity. The analysis of the pyramidal horn uses the sectoral horn approximation, which is commonly employed in practice.

In [28], a specific X-Band isoflux choke ring antenna design is presented for LEO satellite missions, which aims to transmit high-rate image data from space to Earth. Compared to conventional choke ring antennas with uniform sizes, the design incorporates a non-uniform height of choke rings to improve gain and isoflux patterns. The resulting optimised antenna has an impedance bandwidth of > 2 GHz in the X-Band, a gain of 7dB throughout its coverage range, a return loss of less than -42dB at the resonant frequency, an axial ratio of less than 3dB, and a VSWR of less than two within the desired frequency range. The antenna’s radiation pattern exhibits low side and back lobe levels with excellent cross-polarization, ensuring improved polarization purity. This design can be in future LEO satellite missions for high-rate data transmission.

In [29], a multimode monopulse feed design for LEO satellite tracking is presented, which operates in dual-band (X-Ka) frequency ranges. The difference signal is formed using TE21 and TE21* mode, while TE11 mode generates the sum signal for both X and Ka-band. The feed horn for the proposed design is dual-polarized and multimode, intended for use with a 7.5m reflector ground station antenna, and shares a common aperture for both frequency ranges. A Gaussian profile is utilised to achieve dual-band performance over a bandwidth ratio of approximately 3.5, resulting in a gain difference of around 3 dB between the X and Ka bands. Cross-polarisation is better than 22.5 dB and reaches 25 dB for both frequency ranges. The design meets the required gain, cross-polarization, and reflection coefficient specifications for the X and Ka bands. A turnstile junction coupler is employed to extract the tracking modes, TE21 and TE21*, for both frequency ranges.

[30] describes a compact X-band payload telemetry antenna and data handling antenna with simultaneous dual circular polarization for LEO satellite applications. The antenna design employs a waveguide-fed antenna to achieve good power handling and comprises four main components. The first element consists of equal depth and width corrugated rings for amplitude roll-off from antenna boresight to horizon and choke rings to achieve peak gain at an EoC angle of 60 degrees. The second element comprises a dielectric cone and circular waveguide to draw energy from the vertical direction towards the horizontal, which helps reduce the antenna size. The third element is a septum polarizer built in a square waveguide with the desired axial ratio (AR) and good isolation between the ports. The final part includes a one-quarter wave impedance transformer and two waveguide bends to adapt half of the square waveguide of the polarizer to the WR112 waveguide. The proposed design exhibits an axial ratio lower than 2.5dB over the 8.025-8.4 GHz frequency band.

[31] explains that S-band has been used for satellite TT&C applications for a long time, and X-band has also been deployed more recently. The article presents a theoretical design for a new dual S/X-band feed system that can be used in a ground station. The system has S-band transmit and receive capabilities and can receive X-band signals.

2.2 LOW NOISE AMPLIFIER

In satellite systems, amplifying weak signals from the satellite is crucial, and the LNA is typically used for this purpose. Various techniques and technologies have been proposed in the literature to design LNAs that meet specific requirements for different applications. For example, [32] describes the design and fabrication of an LNA using an AlGaN/GaN 0.25 um high electron mobility transistor on silicon carbide technology, which operates in the 9.7-12.9 GHz frequency range. The LNA achieves a noise figure of 1.7-2.1 dB and a small-signal gain of 20-26 dB. On the other hand, [33] proposes a single-stage broadband LNA based on 0.15 um GaN HEMT technology, which operates in the 8-12 GHz frequency range. The LNA provides 9.5 to 10.6 dB with input return loss better than 10 dB and output return loss better than 8 dB in the entire band. The amplifier's noise figure is below 1.9 dB, and the linearity parameters P1dB and third order intercept point (OIP3) are greater than 16 dBm within the operating bandwidth.

In [34] the design and implementation of X and K band LNAs that use 0.18 um SiGe HBT technology are discussed. They propose a method for optimizing the noise match for base inductance in SiGe LNA design with large transistors. The measured X and K band LNAs have a mean noise figure of 1.2 dB and 2.2 dB, respectively, with a peak gain of 24.2 dB and 19 dB at 8.5 GHz and 19.5 GHz. In [35], the authors describe an X-band monolithic three-stage LNA that uses series feedback. The LNA has a noise figure of 1.8 dB, a gain of 30 dB, and an input VSWR of less than 1.2:1 at 10 GHz. In [36], two LNA designs are presented for different frequency ranges in the X-Band: one for 8-10 GHz and the other for 10-12 GHz. The power consumption of both amplifiers is deficient at 0.9 W. The first LNA has a noise figure of 1.1 dB and a peak gain of 27 dB, while the second LNA has a noise figure of 1.3 dB and a peak gain of 25 dB.

A new linearised LNA design for X-band applications that offer flat power gain, low noise performance, and enhanced linearity is proposed in [37]. This study employs a triple-cascade topology with a dual resonant network. The LNA can achieve a peak gain of 18 dB and a minimum noise figure of 1.3 dB over the 8 to 12 GHz frequency range. Another LNA design for X-band satellite receiver applications is presented in [38], using 0.18 um CMOS technology. A two-stage common source configuration with a transformer matching network is chosen to achieve low power consumption, noise, and compact size while maintaining good gain performance. The measured gain is 13.4 dB at 11 GHz, while the noise figure is 3.41 dB.

In [39], a LNA is proposed for X and Ku bands in satellite communication applications. This LNA can receive signals in horizontal and vertical polarizations and is made using 0.15 um GaAs pseudomorphic high electron mobility transistor (pHEMT) technology. The LNA has a power gain of 20.6 and 21.6 from 10.7 to 13.1 GHz and a noise figure of 1.3 dB. Meanwhile, in [40], a GaN cascode LNA is introduced, which can be reconfigured for S and X-bands. It 0.15 um GaN HEMT technology and GaN FET switches to adjust the change operating frequency band. The LNA offers a gain of 13.5 to 14.5 dB for X-band operation, and the noise figure ranges from 1.4 to 2.2 dB.

In addition, [41] and [42] present a low-power X-band LNA that SiGe technology for space applications. [41] reports that this LNA is the first of its kind using Si-based technology to achieve a mean noise figure of less than 2 dB.

2.3 FREQUENCY DOWN CONVERTER

The LEO satellite frequency down converter is a critical element in the receiving chain of LEO satellite communication systems and is responsible for converting the satellite's microwave frequency signal down to a lower intermediate frequency (IF) or baseband signal. In the literature, the down converter design has different techniques and technologies to achieve additional requirements depending on operating principles.

In [43], a microwave hybrid integrated X-band down converter module is introduced. This module can receive microwave signals ranging from 8 to 9 GHz and convert them into an intermediate frequency (IF) signal of 2.43 GHz. To achieve this, a single-frequency conversion approach is used, which involves matching, amplifying, and attenuating the input RF signal. The signal is mixed with the LO signal twice to produce the IF signal, which is filtered, amplified, and attenuated before output. The module has a noise figure of less than 3.8 dB and a conversion gain of approximately 25 dB.

In [44], a down converter designed for a satellite ground station's data acquisition system is discussed. The converter is intended to translate X-band signals to S-band signals using a 5.7 GHz VCO frequency derived by PPL technology. The S-band signal is then further converted to an IF frequency of 720 MHz through mixing with a frequency synthesizer.

Meanwhile, [45] presents a low current GaAs monolithic image rejection downconverter for broadcast satellite applications. The system can convert 11.7 and 12.3 GHz signals to 1 and 1.6 GHz with a conversion gain of approximately 46 dB and a noise figure of less than 3.3 dB.

3. METHODOLOGY

The general block diagram of the satellite ground stations is shown in Figure 3.1. This system is in the X-band (8-8.5 GHz) and is designed for receiver communications. The satellite ground station systems are realized by using parabolic reflector antennas. The signal from the satellite is received with high-gain antennas since the power level of these signals is low. In the design of the ground station, Cassegrain feed is proposed using a 7.3 m reflector antenna. In the system, the signals from LEO satellites are received from ground stations and analyzed by the modem. Since LEO satellites are mobile satellites, signal tracking is performed by the ground station by providing movement on the satellite's route. There is a need for an antenna capable of tracking, an LNA, and a frequency down converter in the specified frequency band.

LEO satellites are located approximately 1000 km above the Earth's surface. The RF signals from satellites have circular polarization and experience attenuation due to the distance between the ground station and the satellite. This attenuated signal is received by a 7.3 m Cassegrain-type ground station. 7.3 m antenna diameter is chosen since the link budget in terms of G/T (32 dB/K), which can provide the desired communication data rate, can be met with this antenna diameter. The signal in the ground station is received by an X-band feed antenna, which is also a feature of signal tracking X-band feed antenna receives the RF signal reaching the ground station with a tracking feature. Since the polarisation of the incoming signal is circular, our antenna will be designed to receive signals with this feature. The X-band feed antenna is a monopulse corrugated horn antenna that supports both right-handed circular polarisation (RHCP) and left-handed circular polarisation (LHCP). The communication signal received by this feed antenna first reaches the corrugated horn and then the septum polariser. The tracking signal is generated by the 4 horns around the corrugated horn. After both the communication and tracking signals are generated, the scan plate processes them. The automatic tracking receiver unit, a separate sub-unit in the ground station system, and the antenna are guided. After the corrugated horn, the RF communication signal reaches the septum polariser, separating it into RHCP and LHCP. The X-band high gain antenna amplifies this RF signal and then transmits it to the LNA mounted just behind the septum polariser. This sub-unit amplifies the communication signal level by slightly changing the noise level of the incoming RF signal in the 8-8.5 GHz frequency band. Since this unit is the first stage after the antenna, it significantly affects the G/T value in the ground station system. Therefore, this sub-unit must have a low noise figure, high gain, and low input back reflection. After the LNA, reducing the RF signal to the L band level is desired. Because the user needs a frequency down-converter sub-system in terms of cost-effectiveness, and elimination of interference, which is one of the disadvantages of high frequency, and because the modem input signals are L band. This unit is expected to downconverter the received RF signal in the 8-8.5 GHz frequency band to 720 MHz frequency with ±200 MHz bandwidth. Since the output of this subsystem will be used by the modem, image rejection, phase noise, noise figure, and LO leakage values should be low. The antenna, low-noise amplifier, and frequency down-converter are designed.

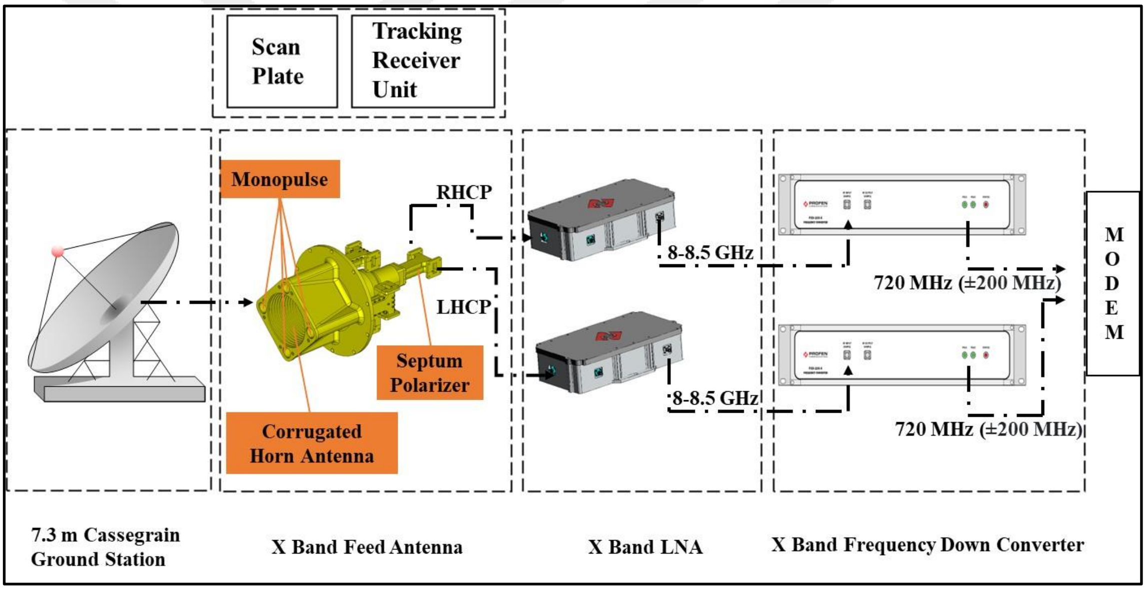

Figure 3.1. The general block diagram of the system

3.1 X-BAND FEED ANTENNA DESIGN

The X-band feed antenna system comprises an X-band feed antenna, X-band monopulse, and X-band septum polarizer and the X-band feed system is placed on the 7.3 m Cassegrain reflector as shown in Figure 3.2. Also, the required RF characteristics of the feed antenna are summarized in Table 3.1.

There are criteria to consider when designing high-frequency communication and tracking applications. Having high efficiency of the system, transferring the communication and tracking signals are separated with high precision and accuracy to the relevant departments, low cross-polarization (XP) and receiving signal without any loss can be given as an example. In designs combining communication and tracking applications, the feeding antenna provides the reception of the communication signal. The tracking signal is collected and processed by taking samples from the communication signal coming to the feed antenna, and this process is done by the monopulse unit. Since the received signal has a circular polarization, septum polarizers perform circular-linear polarization conversion.

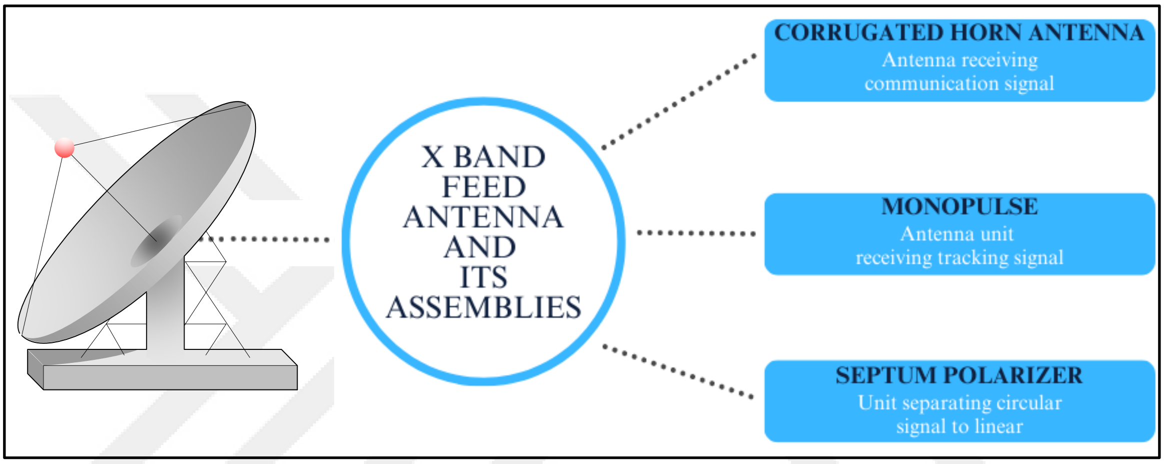

Figure 3.2. The schema of the structural design of the system

Table 3.1. RF characteristics of the X-Band feed antenna

RF Characteristics	Value
VSWR	1:1.5
Port isolation	-20 dB
Gain	53.8 dBi @8250 MHz
Cross polarization	-25 dB
SLL	-15 dB

The monopulse feed antenna tracks remote sensing satellites and receives image data at frequencies of X-band (8 - 8.5 GHz). The five-element feed antenna consists of two different parts. The first one is the corrugated feed antenna which collects the communication signal used as the main element. The second consists of four circular waveguides, two each at the azimuth and elevation of the feed antenna, which are called tracking elements. The circular-linear polarization conversion of the signal is performed by using septum polarizers for the feed antenna and the circular waveguides. Then the error signals are found by using hybrid combiners together. Many studies in communication and tracking applications are based on different operating principles in various frequency bands.

The design and realization of a five-element compact dual-polarized feed for a 4.5m Cassegrain ground station reflector antenna has been presented in [48]. The main feed antenna collects and processes the communication signal, and four tracking antennas are used for the tracking signal. The circular signal received from the four tracking antennas is first converted into a linear polarized signal using a septum polarizer structure and then processed using a hybrid coupler. Furthermore, the principles and techniques of the monopulse method used in tracking systems are provided in [49]. The patent in [25] describes a five-element Cassegrain antenna structure. The main feed antenna with a large aperture in the center collects the communication signal. The tracking antennas are positioned around this wide aperture main feed antenna such that the radiation patterns of the paired tracking antennas intersect at their side lobes. In this patent, the circular signal received from the tracking antennas placed in azimuth and elevation is first converted into a linearly polarized signal with a septum polarizer structure and combined with hybrid couplers. A four-element monopulse technique is analysed using a full beam model as a classical feed at the LEO satellite ground station [50]. In the paper, the monopulse tracking technique is analysed in detail, and the radiation patterns of the feed and tracking antennas are shown depending on the azimuth and elevation angles. The operation of a monopulse tracking radar feed designed with four tracking antennas has been described [51]. The angle-dependent sum and difference signals of the feed and tracking antennas as electromagnetic (EM) waves have been analysed. In addition, the angular tracking error is calculated to design the aperture dimensions of the pyramid antenna. In the antenna system, the linear-circular polarization conversion of the signal is performed with a septum polarizer. The design and performance of septum polarizer structures in the X-band have been presented [52-54].

In this dissertation, a Cassegrain antenna structure in the X-band feeding system is preferred since there is less obstruction in front of the reflector when using two than a single reflector. In the Cassegrain structure, the X-band feed antenna is placed in the virtual focus between the main and second reflectors. The feed antenna provides the receiving part of the communication signal in the X-band feed antenna. The feed antenna is designed as a corrugated antenna.

The monopulse tracking system is used with the communication system to have a tracking feature since the most efficient tracking method uses a monopulse feed. In the monopulse method, waveguides are placed in the azimuth and elevation of the feed antenna. Tracking is performed by calculating the error value between the target and the antenna's boresight with the samples taken from the signal received by the feed antenna in the waveguide. For the feed antenna and waveguides to pass the desired mode, their dimensions must be calculated according to the cut-off frequency of the modes. The design steps of the monopulse tracking system are described later.

A septum polarizer separates RHCP and LHCP signals as linear signals in the feed antenna and waveguides. The insertion loss should be low, and the isolation between the ports should be high to not interfere with the communication signal.

A 180° hybrid coupler and a 2:1 combiner processes the linearly separated signals.

The X-band feeding system consists of a feeding antenna and its assemblies. It is designed to pass the desired mode so that the system can receive the signal for communication and tracking.

The signal contains communication and tracking information. The feeding antenna receives the communication signal. The monopulse tracking part is designed to calculate the tracking signal by sampling the signal. The target error value is calculated from the sampling.

The signal comes as a circularly polarized signal. After the communication signal is received by the feed antenna and the tracking signal is received by the monopulse unit, the signal is converted into a linear polarized signal. The conversion from circularly polarized signal to linear polarized signal is achieved by septum polarizer structure.

The Cassegrain antenna structure reflects the communication and tracking signal from the main reflector and the secondary reflector to the feed antenna. While the feed antenna receives the incoming signal, the tracking signal is calculated by sampling with the monopulse unit. According to the level and phase difference of the signal received by the monopulse unit, the elevation and azimuth error values of the target are calculated. The calculated error value is transmitted to the antenna movement system, and the antenna is directed to the target.

The reflector antenna and RF equipment system to be developed for the Ground Station, which is planned to be used for communication with LEO satellites in polar orbit simultaneously with the sun, includes a 7.3 m diameter reflector antenna, subreflector, X-band feed structures, X-band LNA and X-Band frequency down converters designs.

In conclusion, for the feed antenna to successfully receive the communication and tracking signal and to maintain the system's continuity, the feed antenna's components are the septum polarizer, monopulse unit and corrugated horn, must be properly designed. It is essential that each component provide the required RF characteristics individually, and when all components are combined, the RF characteristics of the system must be maintained.

3.1.1 X-Band Septum Polarizer Design

In this dissertation, a X-band septum polarizer is chosen for the polarization conversion of the signal received by the feed antenna. The structure of the proposed septum polarizer consists of a square waveguide, a segment consisting of several steps called a septum, and two rectangular waveguides. The primary purpose of the design is to linearly transmit half of the power of the right-handed or left-handed circularly polarized wave from the square waveguide to one of the two rectangular waveguides depending on the polarisation characteristics. While achieving this goal, it is necessary to keep reflection values at the inputs and outputs of the structure and the isolation value between the rectangular waveguides low.

The working principle of the septum polarizer structure is based on polarization conversion. There are three different polarization types: linear polarization, circular polarization, and elliptical polarization. All polarization types are a particular case of elliptical polarisation. The phenomenon of polarisation can be clearly understood by considering that the wave is divided into two components. When the angle between these two components is 0° or 180°, the polarisation of the wave is called linear polarisation. The circularly polarized wave can be represented as the sum of two electromagnetic waves with linear polarisation perpendicular to each other. The amplitudes of the composite vectors of the vertical and horizontal components at all points are equal to each other. This is why this type of polarization is referred to as circular polarisation. When the vertical component is one-quarter of a wavelength, i.e., 90° phase difference, ahead of the horizontal component oriented to the right (to the direction of propagation), the wave is RHCP. The vertical component is 90° phase difference ahead of the horizontal component oriented to the left (to the direction of propagation); the wave is called LHCP. All other waves that differ from linear and circular polarisation have elliptical polarisation. A wave is elliptically polarised if the amplitudes of the component vectors of its vertical and horizontal components at different points are not equal or if the vertical and horizontal components are not perpendicular.

In a septum polariser, the circularly polarised electromagnetic wave propagating from the square waveguide to the septum is expressed as the sum of two electromagnetic waves with linear polarisation (one parallel to the septum plane and one perpendicular to the septum plane). In Figure 3.3 (a), the RHCP and LHCP signals are modelled as two electromagnetic waves with linear polarisation. As shown in Figure 3.3 (a), the components of the wave with a 90° phase difference for each circular polarisation are followed separately in the septum. It is evident that the vertical component for the RHCP wave hits the septum steps and becomes two horizontal components with a 180° phase difference at the end of the septum. The horizontal component reaches the end of the septum as a horizontal component again. Since the vertical component propagates along the septum steps more than the horizontal component, the phase differences with the horizontal component are equalized at the end of the septum. The sum of the signals on the left side cancels each other, while the signals on the right side are summed at the end of the septum steps. As a result, the RHCP wave propagating from the square waveguide to the septum reaches the right side as a linear wave at the end of the septum. Considering the signal lost on the left side of the septum, it is clear that the signal reaching the right side of the septum will be half the magnitude of the signal sent from the square waveguide. The modelling of the LHCP wave inside the septum is also shown in Figure 3.3 (b).

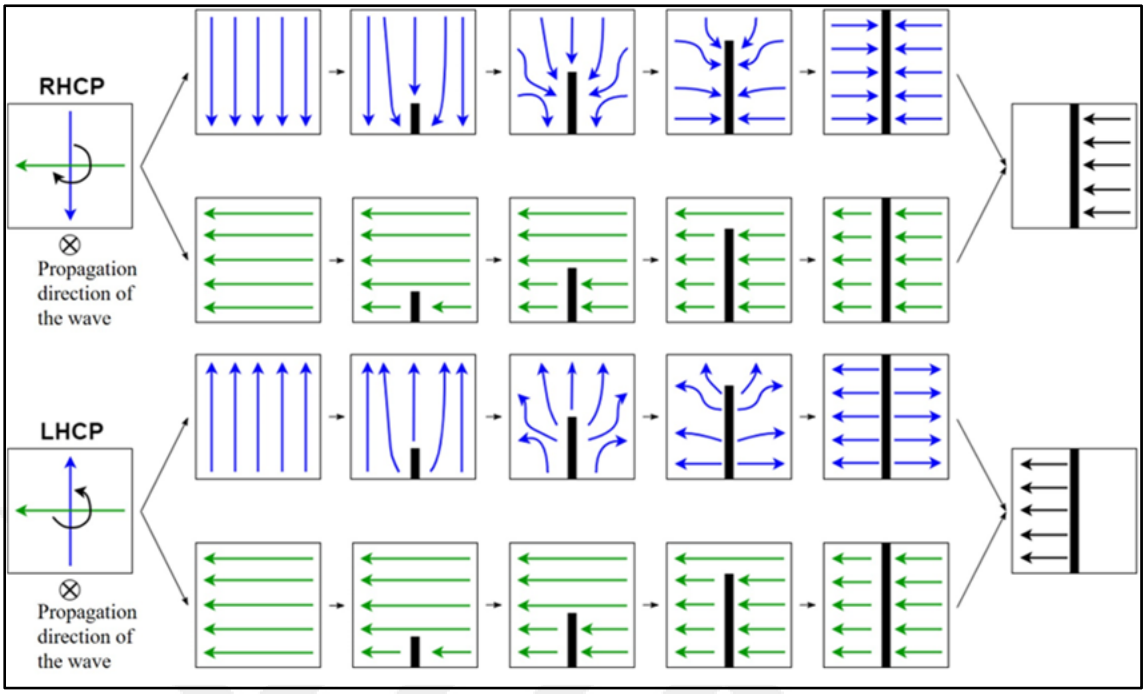

Figure 3.3.The behavior of the circularly polarized wave components in the septum polarizer. (a) RHCP, (b) LHCP

The design of a septum polarizer should consist of three parts; the square waveguide, the septum step structure, and the parts at the end of the septum where linear signals will be received. The square waveguide dimensions are calculated depending on the frequency band. For a rectangular waveguide, the sizes are calculated as follows:

$$f_{c,mn} = \frac{1}{2\pi\sqrt{\mu\varepsilon}}\sqrt{\left(\frac{m\pi}{a}\right)^2 + \left(\frac{n\pi}{b}\right)^2} \tag{3.1}$$

where $\boldsymbol{f_{c,mn}}$ is the cut-off frequency, m, n are the modes, and a and b are the waveguide dimensions. The square waveguide size for 8-8.5 GHz is calculated as 24 mm, and the length of the structure is shown in Figure 3.4.

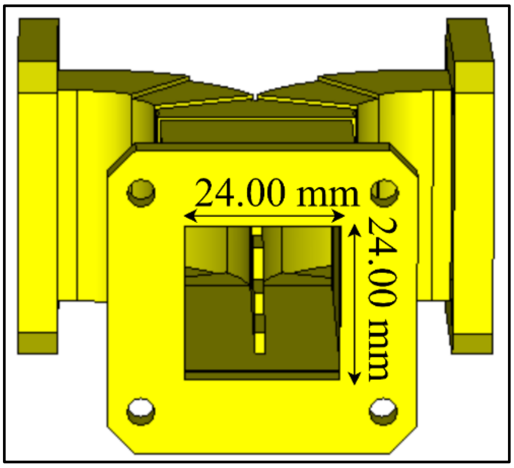

Figure 3.4. The front view of the septum polarizer

In the septum polarizer design, a 4-step septum structure is used. The dimensions of the septum steps are designed concerning the wavelength. In Figure 3.5, the lengths of the septum step structure are shown in letters. Approximate equivalents of these letters in terms of wavelength are given in Table 3.2. For the X-band septum polariser design, the dimensions of all steps are designed as shown in Figure 3.6. In addition, a conductive tooth is designed near the square waveguide for impedance matching in the structure.

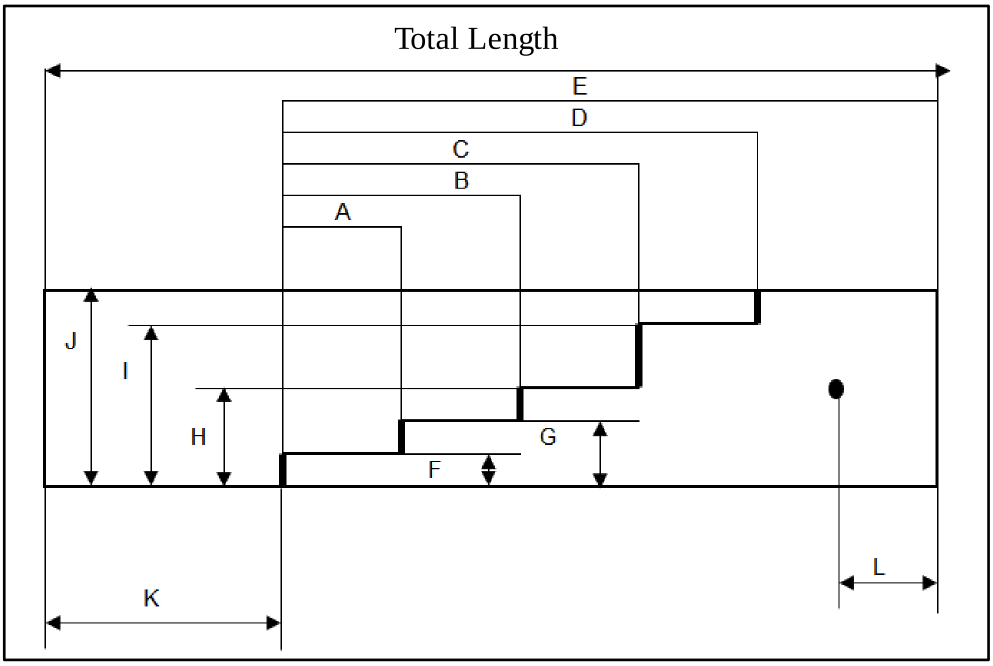

Figure 3.5. The septum step structure and length parameters

Table 3.2. Values of the septum step parameters

Parameter	Length (mm)	Parameter	Length (mm)
A	0.338λ	G	0.178λ
B	0.597λ	H	0.301λ
C	0.868λ	I	0.491λ
D	0.961λ	J	0.626λ
E	1.6λ	K	λ
F	0.08λ	L	0.19λ

Finally, the parts where linear signals are received at the end of the septum are designed. These parts can be designed with a waveguide or pin structure. Rectangular waveguides are used for this design. At the end of the septum, the waveguide is rotated 90° and designed as two waveguides on the right and left sides. The appearance of the structure is given in Figure 3.7.

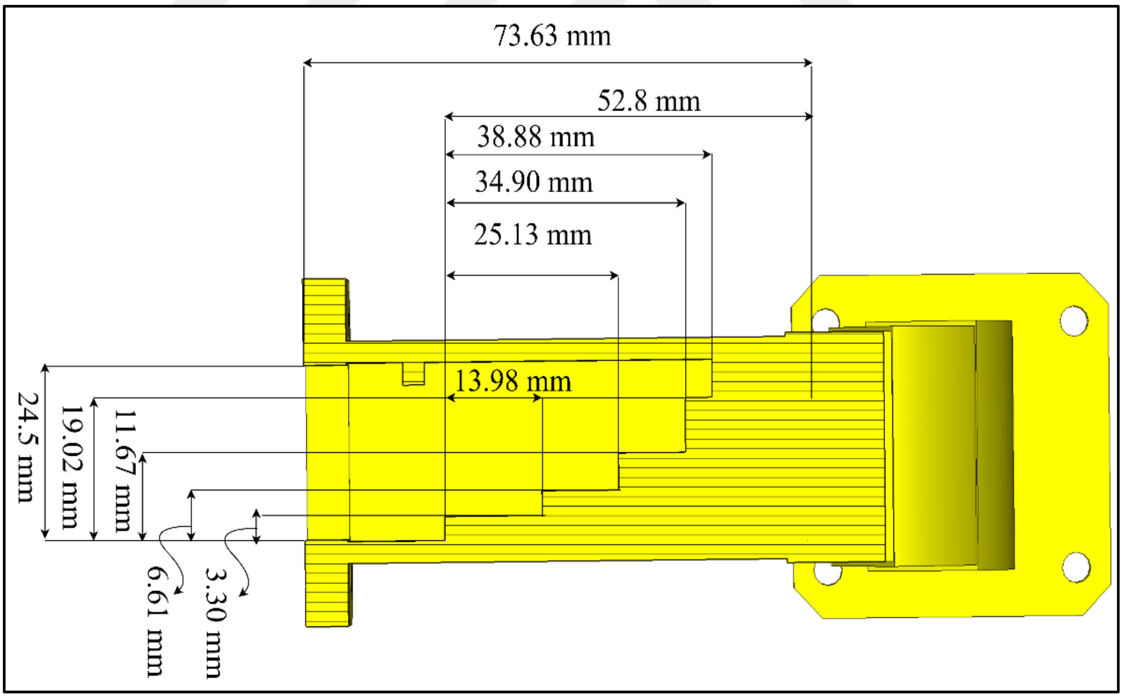

Figure 3.6. Septum step dimensions

The RF designs of the septum polarizer are made by choosing aluminium as the material. The common port is called port 3, where the LHCP signal is received in port 1 (left port in Figure 3.7), and the port where the RHCP signal is received is port 2 (right port in Figure

3.7). Two signals are generated as parallel and perpendicular to the septum plane and summed so that the phase difference between these signals is 90° since it is aimed to obtain a circularly polarised signal at the common port in the design.

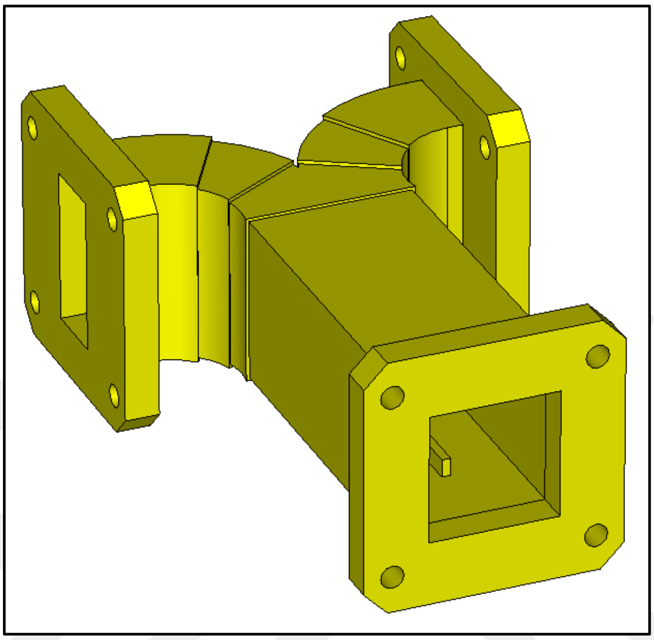

Figure 3.7. The position of a waveguide in the septum polarizer

Theoretically, half of the signal sent from the common port is expected to reach one of the linear ports, corresponding to -3 dB and a 90° phase difference between them. The amplitude of the signal transmitted from the common port to the linear ports is labelled S31 and S32. Insertion loss is shown in Figure 3.8. The phase difference between the linear ports is given in Figure 3.9. The return losses within the linear ports and the isolation value between the linear ports are given in Figure 3.10 and Figure 3.11, respectively.

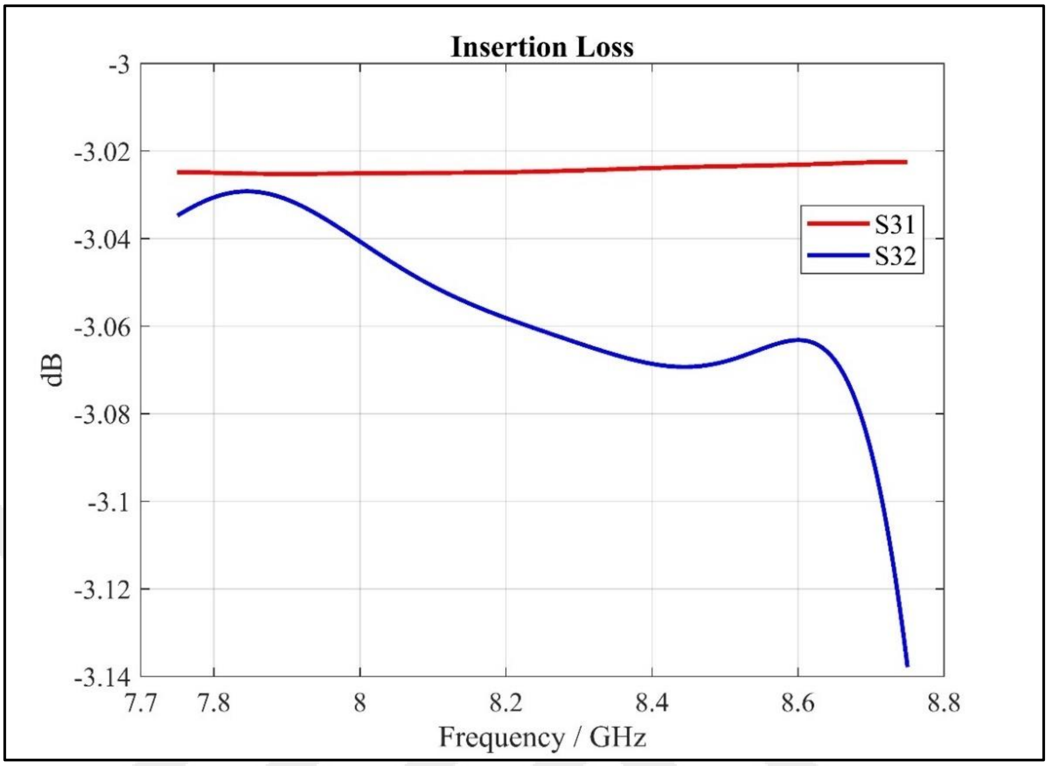

Figure 3.8. Insertion loss of septum polarizer

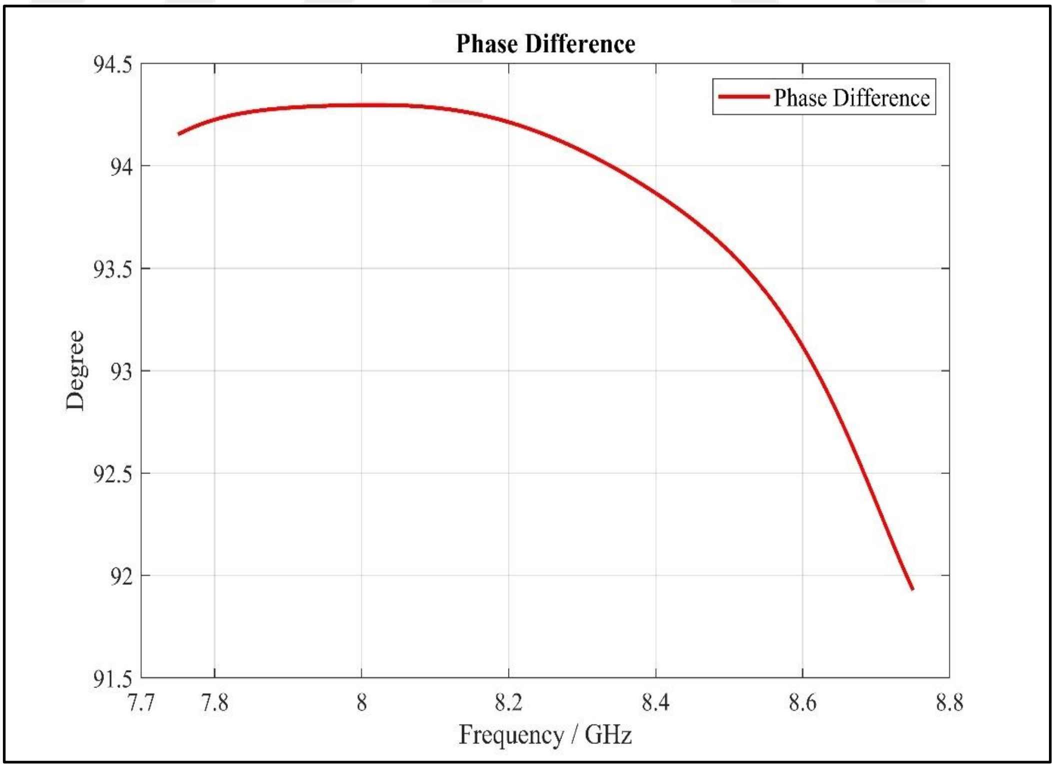

Figure 3.9. The phase difference of septum polarizer

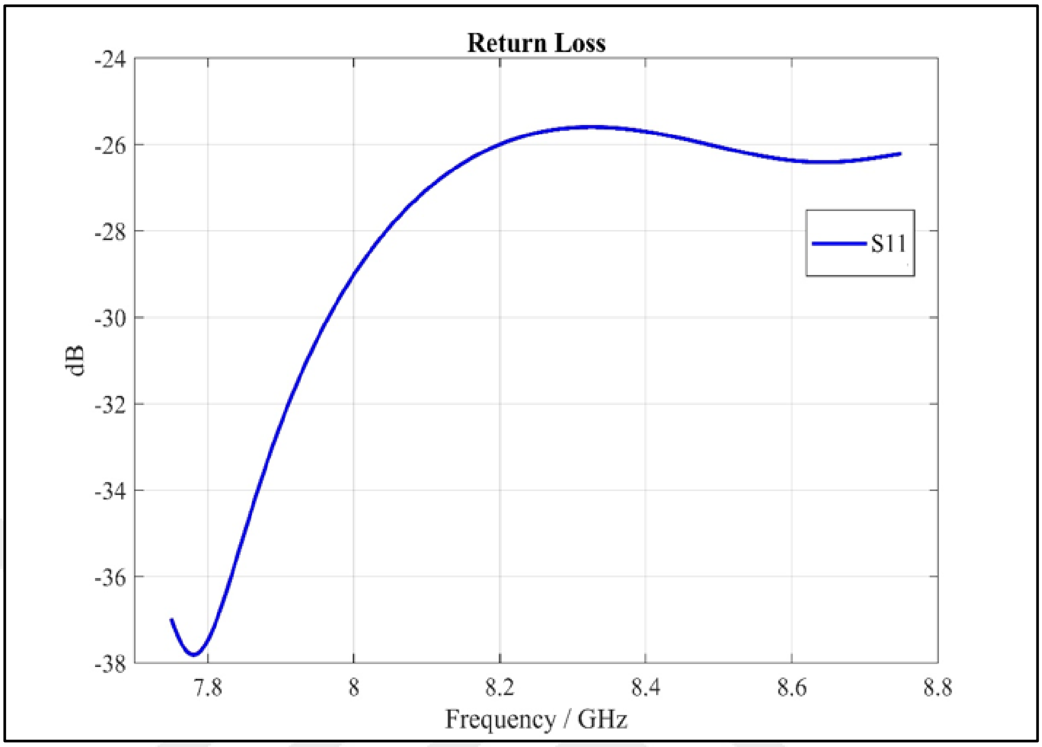

Figure 3.10. The return loss for linear ports of the septum

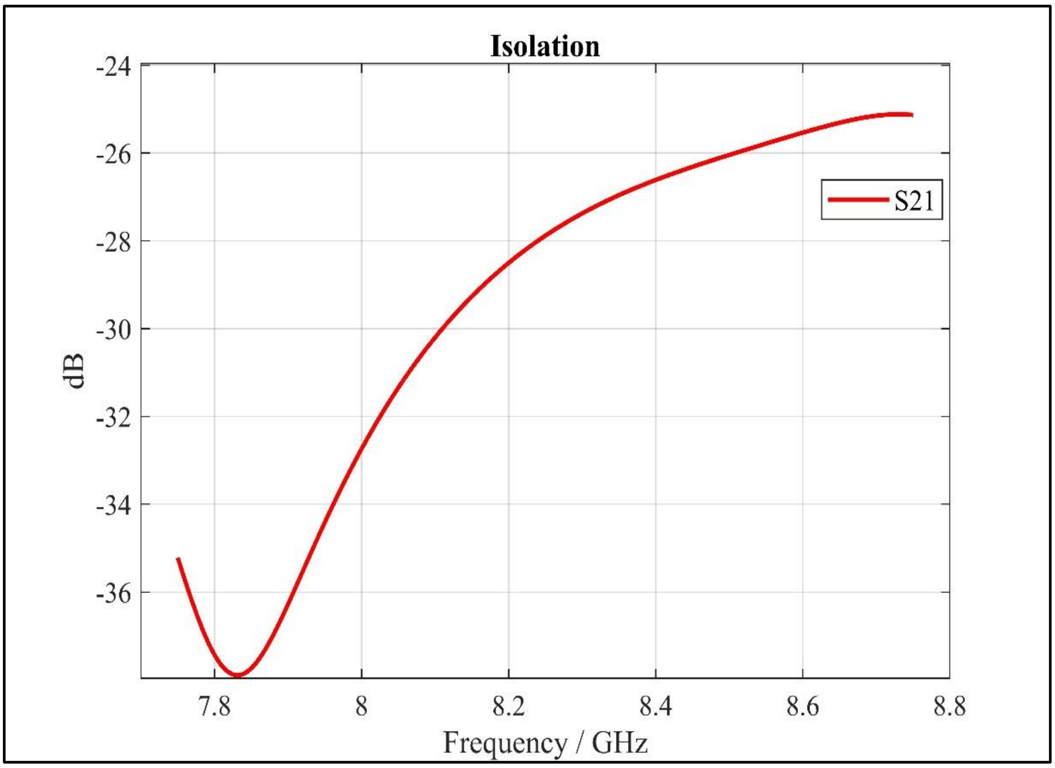

Figure 3.11. Isolation between linear ports of the septum

3.1.2 X-Band Corrugated Horn Antenna Design

The feed antenna is the interstage system that receives the EM wave from the air and transfers it to the transmission line. In this dissertation, the X-band feed antenna is proposed as a corrugated antenna. Corrugations are added after the input radius of the structure is calculated. The depth of the first corrugation placed at the entrance of the antenna is $\lambda/_2$ and the depth of the subsequent corrugations is gradually reduced from $\lambda/_2$ to $\lambda/_4$ with a total of 10 corrugations. The section with ten corrugations with decreasing dimensions is called the mode converter. The depth of the corrugations in the body of the antenna is equal to $\lambda/_4$ and the number of corrugations used in the body is given parametrically. In addition, corrugation widths and tooth thicknesses are also provided as parameters in the Computer Simulation Technology Microwave Studio (CST MWS) program and it optimises the structure by changing the parameter values. The schematic and dimensions of the designed corrugated system are shown in Figure 3.12.

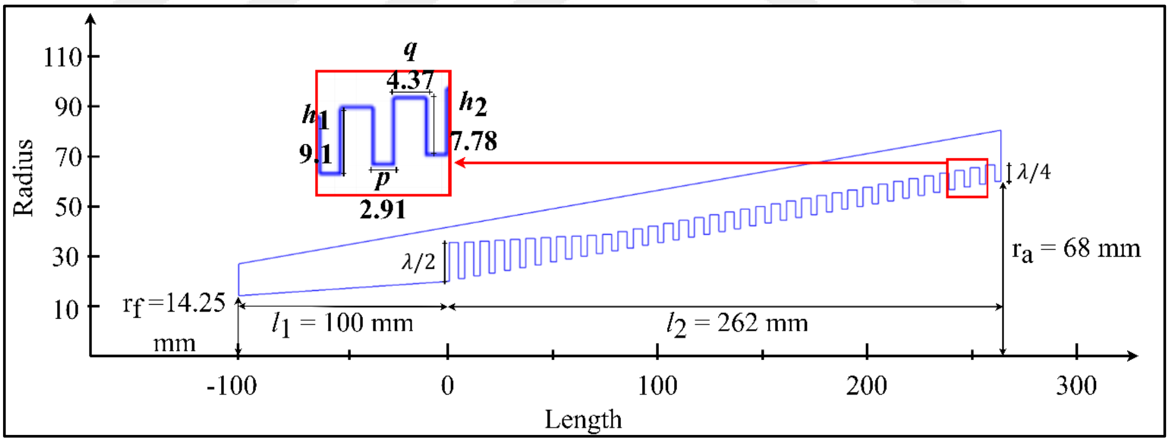

Figure 3.12. The schema of the corrugated structure

The designed corrugated structure is rotated 360° in the waveguide axis, and the mechanical structure is obtained. A cross-sectional view of the mechanical structure of the feed antenna is given in Figure 3.13.

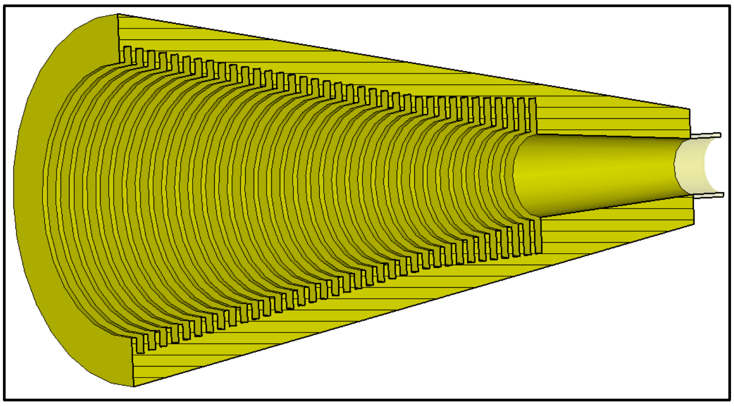

Figure 3.13. Mechanic structure profile of feed antenna

Three critical criteria are taken into consideration in the design of the feed antenna. These are antenna beamwidth, illumination angle phase variation, and feed antenna-air matching. The feed antenna is a matching circuit between the transmission line and the air. In this transition, the power from the transmission line must be harmonized and transmitted with minimum reflection loss. This is analyzed with back reflection and VSWR graphs of the feed antenna port. A VSWR value of 1 indicates that the entire signal is transmitted, while ∞ means that the whole signal is reflected. Therefore, a VSWR value close to 1 is desirable. The VSWR plot for the X-band feed antenna is given in Figure 3.14.

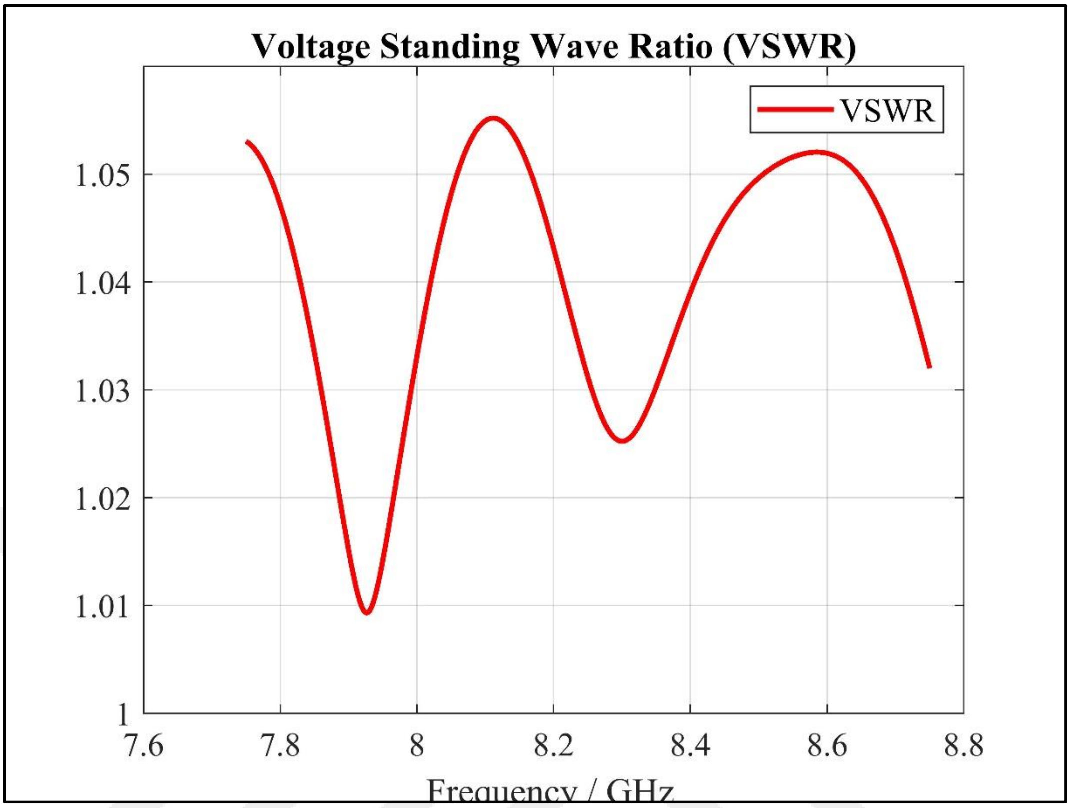

Figure 3.14. VSWR for the feed antenna

The antenna beam indicates how much of the power from the antenna will be reflected by the reflector antenna. This value is known as the edge taper, which is how much the antenna power is reduced at the edge of the illumination angle relative to the main lobe. The radiation pattern showing the antenna gain and side lobe levels is shown in Figure 3.15.

The edge tapers for phi=0° and phi=90° are given in Table 3.3. Low cross-polarization of the signal is one of the antenna design objectives. The cross-polarization of the feed antenna is given in Figure 3.16.

Table 3.3.Edge taper values

	$\boldsymbol{phi = 0°}$	$\boldsymbol{phi = 90°}$
$\boldsymbol{0°}$	$19.48\ dBi$	$19.48\ dBi$
$\boldsymbol{20°}$	$7.43\ dBi$	$7.41\ dBi$
$\boldsymbol{edge\ taper}$	$12.05\ dB$	$12.07\ d$

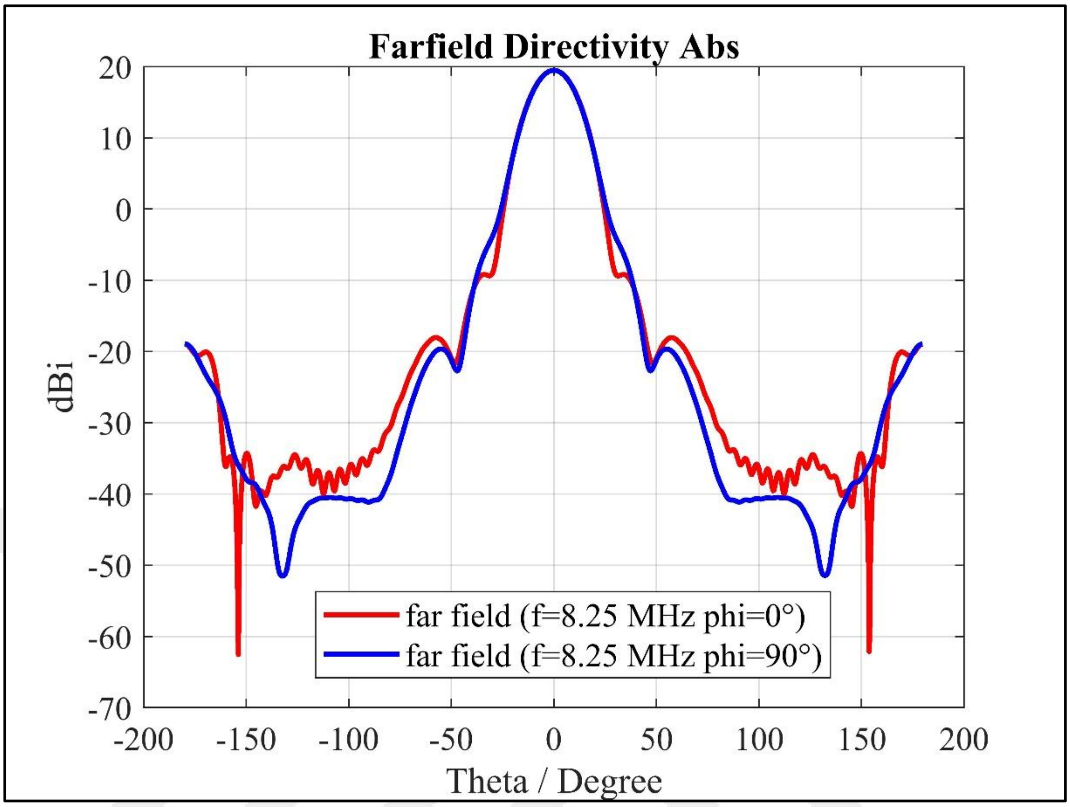

Figure 3.15. The radiation pattern of the feed antenna for phi=0° and phi=90°

The phase curves of the feed antenna for phi=0° and phi=90° are given in Figure 3.17. The circular polarization is transmitted and received in the antenna system. When the phase curve is examined in the circular polarization, the resulting graphic is given in Figure 3.18. Phase difference for phi=0° and phi=90° is low and at the desired level.

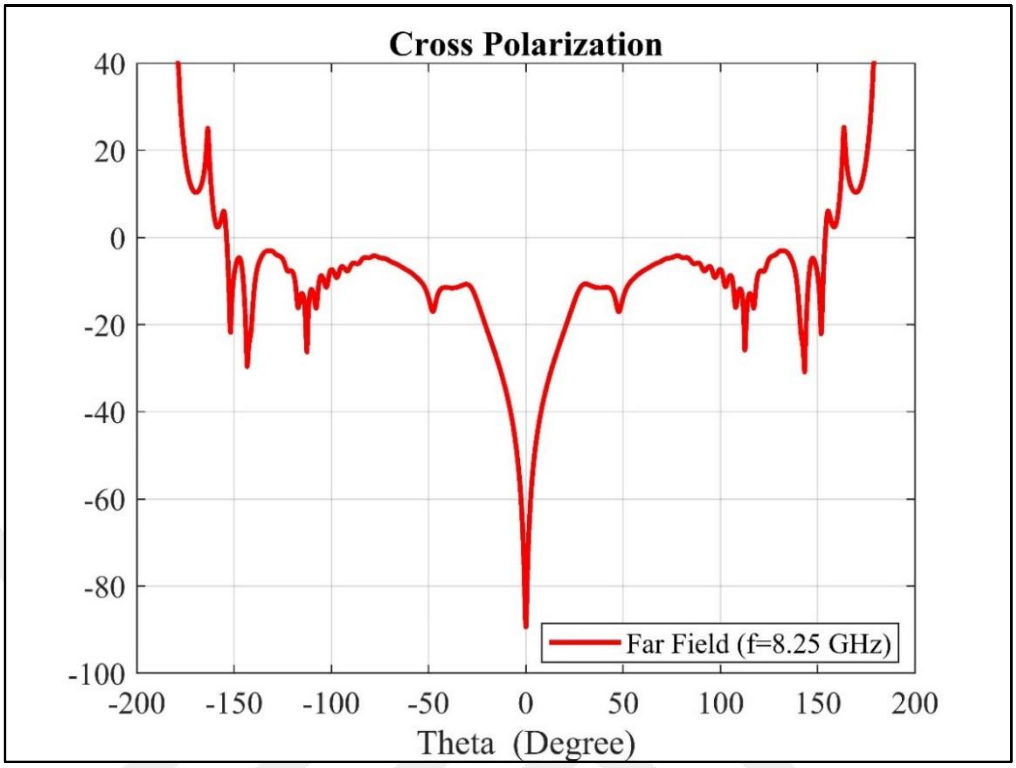

Figure 3.16. The cross-polarization of the feed antenna

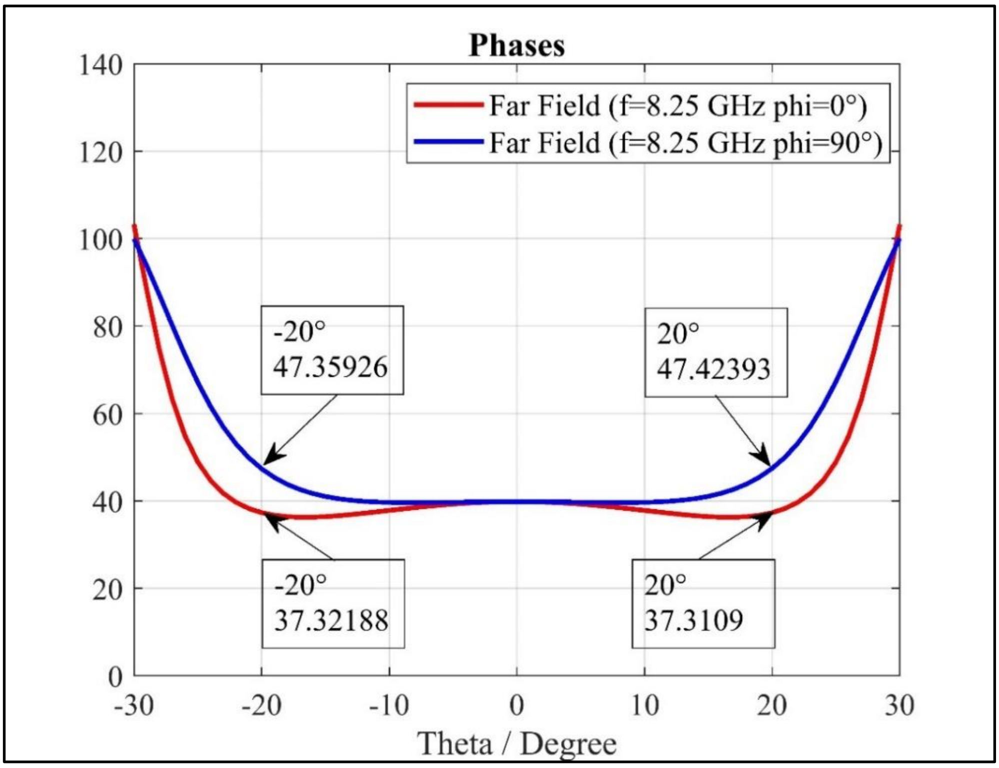

Figure 3.17. The phases of the feed antenna at 8.25 GHz

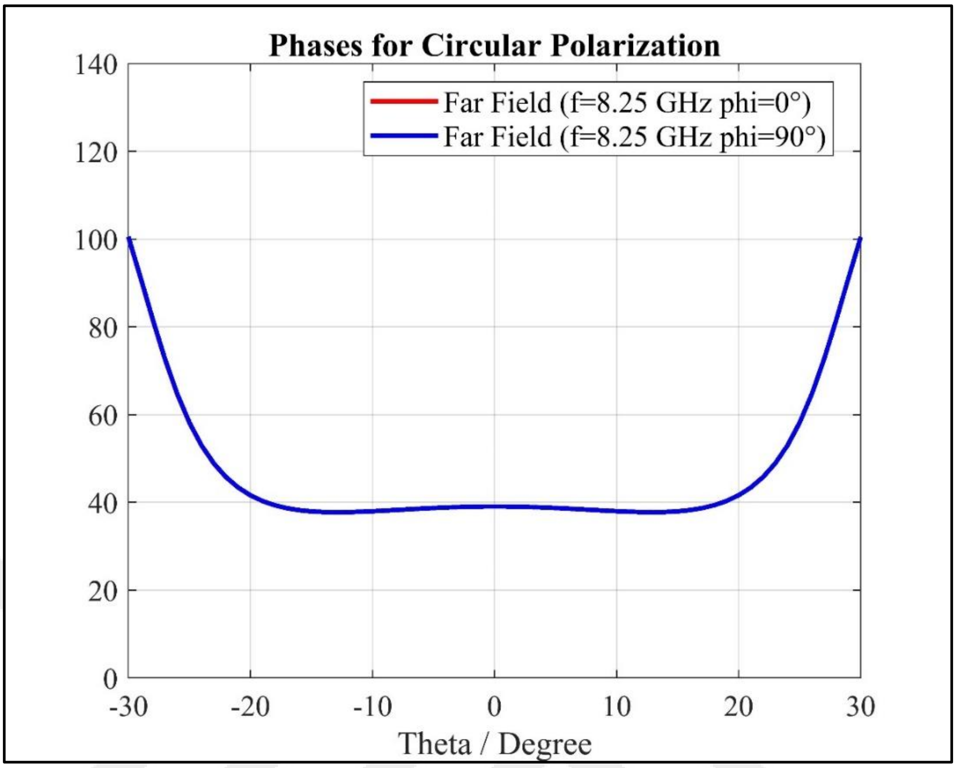

Figure 3.18. The phase curves of the feed antenna for circular polarization at 8.25 GHz

3.1.3 X-Band Monopulse Design

In this dissertation, the X-band monopulse unit is proposed to obtain tracking signals. The monopulse unit calculates the difference between the satellite and the ground station boresight from the signal received by the antenna during satellite communication with the antenna. The monopulse unit is the unit in the feed antenna where the tracking system is realized and consists of four circular waveguides placed two by two in azimuth and elevation of the feed antenna. The number, position, and dimensions of the waveguides used in the monopulse unit are calculated precisely for the design. Firstly, the signal modes are analyzed to calculate the size of the waveguides.

Energy can propagate in a medium or a vacuum, depending on the type of energy and the nature of the medium. The propagation patterns are called by different mode names. In more detail, the mode of electromagnetic radiation is defined as the field pattern of the propagating wave. Different modes have different characteristics; therefore, it is necessary to ensure that the correct modes are excited and unwanted modes are suppressed if they can be supported for any structure.

By looking at wave theory, it is possible to calculate the different modes in which an electromagnetic wave can propagate in a circular structure. The different modes correspond to various components within an electromagnetic wave. The electric field component of an electromagnetic wave, the magnetic field component, and the propagation direction of the wave are perpendicular to each other.

When the electric field component and the magnetic field component of an electromagnetic wave are perpendicular or transverse to the propagation direction in the waveguide, they are called different modes. TE (Transverse Electric) and TM (Transverse Magnetic) are basic modes. TE mode is due to transverse electric waves, characterized by the electric vector always perpendicular to the propagation direction. In TE mode, the electric field component is transverse, while the magnetic field component is perpendicular to the propagation direction. TM mode is characterized by the magnetic vector always being perpendicular to the propagation direction. The magnetic field component is transverse in TM mode, while the electric field component is perpendicular to the propagation direction.

The circular waveguide used in the monopulse unit is given in Figure 3.19.

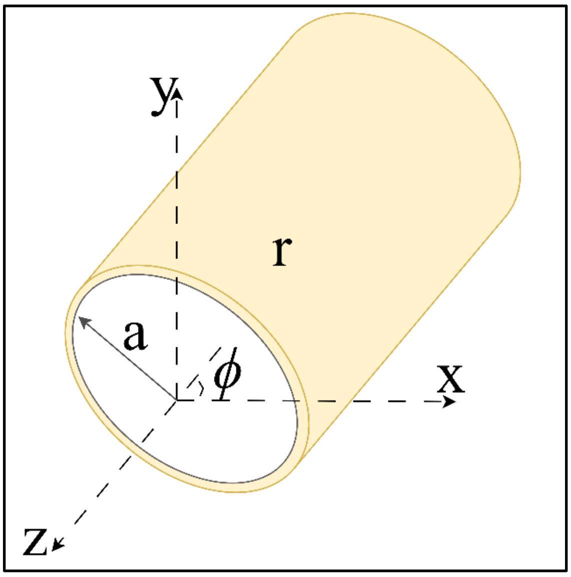

Figure 3.19. The circular waveguide

The signal in Figure 3.19 transmits in the z-direction. In the TE mode, the component of the electric field in the z direction is zero since the electric field is always perpendicular to the propagation direction. Thus, when looking at the solution of the wave equation in the z direction, it is seen that it depends only on the magnetic field in that direction (H_z). It is written as;

$$\nabla^2 H_z + k^2 H_z = 0 \tag{3.2}$$

k is the wavenumber.

Laplace expansion should be done for the solution of the wave equation. The Laplacian expansion of the magnetic field;

$$\nabla^2 H_z = \left(\frac{1}{r}\frac{\partial}{\partial r}\left(r\frac{\partial}{\partial r}\right) + \frac{1}{r^2}\frac{\partial^2}{\partial \phi^2} + \frac{\partial^2}{\partial z^2}\right) H_z \tag{3.3}$$

is written.

When the magnetic field transmits in the r and $\emptyset$ direction, the wave transmits in the z-direction. If the propagation information of the wave is written as $e^{-j\beta z}$, H_z can be expressed as below:

$$H_z(r,\phi,z) = h_z(r,\phi)e^{-j\beta z} \tag{3.4}$$

β, is the propagation constant.

The solution of Equation (3.3), when done through H_z in Equation (3.4):

$$\nabla^2 H_z = \left(\frac{\partial^2}{\partial r^2} + \frac{1}{r}\frac{\partial}{\partial r} + \frac{1}{r^2}\frac{\partial^2}{\partial \phi^2} + \frac{\partial^2}{\partial z^2}\right) h_z(r,\phi)e^{-j\beta z}$$

$$= \left(\frac{\partial^2}{\partial r^2} + \frac{1}{r}\frac{\partial}{\partial r} + \frac{1}{r^2}\frac{\partial^2}{\partial \phi^2} - \beta^2\right) h_z(r,\phi)e^{-j\beta z} \tag{3.5}$$

It is concluded. Equation (3.5) substitute in Equation (3.6),

$$\left(\frac{\partial^2}{\partial r^2} + \frac{1}{r}\frac{\partial}{\partial r} + \frac{1}{r^2}\frac{\partial^2}{\partial \phi^2} - \beta^2\right) h_z(r,\phi)e^{-j\beta z} + k^2 h_z(r,\phi)e^{-j\beta z} = 0$$

$$\left(\frac{\partial^2}{\partial r^2}+\frac{1}{r}\frac{\partial}{\partial r}+\frac{1}{r^2}\frac{\partial^2}{\partial \phi^2}+(k^2-\beta^2)\right)h_z(r,\phi)=0 \tag{3.6}$$

is obtained. If $k_c^2=k^2-\beta^2$ substitutes, Equation (3.6) can be written as below:

$$\left(\frac{\partial^2}{\partial r^2}+\frac{1}{r}\frac{\partial}{\partial r}+\frac{1}{r^2}\frac{\partial^2}{\partial \phi^2}+k_c^2\right)h_z(r,\phi)=0 \tag{3.7}$$

k_c is the cut-off wavenumber.

$h_z(r,\phi)$ contains the r and $\emptyset$ components of the magnetic field. $h_z(r,\phi)$ can be expressed by using the variable allocation method:

$$h_z(r,\phi)=R(r)P(\phi) \tag{3.8}$$

Equation (3.8) variables and Equation (3.7) are solved as below:

$$\frac{\partial^2(RP)}{\partial r^2}+\frac{1}{r}\frac{\partial(RP)}{\partial r}+\frac{1}{r^2}\frac{\partial^2(RP)}{\partial \phi^2}+k_c^2=0 \tag{3.9}$$

$$\frac{r^2}{R}\frac{\partial^2 R}{\partial r^2}+\frac{r}{R}\frac{\partial R}{\partial r}+r^2k_c^2=-\frac{1}{P}\frac{\partial^2 P}{\partial \phi^2} \tag{3.10}$$

The left side of Equation (3.10) depends only r variable, and the right side depends only θ variable. Thus, both sides should be equal to one constant. If this constant, $k_\emptyset^2$, is written, the left and right sides of the Equation (3.10) can be written as equation:

$$\frac{\partial^2 P}{\partial \phi^2}+k_\phi^2P=0 \tag{3.11}$$

$$r^2\frac{\partial^2 R}{\partial r^2}+r\frac{\partial R}{\partial r}+\left(r^2k_c^2-k_\phi^2\right)R=0 \tag{3.12}$$

The solution to Equation (3.11) is as below:

$$P(\phi)=A\sin k_\phi\,\phi+B\cos k_\phi\,\phi \tag{3.13}$$

The solution of h_z for ϕ should be periodic ($h_z(r,\phi)=h_z(r,\phi\pm 2m\pi)$). Therefore, n is an integer, if $k_\phi=n$ is used, Equation (3.13) can be written as below:

$$P(\phi)=A\sin n\,\phi+B\cos n\,\phi \tag{3.14}$$

When using $k_\phi = n$, Equation (3.12) becomes as below:

$$r^2 \frac{\partial^2 R}{\partial r^2} + r \frac{\partial R}{\partial r} + (r^2 k_c^2 - n^2) R = 0 \tag{3.15}$$

The Bessel differential equation is used for the solution of Equation (3.15).

$$R(r) = C J_n(k_c r) + D Y_n(k_c r) \tag{3.16}$$

C and D are constant in Equation (3.16). $J_n(x)$ and $Y_n(x)$ are the first and second Bessel functions, respectively. Bessel functions have a regular singularity at 0 and an irregular singularity at infinity. $Y_n(k_c r)$ is equal to the infinity when $r = 0$. Since this case cannot be accepted for the circular waveguide in terms of physical conditions, D is equivalent to 0.

When Equation (3.14) and (3.16) substitute in Equation (3.8), the solution of hz is expressed as:

$$h_z(r, \phi) = (A \sin n\,\phi + B \cos n\,\phi)\, J_n(k_c r) \tag{3.17}$$

In Equation (3.17), C is combined with A and B since A, B, and C are constant.

Under boundary conditions, it is known that the tangential component of the electric field in the circular waveguide is equal to 0 (E_{tan}=0). Since it is known that E_z=0, E_ϕ is equal to the zero and written for the boundary conditions of the waveguide:

$$E_\phi(r, \phi) = 0 \qquad at\; r = a \tag{3.18}$$

$E_\phi(r, \phi, z)$ is found from $H_z(r, \phi, z)$ as below:

$$E_\phi(r, \phi, z) = \frac{jw\mu}{k_c}(A \sin n\,\phi + B \cos n\,\phi) J_n'(k_c r) e^{-j\beta z} \tag{3.19}$$

$J_n'(k_c r)$ is the derivative of the Bessel function. The tangential component, E_ϕ, should be zero at $r = a$. Thus, the value that makes the right side of Equation (3.19) zero should be written at $r = a$.

$$J_n'(k_c a) = 0 \tag{3.20}$$

There are different root values satisfying Equation (3.20). If p_{nm}' is defined as the mth root of the $J_n'(k_c a)$ ($J_n'(p_{nm}' a) = 0$), k_c should be expressed;

$$k_{c_{nm}} = \frac{p'_{nm}}{a} \tag{3.21}$$

$k_{c_{nm}}$ is the cutoff wavenumber. Here p'_{nm}, which varies according to the values of m and n, is the constant that determines the TE modes in the circular waveguide. p'_{nm} values are given in 4.

Table 3.4. p'_{mn}values TE modes of the circular waveguide

$\boldsymbol{n}$	$\boldsymbol{p'_{n1}}$	$\boldsymbol{p'_{n2}}$	$\boldsymbol{p'_{n3}}$
0	3.832	7.016	10.174
1	1.841	5.331	8.536
2	3.054	6.706	9.970

TE modes are represented with integers TE_{mn}. The m and n represent the mode numbers within the waveguide and are integers that can take different values from 0 or 1 to infinity. Depending on the waveguide dimensions and type, only a limited number of different m and n modes can propagate through a waveguide. Depending on the radius, the mode that can propagate in the waveguide is calculated based on the cut-off frequency. The relationship among the radius of a circular waveguide, the mode numbers m and n, and the cut-off frequency are expressed as follows:

$$f_{c_{m,n}} = \frac{p'_{nm}}{2\pi a\sqrt{\mu\varepsilon}} \tag{3.22}$$

where μ is the relative magnetic permeability of the waveguide, and ε is the relative electrical permeability of the waveguide. $f_{c_{m,n}}$is the cut-off frequency in m and n modes.

From the cut-off frequency found with the waveguide radius and the desired mode numbers, the signal propagates in m and n modes. The propagation of the signal in the circular waveguide for some m and n modes is shown in Figure 3.20.

In the design, the input of the feed antenna is designed as a circular waveguide since the signal arrives at the antenna as a circularly polarised wave. The feed antenna must receive the communication mode of the signal. The communication mode corresponds to TE_{11}

among the circular waveguide modes. Therefore, the value of p'_{11} in Table 3.4 is used for the constant in the equation when finding the radius of the waveguide. The X-band feed antenna is required to operate in the 8-8.5 GHz frequency band. The cut-off frequency should be lower than the minimum frequency value so that the structure can operate efficiently after 8 GHz. For this design, the cut-off frequency is chosen as 7 GHz. With all the given information, the input radius of the circular waveguide is calculated as 12.56 mm from Equation (5.21). As a result of the simulations, the optimum radius value is 14.25 mm.

For a high gain, narrow beamwidth reflector, the criticality in designing an accurate tracking system with optimum sum and difference patterns is mainly based on the feed design. After the feed antenna design described in section 0, the monopulse section is added to the structure. The monopulse section samples the signal from the feed antenna. For this reason, the dimensions of the circular waveguides in the monopulse unit are designed as 14.25 mm. Data in elevation and azimuth are required to calculate the error signal by sampling the signal to the antenna. Therefore, four couplers are designed to receive data from the circularly polarised signal in each axis. These couplers are placed two each in azimuth and elevation of the feed antenna. The five-element structure consisting of a corrugated antenna and four circular waveguides is shown in Figure 3.21.

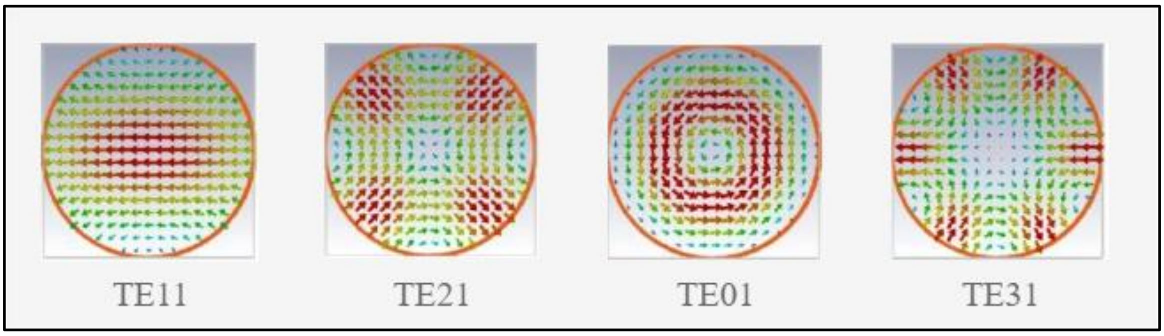

Figure 3.20. Some TE modes in the circular waveguide

The signal arrives at the waveguides in circular polarization. The circular-linear polarisation conversion is done by septum polarizers connected to the waveguides. Each waveguide has two linear ports. These ports are where RHCP and LHCP signals are output separately when converted to linear. Each polarization type is processed in its way.

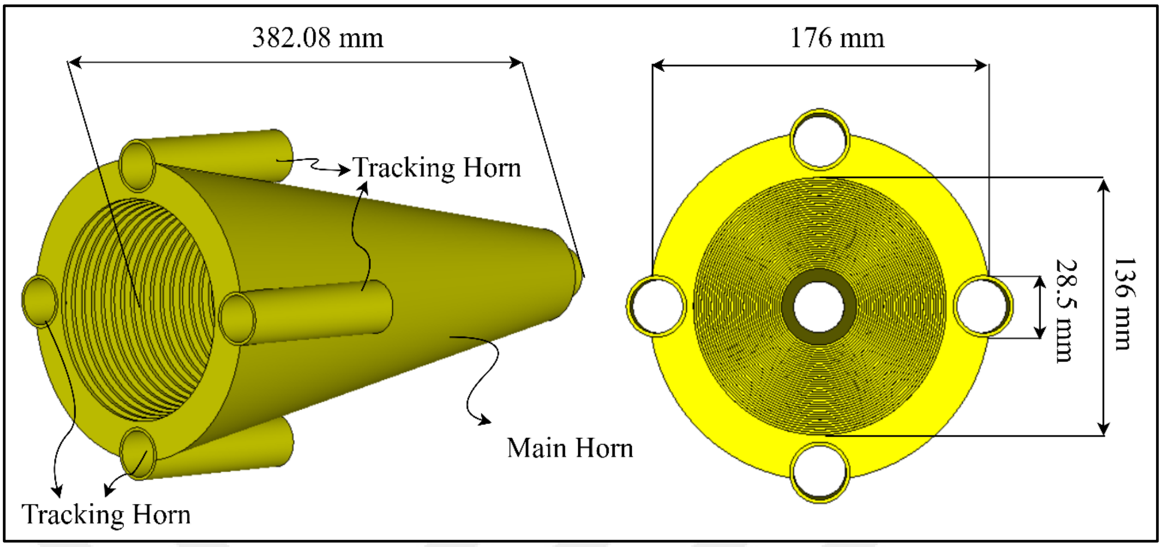

Figure 3.21. Feed and tracking antenna (a) three-dimensional view (b) front view

Figure 3.22 shows the block diagram of the monopulse monitoring for one polarization, and the schema will be the same for the other polarization. The signals received from the waveguides E_1 and E_2 on the elevation axis of the feed antenna are processed with a 180° hybrid to extract the elevation error (EL). The azimuth error (AZ) is subtracted by processing the signals received from the waveguides A_1 and A_2 located on the azimuth axis of the feed antenna with a 180° hybrid. The EL and AZ errors are sent to the scanner plate, and the error signal is calculated. This error signal, together with the total signal from the feed antenna, is the input of a 6 dB coupler. The tracking signal at the output of the 6 dB coupler is transmitted to the tracking receiver, which derives the EL and AZ to drive the servomotor, enabling the antenna system to be used as a tracking antenna. With this tracking method, angular information is obtained simultaneously in both azimuth and elevation. If the error signal is zero, the servomotor is informed that the tracked satellite is directly opposite the antenna, and the motor does not move. However, with the error signal captured in azimuth or elevation, the degree of deviation between the target and the antenna is determined by the error signal and transmitted to the servo motor. The movements required for the antenna system to be directly opposite the target are defined, and the target is moved directly opposite the antenna.

It is essential in design to ensure the same orientation of the septum and the exact orthogonality of the difference element in the two-hybrid elements. Otherwise, movement in the elevation axis will cause an undesired error in the azimuth axis and vice versa, known as crosstalk. Once the design and fabrication of the feed are completed, the position of the feed in the reflector is decided by ensuring that the phase center of the feed is aligned with the focus of the reflector.

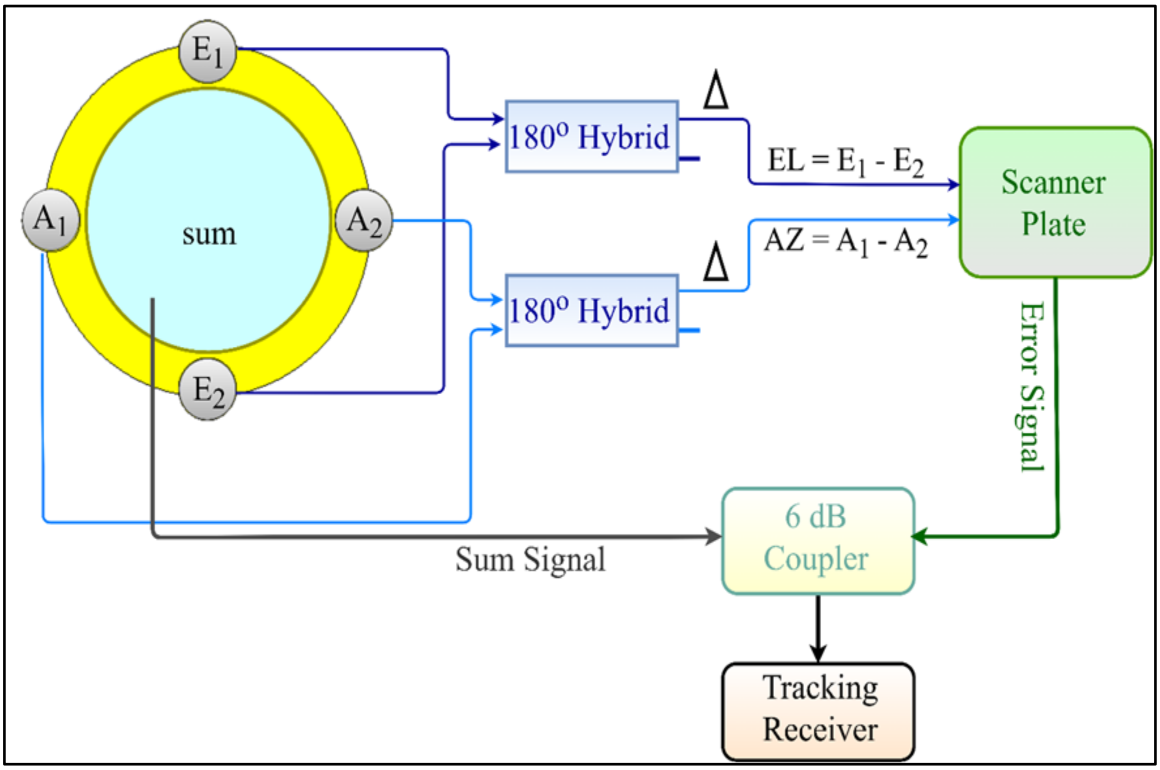

Figure 3.22. Monopulse tracking block diagram

It is essential that the signal from which communication and tracking information is received and processed with high efficiency and low loss. The signal level decreases if the communication signal experiences a loss while passing through the antenna, and communication cannot be provided at the desired performance. In order not to affect communication, transmission loss must be minimized. Since the conductor loss will affect the transmission loss, aluminium is chosen as the material for low conductor loss and ease of production.

All VSWR values for the X-band monopulse unit and the feed antenna are given in Figure 3.23. Port isolations between the monopulse unit and feed antenna are shown in Figure 3.24.

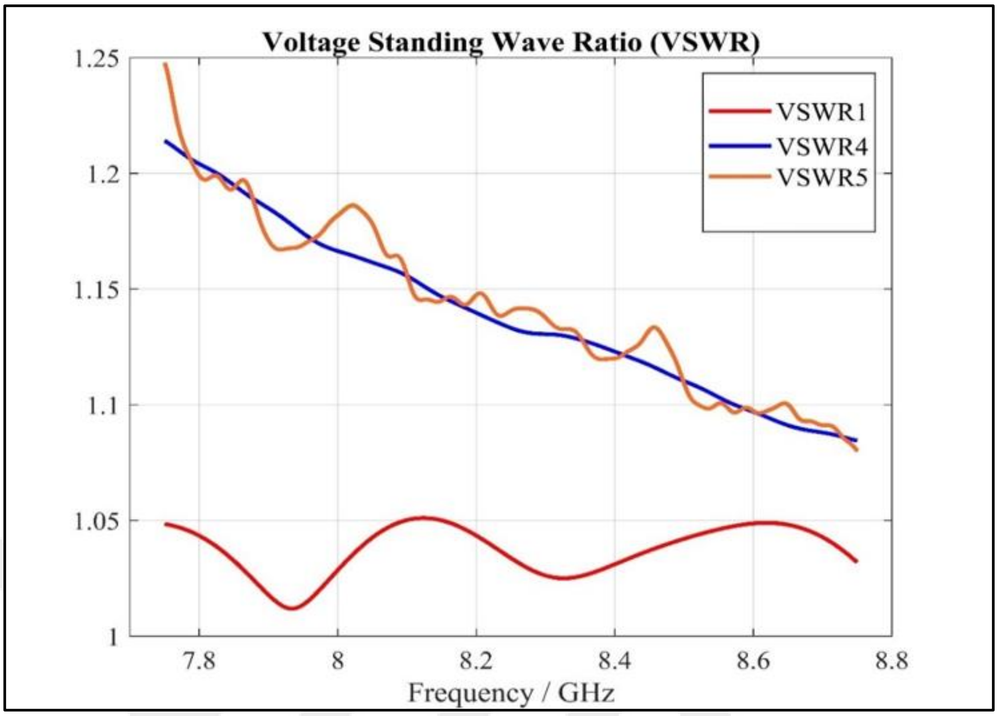

Figure 3.23. VSWR for monopulse unit and feed antenna

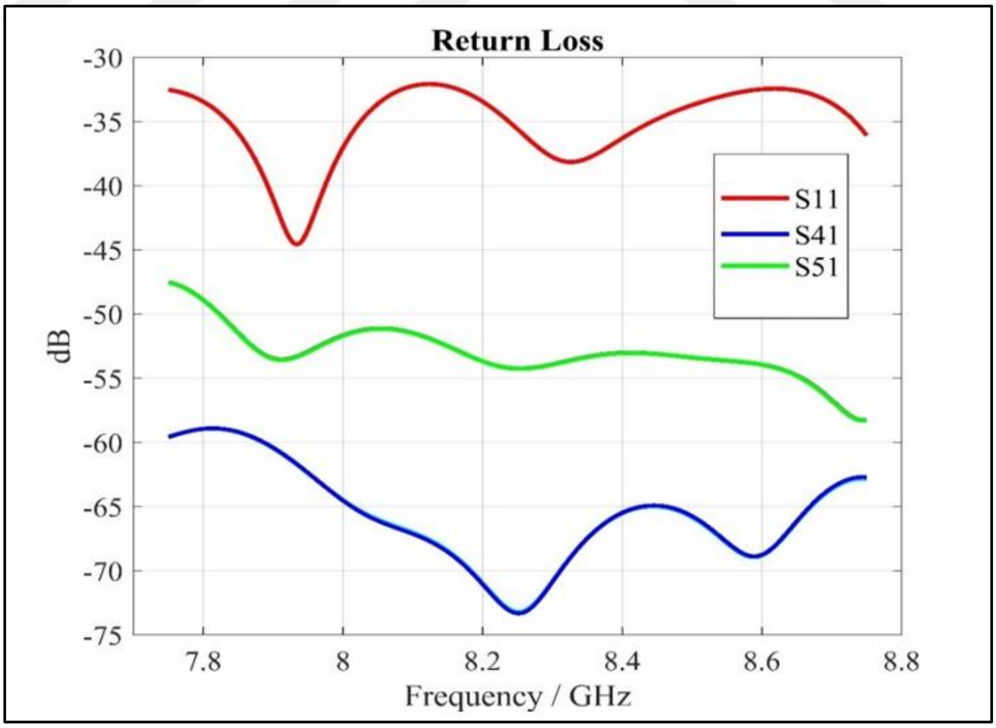

Figure 3.24. Port isolations between the monopulse unit and feed antenna

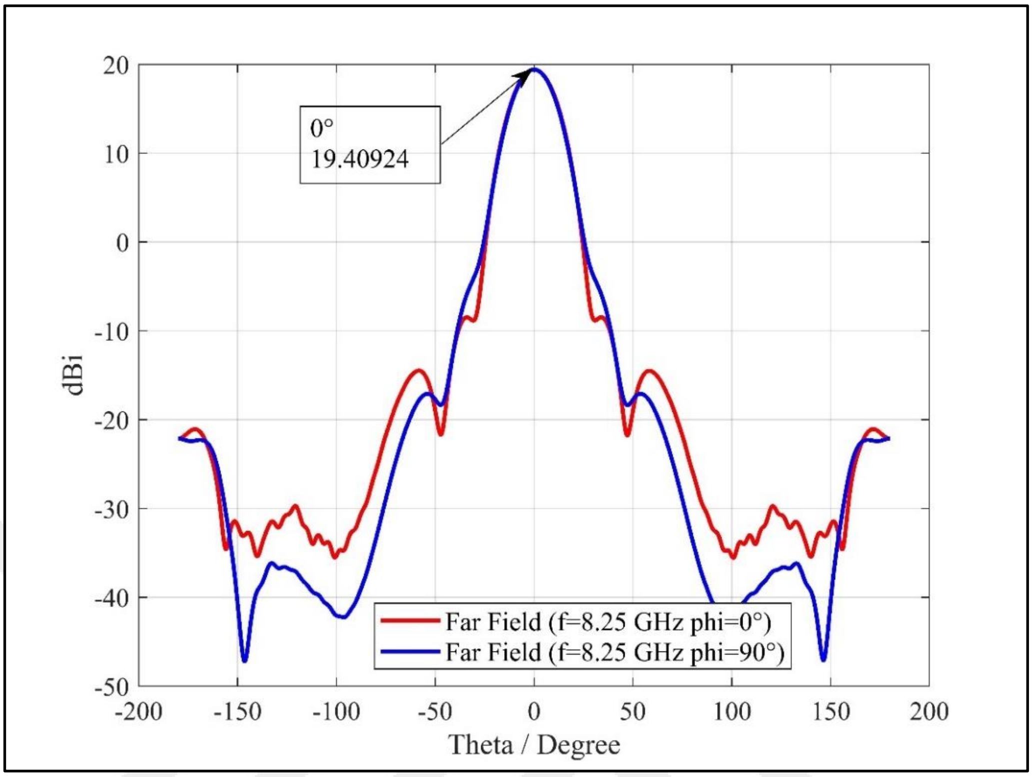

Figure 3.25. The radiation pattern of monopulse unite and the feed antenna at phi=0° and phi=90°

Table 3.5. Edge taper values for monopulse unit with feed antenna

	$\boldsymbol{phi = 0°}$	$\boldsymbol{phi = 90°}$
$\mathbf{0°}$	$19.41\ dBi$	$19.41\ dBi$
$\mathbf{20°}$	$7.41\ dBi$	$7.21\ dBi$
$\boldsymbol{edge\ taper}$	$12\ dB$	$12.2\ dB$

The radiation pattern of the system consisting of the monopulse unit and the feed antenna, showing the antenna gain and side lobe levels, is given in Figure 3.25. Table 3.5 provides edge taper values for phi=0° and phi=90°. The phase curves of the feed antenna for phi=0° and phi=90° are shown in Figure 3.26. The highest phase difference is 11°. A phase change of less than 25° increases the reflector aperture efficiency.

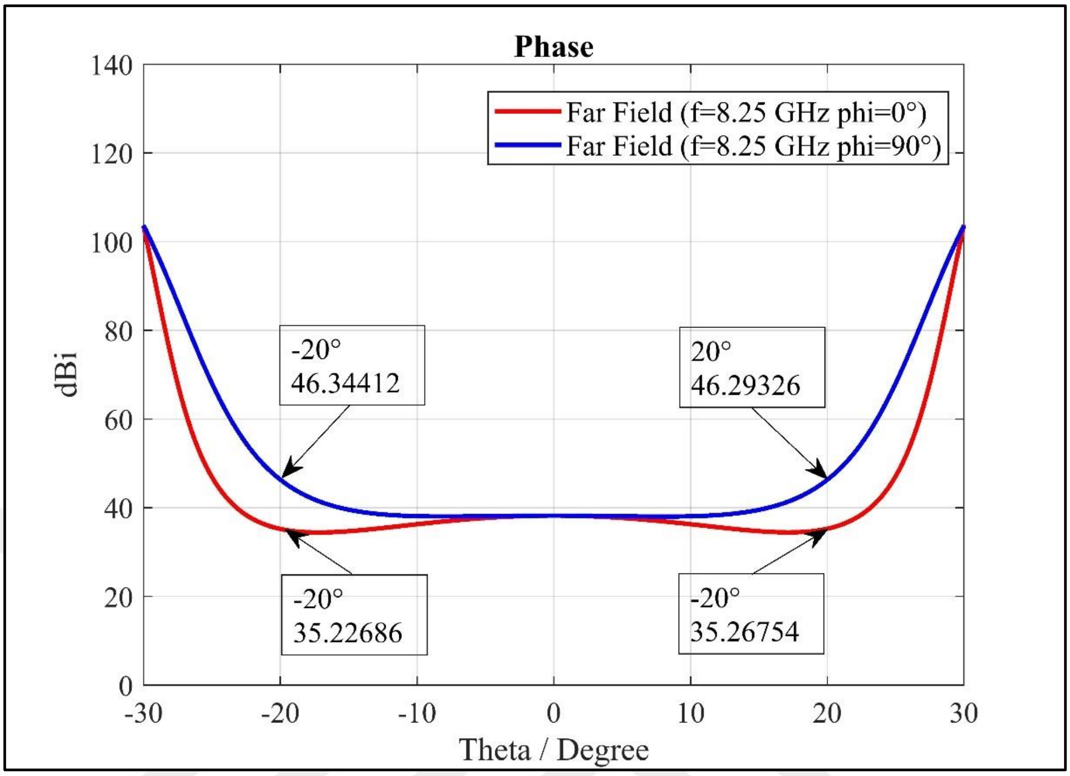

Figure 3.26. Monopulse unit and feed antenna phase curves at 8.25 GHz

3.1.4 Merging of Feed Antenna and Its Assemblies

The feed antenna, monopulse unit, and septum polarisers are combined and simulated. The simulated design is shown in Figure 3.27. Ten ports are defined on the structure. Two of these ports are the ports that will receive the linear polarised communication signal. Four ports are the ports of the circular waveguides on the elevation axis for the tracking signal; the other four ports are the ports of the circular waveguides on the azimuth axis for the tracking signal. Two linearly polarised ports are defined for each circular waveguide because the signal coming to the circular waveguide as RHCP or LHCP is transmitted linearly polarised to the right or left port at the end of the septum. The numbers of each port defined for the monopulse unit using the configuration in Figure 3.22 are listed in Table 3.6.

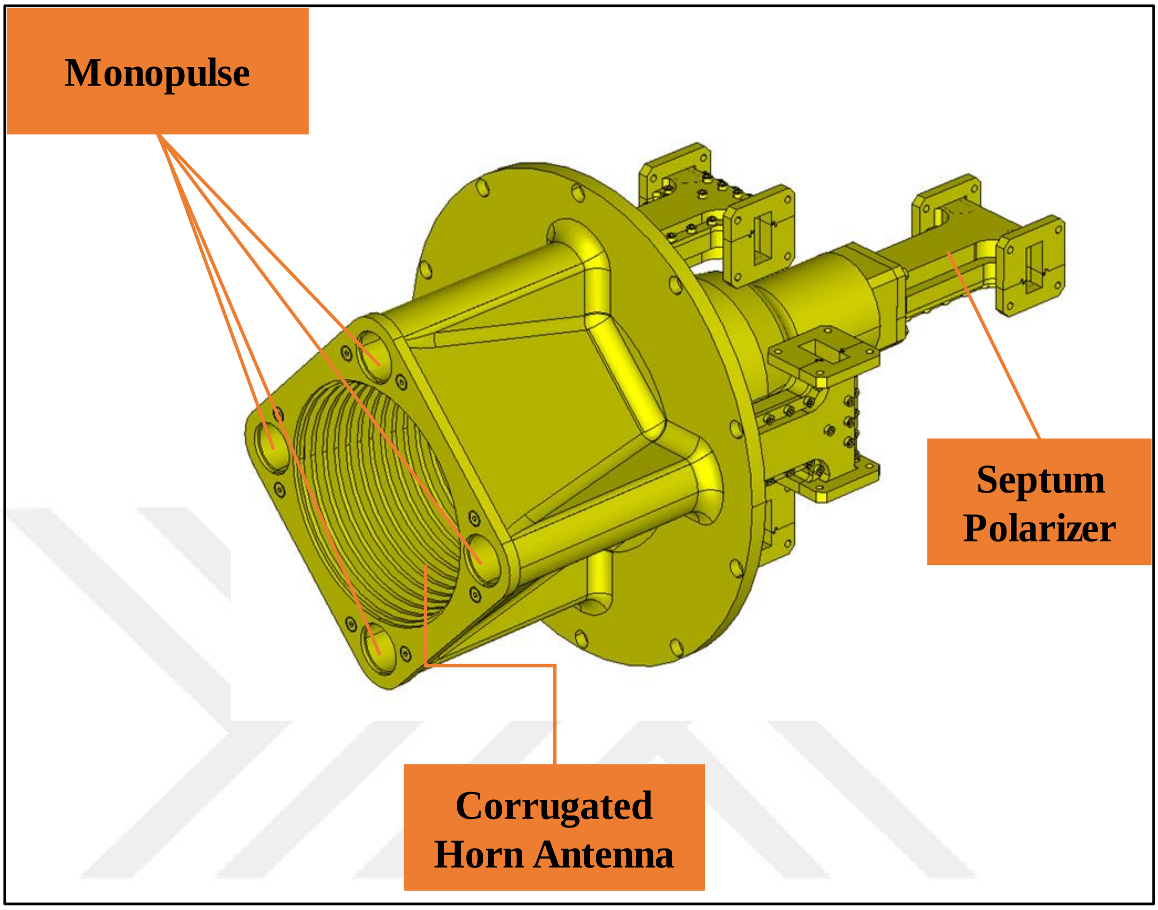

Figure 3.27. X-Band antenna and its assemblies

Table 3.6. Defined port numbers for analyzing X-Band feed antenna and assemblies

Port Number	Position
1	Feed Antenna RHCP
2	Feed Antenna LHCP
3	Elevation 1 RHCP
4	Elevation 1 LHCP
5	Elevation 2 RHCP
6	Elevation 2 LHCP
7	Azimuth 1 RHCP
8	Azimuth 1 LHCP
9	Azimuth 2 RHCP
10	Azimuth 2 LHCP

After the design of the feed antenna, four circular waveguides, called monopulse units, are added in azimuth and elevation. Septum polarisers for the feed antenna and circular waveguides are added to the structure. The cross-sectional view and lengths of the design are given in Figure 3.29. The feed antenna, circular waveguides, and septum polarizers are aluminium. The elements are connected with bolts, and sealing elements are used between them. The antenna system consists of 3 main structures: corrugated horn antenna, monopulse unit and septum polarizer.

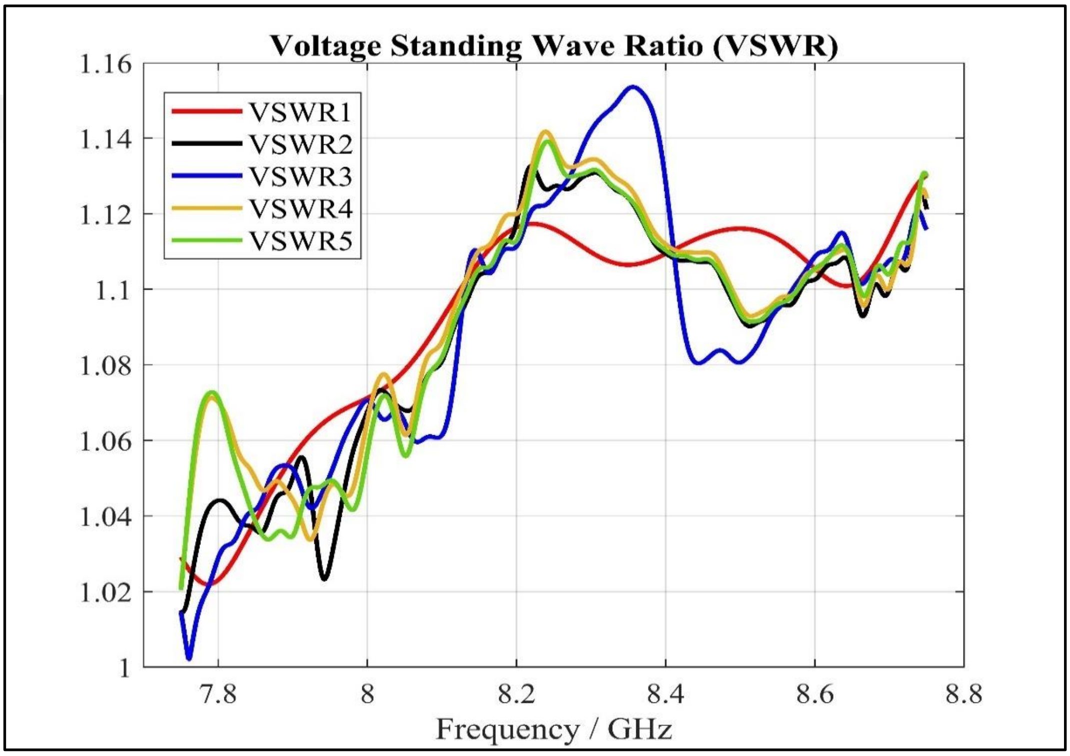

Figure 3.28. VSWR for feed antenna and its assemblies

The VSWR graph of all septum ports named in Table 8 for the X-band feed antenna system is given in Figure 3.28. For 8, 8.25, and 8.5 GHz, the radiation patterns showing the antenna gain and side lobe levels are presented in Figure 3.30 for phi=0° and Figure 3.31 for phi=90°.

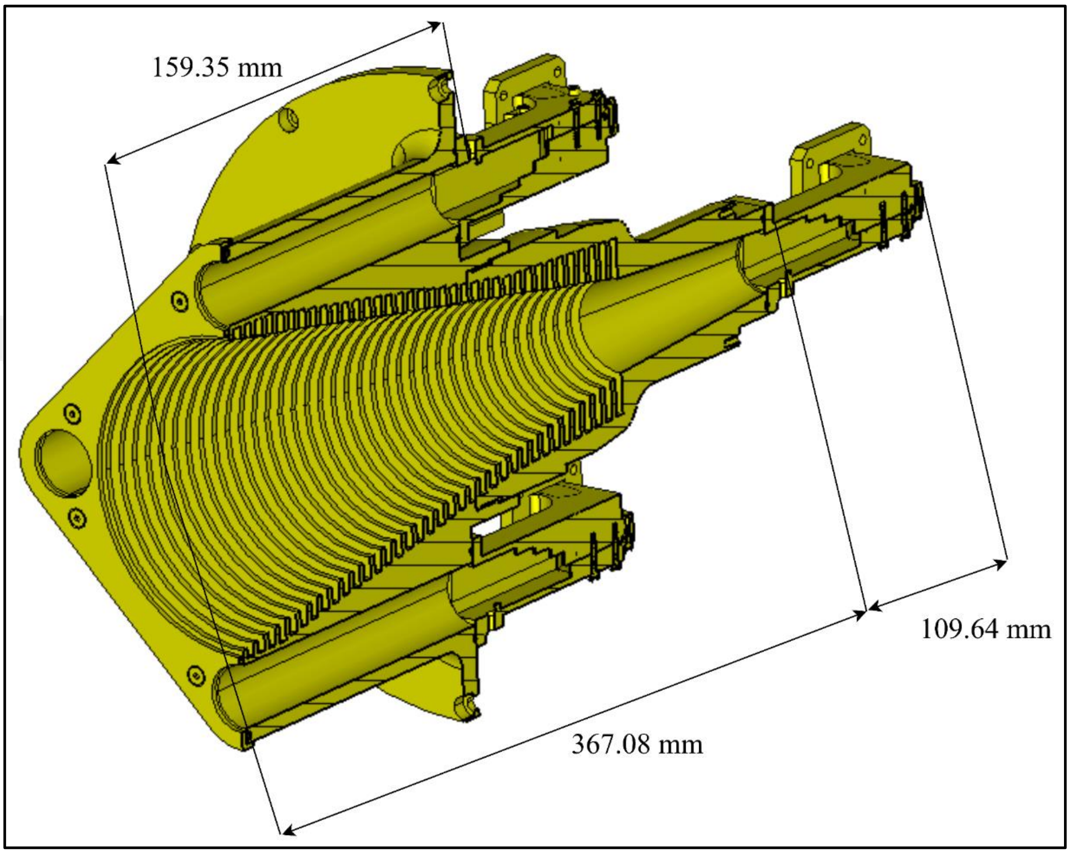

Figure 3.29. Dimensions of feed antenna and assemblies

The phase curves of the feed antenna for phi=0° and phi=90° are shown in Figure 3.32. The maximum phase difference is 2°. A phase change of less than 25° increases the reflector aperture efficiency.

Circular polarization is transmitted and received in the antenna system. When the phase curves are analyzed in circular polarisation, the resulting graph is given in Figure 3.33. The phase difference for phi=0° and phi=90° is slight and at the desired level.

The three-dimensional radiation pattern of the X-band feed antenna and its assemblies is shown in Figure 3.34. The gain of the antenna system is 19.40 dBi. Also, sum and difference pattern of the feed antenna are shown in Figure 3.35 and Figure 3.36.

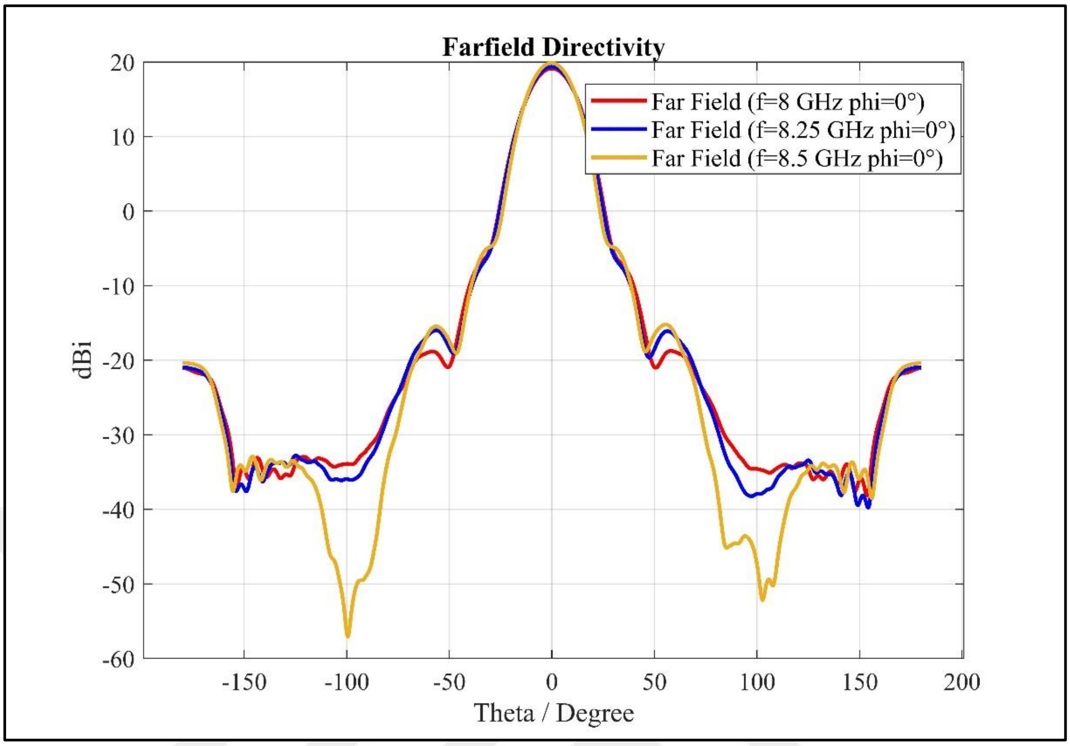

Figure 3.30. The radiation pattern of the feed antenna and its assemblies at 8 GHz, 8.25 GHz, and 8.5 GHz at phi=0°

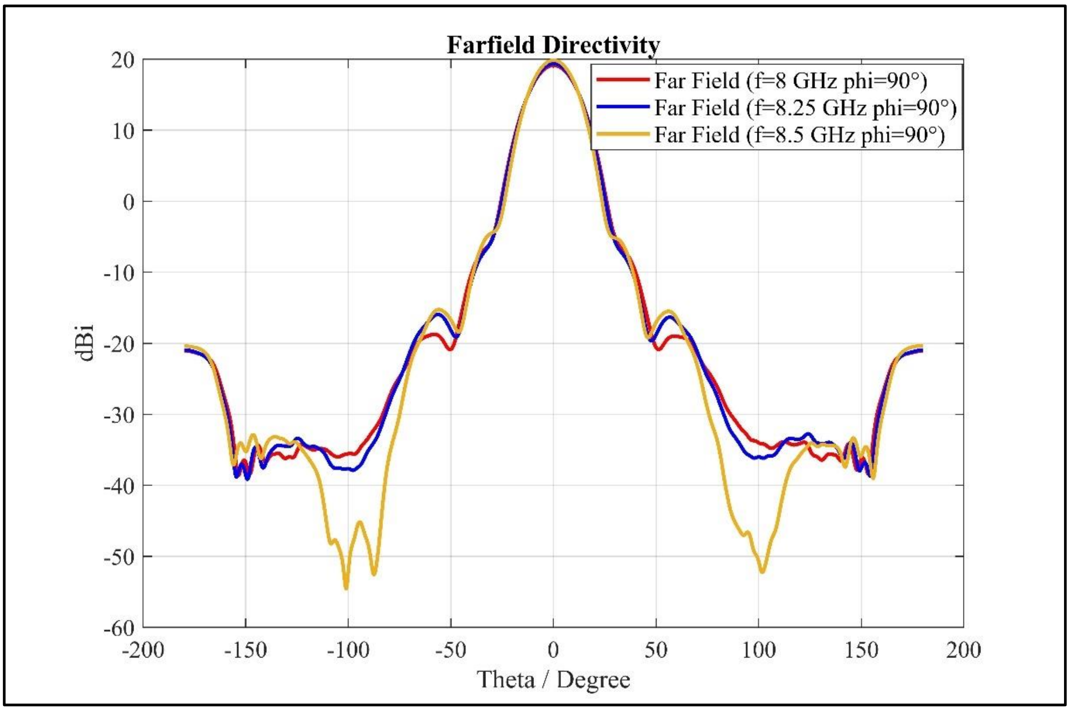

Figure 3.31. The radiation pattern of the feed antenna and its assemblies at 8 GHz, 8.25 GHz, and 8.5 GHz at phi=90°

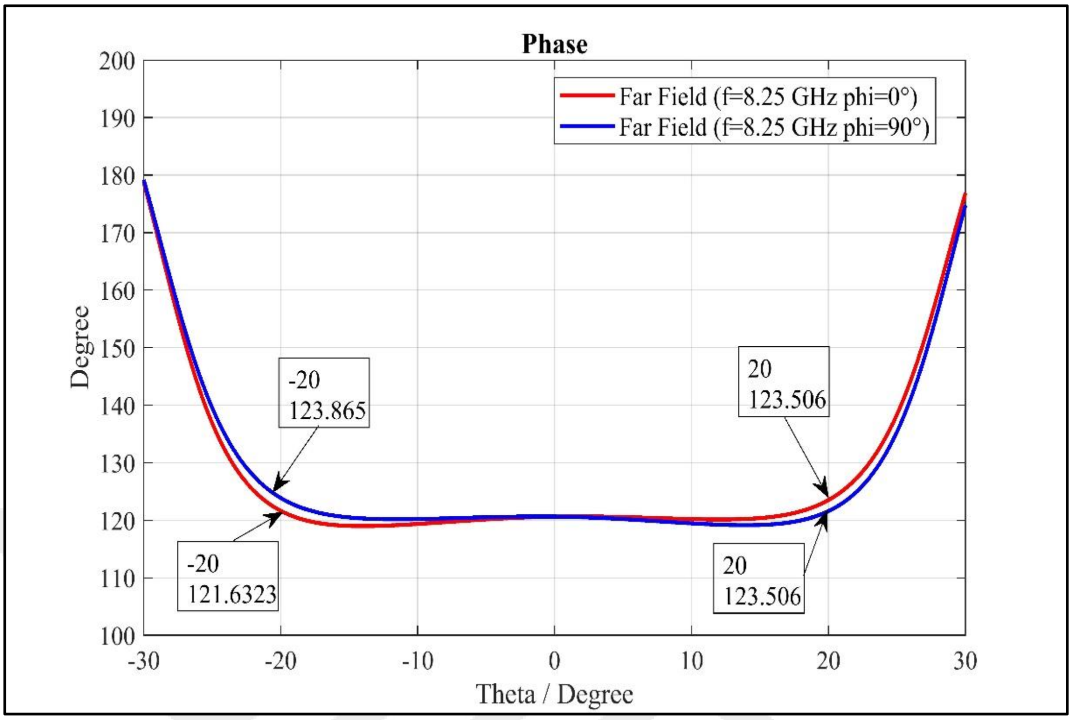

Figure 3.32. Phase curves of feed antenna and its assemblies at 8.25 GHz

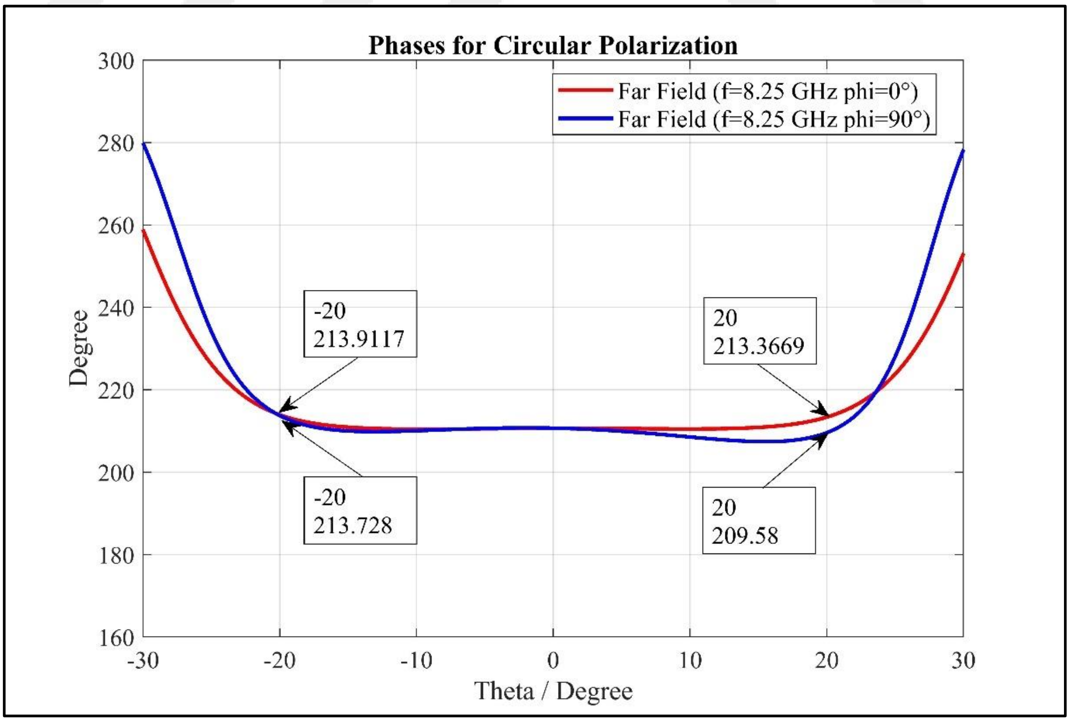

Figure 3.33. Phase curves of feed antenna and its assemblies for circular polarization at 8.25 GHz

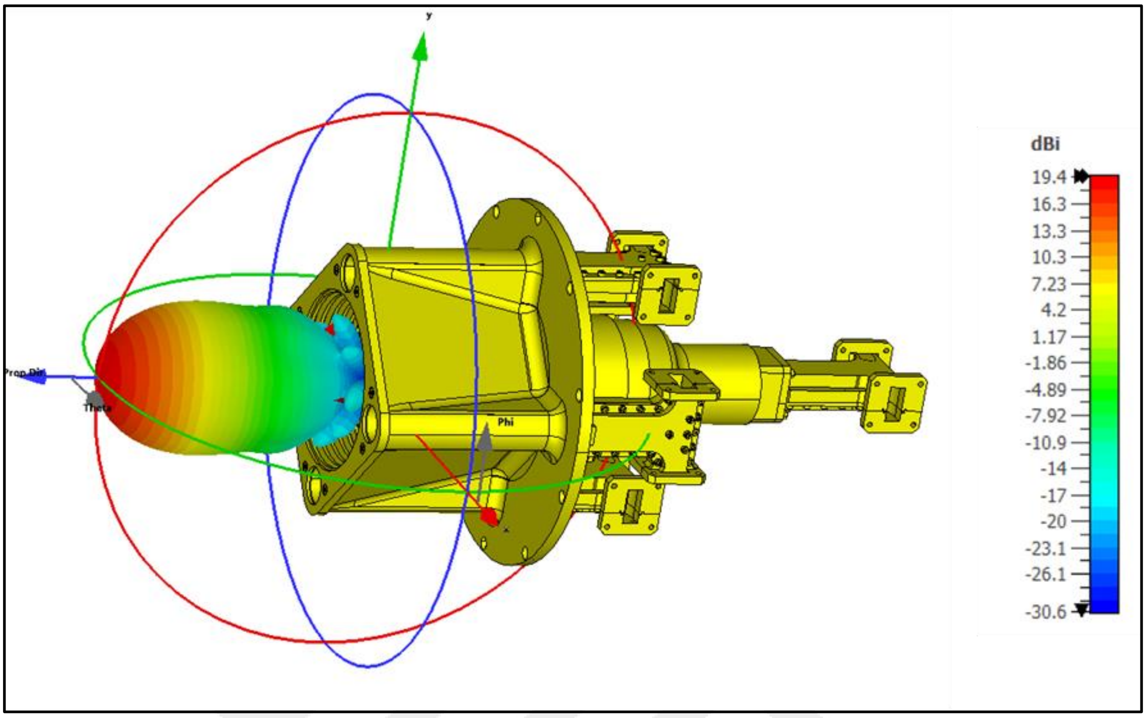

Figure 3.34. The radiation pattern of the antenna system

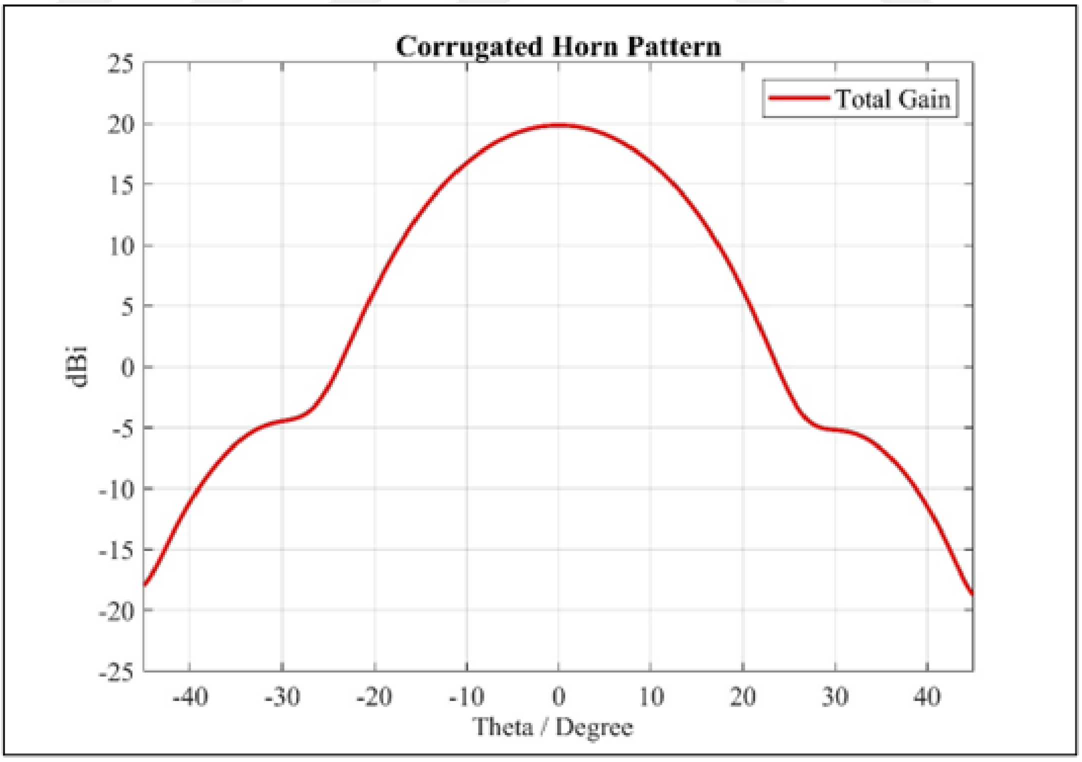

Figure 3.35. Corrugated horn antenna gain (total) plot

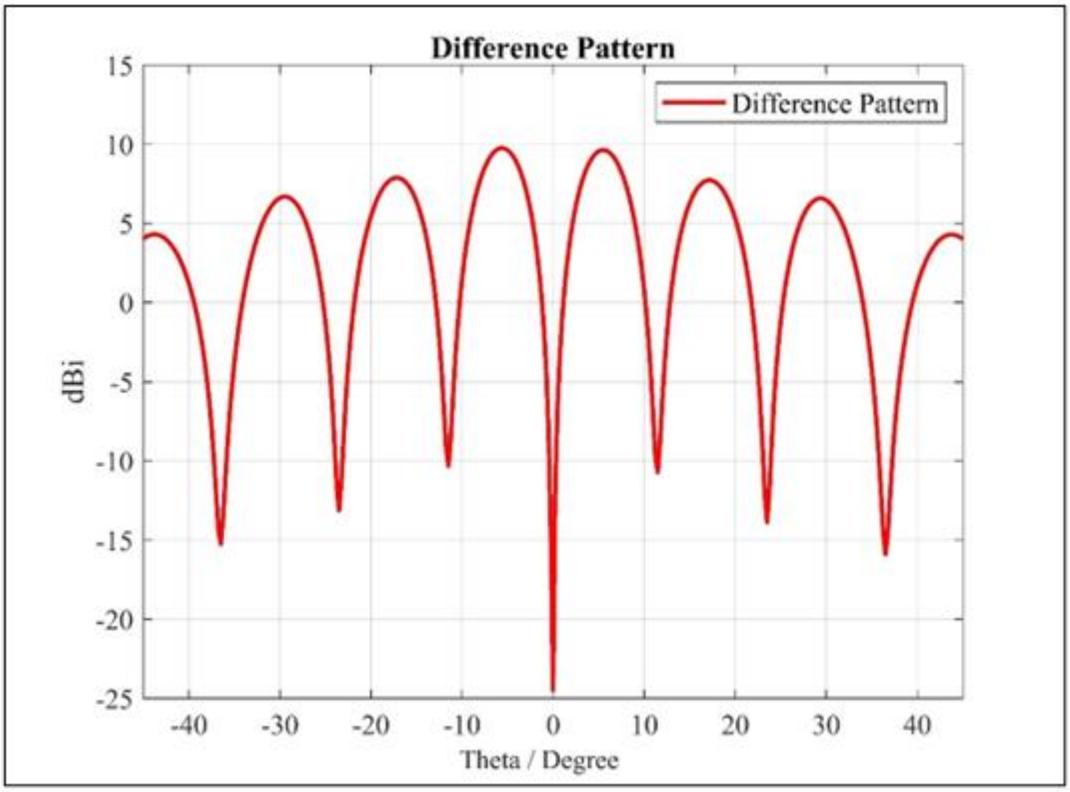

Figure 3.36. Difference pattern plot

Cassegrain reflector antennas are referred to as dual reflector antennas in the literature. This type of antenna has two reflectors: a main parabolic reflector and a hyperbolic subreflector (auxiliary reflector, secondary reflector). The main parabolic reflector has a prime focal point, and the hyperbolic subreflector has a prime and imaginary focal point. In the Cassegrain antenna structure, the focal points of the main parabolic reflector and the hyperbolic subreflector are overlapped. Therefore, there are a total of two focal points in the system. The mentioned Cassegrain-type reflector structure is shown in Figure 3.37.

The point indicated by f_2 in Figure 3.37 shows the focal points of the main parabolic reflector and the hyperbolic subreflector, as can be seen, the focal points of both structures are placed so that they overlap. The point indicated by f_2 is the virtual focal point of the hyperbolic subreflector.

The principle of operation of the binary structure is as follows: The waves coming from the virtual focal point (f_2) onto the hyperbolic subreflector travel in the direction of the real focal point of the hyperbolic reflector (shown as dashed lines in Figure 3.37) and reach the main parabolic reflector. The focal point f_2 is also the focal point of the main parabolic reflector, and for the main parabolic reflector, all waves coming from the focal point travel in a straight line. Therefore, the waves from f_2 are reflected once from both reflectors and propagate as plane waves. In the Cassegrain structure, the feed antenna is placed at the focal point f_2. The waves from the far field can be considered plane waves, and the incident waves are reflected from the reflector structures and collected at the focal point, and vice versa.

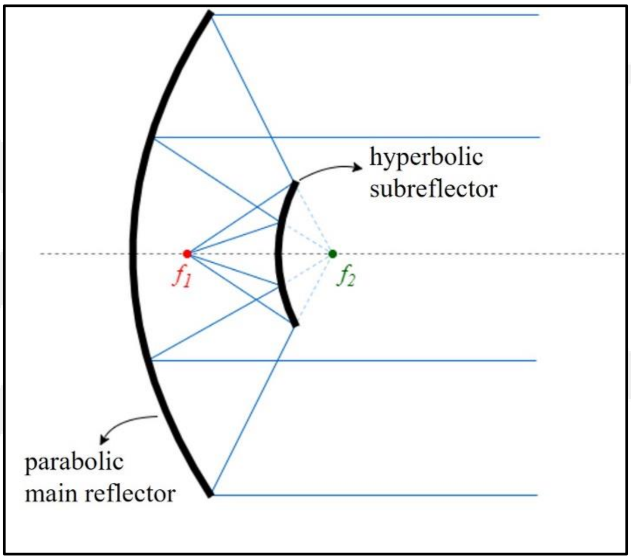

Figure 3.37. The structure of the Cassegrain antenna structure

A Cassegrain reflector structure is used in the X-band feed antenna system. As a result of the simulations performed on CST Studio Suite, the phase center and sigma value of the feed antenna are found. Sigma is the magnitude of the phase variations at all points in the spherical coordinate system where the antenna is located. If the sigma value is small, the phase variations at all points are slight. The phase center of the feed antenna is placed at the focal point f_2. The sigma value helps to optimize the position of the antenna. The X-band feed antenna is planned to illuminate 20° on the secondary reflector. After the feed antenna system is placed on the focus of the 7.3 m Cassegrain reflector antenna. The difference model is calculated for the RHCP ports; the LHCP ports are the same as the RHCP ports. The simulated sum and difference models are shown in Figure 3.35 and Figure 3.36, respectively.

Figure 3.38 shows the feed antenna placed on the Cassegrain reflector antenna. The gain of the system is 54.6 dBi when the feed antenna system is placed on the focus of a 7.3 m Cassegrain reflector antenna.

The secondary sum and difference models are optimized for the given reflector and subreflector profile to maximize the secondary gain. The simulated secondary sum and difference pattern are shown in Figure 3.39. The sum pattern fulfills the gain requirement, while the difference pattern provides the required depth and slope.

As can be seen from the additional zoomed diagram in Figure 3.39, there is no undesirable distortion in the difference pattern. Although the difference pattern provides a broader tracking pointing accuracy, reliable tracking is achieved by operating the system in the main lobe of the sum beam. This is achieved by providing appropriate threshold-level adjustments for tracking errors at the tracking receiver.

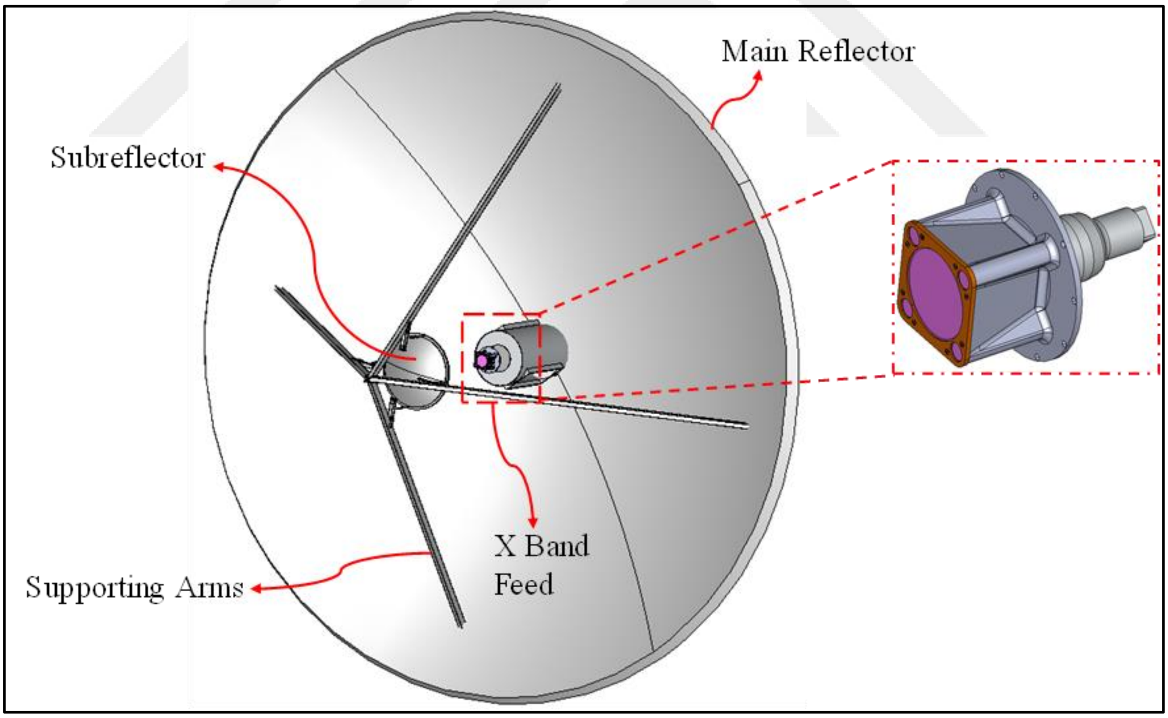

Figure 3.38. The feed antenna position on the 7.3 m Cassegrain reflector

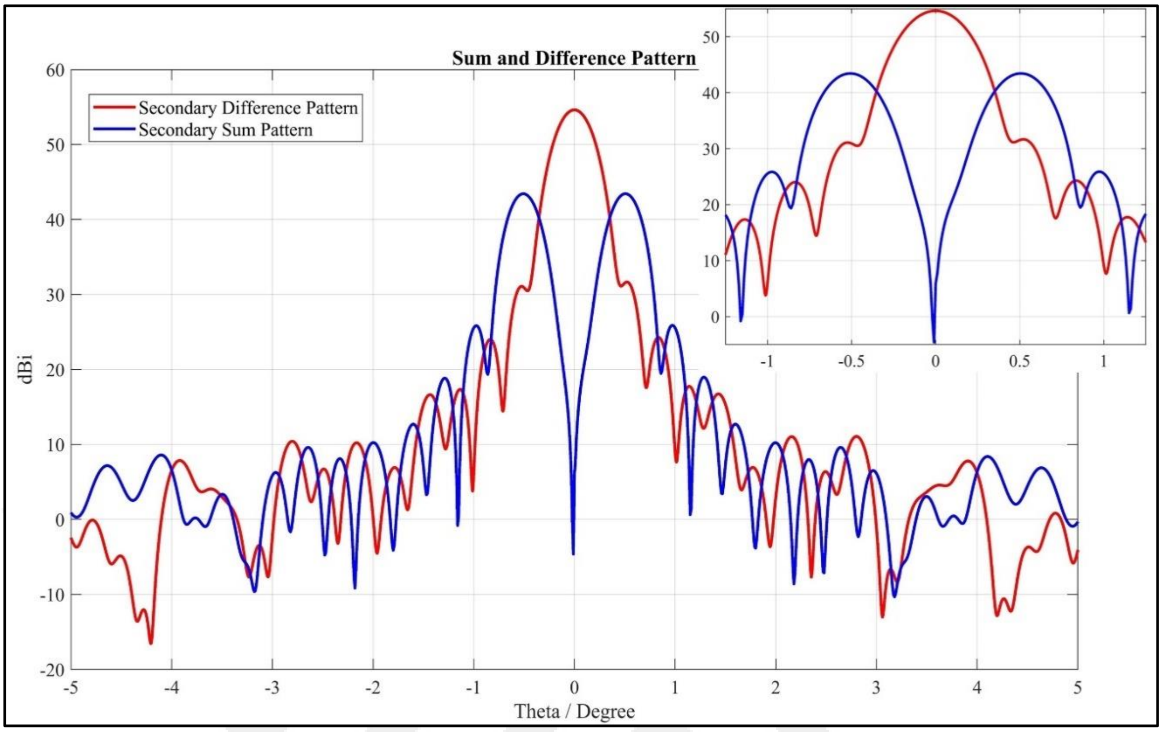

Figure 3.39. Secondary sum and difference pattern plot for 7.3 m Cassegrain antenna

3.2 X-BAND LNA DESIGN

The amplifier designed in this dissertation is decided to be a 4-stage structure. The first two stages are designed using transistors, and the last two stages are designed using MMIC low-noise amplifiers. The LNA is intended to have a 4-layer structure and to operate appropriately between 8 GHz and 8.5 GHz. Since the first two stages are transistor-based designs, the first stage is used as a pre-amplifier stage for the second stage. The S parameters of the transistors used are taken from the data sheets, and the transistors are first modelled as 2-port circuits, and the stability regions of the transistors are examined. Then, the conjugate impedance matching of the input and output for maximum gain and minimum noise figure and the matching between the two stages are made. Finally, the biasing circuits of the transistors are designed.

The frequently used method in RF and microwave receiver circuit designs is designing LNAs in the simulation program and making realization, then measuring S parameters and noise factor and comparing results with theoretical results.

- Choosing a transistor having the lowest noise level and sufficient catalog values for the frequency band
- Designing a DC feeding circuit to obtain the same S-parameter values in the catalog
- Making stability analyses and providing solutions to obtain unconditional stability
- Finding the input and output impedance or reflection coefficients for the input and output matching circuits, respectively, with the help of S-parameter analysis to obtain maximum power gain and minimum noise factor by evaluating the power gain and noise factor circles together,
- Designing of matching circuits for maximum bandwidth and minimum reflection using lumped-parameter circuit elements or microstrip transmission lines,
- The layout and realization of the entire circuit obtained for PCB (Printed Circuit Board),
- The design is made by converting and measuring the values found in the practical circuit.

Figure 3.40 shows the schematic of the proposed LNA. As shown in the figure above, an input-matching circuit for CE3512K2 and an output-matching circuit for MGF4935AM should be made. An interstage matching circuit must be designed for the cascade connection of these two transistors. The design of the input matching circuit is described in detail below.

Figure 3.40.The schematic of the proposed LNA circuit

The design specifications of the X-band LNA are given in Table 3.7. As can be seen, a four-stage design is required to achieve the desired gain. This cascade structure uses microstrip technology in the 8 – 8.5 GHz frequency band. The scattering parameters of the transistors used in the design are analyzed using S parameter data. For nonlinear results, the spice model of the transistors is considered. The passive element (capacitor) used on the RF line belongs to Murata company, and the Netlist model is used. Simulations and PCB design are designed with AWR program. It is simulated in the AWR program using the products given in Table 3.8.

Table 3.7. X-Band LNA properties

Parameter	Value
Frequency band	8 – 8.5 GHz
Gain	50 dB
Noise figure	maximum 0.7 dB
Input reflection rate	14 dB
Output reflection rate	14 dB
1 dB compression power	minimum 10 dBm
Input standing wave ratio	1.5:1
Output standing wave ratio	1.5:1
Input connector type	N-type
Output connector type	SMA

Table 3.8. IC components utilizing the LNA design

Manufacturer	Product part number	Product explanation
CEL	CE3512K2	Transistor
Mitsubishi Elec.	MGF4935AM	Transistor
Analog Devices	HMC902LP3E	MMIC LNA
Analog Devices	ADM7160	Regulator
Texas Ins.	TPS72325	Negative regulator
Texas Ins.	LM2931AMX	Regulator
Microchip	TC7660	Negative feeding (charge pump)

For a low-noise amplifier operating in the X-band, it will be advantageous to be designed using the amplifier's S parameters since the operating frequencies are high. After selecting the transistor used in the amplifier, the S parameters of that transistor can be accessed from the datasheet. If it is unavailable in the datasheet, it can be requested from the manufacturer or obtained by measurement. S parameters for a transistor vary with frequency for a given drain-source voltage and drain current. Using the S parameters of the transistor, the regions where the transistor is stable should be found first, and whether it is stable in the desired region should be controlled. If there is instability, the transistor can be stabilized with feedback circuits, etc. While selecting the transistors to be used in this dissertation, the datasheets of the transistors are first read. The transistors that meet the required qualifications are selected. HMC902LP3E wideband MMIC LNA is chosen for the third and fourth stage of the four-layer design. When the data sheet of this LNA is analyzed, it is seen that its gain is 19dB, the noise figure is 1.8dB, and the P1dB output power is 19 dBm. In the first two stages, a transistorized structure is designed. It is decided to use the CE3512K2 transistor in the preamplifier stage of this first two-stage design and the MGF4935AM transistor in the next stage. When the data sheet of the transistor in the first stage is examined, it is reached that the gain is 13.2 dB at 8.25 GHz. Considering the effect of the wide band in the 8-8.5 GHz operating band, it can be predicted that the gain value obtained from the last stages will be between 38 dB on average. Therefore, a total gain of 65 dB is expected from the four-stage X-band LNA. The S parameters of these transistors are found, and these transistors are modeled as two ports in AWR.

A new project is created in AWR, and the S parameters files created for CE3512K2 and MGF4935AM are imported to this dissertation. The S parameters given for VDS=2V and ID=10mA, VG= -0.47V in CE3512K2 and VDS=2V and ID=10mA, VG= -0.3V in MGF4935AM are used. Figure 3.41 shows the S parameter files of CE3512K2 and MGF4935AM saved in the project in AWR.

After these files are saved in the project, transistors with these S parameters are created as two ports in the subcircuits category in the circuit elements tab. CE3512K2 and MGF4935AM as two-port subcircuit elements are given in Figure 3.42.

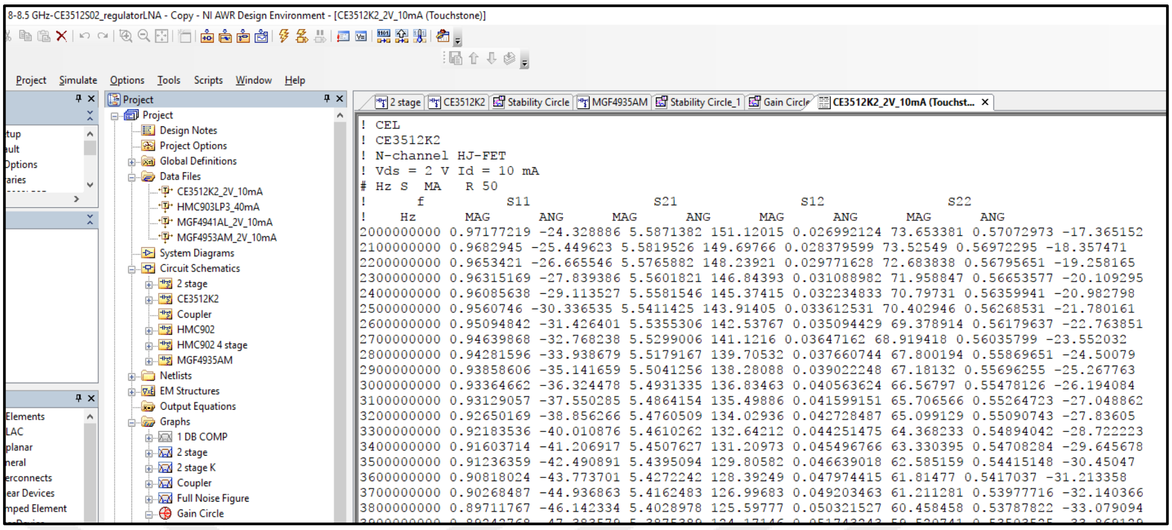

Figure 3.41. CE3512K2 S parameters

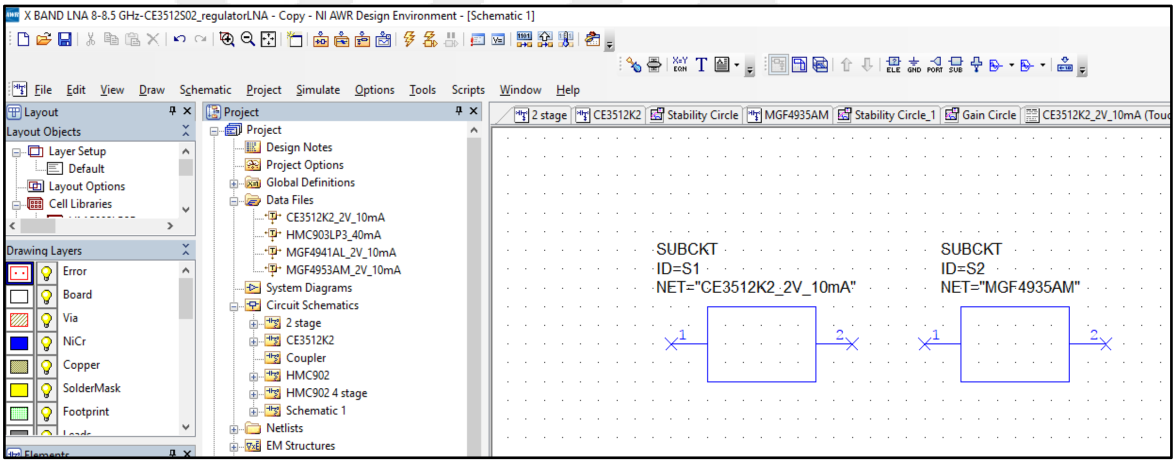

Figure 3.42. Two ports representation of CE3512K2 and MGF4935AM

For a circuit element with S parameters in MWO, stability circles can be plotted on Smith Chart. Figure 3.43 shows the input and output stability circles drawn in AWR at 8-8.5 GHz for CE3512K2, and Figure 3.44 shows the input and output stability circles drawn in AWR at the same frequency band for MGF4935AM. In MWO, the SCIR1 and SCIR2 functions should be selected for the input and output stability circles, respectively.

It is $|S_{11}| < 1$ and $|S_{22}| < 1$ for both transistors. In the 8 – 8.5 GHz operating band, they are stable everywhere within the Smith Chart except for the intersection regions of these circles with the Smith Chart.

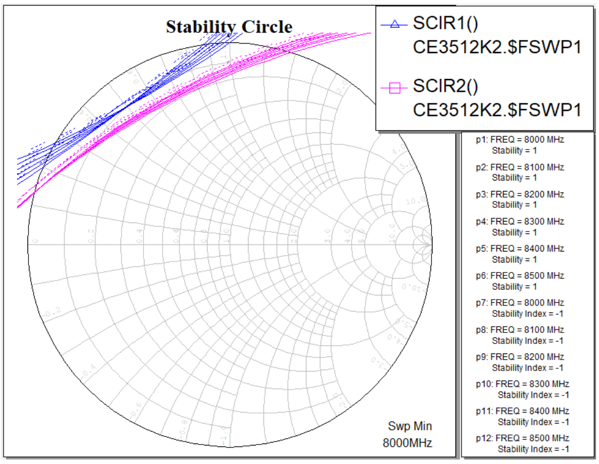

Figure 3.43. Input and output stability circles of CE3512K2

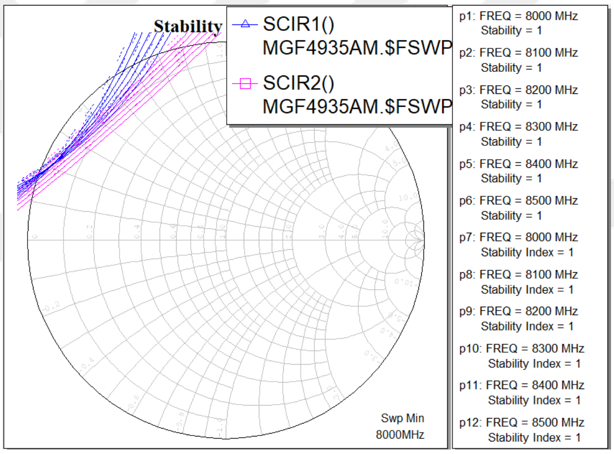

Figure 3.44. Input and output stability circles of MGF4935AM

The source impedance, input and output impedances of the LNA are represented by Z_S, Z_{in} and Z_{out}. After deciding what the values of $Z_S = Z_{in}^*$ and $Z_S = Z_{out}^*$will be for maximum power transfer; these values must be matched to $Z_0 = 50\ \Omega$. This process is called conjugate impedance matching. Impedance-matching circuits can be made with circuit elements such as capacitors, coils, or microstrip lines. In this dissertation, the matching circuits are realized with microstrip lines. Because microstrip lines take up less space, are lighter, and cost not very high. Any impedance-matching circuit provides perfect matching for a single frequency. Various conventional approaches, such as compensated matching circuits, resistive matching circuits, negative feedback, balanced amplifiers, and distributed amplifiers, are used for wideband impedance matching circuits. In this dissertation, compensated matching circuits approach is used. Since the design of the project is intended to operate between 8-8.5 GHz, the adaptations are made for 8.25 GHz and then compensated by using the AWR's non-compliance feature and made to operate between 8-8.5 GHz. This process caused a slight decrease in the maximum gain that could be achieved, but this decrease is tolerated to increase the bandwidth. The matching circuits used in this dissertation are designed with the help of the Smith Chart. There are many methods for impedance matching, such as single stub matching, double stub matching, quarter-wave transformer, single-part converter, and multi-part converter. The most common methods are single-stub matching and double stub matching. Both matching techniques are tried in this dissertation, and whichever provides better matching is preferred. In addition, single stub and double stub can be parallel or series. Since the former is easier to realize in real-life applications, it is used in this dissertation. The main function of stubs is to make RF short circuit DC open circuit or RF open circuit DC short circuit. In other words, it works like a capacitor. This process is realized on low-impedance lines. Reducing the impedance also increases the size of the line, which is undesirable. Using a quarter wave stub is a perfect solution for this problem. The quarter wave stub shows low impedance in a wideband and has small dimensions compared to the stub with the same function. Thus, it has fewer parasitic effects and less space in the circuit. This work uses a radial stub instead of a stub with large dimensions. Figure 3.40 shows the block diagram of the X-band low-noise amplifier designed for the project.

Using the S parameters, the input constant gain circles are drawn on the Smith Chart as a first operation to obtain the maximum gain from the CE3512K2 transistor modelled in AWR. This process can be done in AWR. Then, the closest point of this circle, which represents the maximum gain, to the center of the Smith Chart is selected. This selected point gives z_{in}. These values are multiplied by 50 and Z_{in} is obtained. Z_s=Z_{in}^*, the Z_S value is determined, which is matched to the $50\ \Omega$ input port. This matching process is done by marking the z_s point on the Smith Chart as z_s=Z_S/50.

Figure 3.45 shows the input constant gain circle of the CE3512K2 plotted in AWR. This circle is for the maximum gain, and the maximum gain that can ideally be obtained from CE3512K2 is 16.67 dB, as can be read from the figure. The point of this circle closest to the center of the Smith Chart is marked on the figure which is z_{in}.

The matching process is performed according to the complex conjugate point of this point, zs, for maximum gain. Another issue is that the point to be matched should be in the region where CE3512K2 is stable, within the stability region given in the figure above for CE3512K2. The zin value in the figure above and the zs value, which is the complex conjugate of this value, are given below:

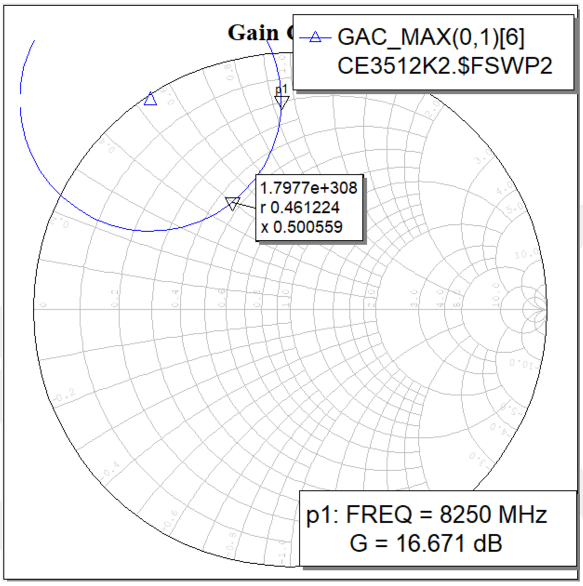

Figure 3.45. Input constant gain circle for CE3512K2

$$zin = 0.46 + j0.5 \tag{3.25}$$

$$Z_{in} = zin * 50 = 23 + j25 \tag{3.26}$$

$$Z_s = 23 - j25 \tag{3.27}$$

$$zs = {}^{Z_s}/_{50} = 0.46 - j0.5 \tag{3.28}$$

The intended operation here is to match Z_s to $Z_O = 50\ \Omega$. For this process, both single stub and double stub matchings are tried and simulated in AWR. For this circuit, it is decided to make a single stub matching since the results of the single stub matching are better. The stubs are designed to be open circuit. The open circuit stub acts as a capacitor. The short circuit stub acts as inductance. At high frequencies, connecting the inductance directly to the ground creates a problem because the inductance may short-circuit as the frequency increases. For this reason, it is decided to make the stubs open circuit. This matching is tried for several values in the project, and the best value is selected. Excess line length brings an extra loss. Therefore, the distance, d, should be chosen as small as possible. In this dissertation, $d = 0.1\lambda$ is set for the CE3512K2 input matching circuit. λ is the signal wavelength and is expressed as $\lambda = vP/f$, where vP is the phase velocity, and f is the frequency. The distance of the stage to the load is also arbitrarily chosen to be 0.1λ (provided that it is consistent). In this case, the stub distance (distance l) is calculated as l= 4.23mm. The operations performed while reaching these values are as follows. These operations are not completed in the AWR environment but with the interactive Java-based cymbidium impedance matching program on Amanogawa's web page [62].

The interface of the program is given in Figure 3.46. At the beginning of the program, whether the stubs should be open or short circuits should be selected. After zs is determined, a standing wave ratio circle with radius |zs| is drawn. After the first stub is included in the circuit, a circle is drawn for the admittances that can provide the matching. The distance from the load (from zs) is traveled on the Smith Chart for the length of the determined stub.

From the point reached, a point on the pink circle is reached by traveling a distance l. From this point, the distance d is traveled. From the last point, go to the center of the Smith Chart.

Due to the inductive effect at high frequencies, the stubs should not be too long. Since the second solution is more appropriate in this respect, the results of the second solution are used in the matching process.

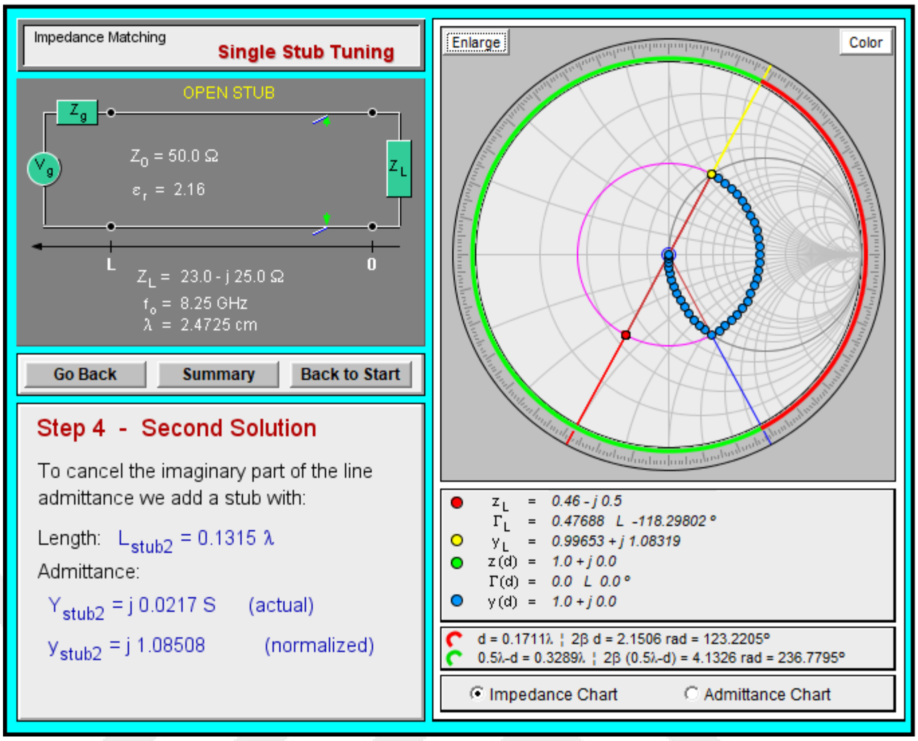

Figure 3.46.The interface of the simulation program for using single stub tuning

At this stage, a project should be created in AWR using the values found above, and S parameter simulations should be performed to determine whether the matching is appropriate. The circuit diagram designed to simulate the matching is given in Figure 3.47.

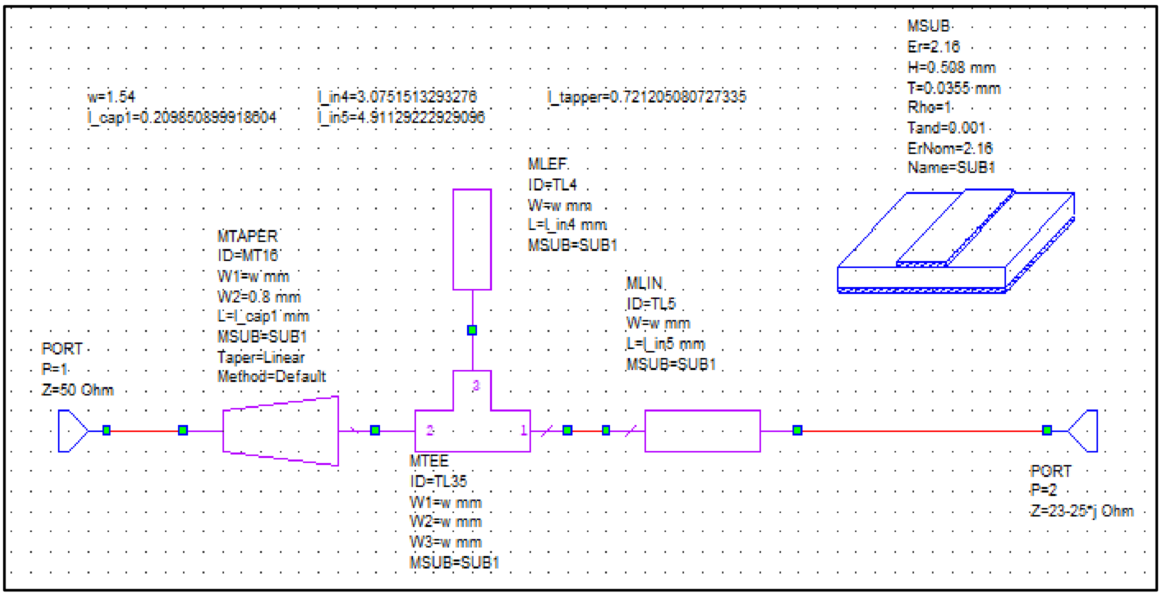

Figure 3.47. CE3512K2 input impedance tuning circuit

While creating this circuit, the following operations are performed respectively. Firstly, two ports with Z_O and Z_S values are created. Microstrip lines (MLIN and MLEF) are available in AWR (MLIN and MLEF), where the distance to the side line with l value is calculated for impedance matching, and the distance d can be created as parameters. These lines are added to the circuit, and their parameters are entered. Then a T-junction (MTEE) is added between the lines to reduce the discontinuity between the lines. The width of the lines is selected as 1.46 mm. This value is calculated with the TXLINE option of AWR. TXLINE interface is given in Figure 3.48 below. Here, it is seen that the line impedance is 50 Ω, the frequency is 8.25 GHz, and the line width is 1.46 mm when written in the relevant places in the lower left pane and pressing the right arrow. Here, the substrate properties must be entered before calculating w. MSUB represents the substrate in the CE3512K2 input impedance matching circuit. The line thickness is 0.035 mm. It is designed on 0.508 mm thick RT Duroid 5880 with the dielectric constant of 2.16. It is crucial to enter these values correctly because w and therefore, simulation results change significantly depending on these values. For this reason, it is necessary to contact the PCB manufacturer in advance and find out all properties of the material.

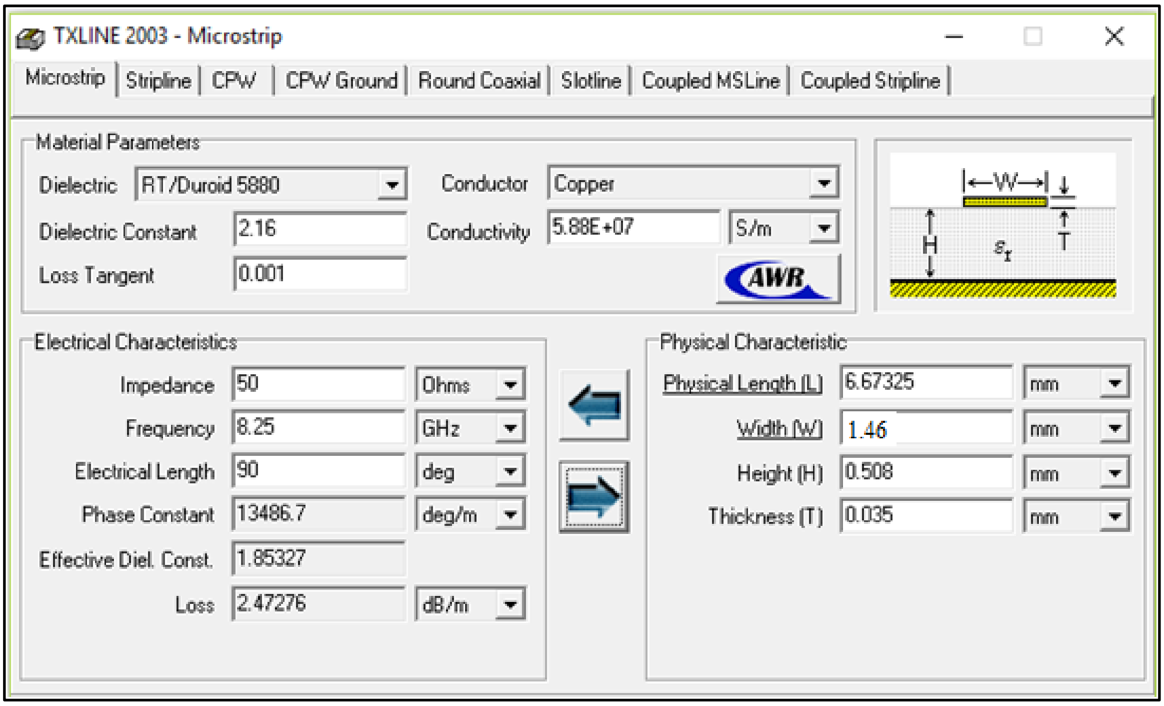

Figure 3.48. Interface of TXLINE

After these operations, simulations should be performed. A new graphic file should be created, and S parameters should be plotted between 8-8.5 GHz. $|S_{11}|$ and $|S_{22}|$ must be less than -10 dB for the matching circuit to be considered to be working correctly. The S parameters plotted in AWR (Figure 3.49).

The results show that the tuning circuit works well. After this stage, if desired, these results can be further improved by using the optimization option of AWR. It is done during the project work process. The optimization tool of AWR is used to achieve the desired requirements with the necessary adaptations. However, it is realized that it is not required to perform the tuning process at this stage since a final tuning process is performed again when these tunings performed separately are combined. The tuning process can be achieved with both the L and W parameters.

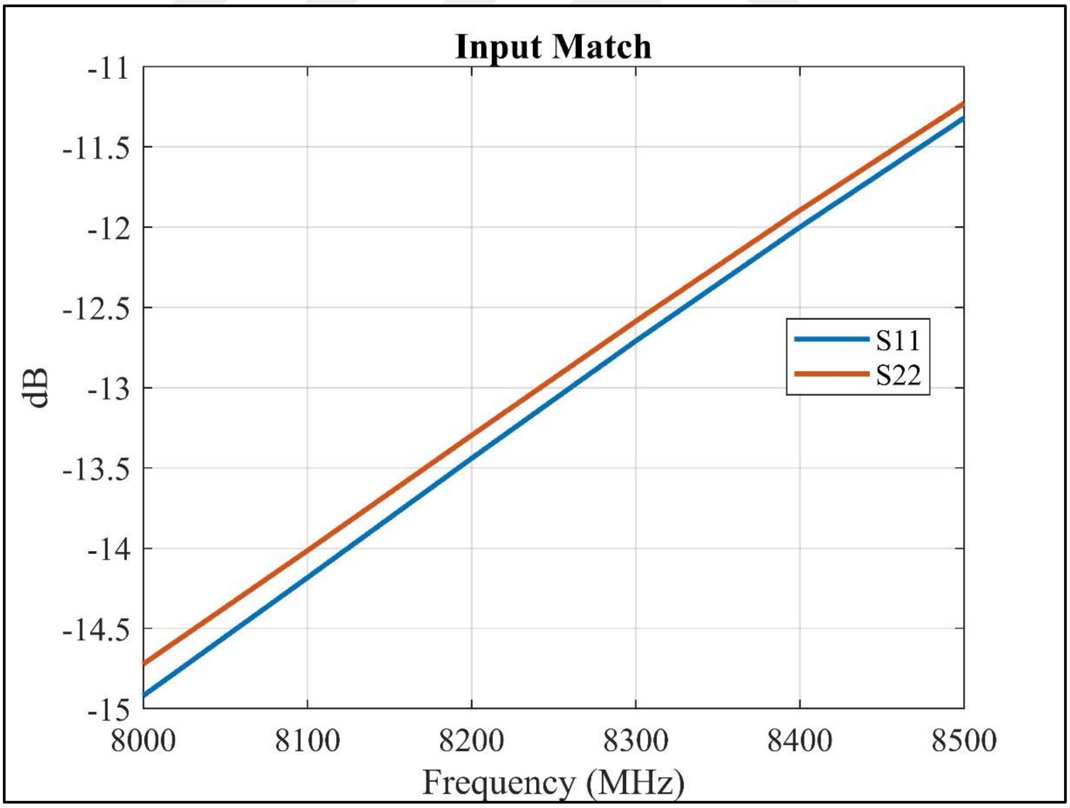

Figure 3.49. S parameters of the input tuning circuit

Figure 3.50 shows the block diagram of the X-band LNA circuit. Here the purpose is to show each matching circuit individually since all the matching circuits cannot be given together.

The coupler design is shown in Figure 3.51 among the blocks that make up the X-band LNA. Figure 3.52 shows the input matching circuit of the CE3512K2 transistor. A quarter wave sideline is used in the input matching circuit. The quarter wave sideline is referred to as MRSTUB2W in AWR. MRTSUB2W has a radius (R_0), thickness (W) and angle (Theta) parameters. It is appropriate that the angle is 90°. A project is created in AWR to calculate the dimensions of the quarter wave sideline that should be used instead of the normal sideline. In this work, a normal sideline is connected to one port (port 1), and a quarter-wave sideline is connected to another (port 2). Firstly, the impedance seen from the input of port 1 is checked. Then, the impedance seen from the input of port 2 is equalized to the impedance seen from the input of port 1 by adjusting the W and R_0 parameters of the quarter wave sideline with the matching process. When the equalization is achieved, the quarter wave sideline obtained can be used instead of the normal sideline in the circuit. It provides a high bandwidth since it is operated at a high frequency. In Figure 3.53, an interstage matching circuit is designed to adjust the impedances of CE3512K2 and MGF4935AM transistors. In the design of the matching circuit, it should be noted that the stages are DC isolated from each other. In this process, high-value capacitance could have been used, but coupled line is used in the design because of its high effect on the noise figure. Figure 3.54 shows the output-matching circuit design for the MGF4935AM transistor. Figure 3.55 and Figure 3.56 show the input and output impedance matching circuit for HMC902LP3E MMIC LNA. Figure 3.57 and Figure 3.58 show the input and output impedance matching circuit design for the MMIC LNA used at the 4th stage.

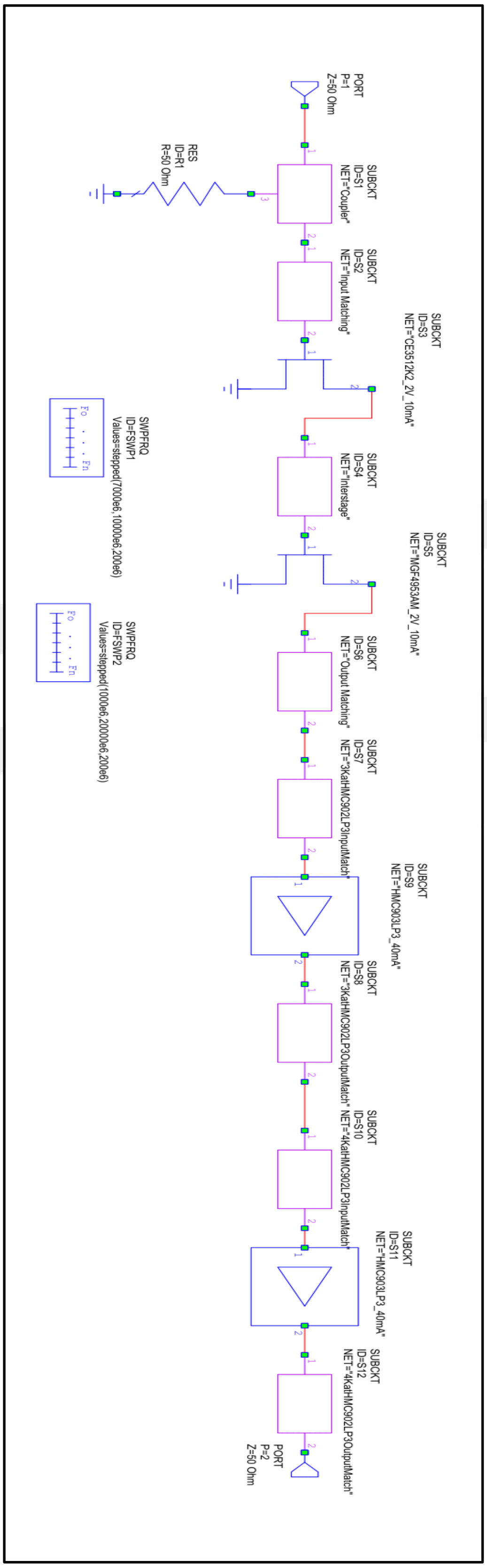

Figure 3.50. X-Band LNA block diagram on AWR

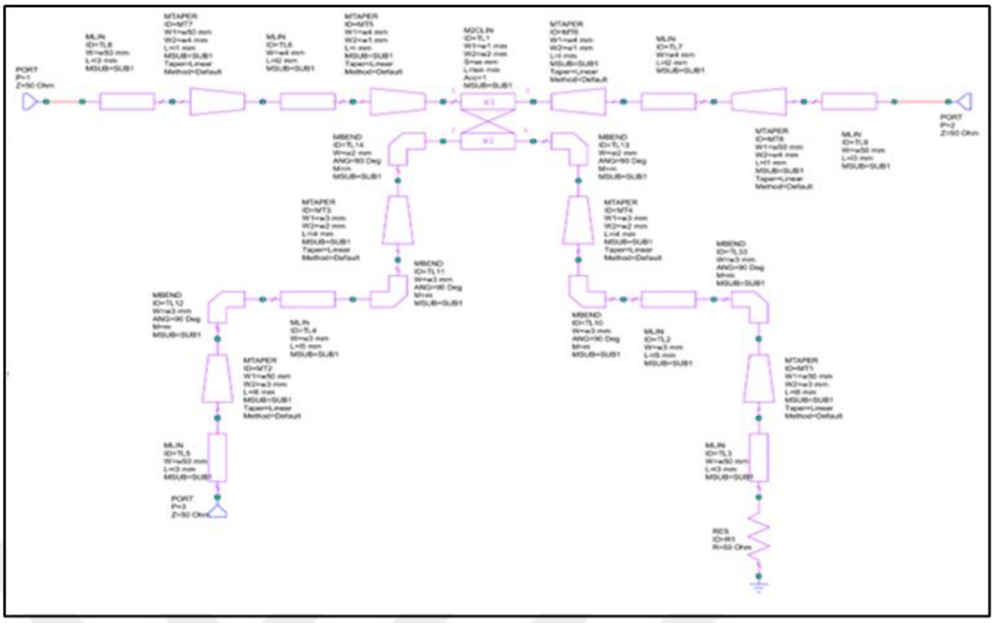

Figure 3.51. Coupler design for test output port of X-Band LNA

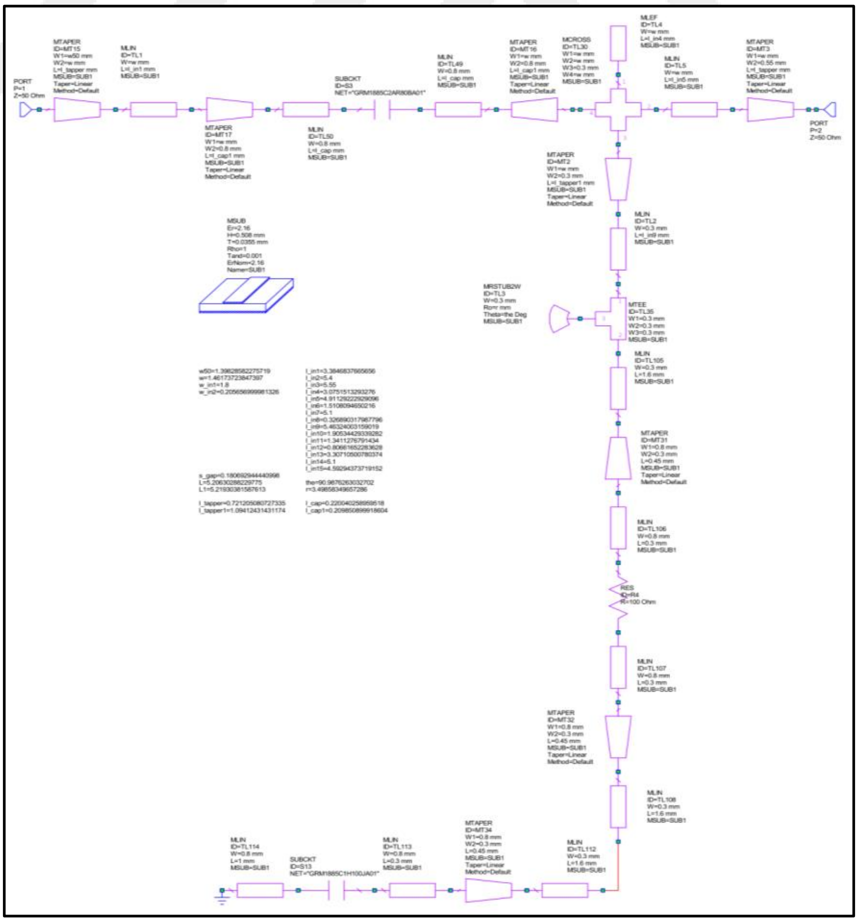

Figure 3.52. Input tuning circuit for X-Band LNA

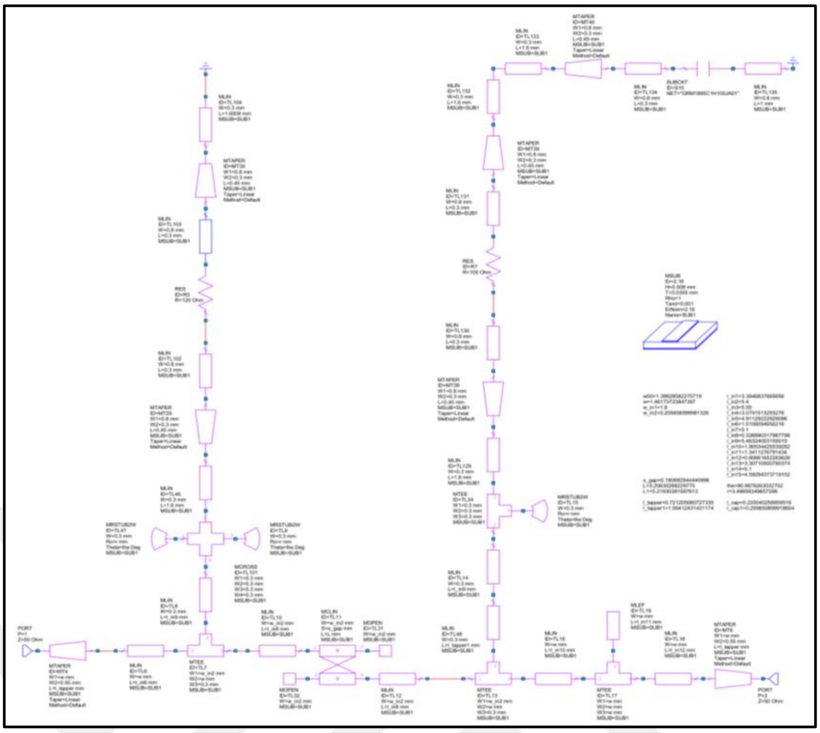

Figure 3.53. Interstage tuning circuit for X-Band LNA

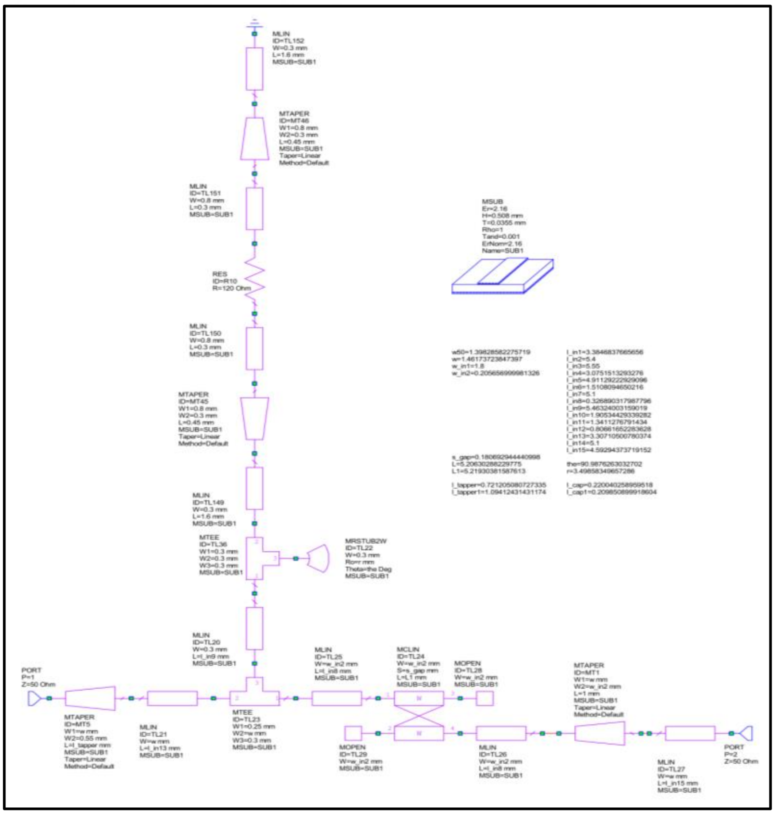

Figure 3.54. Output tuning circuit for X-Band LNA

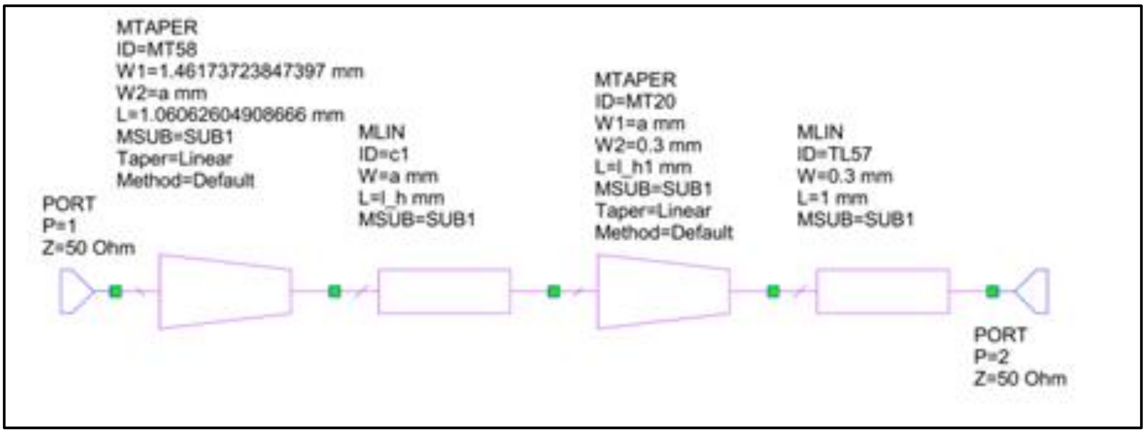

Figure 3.55. 3rd layer Tuning circuit for X-Band LNA

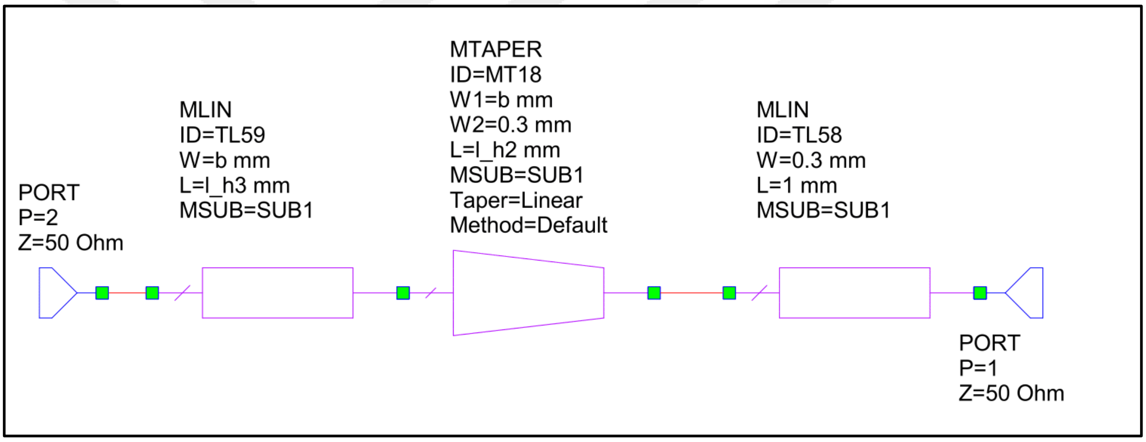

Figure 3.56. 3rd layer output tuning circuit for X-Band LNA

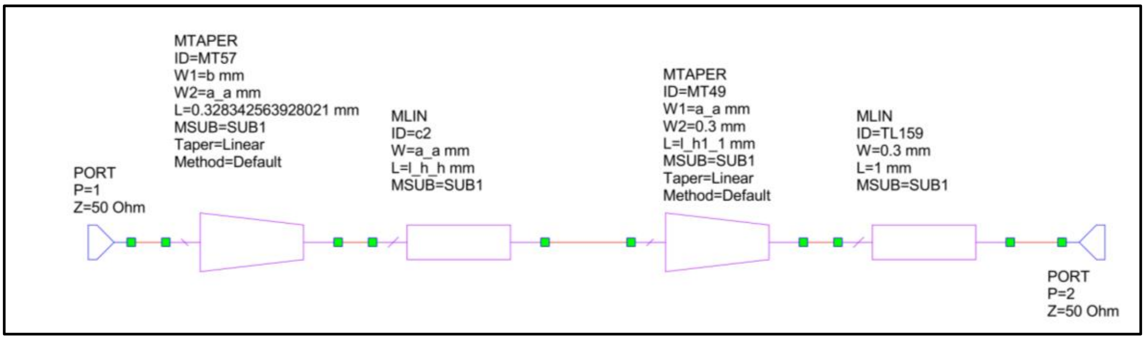

Figure 3.57. 4th layer tuning circuit for X-Band LNA

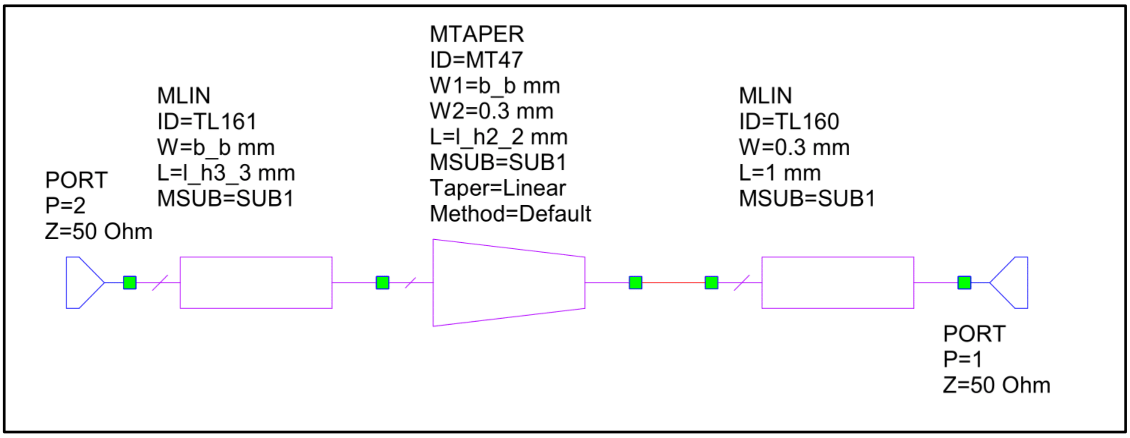

Figure 3.58. 4th layer output tuning circuit for X-Band LNA

3.2.1 Effects of Design Processes on The Performance of The LNA

Initially the first step of X-band LNA is designed (Figure 3.59). Figure 3.59 shows the AWR layout of the transistor in the first stage with the matching circuit. According to the simulation results, the results of the S parameter are shown in Figure 3.60. Figure 3.61 shows the noise figure, and Figure 3.62 shows the Roulette stability k-factor.

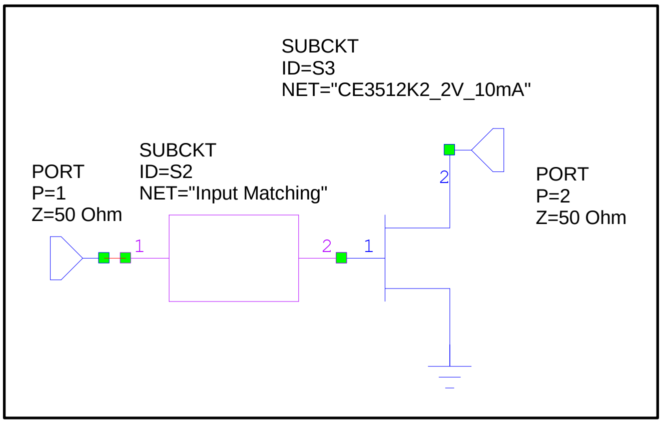

Figure 3.59. AWR representation of the first step of X-Band LNA

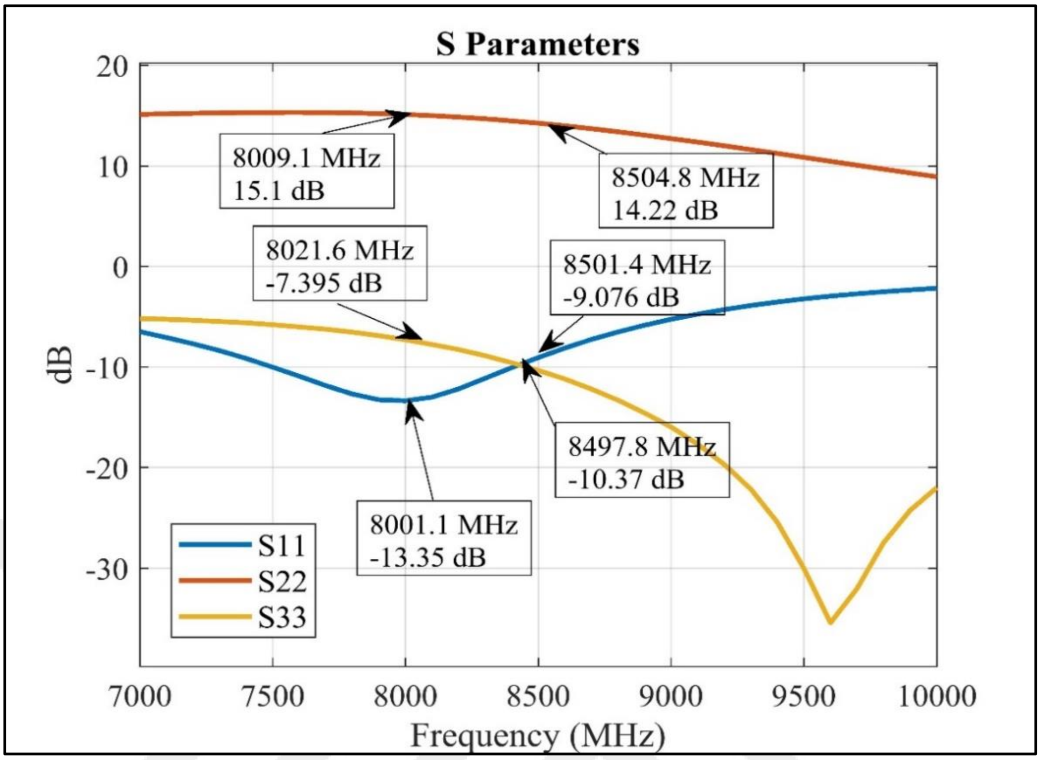

Figure 3.60. S parameters of the first step of X-Band LNA

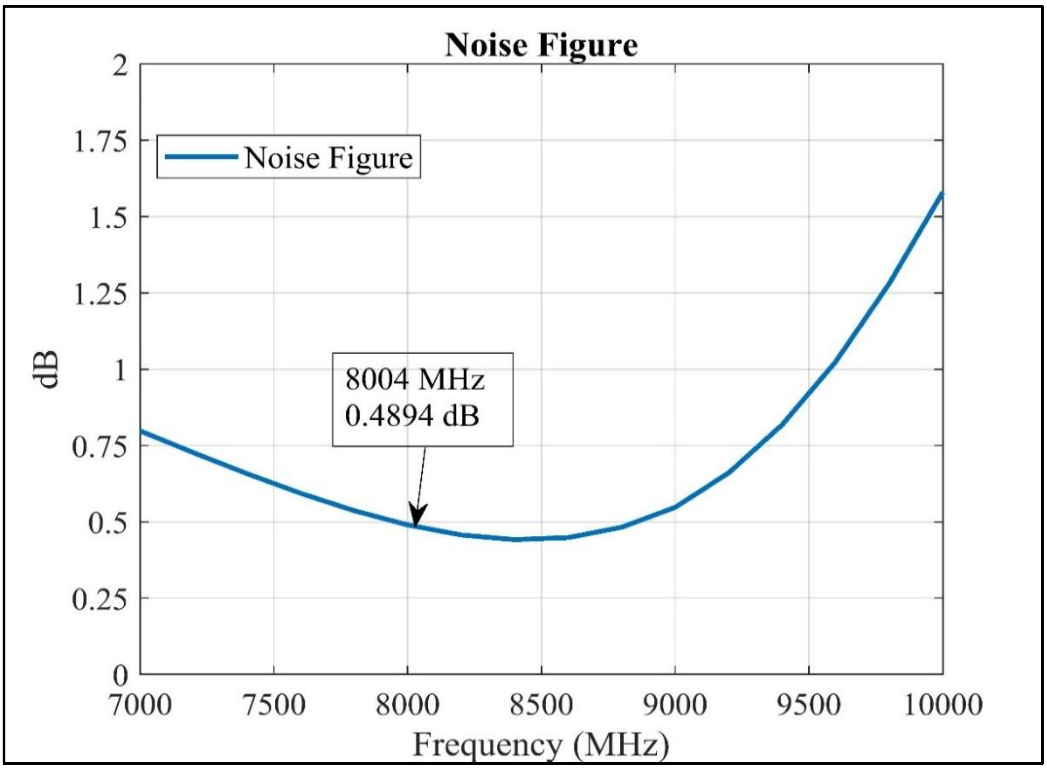

Figure 3.61. The noise figure of the first step of X-Band LNA

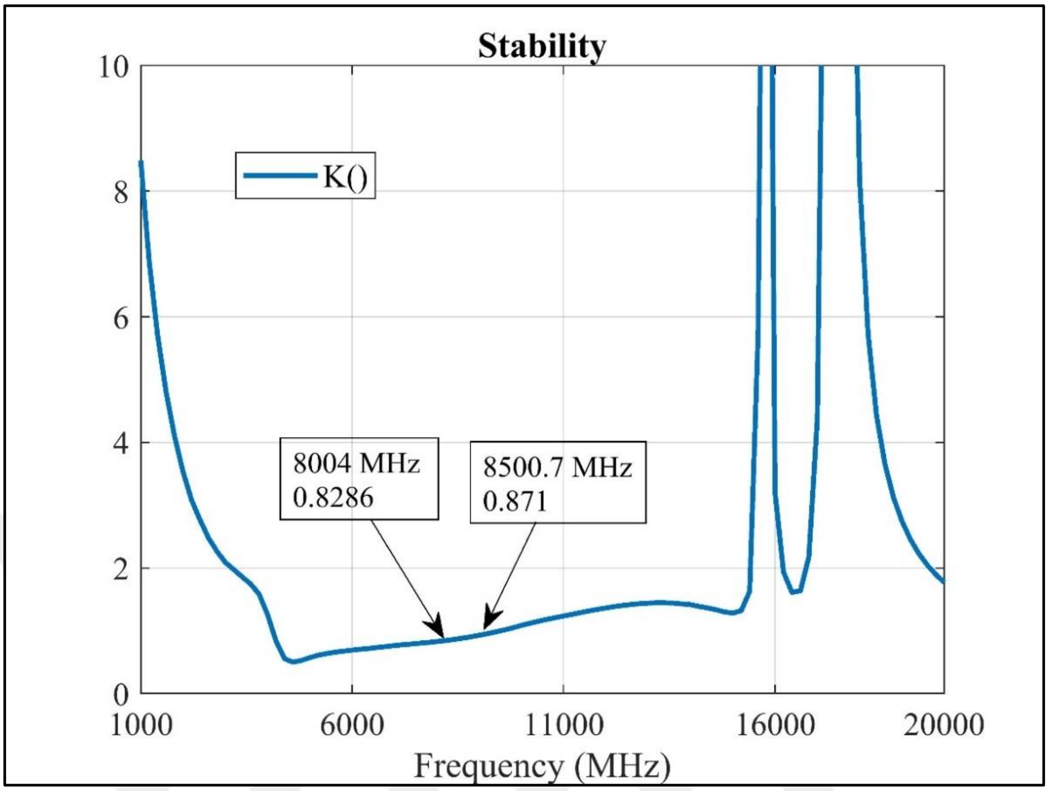

Figure 3.62. Roulette stability k-factor of the first step of X-Band LNA

Figure 3.63 shows the AWR layout with the first and second-stage transistors, input, and interstage matching circuit. According to the simulation results, the S parameters results are shown in Figure 3.64. Figure 3.65 shows the noise figure, and Figure 3.66 shows the Roulette stability k-factor.

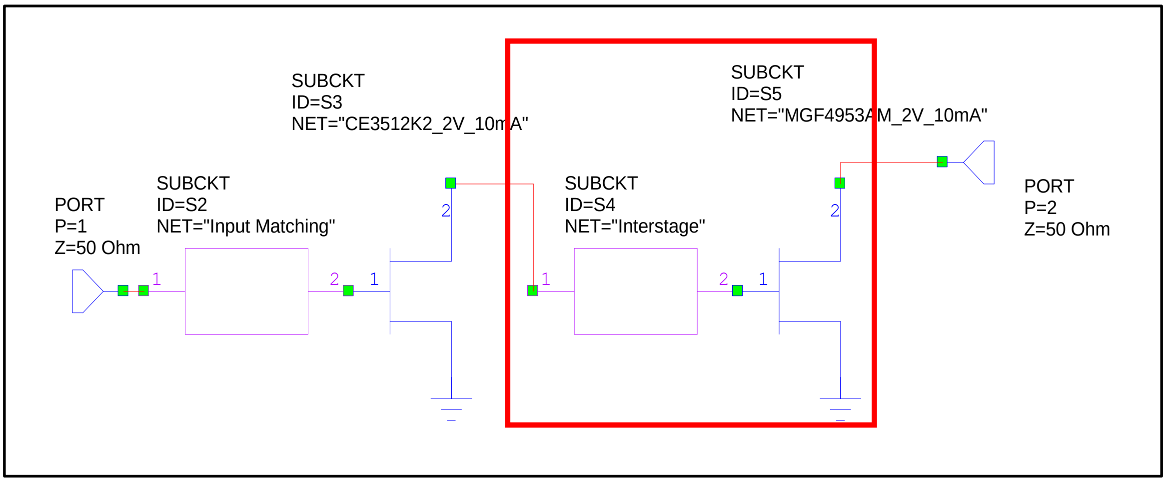

Figure 3.63. AWR representation of the second step of X-Band LNA

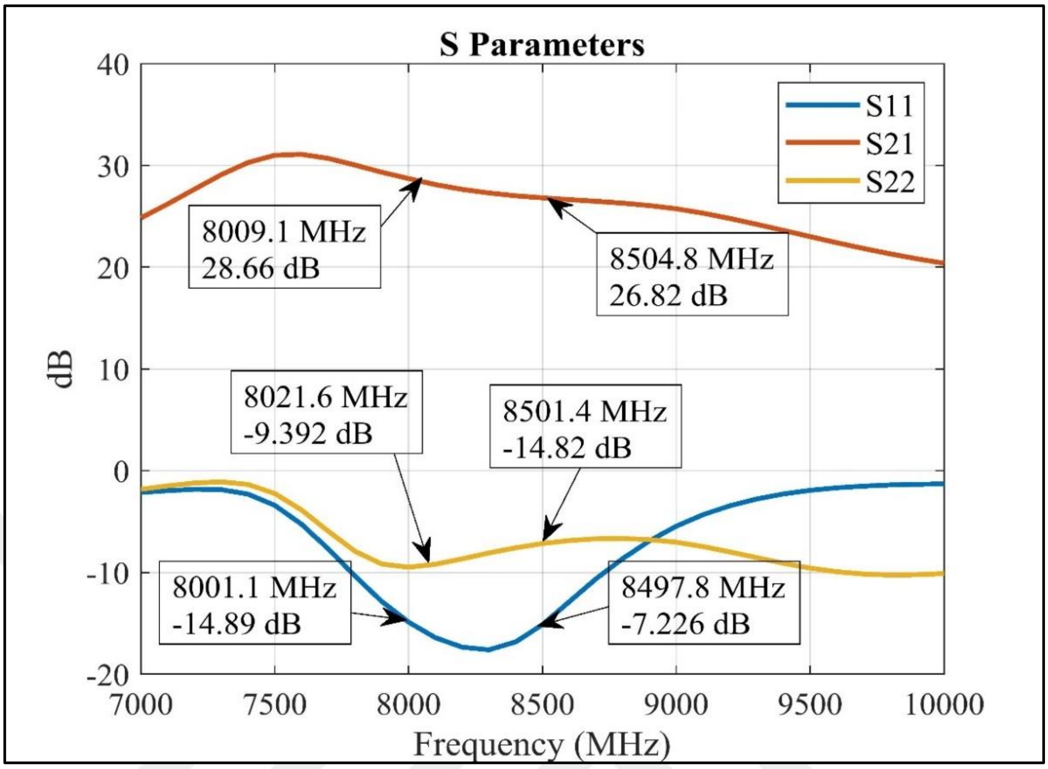

Figure 3.64. S parameters of the second step of X-Band LNA

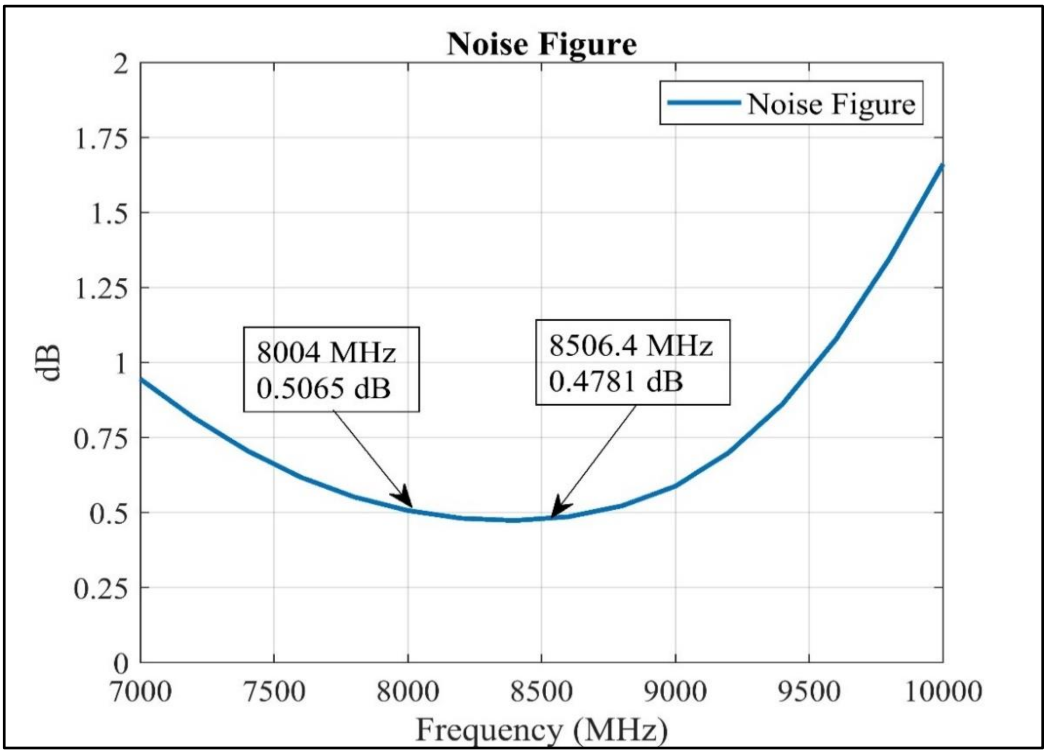

Figure 3.65. The noise figure of the second step of X-Band LNA

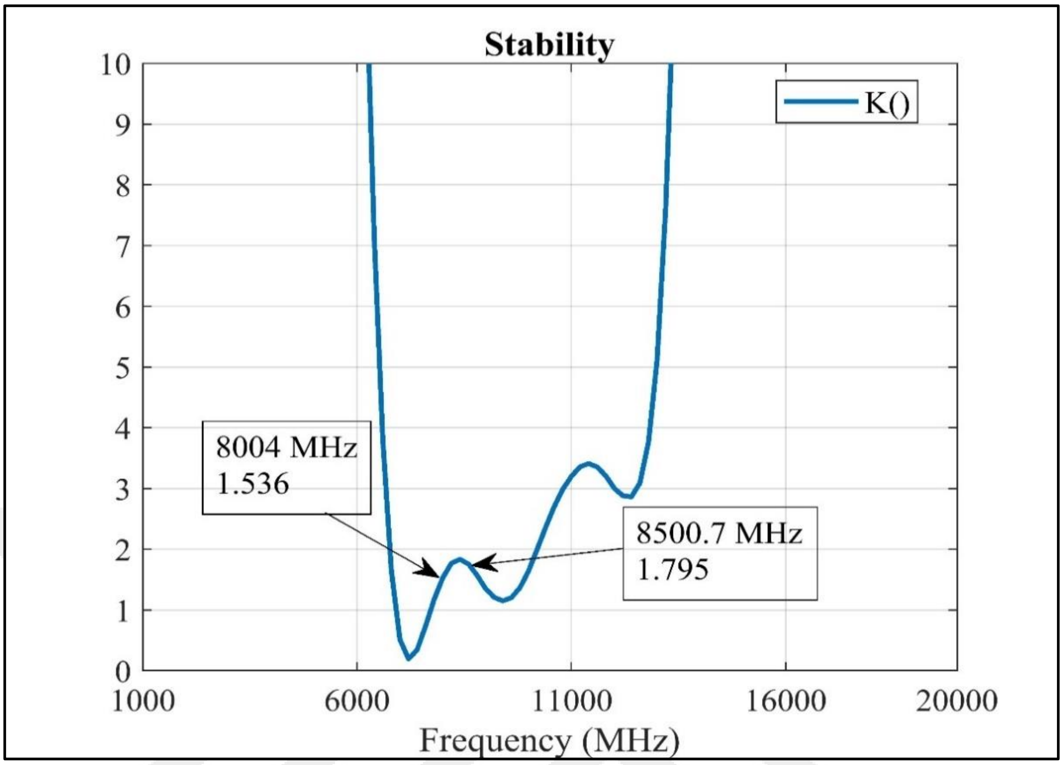

Figure 3.66. Roulette stability k-factor of the second step of X-Band LNA

Figure 3.67 shows the AWR design of the MGF4935AM transistor with the output matching circuit. According to the simulation results, the S parameter results are shown in Figure 3.68. Figure 3.69 shows the noise figure, and Figure 3.70 shows the Roulette stability k-factor.

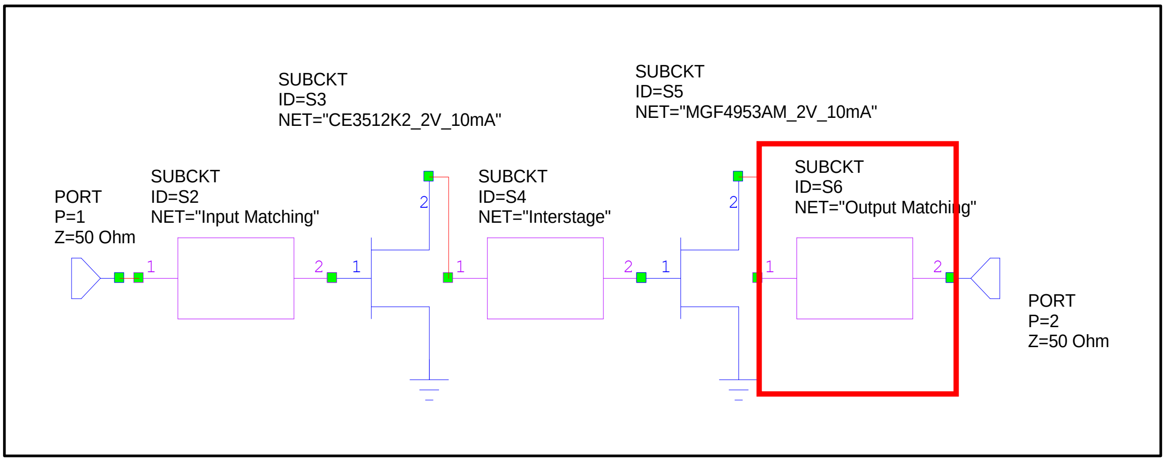

Figure 3.67. AWR representation of the third step of X-Band LNA

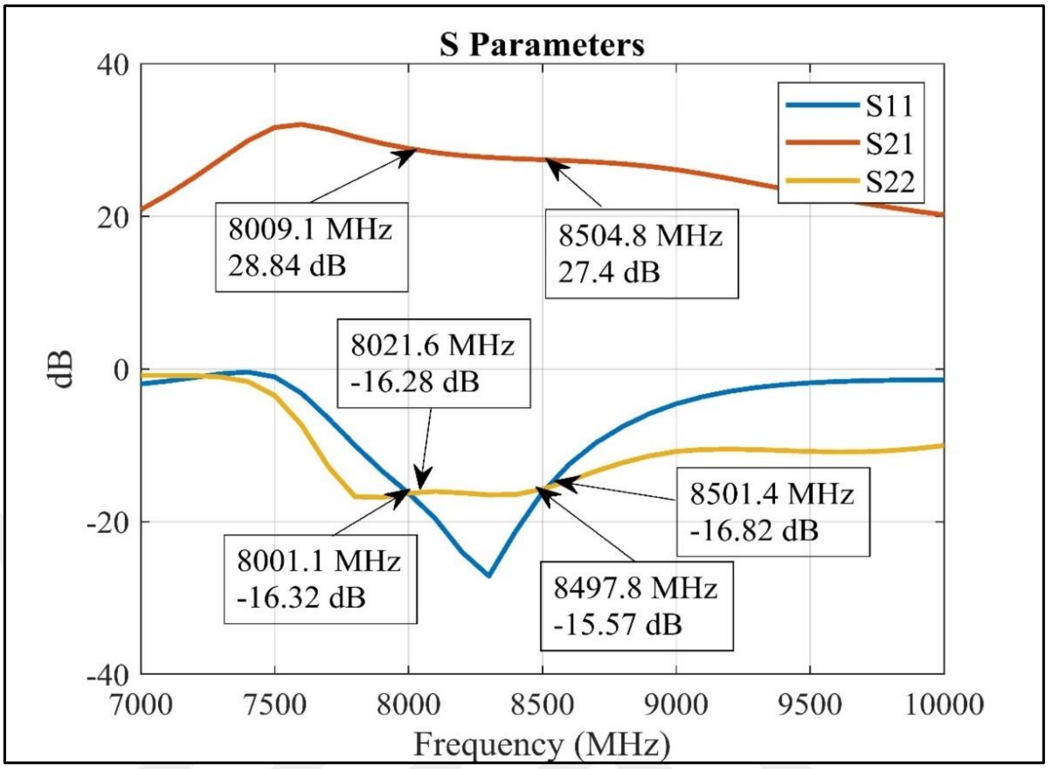

Figure 3.68. S parameters of the third step of X-Band LNA

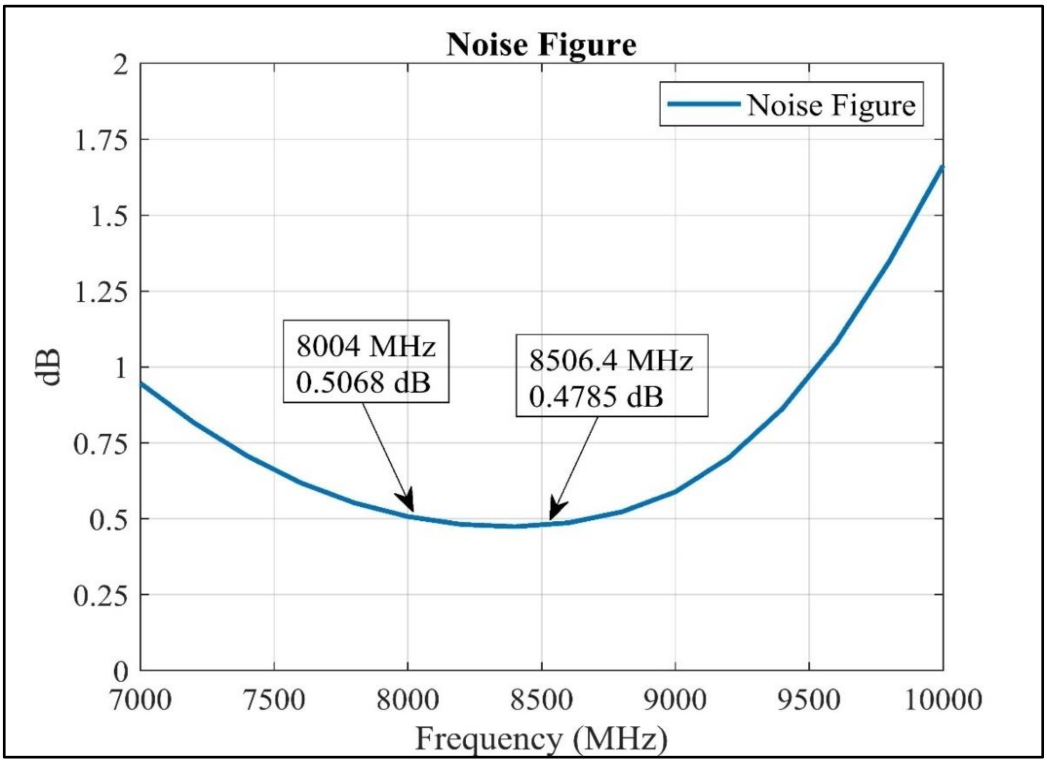

Figure 3.69. The noise figure of the third step of X-Band LNA

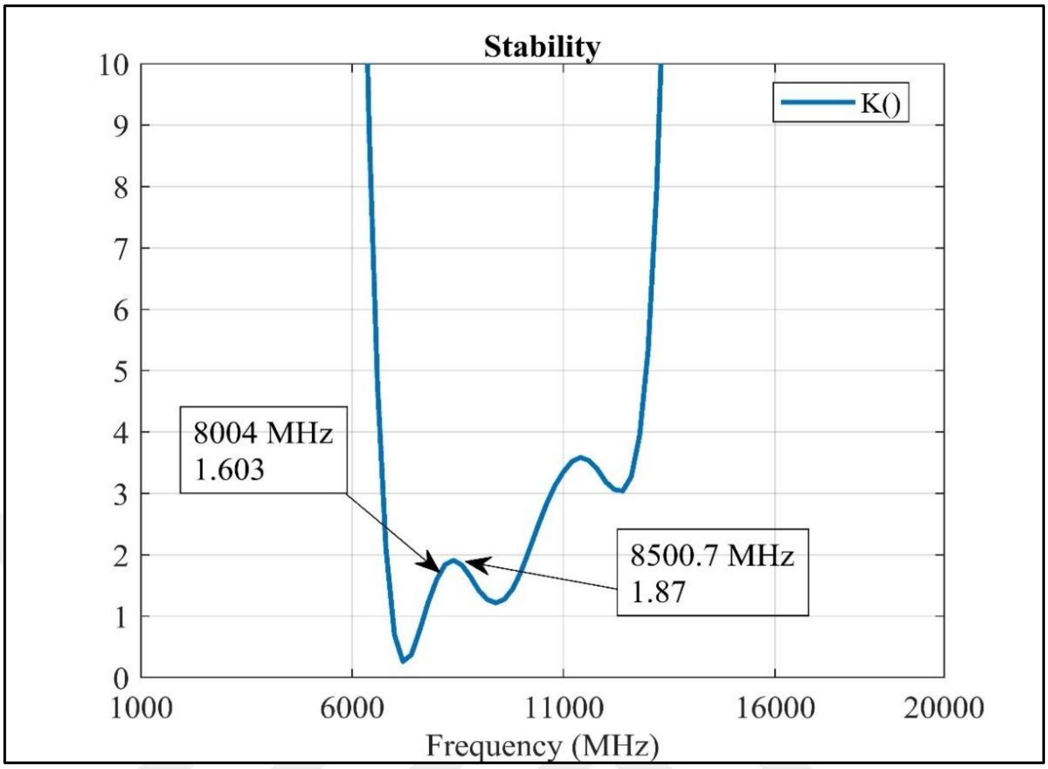

Figure 3.70. Roulette stability k-factor of the third step of X-Band LNA

In addition to the 3rd stage, Figure 3.71 shows the AWR layout of the MGF4935AM transistor with the output matching circuit. According to the simulation results, the S parameter results are shown in Figure 3.72. Figure 3.73 shows the noise figure, and Figure 3.74 shows the Roulette stability k-factor.

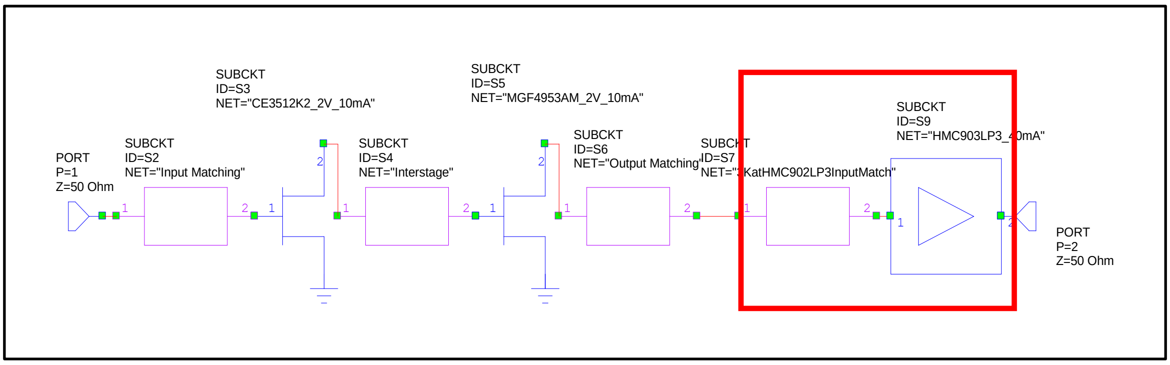

Figure 3.71. AWR representation of the fourth step of X-Band LNA

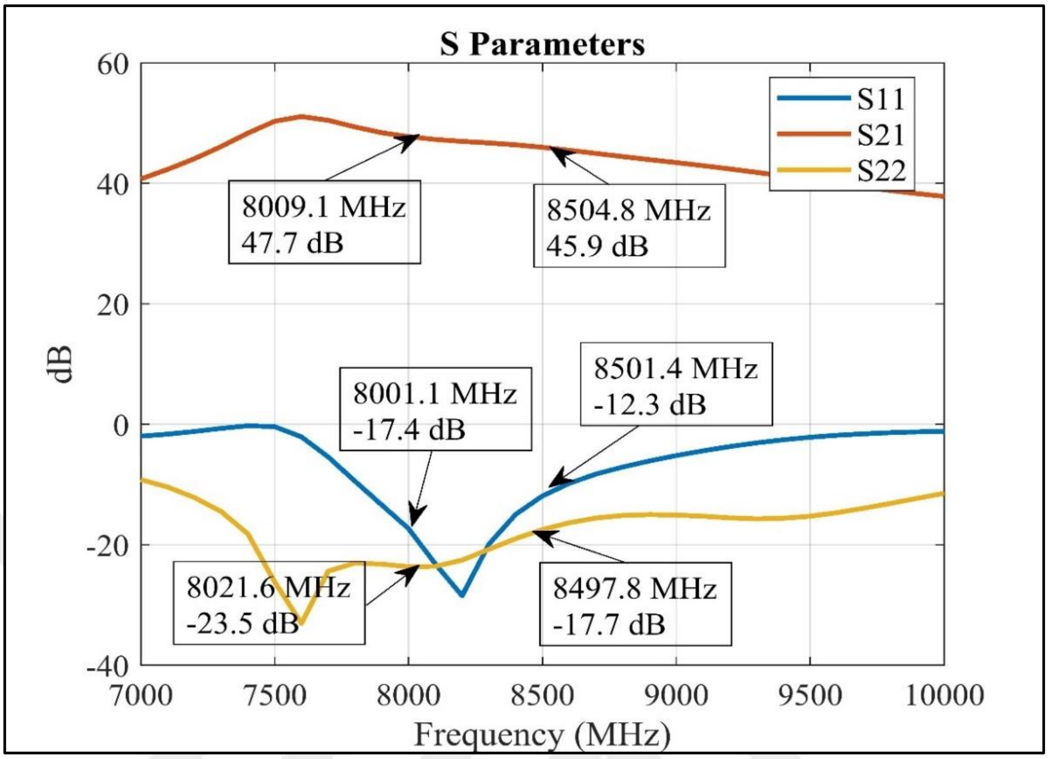

Figure 3.72. S parameters of the fourth step of X-Band LNA

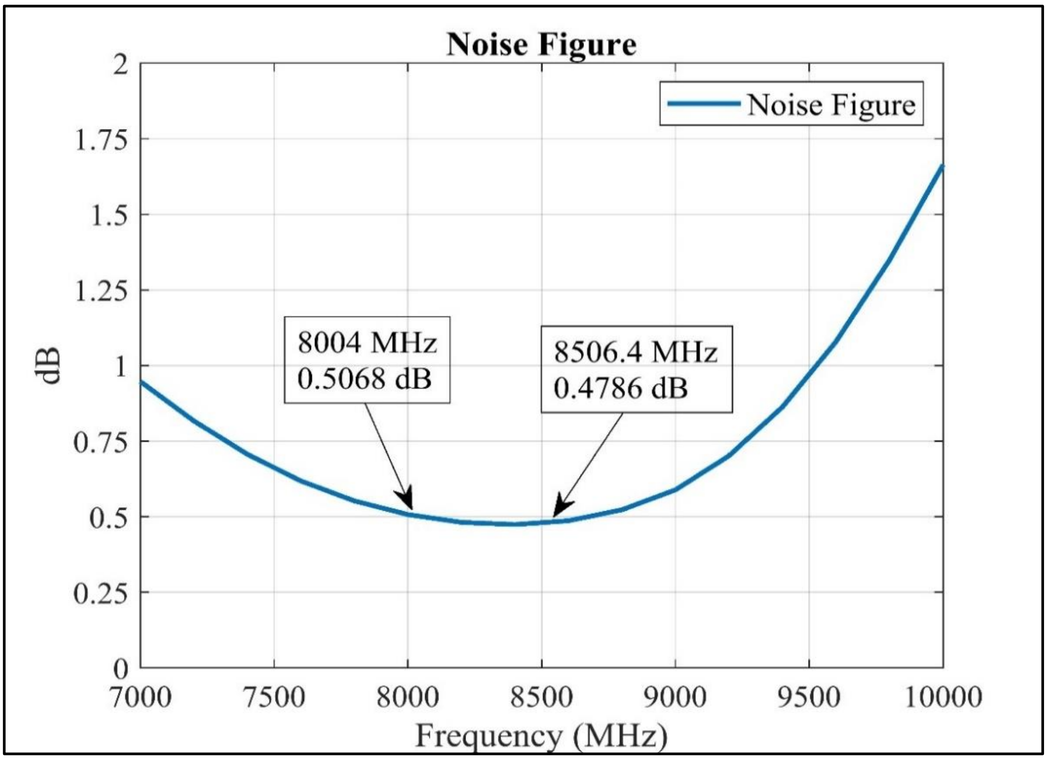

,

Figure 3.73. The noise figure of the fourth step of X-Band LNA

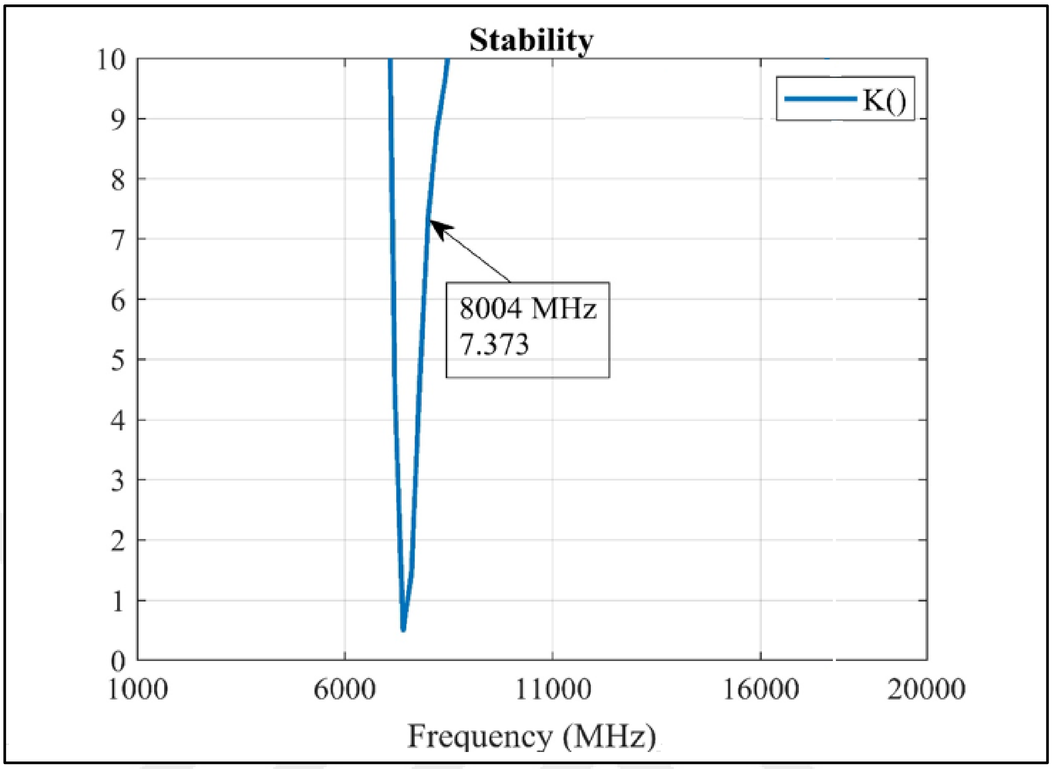

Figure 3.74. Roulette stability k-factor of the fourth step of X-Band LNA

Figure 3.75 shows the AWR layout of the HMC902LP3E MMIC LNA with the output matching circuit in addition to the 4th stage. According to the simulation results, the S parameter results are shown in Figure 3.76. Figure 3.77 shows the noise figure, and Figure 3.78 shows the Roulette stability k-factor.

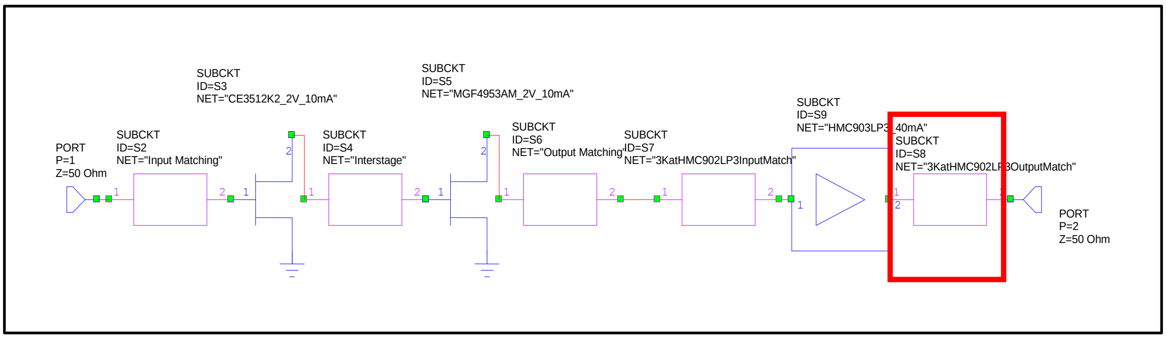

Figure 3.75. AWR representation of the fifth step of X-Band LNA

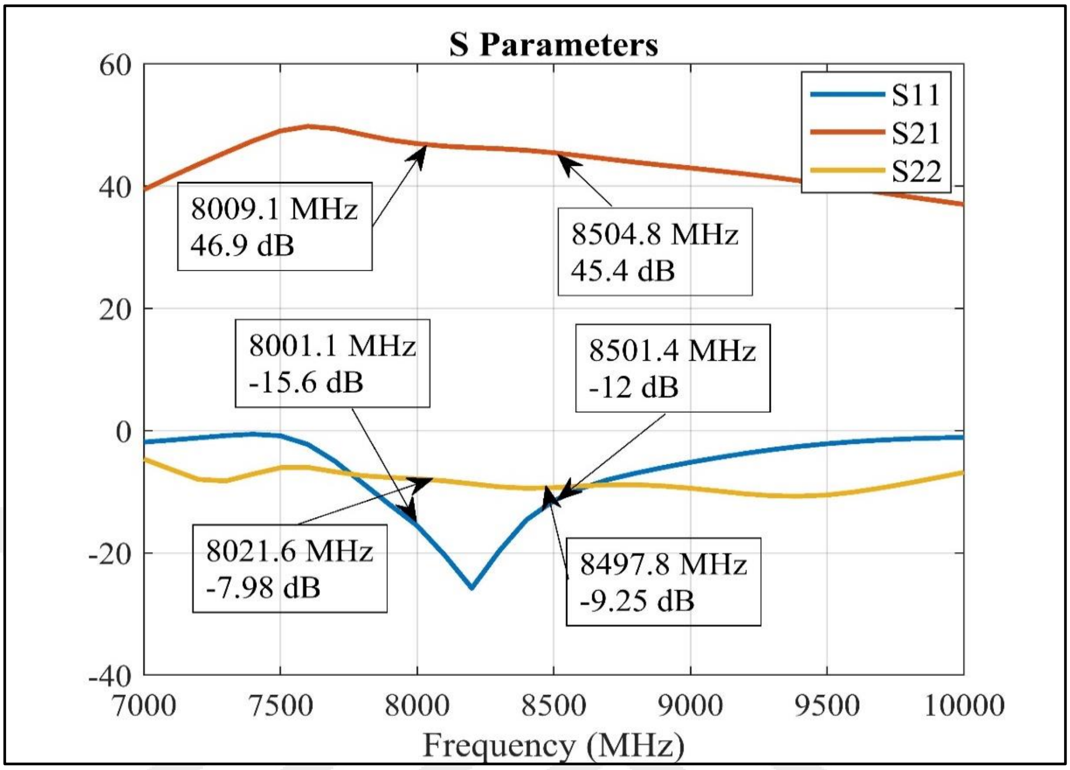

Figure 3.76. S parameters of the fifth step of X-Band LNA

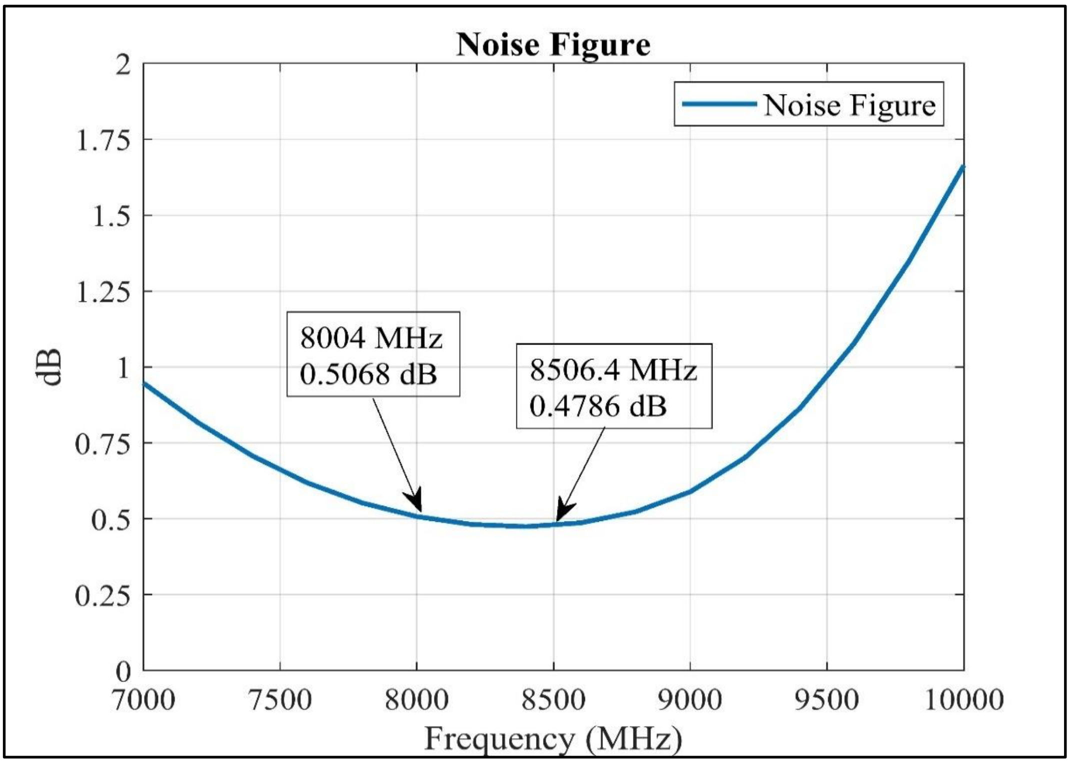

Figure 3.77. The noise figure of the fifth step of X-Band LNA

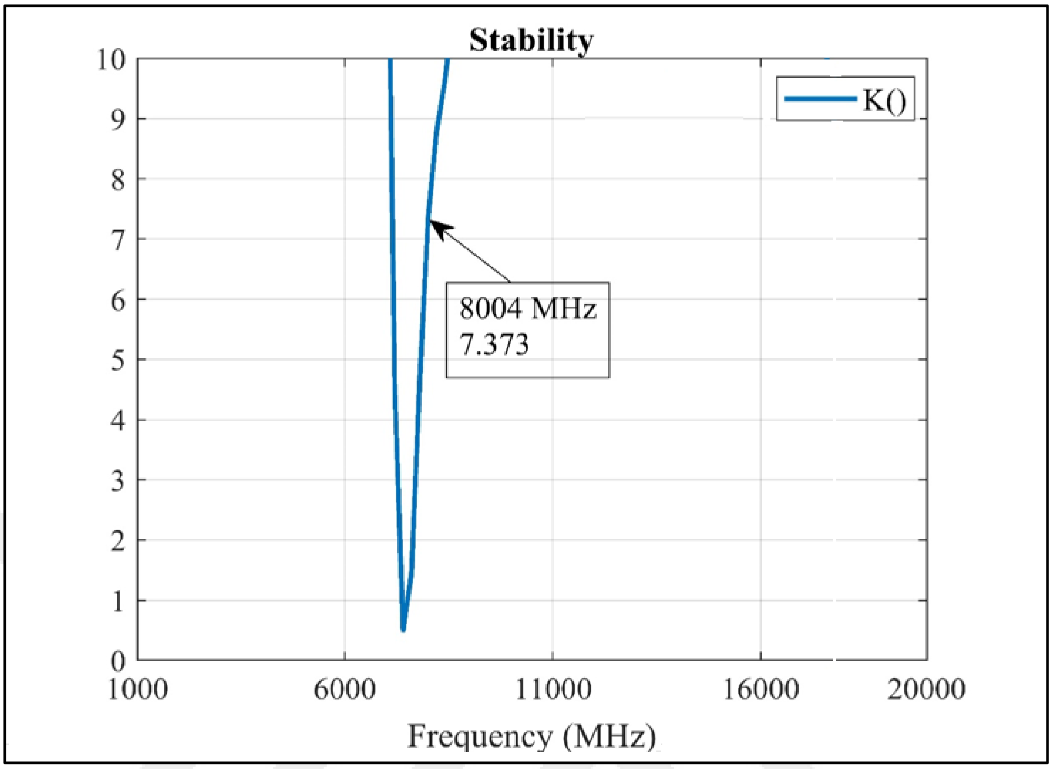

Figure 3.78. Roulette stability k-factor of the fifth step of X-Band LNA

Figure 3.79 shows the AWR layout with the HMC902LP3E MMIC LNA and input matching circuit on the 4th stage in addition to the 5th stage. According to the simulation results, the S parameter results are shown in Figure 3.80. Figure 3.81 shows the noise figure, and Figure 3.82 shows the Roulette stability k-factor.

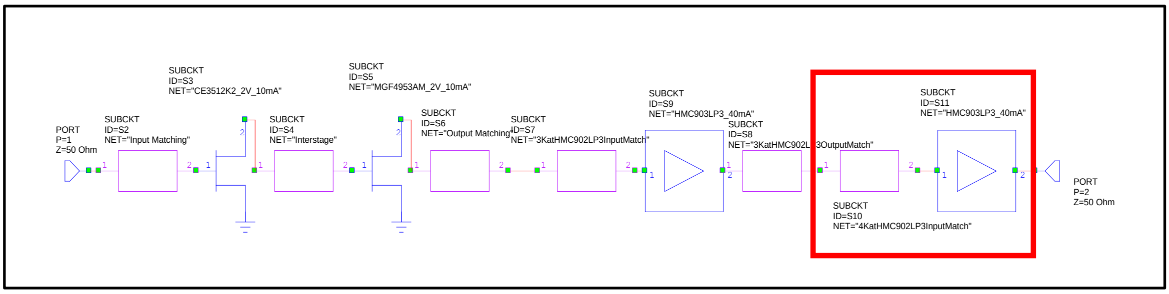

Figure 3.79. AWR representation of the sixth step of X-Band LNA

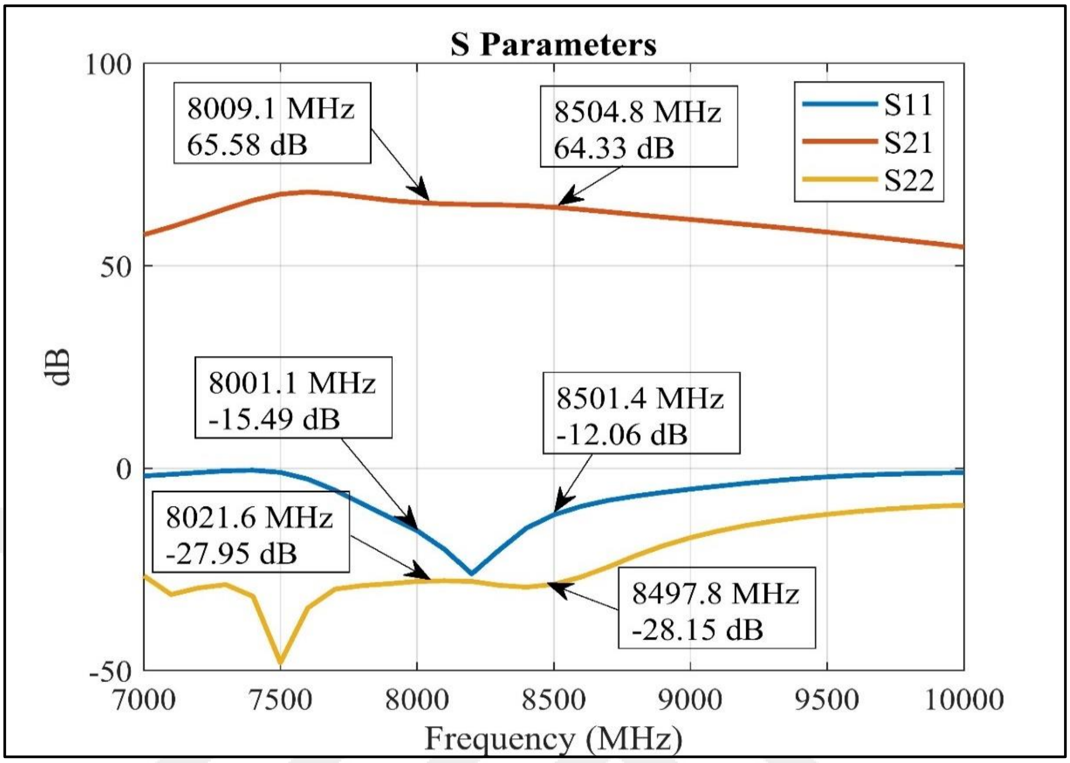

Figure 3.80. S parameters of the sixth step of X-Band LNA

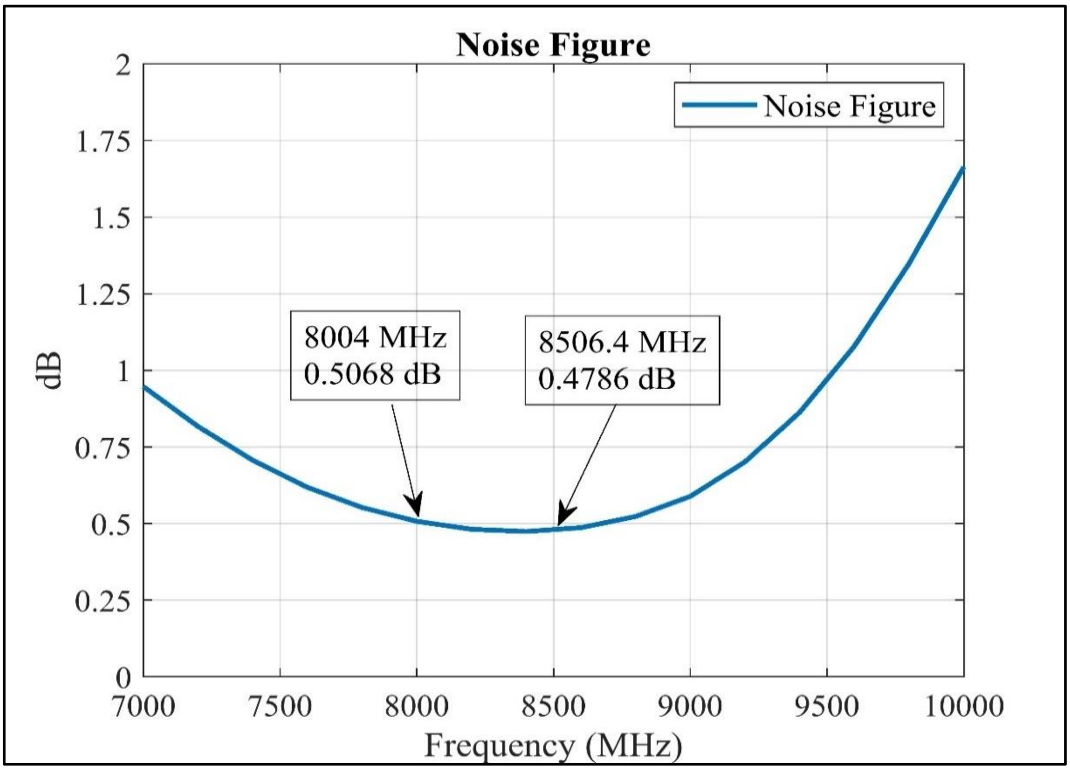

Figure 3.81. The noise figure of the sixth step of X-Band LNA

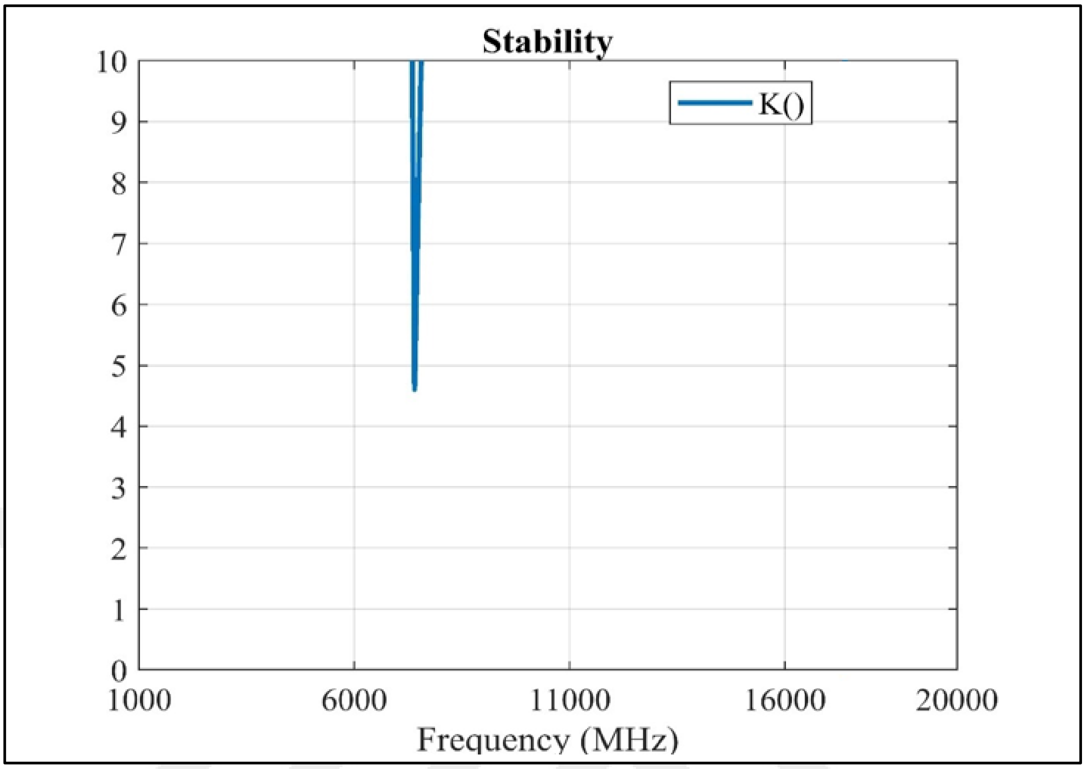

Figure 3.82. Roulette stability k-factor of the sixth step of X-Band LNA

Figure 3.83 shows the AWR layout of the HMC902LP3E MMIC low-noise amplifier on the 4th stage with the output matching circuit in addition to the 6th stage. According to the simulation results, the S parameter results are shown in Figure 3.84. Figure 3.85 shows the noise figure, and Figure 3.86 shows the Roulette stability k-factor.

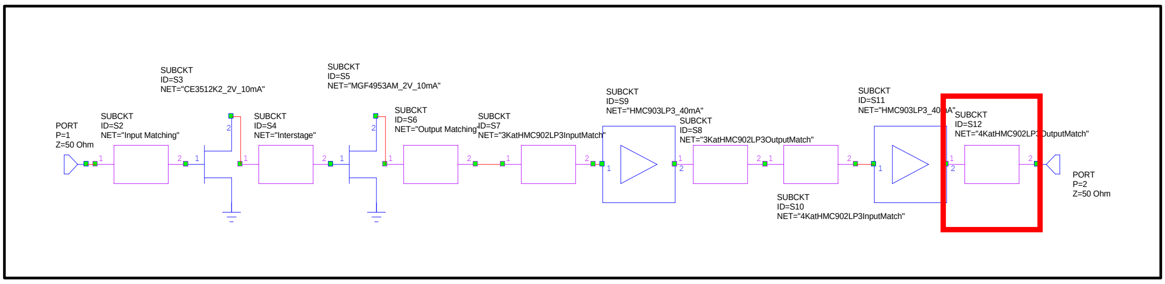

Figure 3.83. AWR representation of the seventh step of X-Band LNA

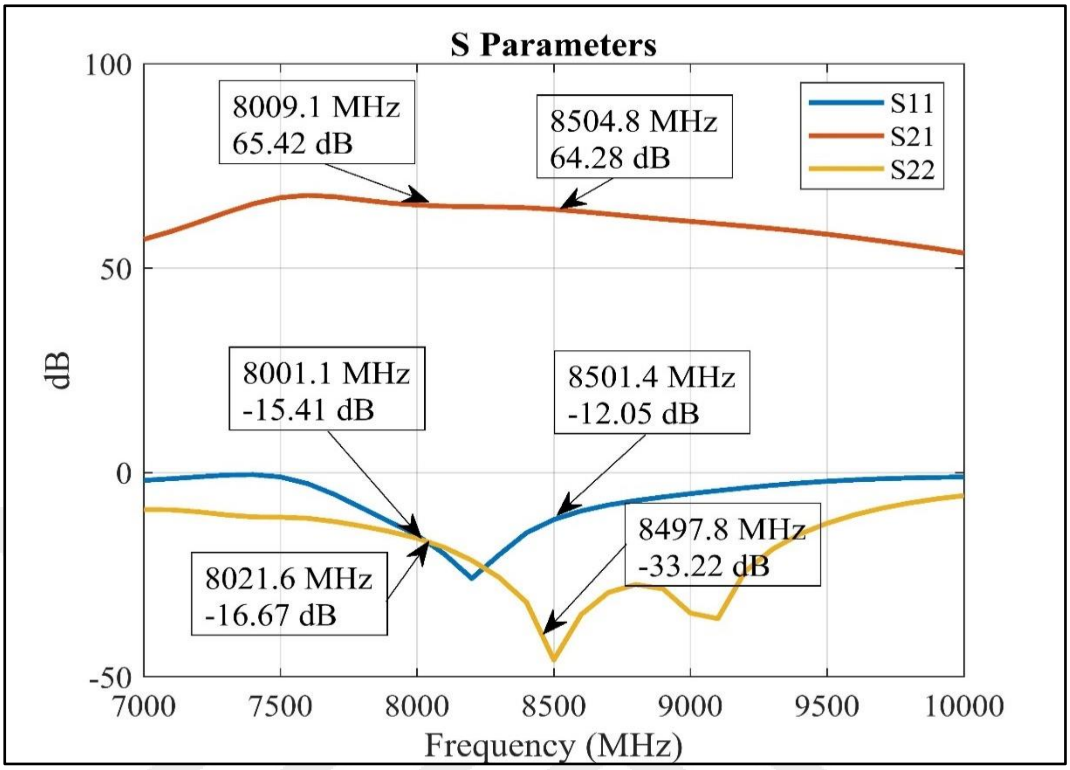

Figure 3.84. S parameters of the seventh step of X-Band LNA

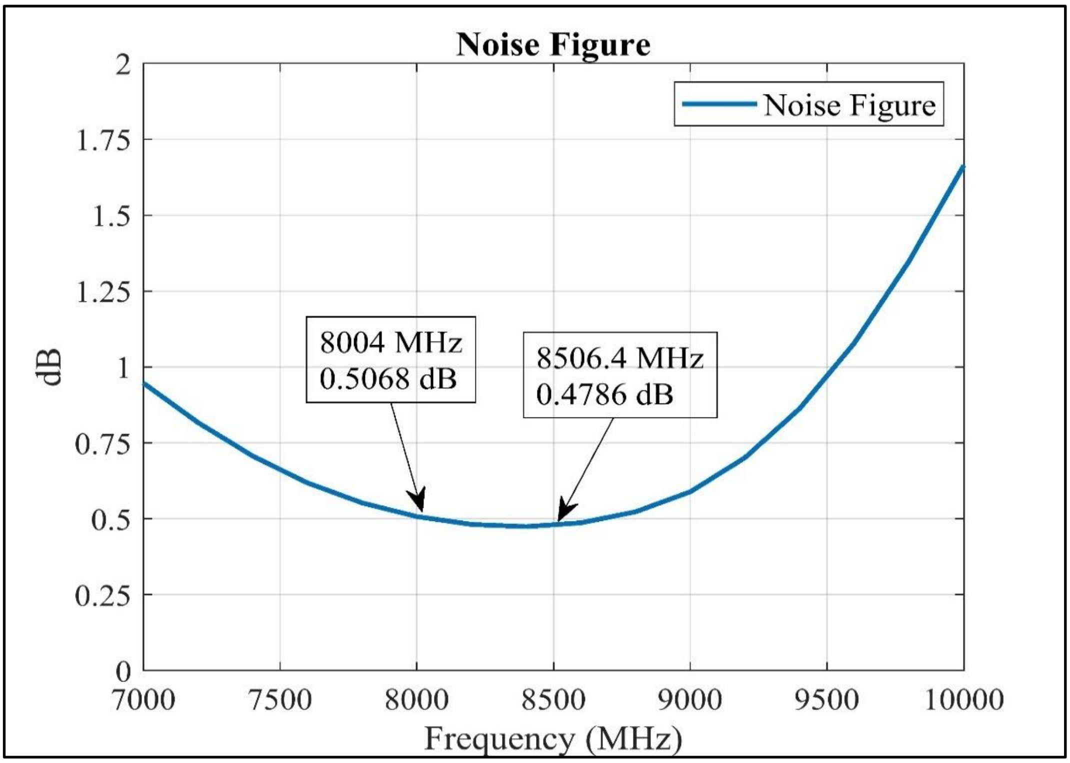

Figure 3.85. The noise figure of the seventh step of X-Band LNA

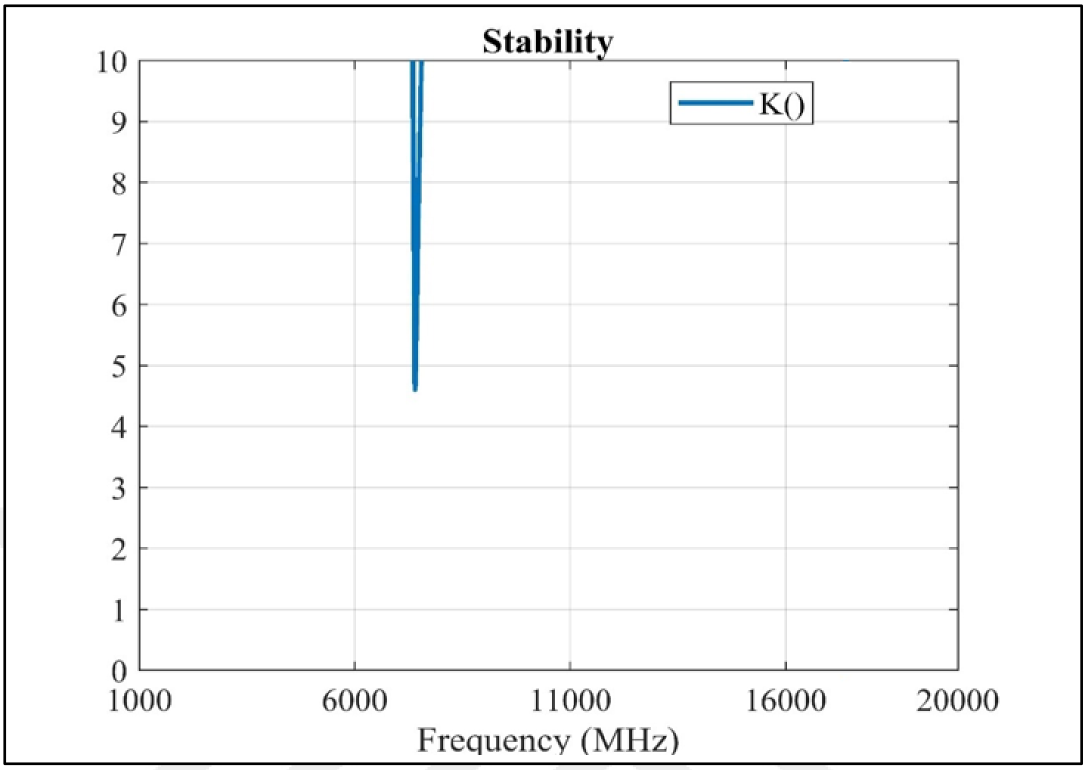

Figure 3.86. Roulette stability k-factor of the seventh step of X-Band LNA

In the design, a coupler is used in the RF input as shown in Figure 3.87. The coupler designed for 8-8.5 GHz is shown in Figure 3.89.

Also, the 2D layout of the proposed X-band LNA is demonstrated in Figure 3.88. The signal is received by attenuating the RF signal by 35 dB at the coupling port. This signal is used for the test port.

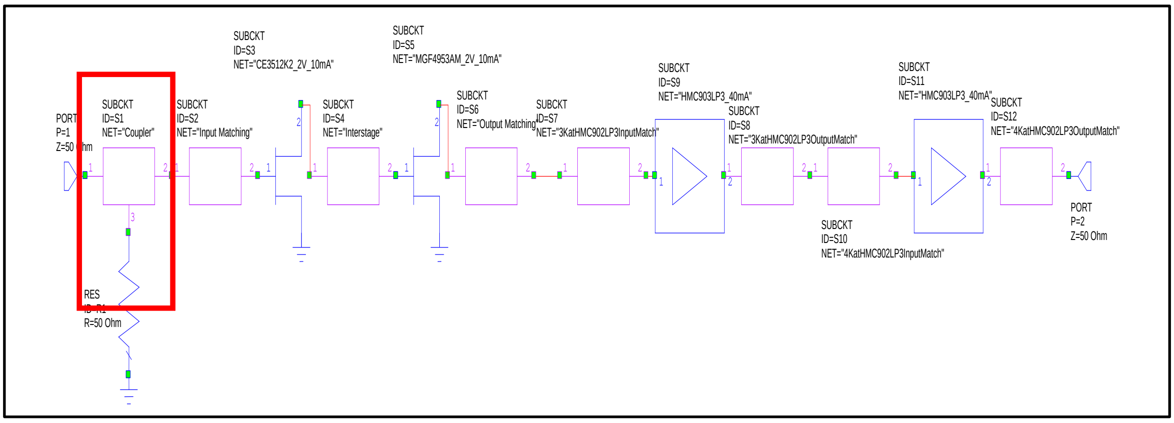

Figure 3.87. AWR representation of the eighth step of X-Band LNA

During the matching process, the following steps are taken into consideration. The width of the microstrip line should be between 0.2 mm and 5 mm. While smaller than 0.2 mm can be challenging in terms of fabrication, greater than 5 mm increases parasitic effects. Therefore, line width should choose carefully. A critical point when selecting the line thickness is that the thickness of the lines connected to the input and output of the transistors should not be smaller than the thickness of the input and output legs of the transistor. If it is smaller, some of the transmitted RF signals may be lost before entering the line. For this reason, the leg thicknesses of the transistors should be checked from the data sheets, and the thickness of the lines to be connected to these legs should be at least as thick as the transistor's leg thickness. As mentioned before, microstrip lines are not desired to be too long due to their parasitic effects, and they must be considered in the matching process. The S parameters should not be too dependent on the length or thickness of any line. For example, when the thickness of any line is changed by 0.1 mm, the S parameters should not change too much because the printed circuit production is not a completely ideal process. There may be slight changes in the thickness and length of the lines during fabrication. The circuit should be tolerant of these small changes. Especially the stub lengths should not be too long. Because as the line length increases, it will show an inductive effect.

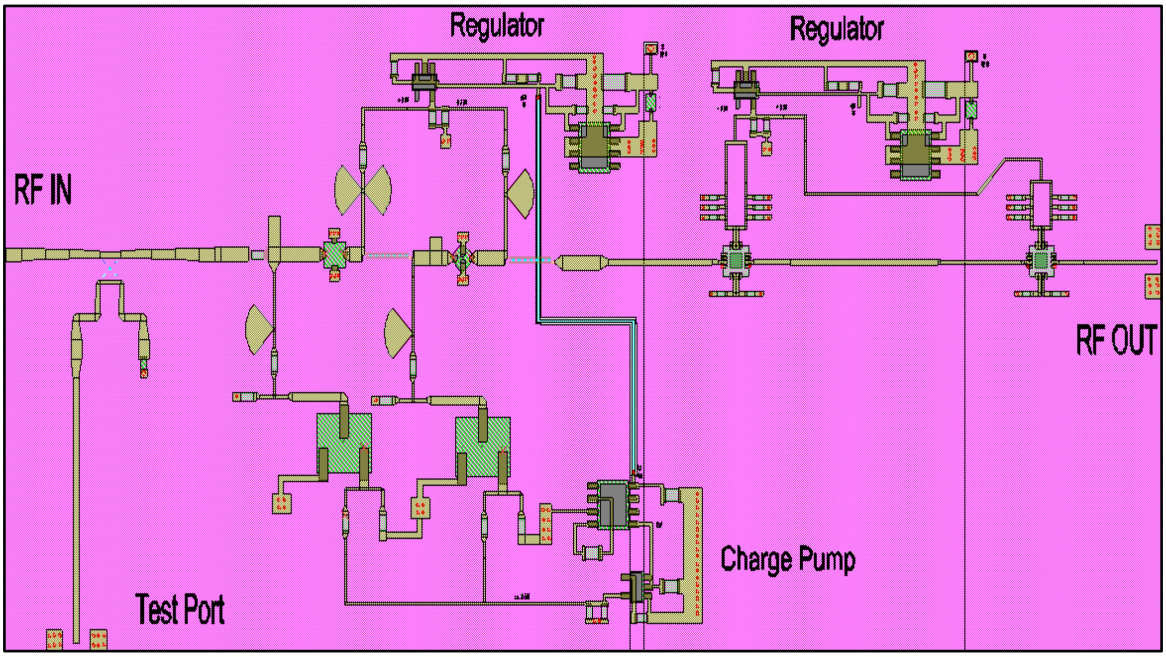

Figure 3.88. 2D Design of X-Band LNA

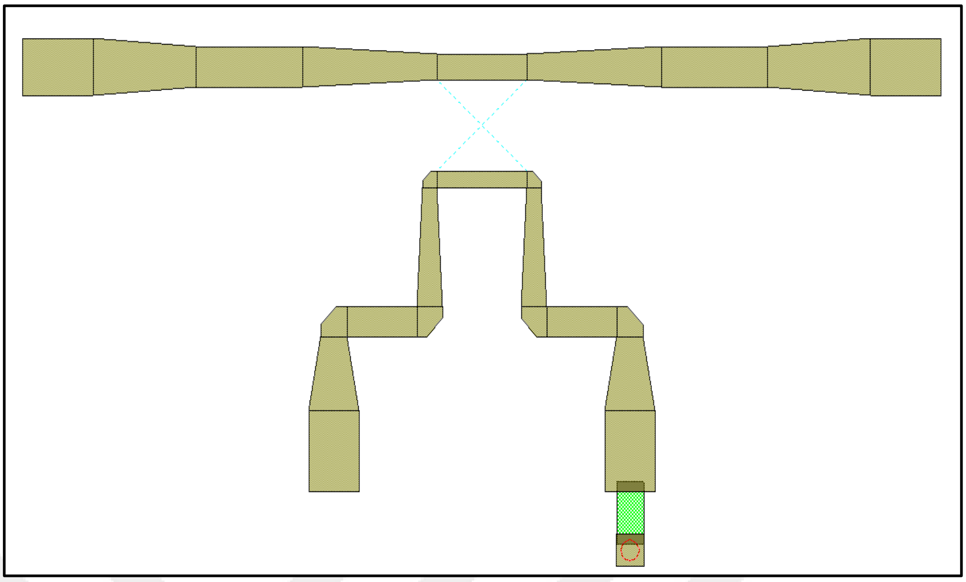

Figure 3.89. Coupler for designing test output port

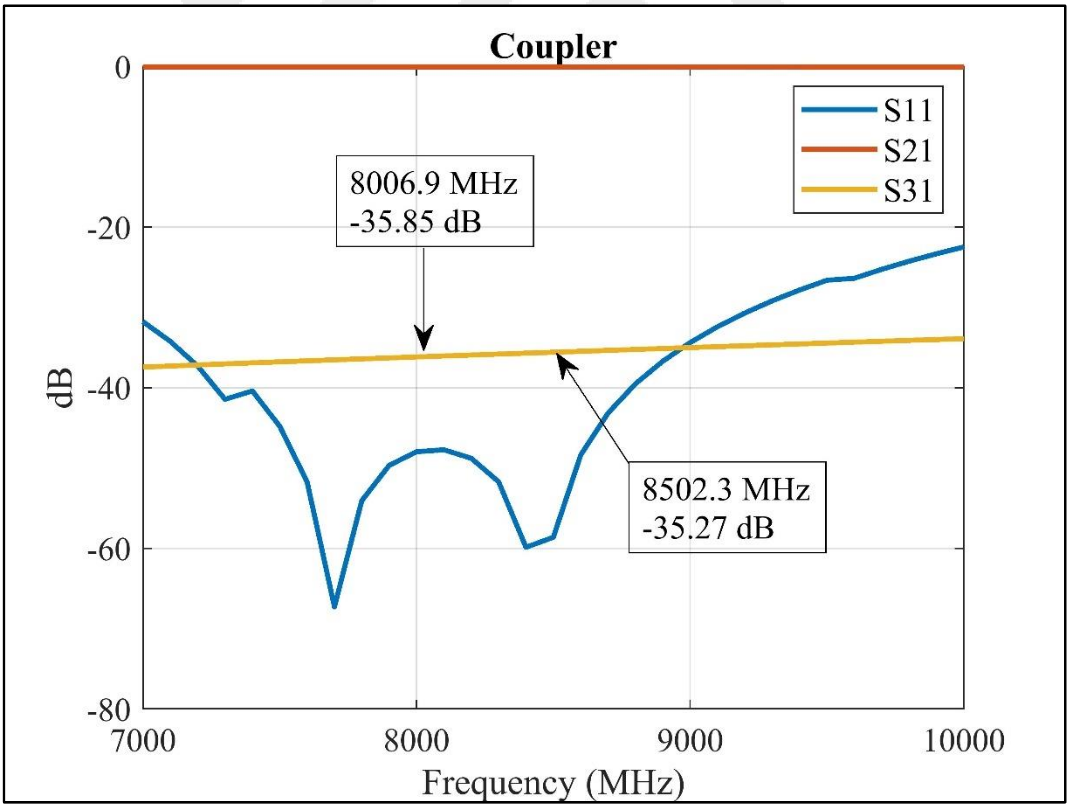

Figure 3.90. Simulation results of coupler design

In the design, an isolator, shown in Figure 3.91, is used at RF output. It is used to make the output reflection value better. The chosen isolator is with an SMA connector and is connected to the X-band LNA output port. This isolator has a 0.3 dB insertion loss and 20 dB isolation value.

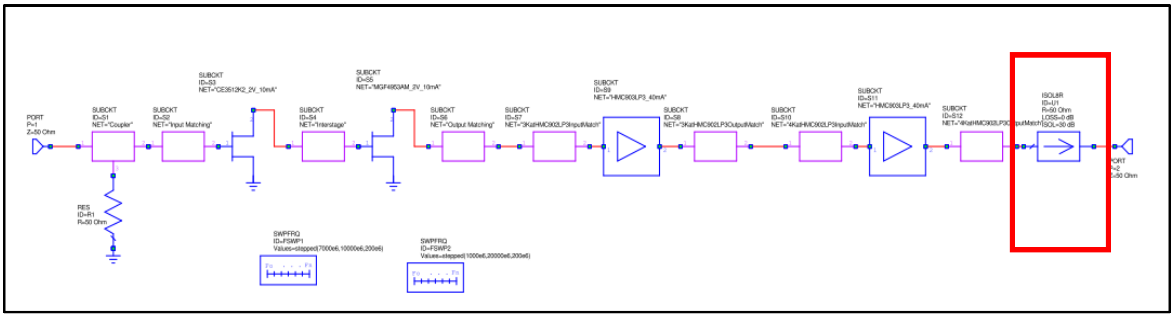

Figure 3.91 AWR representation of the ninth step of X-Band LNA

3.2.2 Regulator Design

The regulator circuit operates with a 12 V input signal. Figure 3.92 shows the regulator circuit. The RF transistors in the first two stages require a DC voltage of 3.3 V at the drain end and -0.47 V and -0.47 V at the gate end. The MMIC LNAs in the third and fourth stages require a voltage of 3.5 VDC.

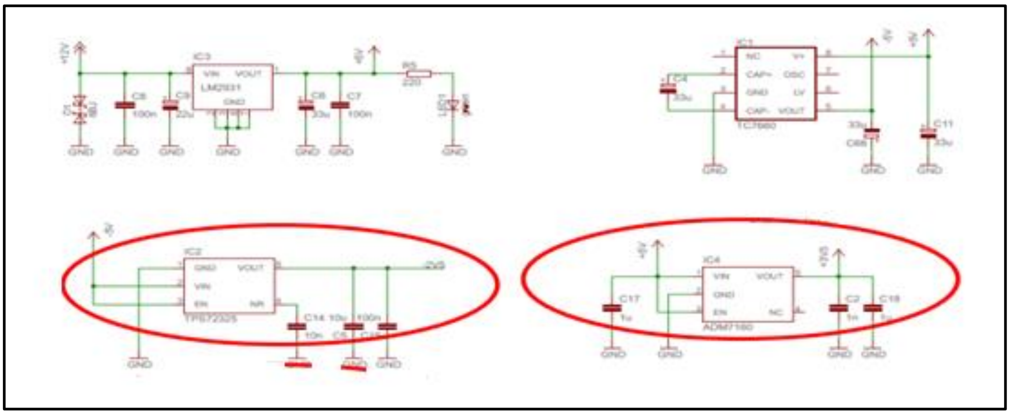

Figure 3.92. Regulator design

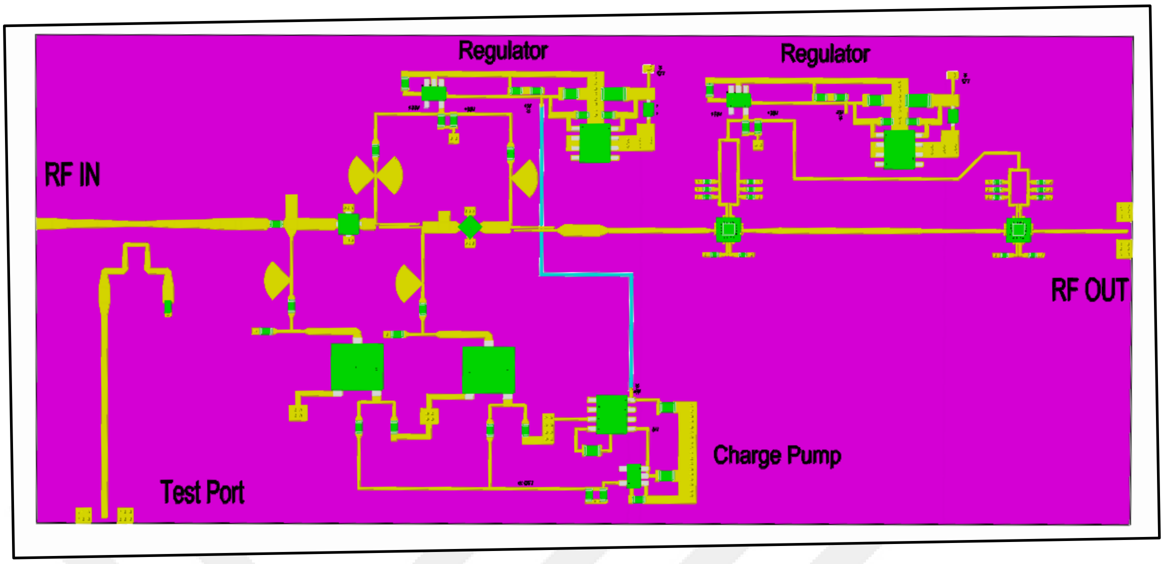

Figure 3.93. 3D representation of X-Band LNA

3.2.3 Merging of Assemblies of The LNA and Regulator

According to the block diagram in Figure 3.91 and Figure 3.93, a coupler is added to the test port as the 9th step. Simulation results, EM analyses, and essential optimizations are done.

According to the X-band LNA simulation, the operating frequency is between 8 and 8.5 GHz. S parameters of the X-band LNA are shown in Figure 3.94. The figure shows that the gain is 64.5 dB, which meets the technical specification requirement.

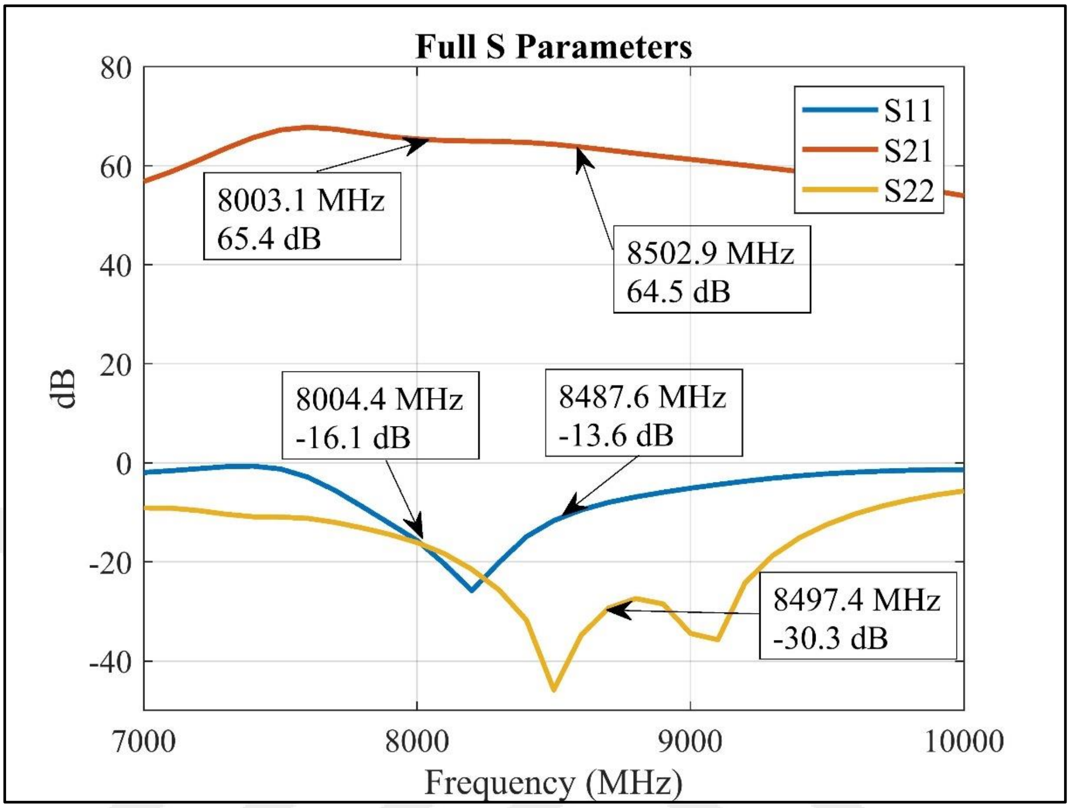

Figure 3.94. S parameters of the X-Band LNA

According to the scattering parameters in Figure 3.94, the input and output reflection ratio is below - 14 dB. According to this value, VSWR is 1.5. This value is met in the technical specification requirement. Figure 3.95 shows the noise figure graph, and according to the graph, the maximum value of 0.7 dB meets the requirement. The simulation result shows a maximum value of 0.6 dB in the 8 – 8.5 GHz frequency range.

According to the simulation results, the transistors should be stable in all frequency bands. According to Figure 3.96, the Roulette stability k-factor is above 1 in the frequency band 0 - 20 GHz. According to this result, the simulation for the Roulette stability factor in cascaded circuits is necessary but insufficient. It must be terminated with passive terminators between the layers to meet the Roulette condition fully. In Figure 3.97, the P1dB is 14 dBm. It meets the minimum requirement of 10 dBm given in the technical specification.

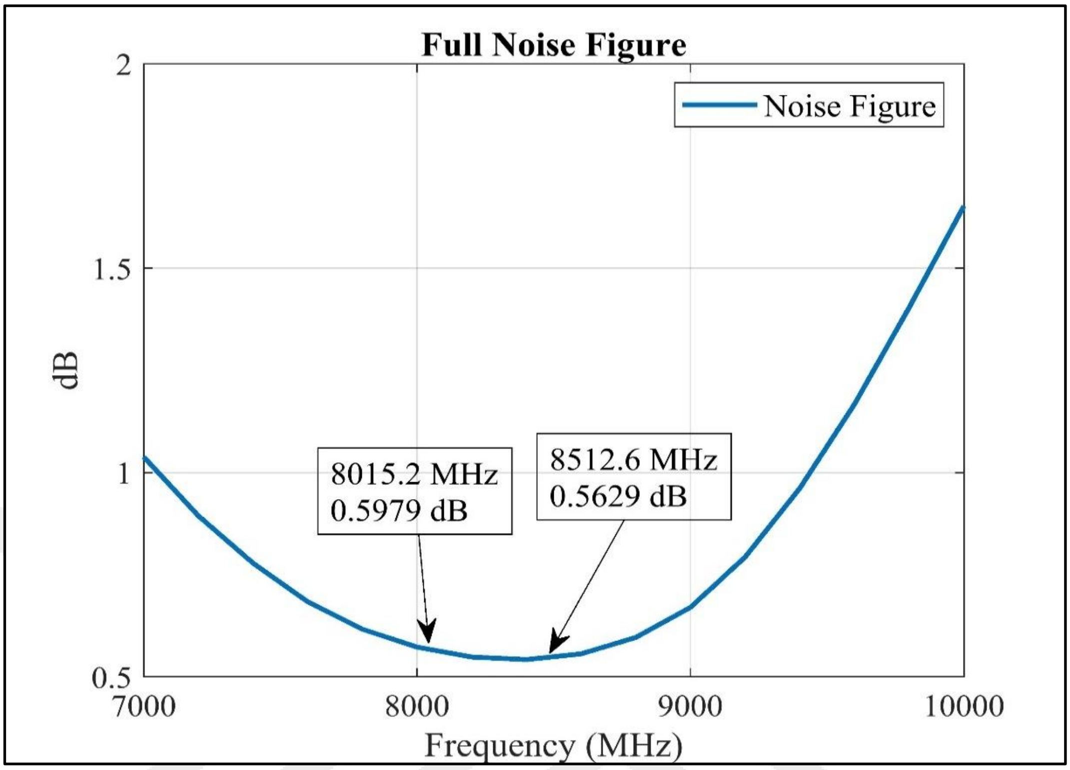

Figure 3.95. The noise figure of X-Band LNA

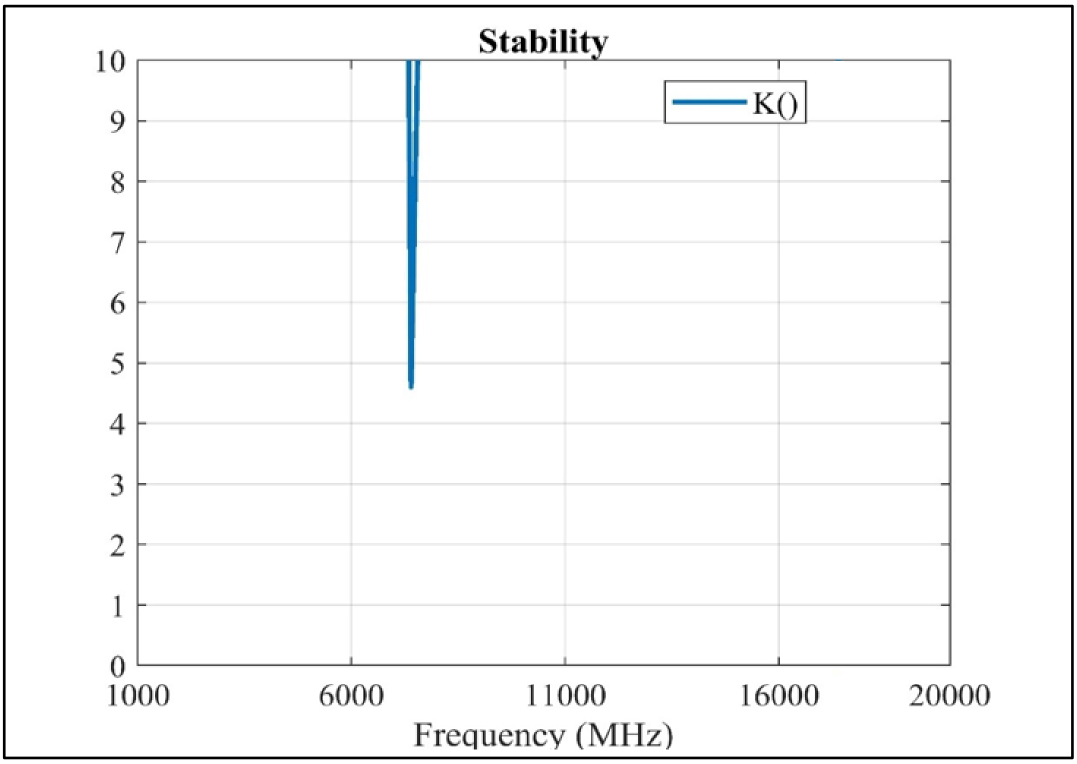

Figure 3.96. Roulette stability factor of X-Band LNA

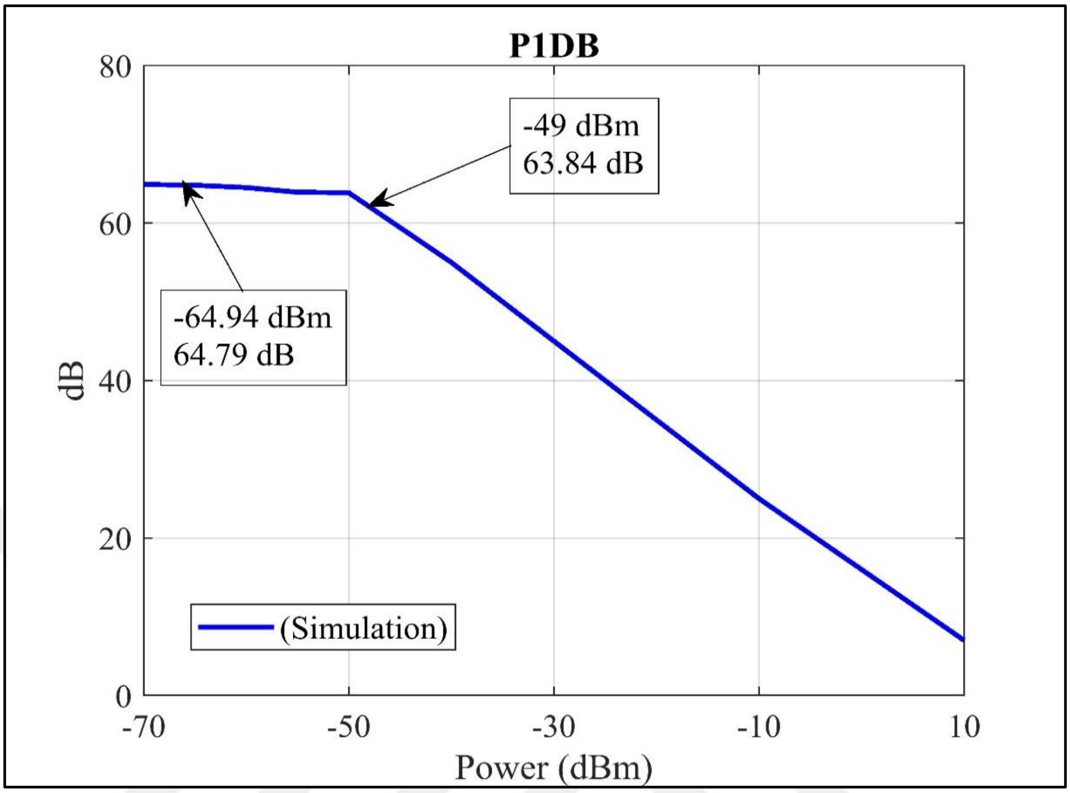

Figure 3.97. P1dB of X-Band LNA

According to the results of the thermal and electromagnetic simulations of the designed RF circuits, the mechanical design of the RF circuit boxes is made to minimize the adverse effects that may arise from thermal and electromagnetic interaction as a result of system integration. The dimensions determined in the mechanical design are considered by the boundary condition provided by the AWR program. Since the boundary condition in the AWR program can only be specified for height, height information is obtained using this condition in the mechanical box design. The product will be outdoor equipment.

In the design, the input of the X-band LNA is designed as SMA. An N-type connector is used at the output of the connector.

A three-dimensional view of the designed box is given in Figure 3.98 and Figure 3.99. Dimensions of the mechanic box to be designed for X-band LNA is shown in Figure 3.100.

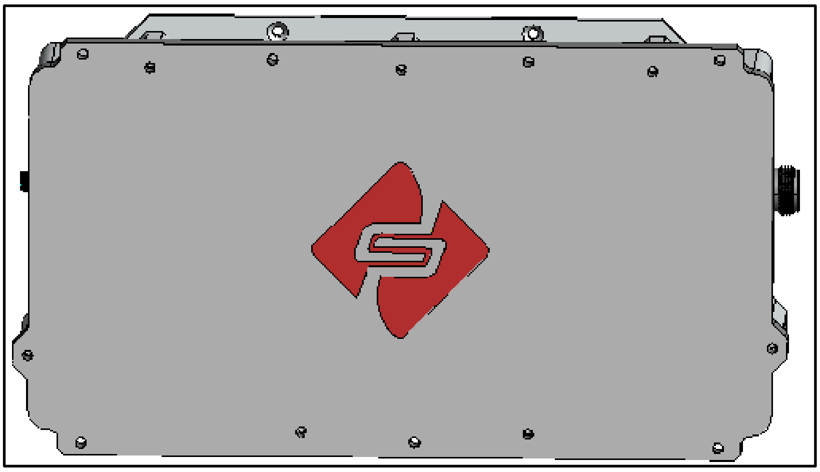

Figure 3.98. General view of X-Band LNA box

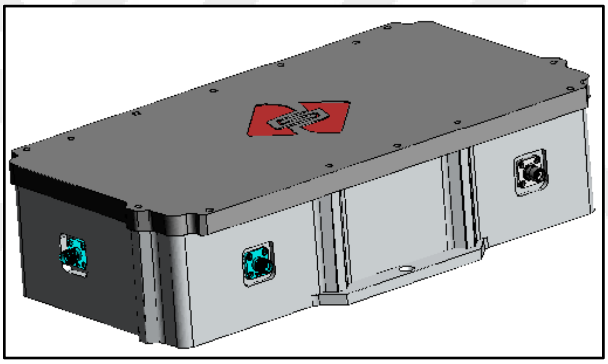

Figure 3.99. Side view of X-Band LNA box

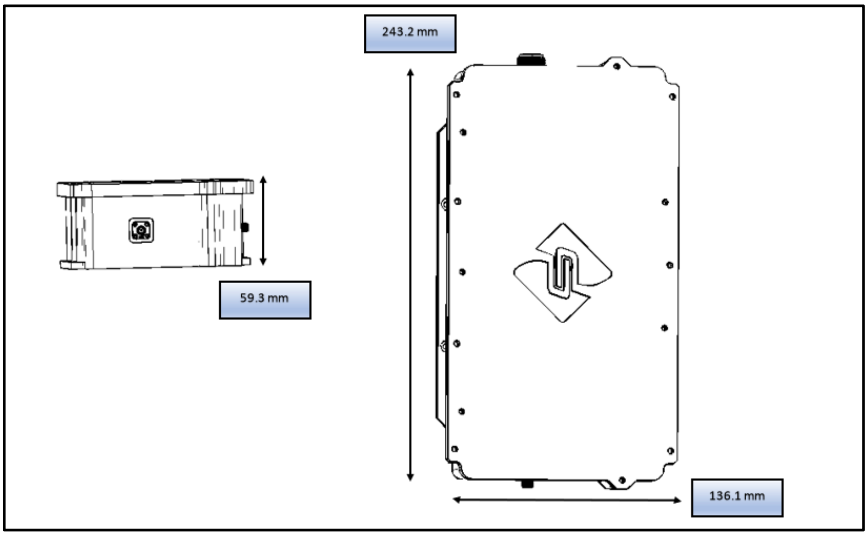

Figure 3.100. Dimensions of X-Band LNA box

3.3 X-BAND FREQUENCY CONVERTER DESIGN

The requirements that frequency converters should meet are spurious levels, gain ripples, VSWR, noise figure, output signal power level, and signal linearity. The essential working concept for these requirements is given below: In this dissertation study, the following units were designed separately. AWR software program was used in all designs.

- Generating RF block diagram and simulation
- Filter and Coupler
- X-L band circuit design
- PLL (phase-locked loop) circuit design
- Control Circuit Design
- Regulator Circuit Design

An important parameter is the image rejection level of the frequency downconverter to be used at the receiver side of the satellite communication system. This parameter is related to the characteristics of the filter to be used at the input. According to the input and output frequencies, the frequency band of the imagine frequency is calculated, and the filter is selected accordingly. X-band frequency down converter specifications are shown in Table 3.9.

The phase noise is another determining parameter for the frequency down converter. The low phase noise of the design is critical in satellite communication links where phase modulation is generally used. The level of spurious signals is also an essential parameter for the cleanliness of the signal band.

Table 3.9. X-Band frequency down converter specifications

Parameter	**Value**
Input operating frequency	8 – 8.5 GHz
Output operating frequency	720 MHz (±200MHz)
P1dB	+10 dBm
Gain adjustment step	1 dB
Input reflection ratio	15 dB

Output reflection ratio	15 dB
Local oscillator frequency	7.28 – 7.78 GHz
Local oscillator leakage	-35 dBm
image frequency suppression ratio	-50 dB
External reference oscillator frequency	10 MHz
External reference oscillator signal level	-5 ... +5 dBm
Noise factor	Max 20 dB
Phase noise	-60 dBc/Hz (@1KHz)
Feed voltage	220V AC
Input connector type	N
Output connector type	N

The block diagram of the X-band frequency down converter is given in Figure 3.101. The simulations are done in AWR simulation program using the products shown in Table 3.10. The RF and PLL parts are presented as separate design diagrams in the design. The procedure is done like this because it observes the effect of the spurious level coming from PLL.

Table 3.10. Integrated circuits used in circuit

Manufacturer	**Product part number**	**Product detail**
RFCi	RFSL2950	Isolator
MiniCircuits	ADC-10-4	Coupler
MiniCircuits	SIM-14H+	Mixer
MiniCircuits	XLF-861	Low pass filter
MiniCircuits	MNA-2W	Amplifier block
MiniCircuits	LFCN-1400	Low pass filter
MACOM	AT-106-PIN	Digital RF attenuator
MiniCircuits	LFCN-1200	Low pass filter
MiniCircuits	PHA-101	Amplifier block
MiniCircuits	LFCN-1000	Low pass filter
MiniCircuits	RDP-2R15+	Diplexer

Analog Devices	HMC3653LP3BE	Amplifier block
MiniCircuits	VLF-1500+	Low pass filter
MiniCircuits	VLF-1575+	Low pass filter

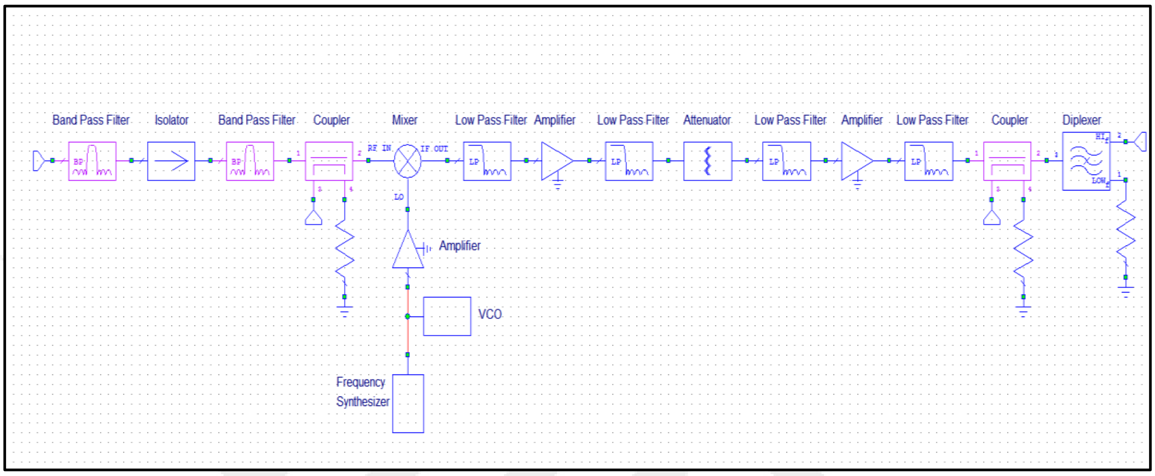

Figure 3.101. An overall diagram of the X-Band frequency down converter

The design of the Hairpin filter and coupler is realized since no suitable filter has the desired suppression level at the RF signal input port, the frequency down converter, as shown in Figure 3.101.

3.3.1 Filter and Coupler Design

In the design of the X-band frequency down converter system, band pass filter, isolator, and band pass filter are used at the input of the RF block diagram given in Figure 3.101. These filters are not integrated filters but designed within Profen. These filters are "Hairpin" filters operating in the frequency range of 8-8.5 GHz, and their design is shown in Figure 3.102. The aim is to keep the image rejection value at the value in the technical specification. The mixer generates image frequencies. While an RF signal source drives the mixer, the oscillator signal from the LO (Local Oscillator) port and the harmonics obtained at the output port are observed. When a mixer is used for frequency amplification, the input and output ports are IF and RF.

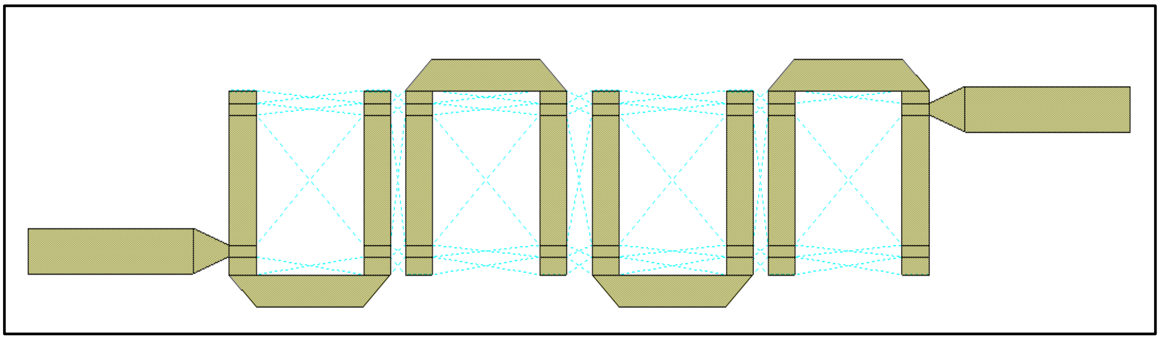

Figure 3.102. Bandpass filter design (Hairpin)

In the X-band frequency down converter system design, the coupler used at the input in the RF block diagram in Figure 3.101 is not integrated. The 10 dB directional coupler design in the 8-8.5 GHz range is shown in Figure 3.104. Thanks to the couplers used at the input and output, input and output sampling data are received and processed. Figure 3.105 shows the results of the designed coupler.

The three-dimensional layout of the RF design circuit is shown in Figure 3.106. The design simulations are obtained by making integrated connections with input and output matching circuits. At the input of the circuit, the Hairpin bandpass filter shown in Figure 3.102 is used, followed by an isolator operating at X-band frequency and again a Hairpin filter with the same characteristics as the bandpass filter at the input. Figure 3.103 shows the S parameters of the filter. The aim here is to suppress the image frequencies. Image frequencies fall in the 6.56 – 7.06 GHz range in the X-band frequency down converter system. A cascade design is applied to suppress this frequency range in the filter design. After the bandpass filter, the signal passes through a directional coupler and reaches the mixer.

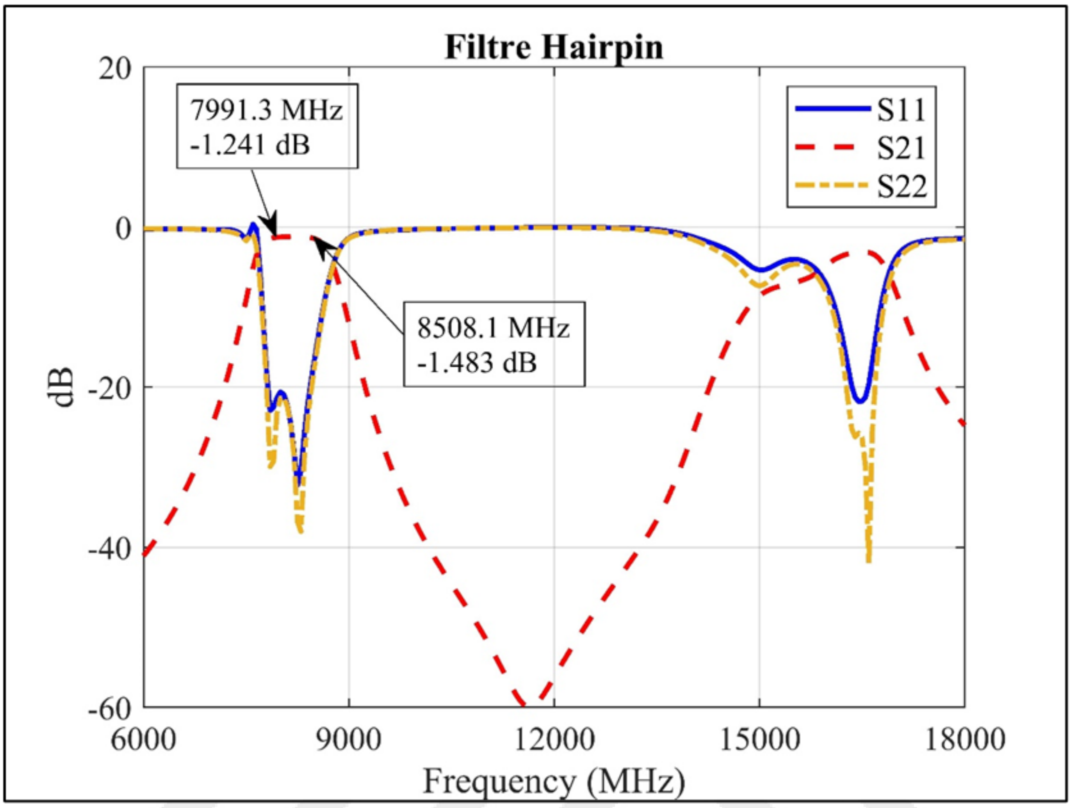

Figure 3.103. Bandpass filter simulation result

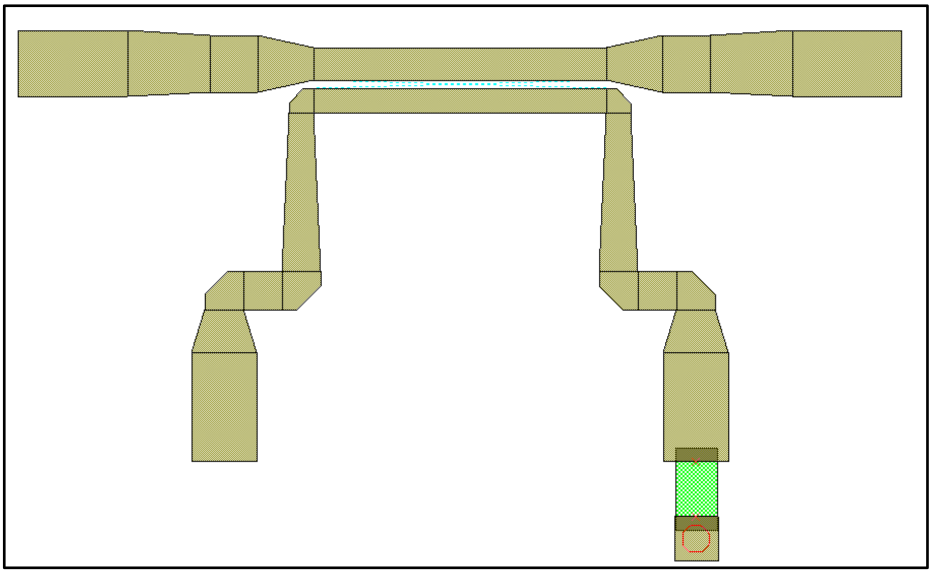

Figure 3.104. Directional coupler design

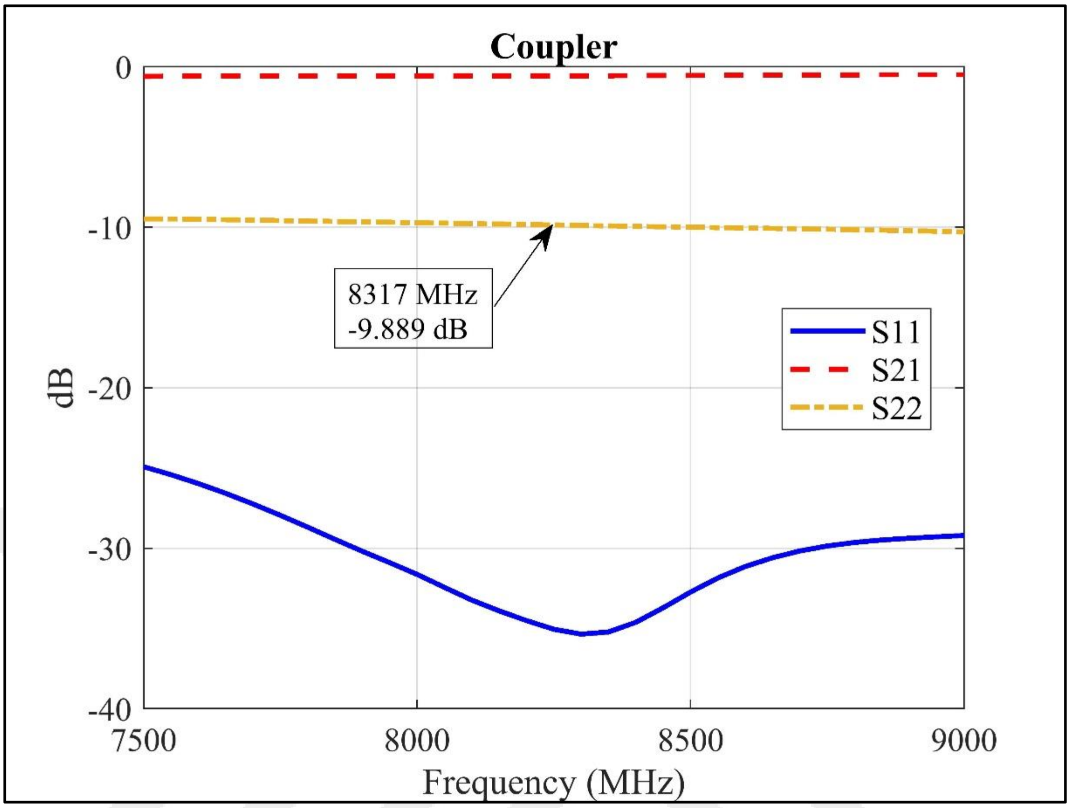

Figure 3.105. Directional coupler simulation result

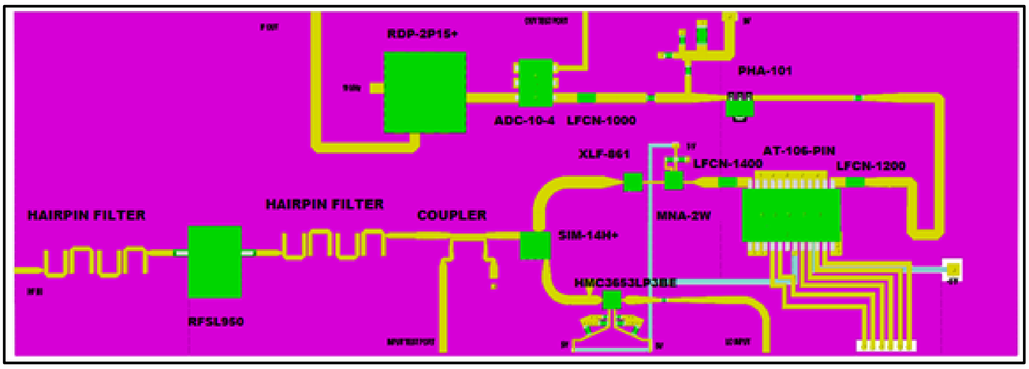

Figure 3.106. The RF layout of the X-Band frequency down converter layout

The signal level at the input of the mixer should be less than 10 dB than the local oscillator signal. The expected signal level at the LO input of the mixer is +7 dBm. Therefore, the IF input of the mixer should be at most -7 dBm. The mixer receives a 7 dBm signal from the PLL part. The LO power value of the selected mixer is +14 dBm. A buffer amplifier is used in the LO section to operate the mixer. The desired LO power is provided for the mixer with the amplifier used. A reflectionless low-pass filter suppresses the harmonic and spurious signals generated after the mixer. After the filtering process, the signal is amplified with the MNA-2W. After the amplification process, a low-pass filter suppresses the harmonics. MACOM AT-106-PIN is a 6-bit digital attenuator. A microcontroller unit manages it. The digital attenuator provides a range of ±20 dB with its 6-bit and the criterion of being adjustable in 1 dB steps.

After the digital attenuator, the RF signal is passed through a low pass filter and then amplified with the PHA-101. The RF signal is fed to the directional coupler, where a 720 MHz center frequency signal is generated at the upper-frequency output of the diplexer. At the lower frequency output, 10 MHz external signal output is received. 10 MHz external signal output is used for VCO. An N-type connector is used at the input and output ports, and the impedance value is 50 Ohm.

3.3.2 PLL Design

As shown in Figure 4.7, the phase-locked loop circuit mainly consists of a phase sensor, load pump, filter, voltage-controlled oscillator, and N-divider.

With the developing integrated circuit technologies, phase sensors, frequency dividers, and load pumps can be designed as integrated on the PLL Synthesiser IC. As a result, in addition to dimensional gain, phase noise performance has also been improved. These combiners (Synthesizers) are divided into two categories as integer and fractional. For example, In integer combiners, the N value shown in Figure 3.107 can be integer numbers such as 200 and 201. In fractional combinators, these values can be 200.4 and 205.3. Both types of combiners have profits and losses on each other. Fractional combiners can achieve higher phase sensor frequencies for a given output frequency, which reduces phase noise and improves signal quality. However, at the same time, they generate unwanted signals (spurious) at considerably higher levels than integer combiners, which is one of the most severe drawbacks of fractional combiners.

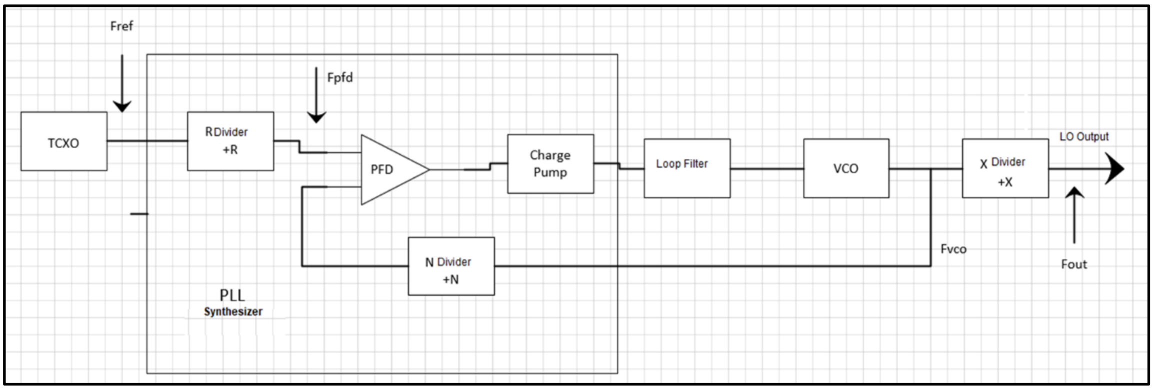

Figure 3.107. The block diagram of a phase-locked loop circuit

Table 3.11. IC components to be utilized in PLL design

Manufacturer	**Product part number**	**Product detail**
Analog Devices	HMC508LP5	VCO
Analog Devices	HMC703LP4E	PLL
Analog Devices	HMC860LP3E	Voltage regulator
Analog Devices	HMC976LP3E	Voltage regulator
IQD	CFPT-9301	TCXO

The design of the active filter is carried out with the simulation and analysis software provided by the company (Analogue Devices) for which the combiner is designed.

Again, the structure in Figure 3.107 is analyzed with the help of the phase-locked loop circuit design program written by the company for which the combiner is designed. Also, the IC components used in the PLL design is listed in Table 3.11.

The value of -60dBc/Hz at 100Hz is expected to be obtained in the project output. However, it is calculated as -64dBc/Hz due to the analysis of the currently designed circuit. This value is better than the value targeted in the project output. The agreement between the analysis and reality will be questioned by producing the design through the printed circuit and making the necessary measurements. The three-dimensional version of the phase-locked loop circuit board planned to be fabricated is given in Figure 3.108.

The board design given in Figure 3.108 is made in four stages. The reference oscillator design, which will be discussed in the next section, is also on this board. The design is made on the AWR program. Coplanar waveguide technology is used in the high-frequency lines of the design. Since the high-frequency terminals of the chips used in the design are matched to 50 ohms, no matching circuit is designed. On some lines, especially on the feedback lines, there are attenuator designs for the desired power values of the chip leads. Decoupling capacitors are used when it is necessary. The regulator circuits required for the chips are also placed on the board. Burried via circuits are used on the board, providing passing options between interstage layers.

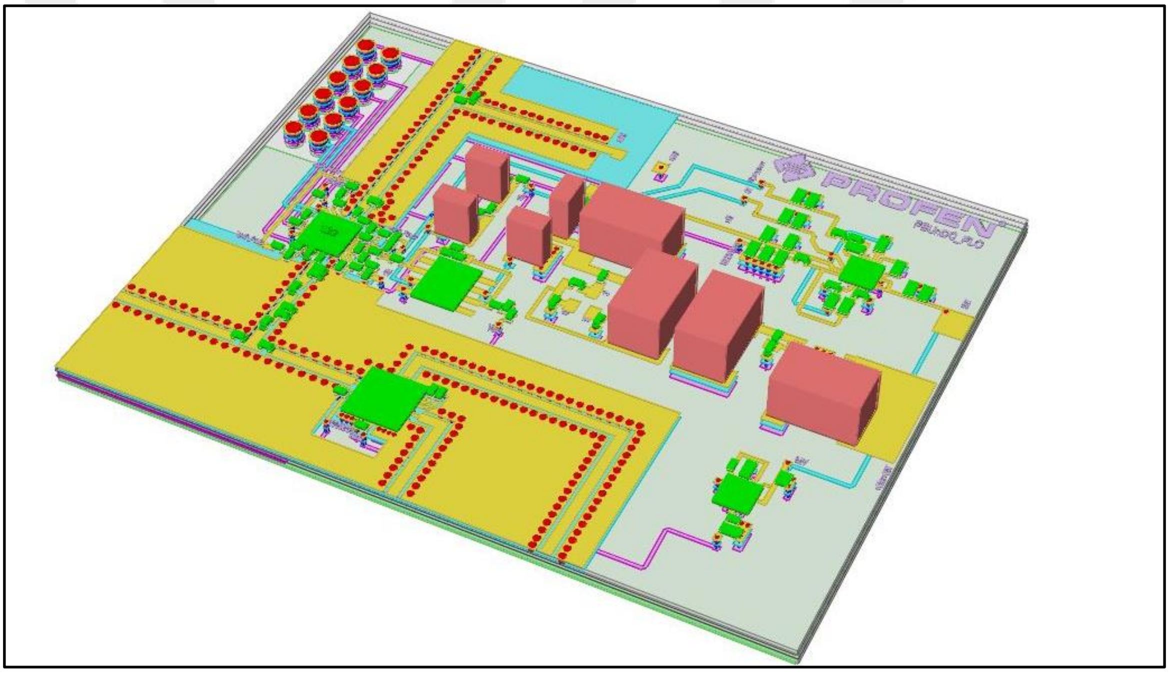

Figure 3.108. 3D design of the phase-locked loop circuit and reference oscillator card on the AWR

The crystal oscillator features decided and researched for the design are given below.

- Temperature tolerance (TXCO/ VCTCXO)
- 10 MHz output frequency
- Low phase noise
- Square wave as output signal characteristic
- Tristate

In light of the specifications mentioned above, a crystal oscillator is found. The phase noise characteristic is considered in Figure 3.108 in the design analysis part of the phase-locked loop circuit design section. Again, as mentioned in the PLL design section, the reference oscillator and PLL design are realized on the same circuit. TXCO, selected as the internal frequency source, has a frequency stability of ± 1 ppm and a maximum wear-out of ± 1 ppm/year.

3.3.3 Regulator Circuits

The regulator circuit converts the 220V AC power signal from the input to 24 V DC value with the LRS-100-24 coded power supply of the Mean Well. With the regulator card used in the system, a 24 V DC voltage value is used for the frequency down converter. The 24V DC output from here is connected to the linear LDO (Low-Dropout Regulator). The 24V coming to the LDO circuit is converted into 5V, 5.5V, 15V, 9V, -5V, 12V, 3.3V, and -2V and supplies other circuits. Figure 3.109 shows the 24V input of the circuit and the DC voltage outputs and Table 3.12 shows the integrated circuits in the regulator design.

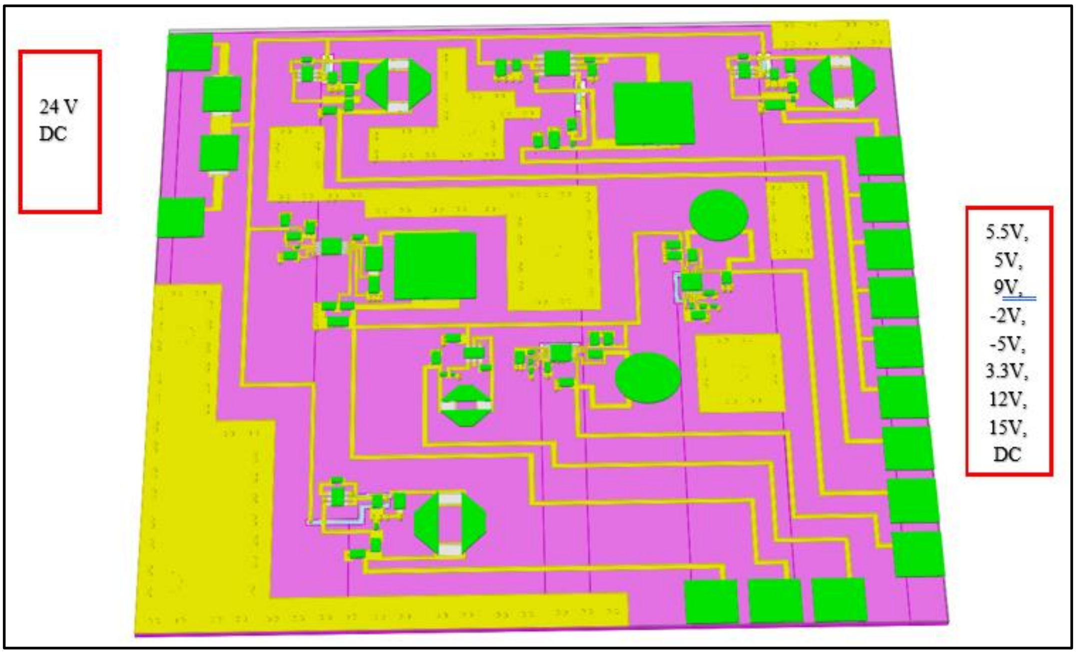

Figure 3.109. 24V input voltage and DC voltage outputs

Table 3.12. Types of components to design regulator card

Manufacturer	Product Number	Product Detail
Texas Instruments	LMR14010A	Voltage Regulator
Texas Instruments	LMR33630A	Voltage Regulator
Texas Instruments	LM25011	Voltage Regulator
Texas Instruments	TPS561208	Voltage Regulator
Texas Instruments	TPS63710	Voltage Regulator
Texas Instruments	LMR14006Y	Voltage Regulator

3.3.4 Merging of Assemblies of the Frequency Down Converter

The active RF products used in the overall block diagram given in Figure 3.101 need a DC supply. The DC voltage card shown in Figure 3.109 is designed, and all units are fed through this card. The input frequency range of the designed X-band frequency down converter system is between 8-8.5 GHz. The output frequency band is at 720 MHz center frequency with +-200 MHz bandwidth.

According to the X-band frequency down converter design simulation results, the in-band gain value for LO power 7 dBm is shown in Figure 3.110 and Figure 3.111 for LO frequency 7280 MHz and 7780 MHz, respectively. According to the simulation results, the loop gain in the operating band is 14 dB.

Figure 3.112 shows the image rejection graph of the frequency down-converter. When the image rejection frequencies of the mixer are calculated, the frequency band 6560 - 7060 MHz is where the image frequencies are located. The 50 dB value given in the technical specification is met according to the simulation result. A cascade band-pass filter of our design is used where the RF input is located to obtain this result. Thus, a value even lower than the desired value is obtained.

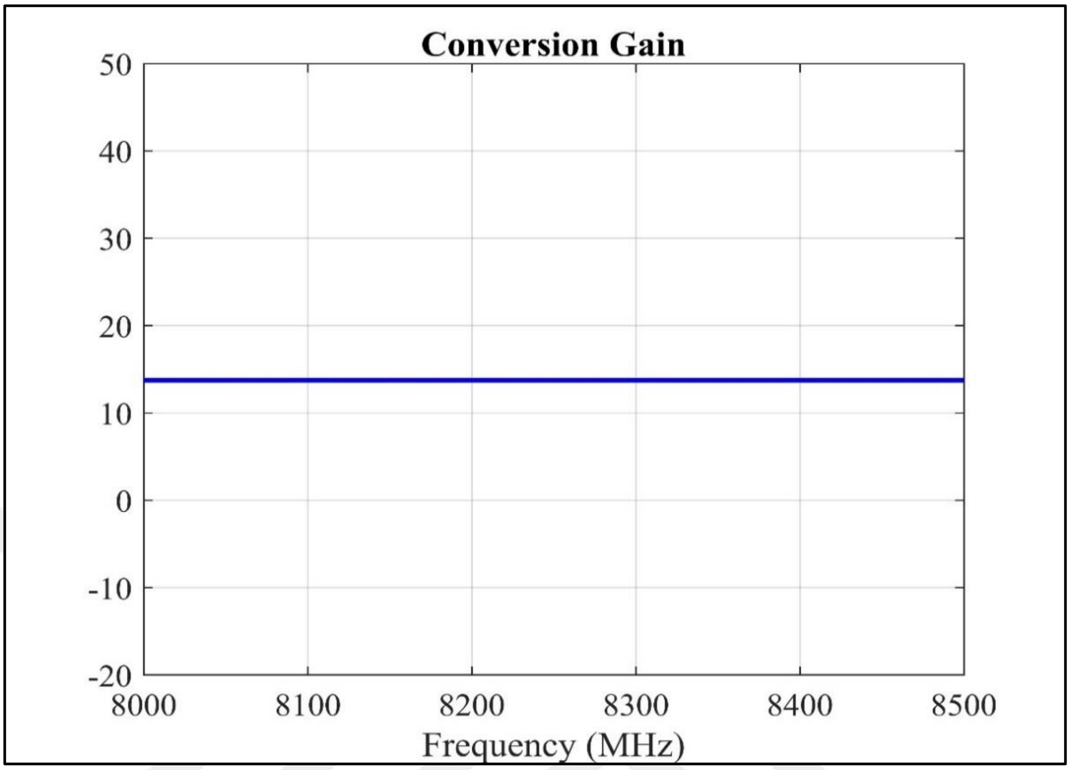

Figure 3.110. In-band loop gain LO:7780 MHz

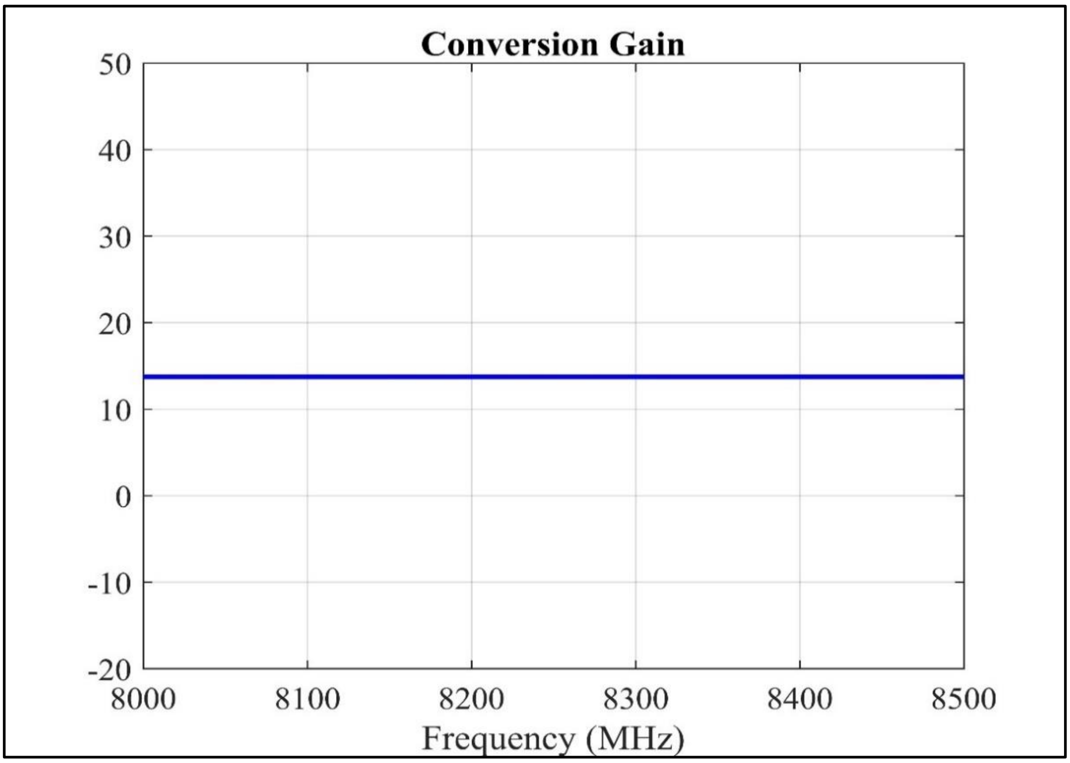

Figure 3.111. In-band loop gain LO: 7280 MHz

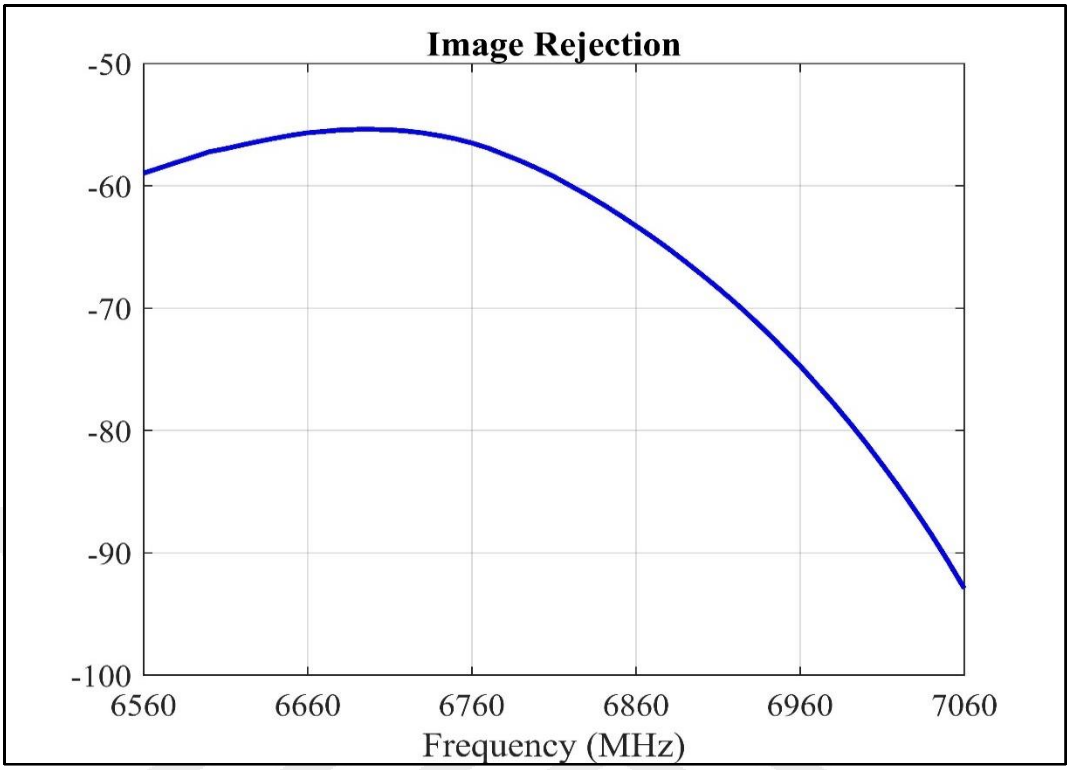

Figure 3.112. Image rejection

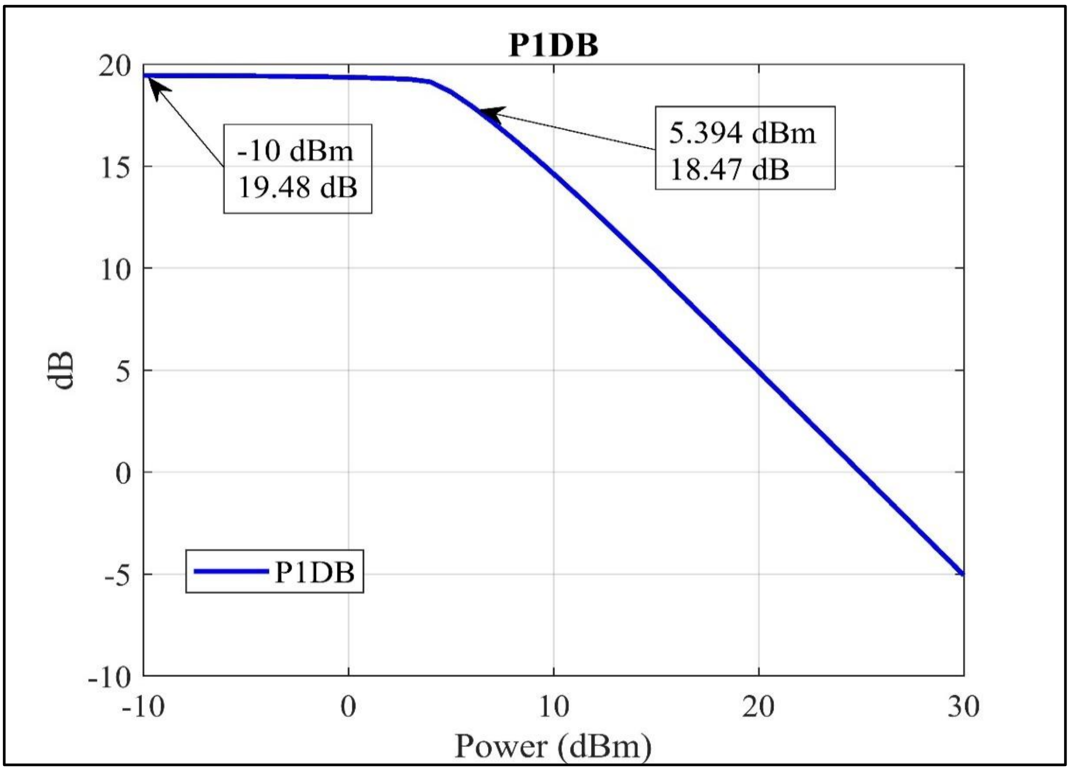

Figure 3.113. P1dB

The P1dB point of the system, shown in Figure 4.14, is +23.6dBm, and it meets the requirements in the technical specification.

Figure 3.114 shows the nonlinear noise factor plot of the X-band frequency downconverter system. The noise figure of the RF design circuit is below 19.6 dB. It meets the maximum noise factor value in the technical specification.

Figure 3.115 shows the in-band and out-of-band spurious signals when the input power is given at -20 dBm. In the given graph, the spurious level is below -63 dBm when LO is at 7280 MHz frequency. Since the X-band frequency down converter will be directly on the communication line, the spurious level becomes more critical. The simulation result suits in-band, out-of-band, and LO leakage levels. In the same case, in the graph in Figure 3.116, when LO is at 7780 MHz frequency, the spurious level is below -78 dBm, both in-band and out-of-band. According to the simulation results, the phase noise value from the PLL is also below -60 dBc.

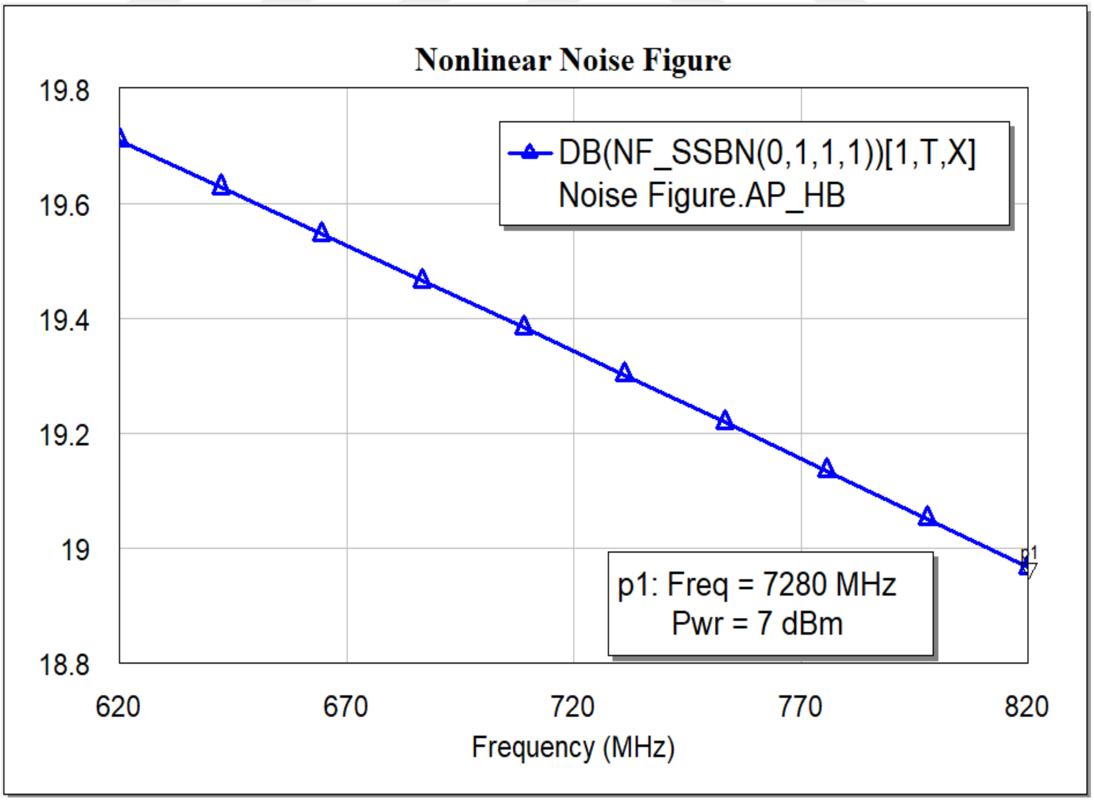

Figure 3.114. Noise factor

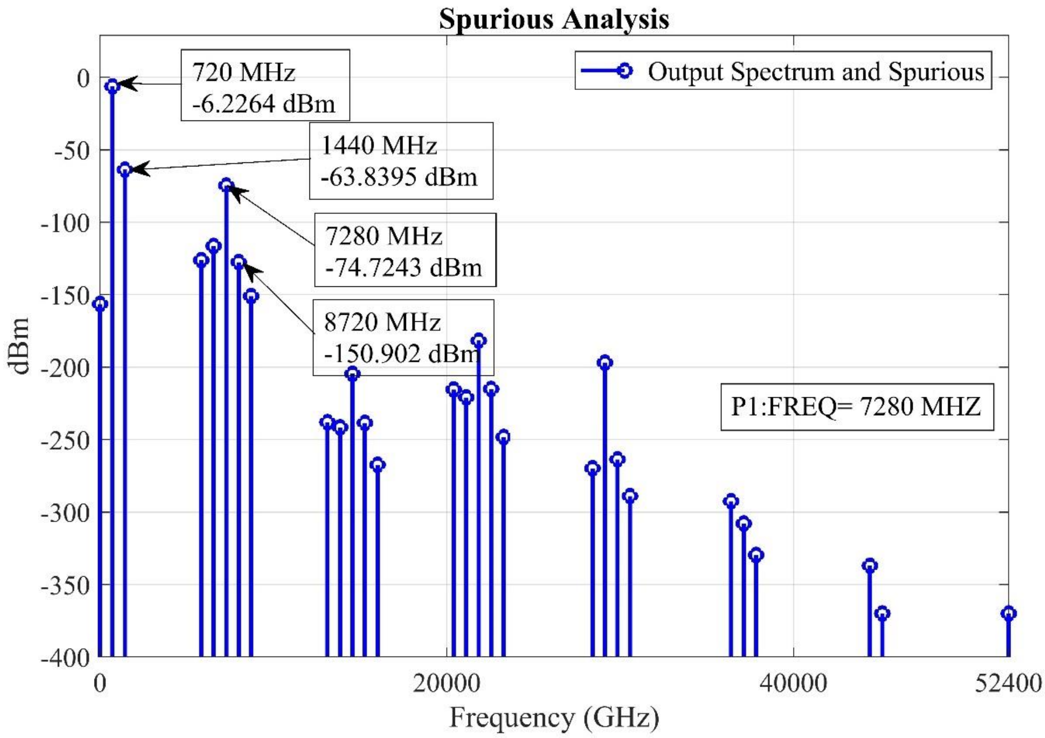

Figure 3.115. Single harmonics at the input and spurious signals LO: 7280

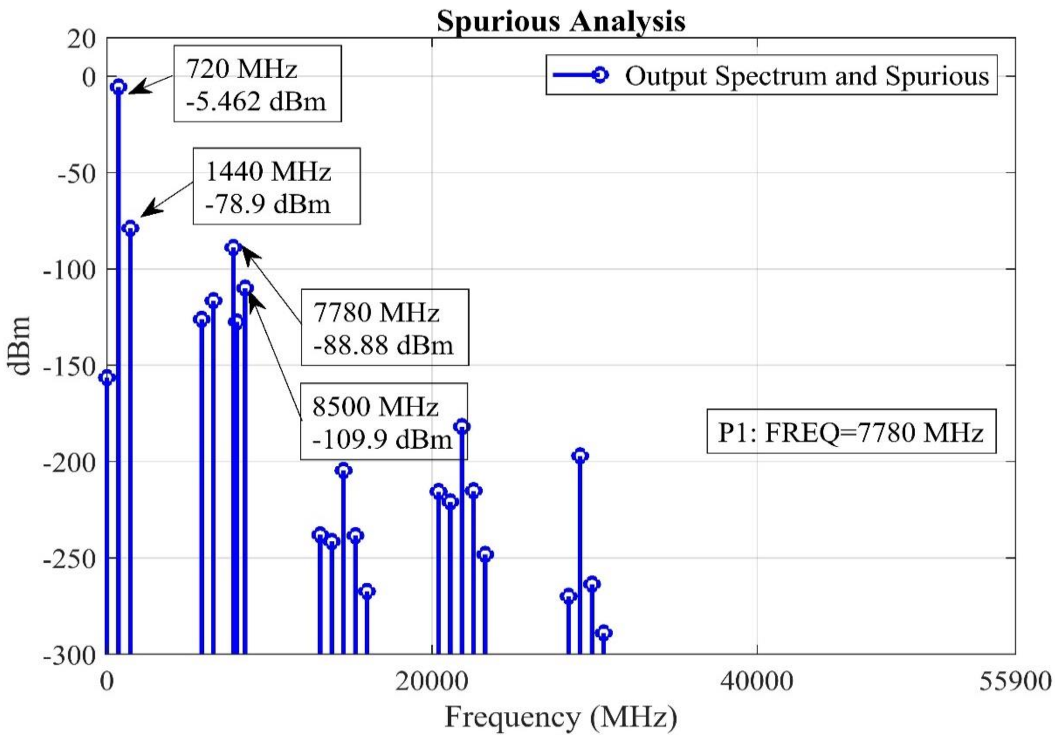

Figure 3.116. Single harmonics at the input and spurious signals LO: 7780

In the graphs given in Figure 3.117 and Figure 3.118, the input and output return loss are below -15 dB. It meets the minimum value given in the technical specification.

The X-band frequency down converter system uses couplers at the input and output. Thanks to these couplers, the input and output frequency will be monitored and adjusted. The microcontroller circuit will manage the RF log detector at the coupling end of the coupler. The gain will be monitored and adjusted by using a 6-bit digital attenuator. The microcontroller circuit can also adjust the digital attenuator in 1 dB steps between the desired ±20 dB. The RF output cancellation feature is a process that can be done by cutting the regulator used. This process can be intervened through the microcontroller using the digital attenuator.

In the overall block diagram given in Figure 3.101, the interface is added after the entire layout is formed. Because both the input frequency is variable and the gain level is desired to be adjustable, controlling it with an Ethernet interface in the ground station system is necessary. Therefore, the interface design is made for the device. The hardware information of the design is given below.

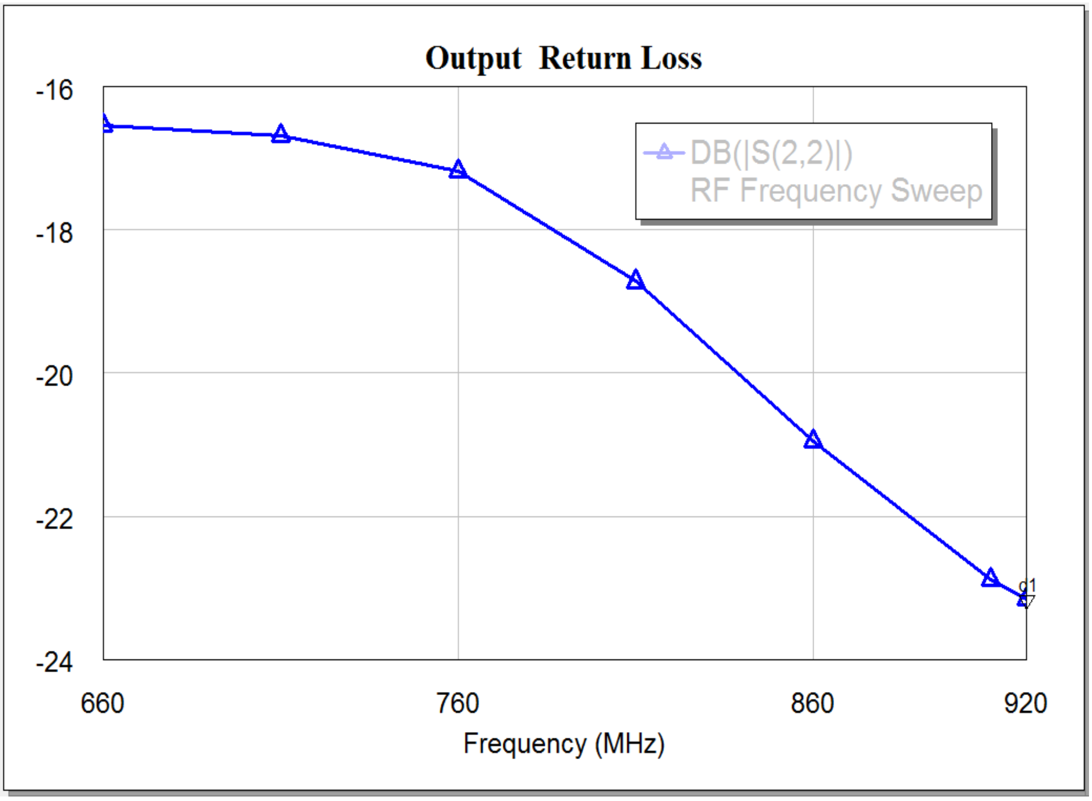

Figure 3.117. Input return loss

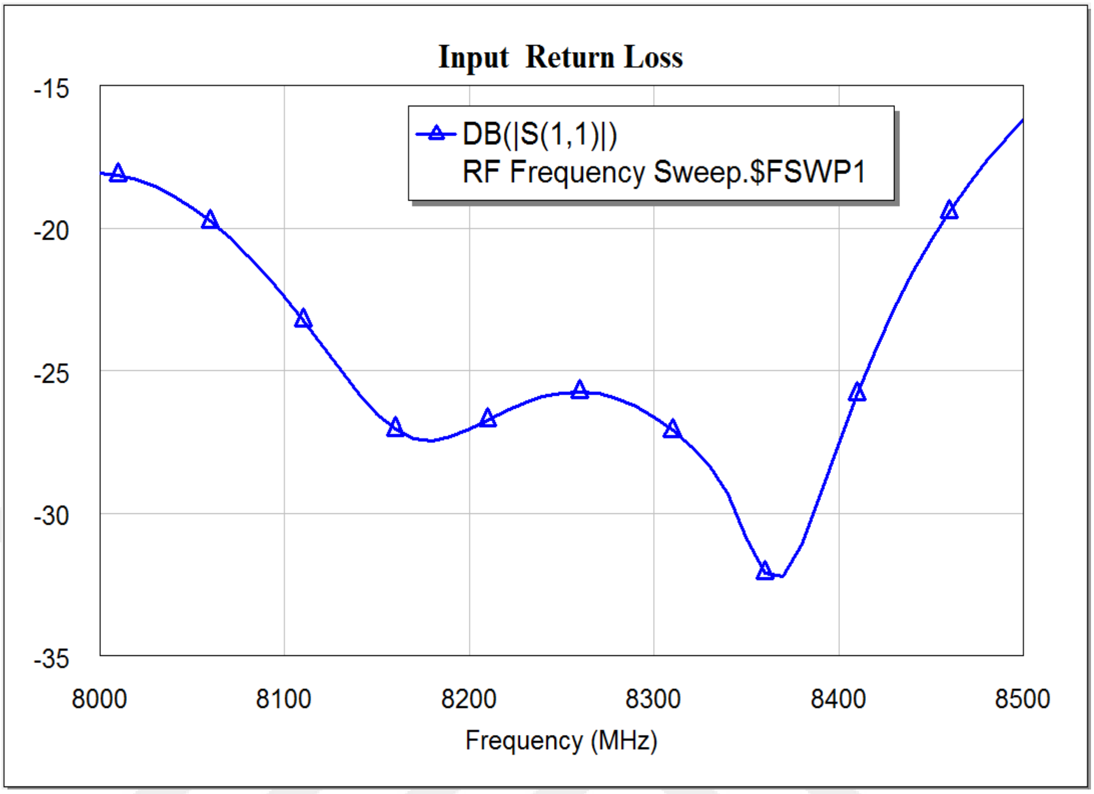

Figure 3.118. Output return loss

In the software design of the frequency down converter, the control work of the frequency down converter will be done with Nucleo-F429ZI.

Nucleo-F429ZI X-band frequency down converter circuit tasks:

- Adjusting the attenuation amounts of the RF digital attenuator,
- Measuring the power level with the analog output of the RF Log power detector,
- Making SPI (Serial Peripheral Interface) communication with a phase-locked loop synthesizer,
- Setting the operating sequence of switching power supplies,
- To control RF Mute Mode.
- Sending power and attenuation information on the circuit to different circuit boards via serial communication.

According to the results of thermal and electromagnetic simulations of the designed RF circuits, the mechanical design of the RF circuit boxes has been made to minimize the negative effects that may arise from thermal and electromagnetic interaction due to system integration. The product will be outdoor equipment.

Figure 3.119 and Figure 3.120 show the images of the front and back panels of the designed mechanical box designed on Solidworks. The frequency down converter will be mechanically enclosed in a Rack type 2U box.

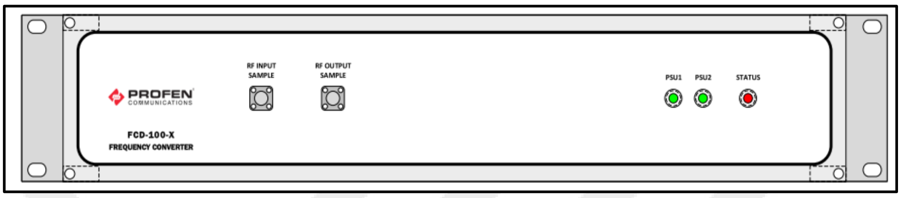

Figure 3.119. The front panel view of X-Band frequency down converter box design

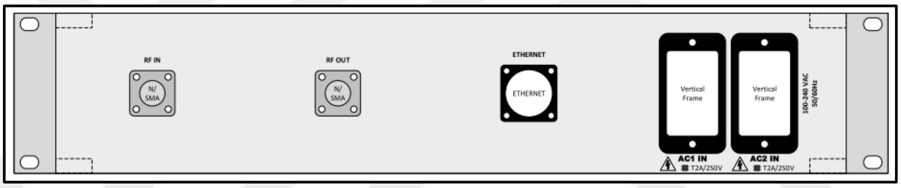

Figure 3.120. The back panel view of X-Band frequency down converter box design

4. EXPERIMENTAL RESULTS

4.1 MEASUREMENT RESULT OF X-BAND FEED ANTENNA

While Figure 3.27 shows the completed version of the X-band feed antenna, Figure 4.1 shows its fabricated form. Here, RF measurements of the X-band feed antenna are performed in an anechoic chamber in the Profen R&D laboratory. The measurements are tested at 8 GHz, 8.25 GHz and 8.5 GHz frequencies. The X-band feed antenna is placed on a motion pedestal in the anechoic chamber tests. On the opposite side of the pedestal, a reference antenna with a known gain, frequency range, cross-polarization value, and input reflection value, shown in Figure 4.2, is placed in a line of sight. It is noted that the reference antenna is required to have the same polarisation as the proposed antenna. After the placement, the X-band feed antenna, which Profen manufactures, is moved in azimuth and elevation on the movement pedestal. Patterns are realised with the spectrum analyzer, as shown in Figure 4.3.

Firstly, the feed antenna's VSWR is measured. The comparison of the measurement and simulation results is given in Figure 4.4. The radiation pattern showing the antenna gain and side lobe levels of the feed antenna is analyzed, and the measurement and simulation results of the antenna are shown in Figure 4.5. The cross-polarization measurement of the feed antenna is illustrated in Figure 4.6.

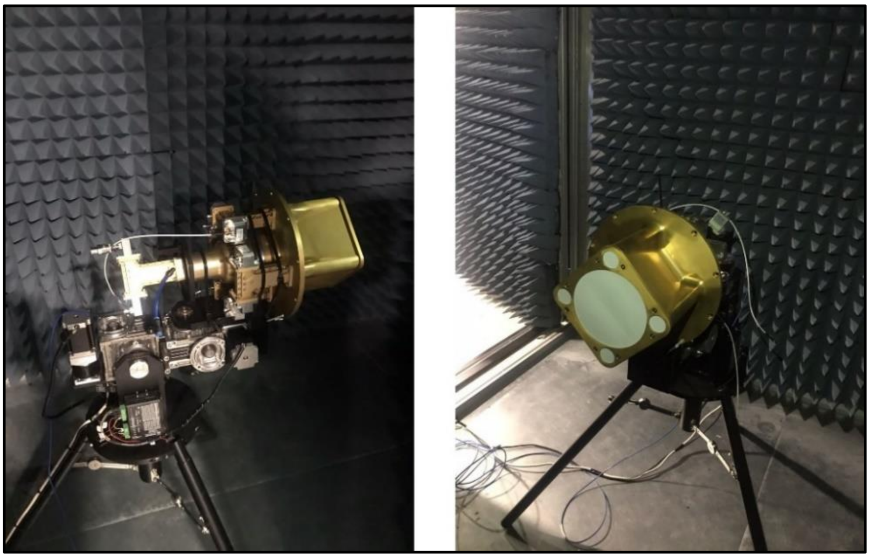

Figure 4.1. The measurement setup of the feed antenna

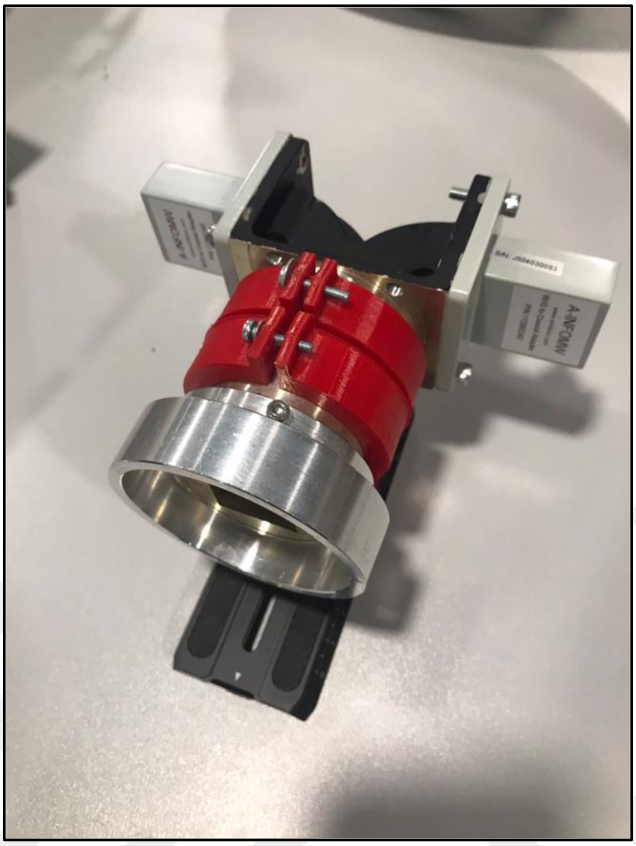

Figure 4.2. The fabricated reference antenna

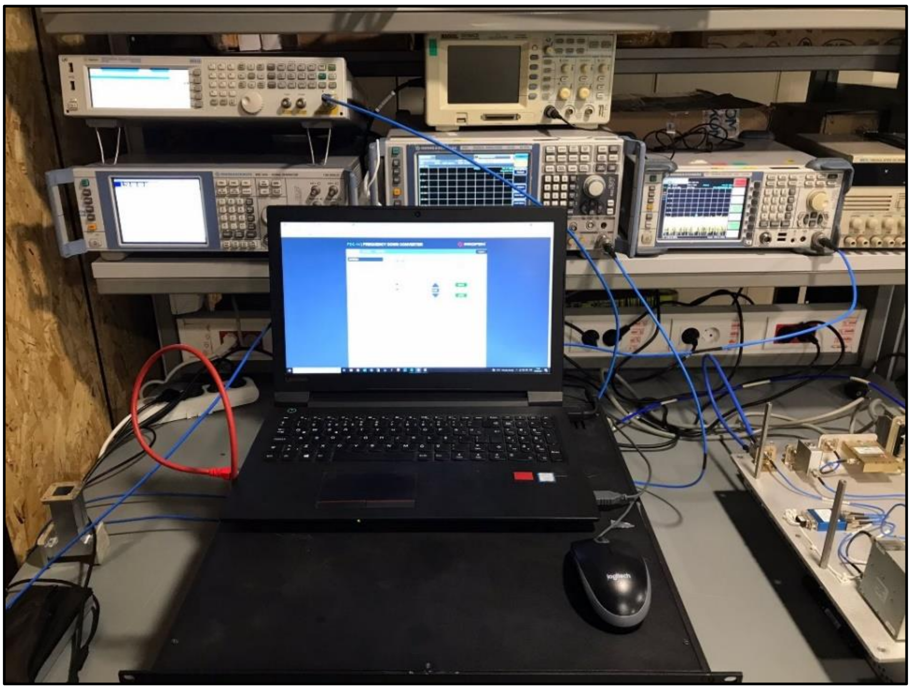

Figure 4.3. The control panel of the measurement

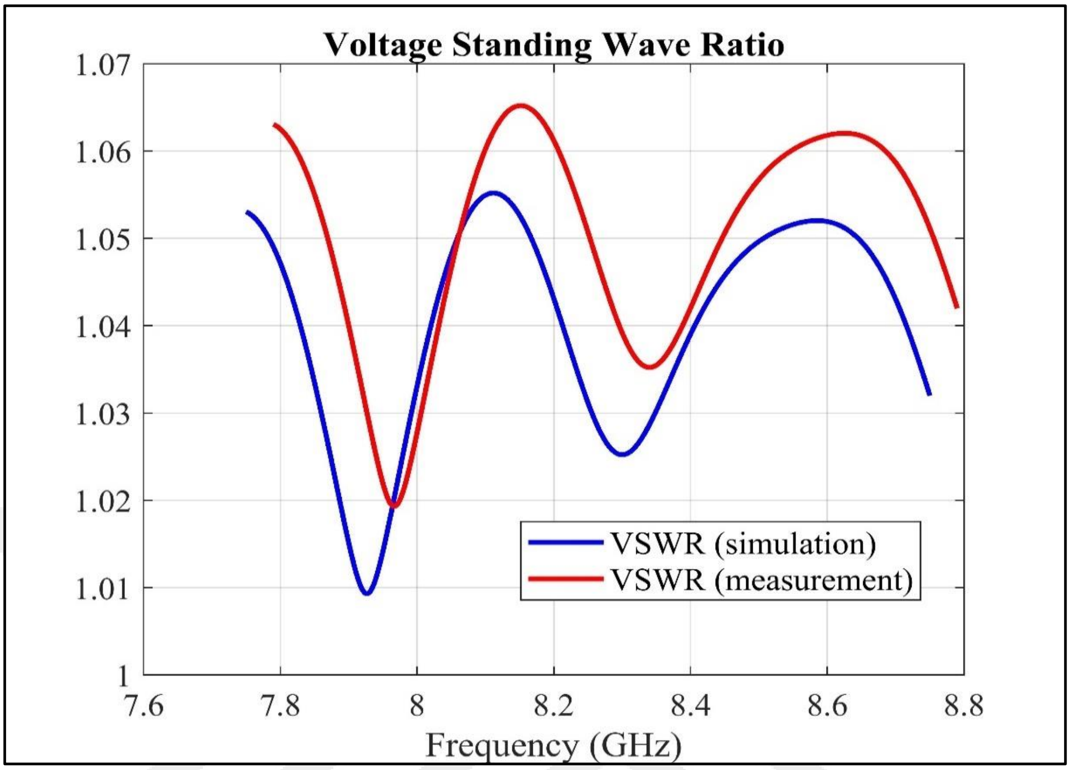

Figure 4.4: Measurement and simulation results of VSWR the feed antenna

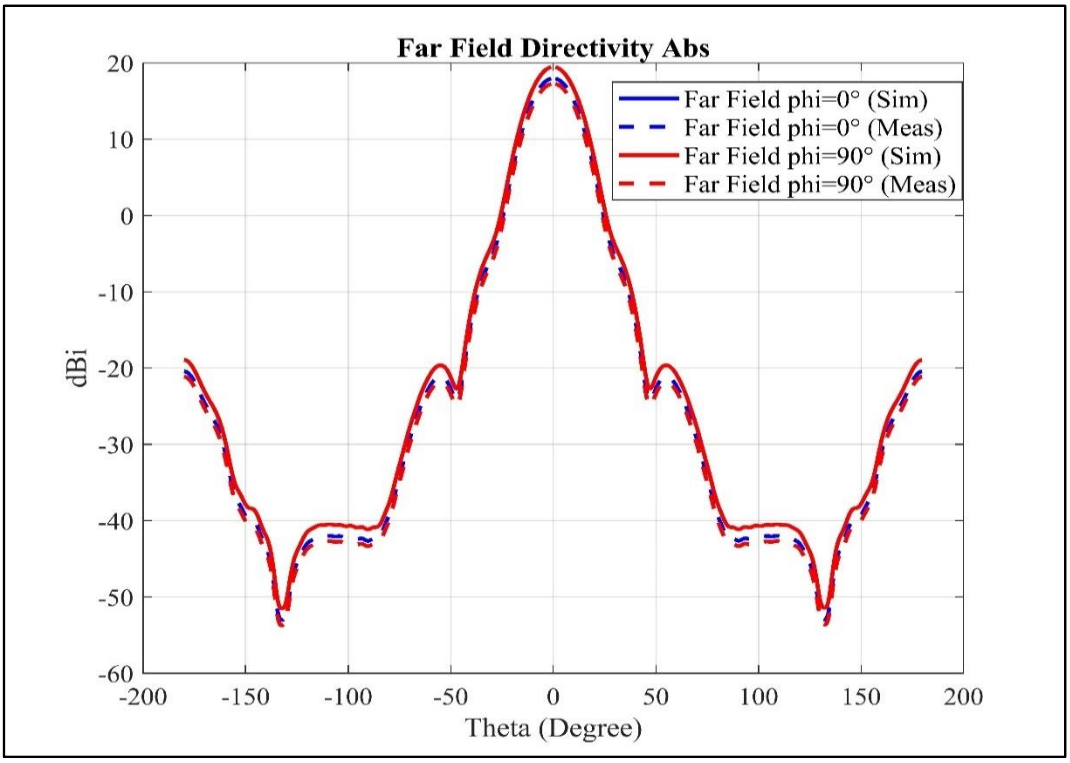

Figure 4.5. Measurement and simulation results of the radiation pattern of the feed antenna

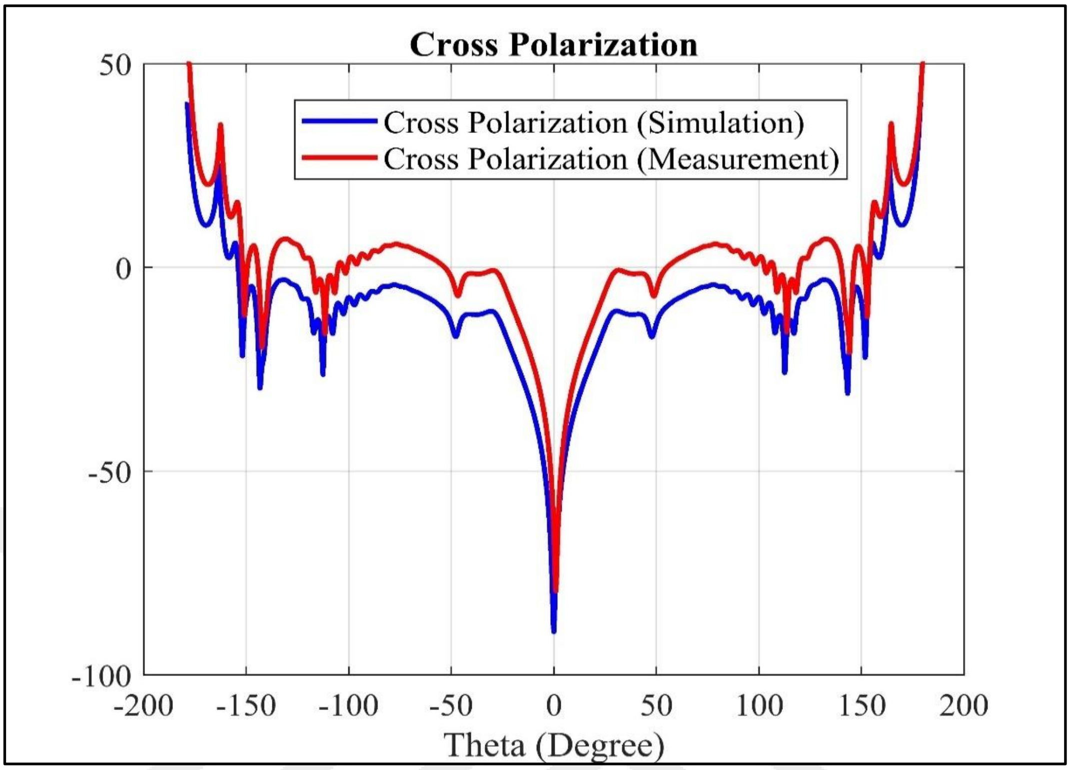

Figure 4.6. Measurement and simulation results of the cross-polarization of the feed antenna

In the monopulse unit, the VSWR of the ports is analyzed. Figure 4.7 shows the measurement and simulation results of the VSWR of the monopulse ports. In addition to VSWR, port isolations are simulated and measured (Figure 4.8). Then, the feed antenna is added to the monopulse unit. The radiation pattern of this combination at 8.25 GHz is shown in Figure 4.9. In the septum polarizer design, the port isolation measurement is first analyzed. Figure 4.10 shows the measurement and simulation results of the insertion loss of the septum polarizer ports. Also, the return loss measurement of the first and second ports of the septum polarizer is shown in Figure 4.11. The isolation between linear ports of the septum polarizer is shown in Figure 4.12. Finally, all unit of the feed system is combined. Firstly, VSWR measurement is achieved for all ports (Figure 4.13). The radiation pattern of the system for phi= 0° and phi=90° are demonstrated in Figure 4.14 and Figure 4.15, respectively. Also, Figure 4.16 and Figure 4.17 demonstrates the total gain of the corrugated horn antenna and the difference pattern of the corrugated horn antenna, respectively.

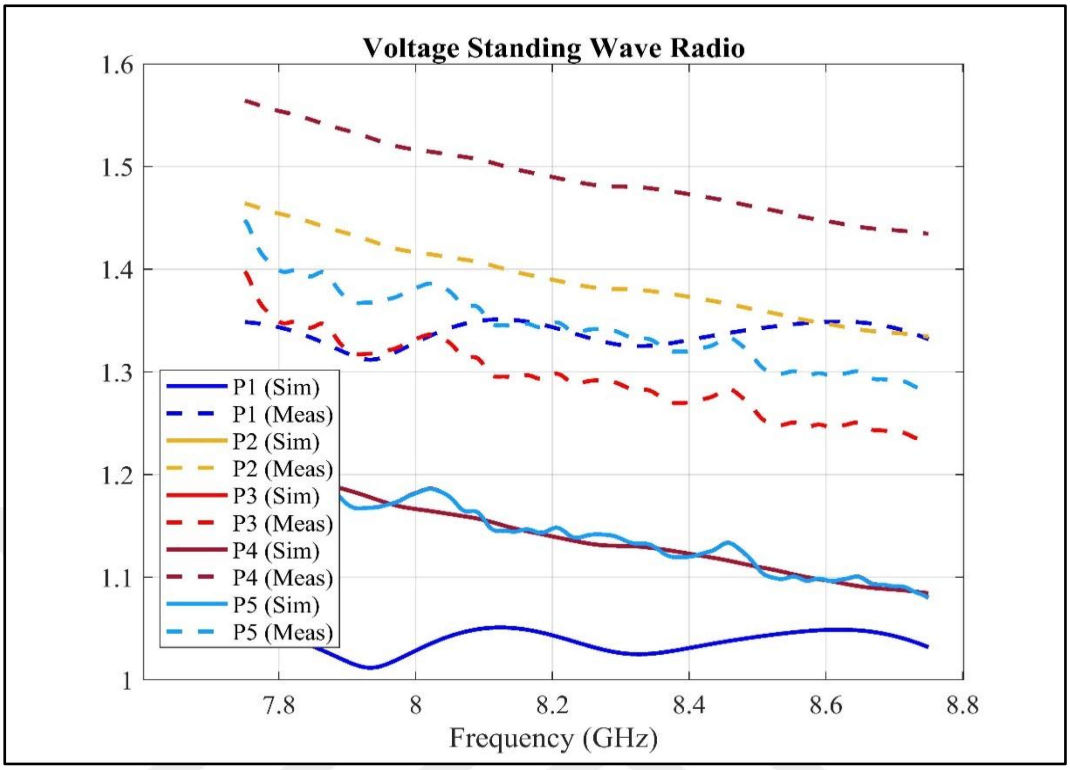

Figure 4.7. VSWR for all ports

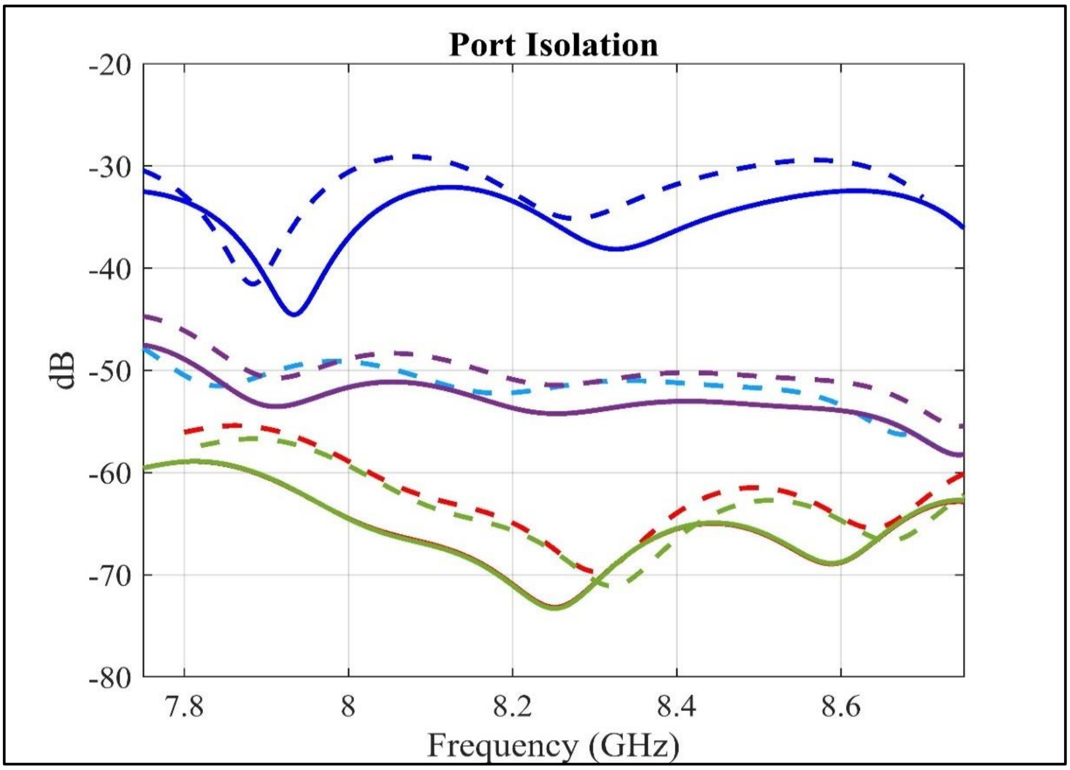

Figure 4.8. Measurement and simulation results of the port isolations of the monopulse unit

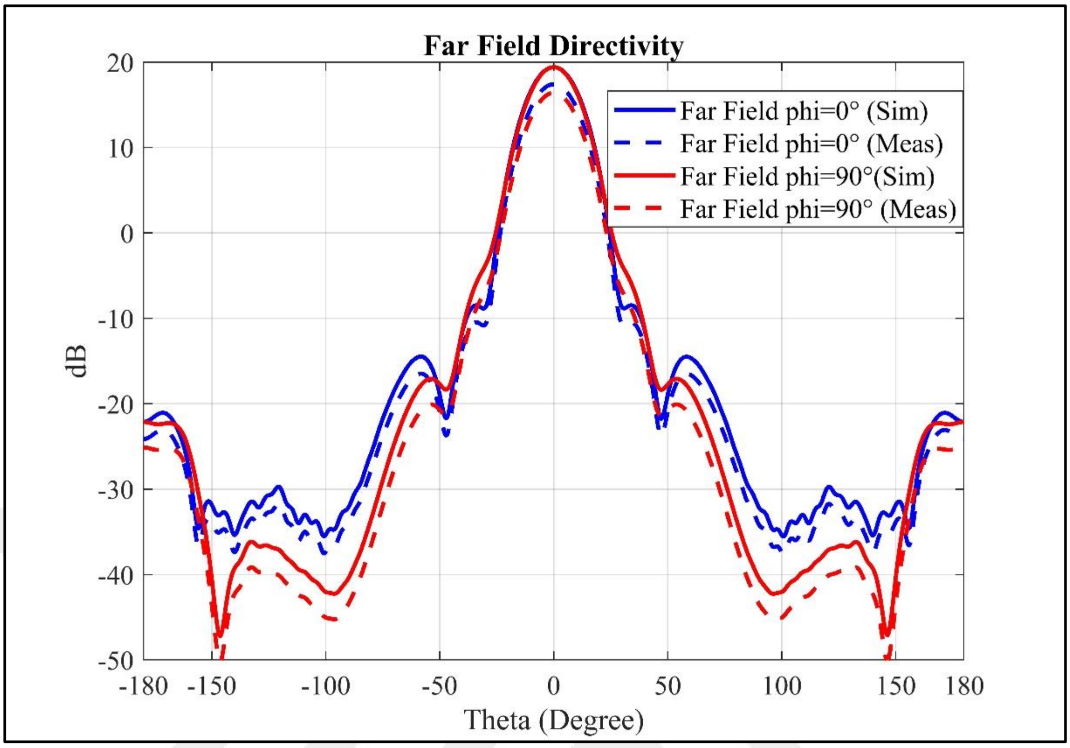

Figure 4.9. Measurement and simulation of the radiation pattern of the feed antenna and monopulse unit at 8.25 GHz

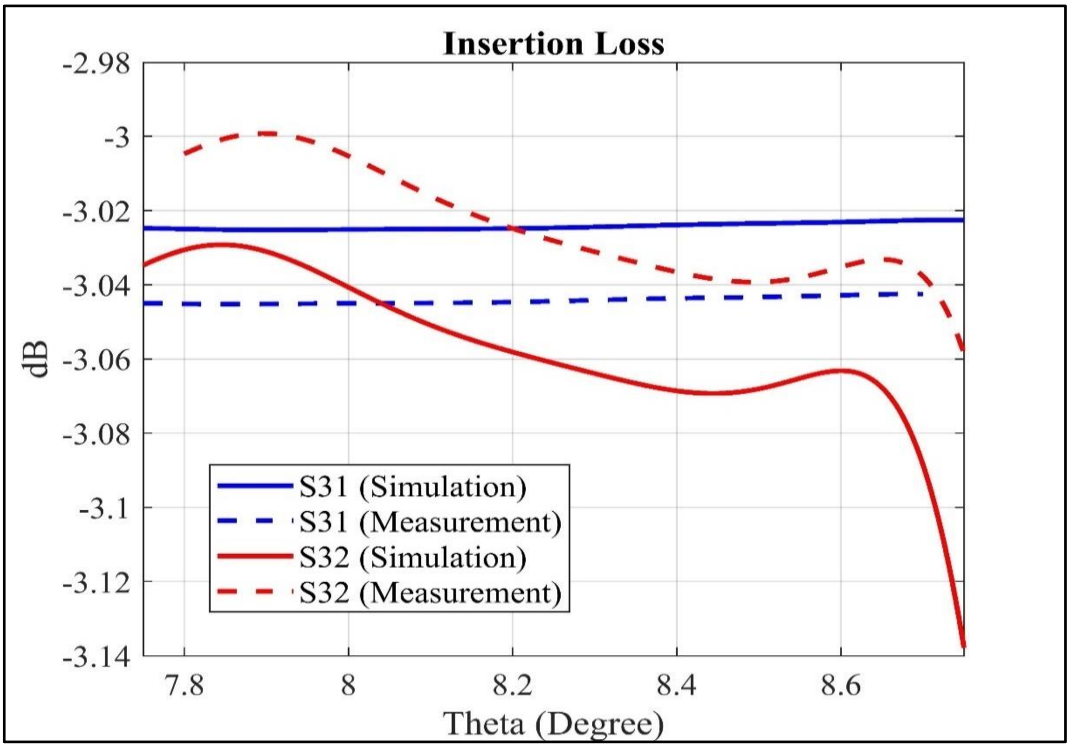

Figure 4.10. Measurement and simulation of the port isolations of the septum polarizer ports

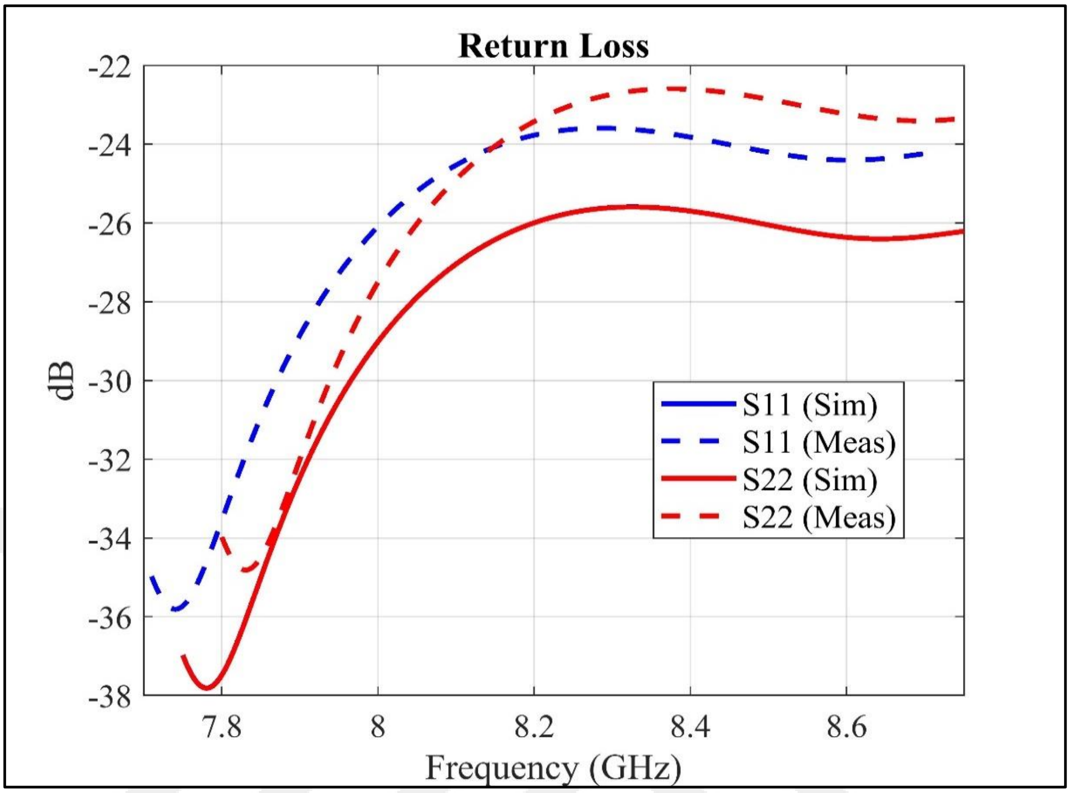

Figure 4.11. The return loss of the first and second ports of the septum polarizer

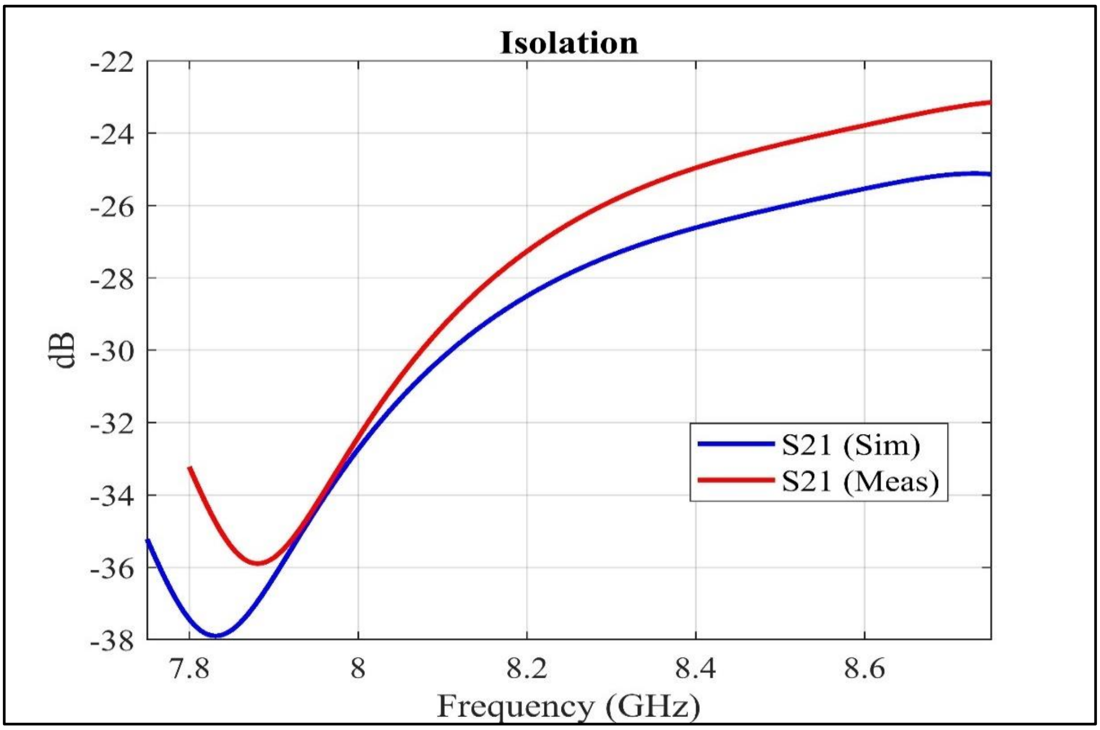

Figure 4.12. Isolation of the linear ports of the septum polarizer

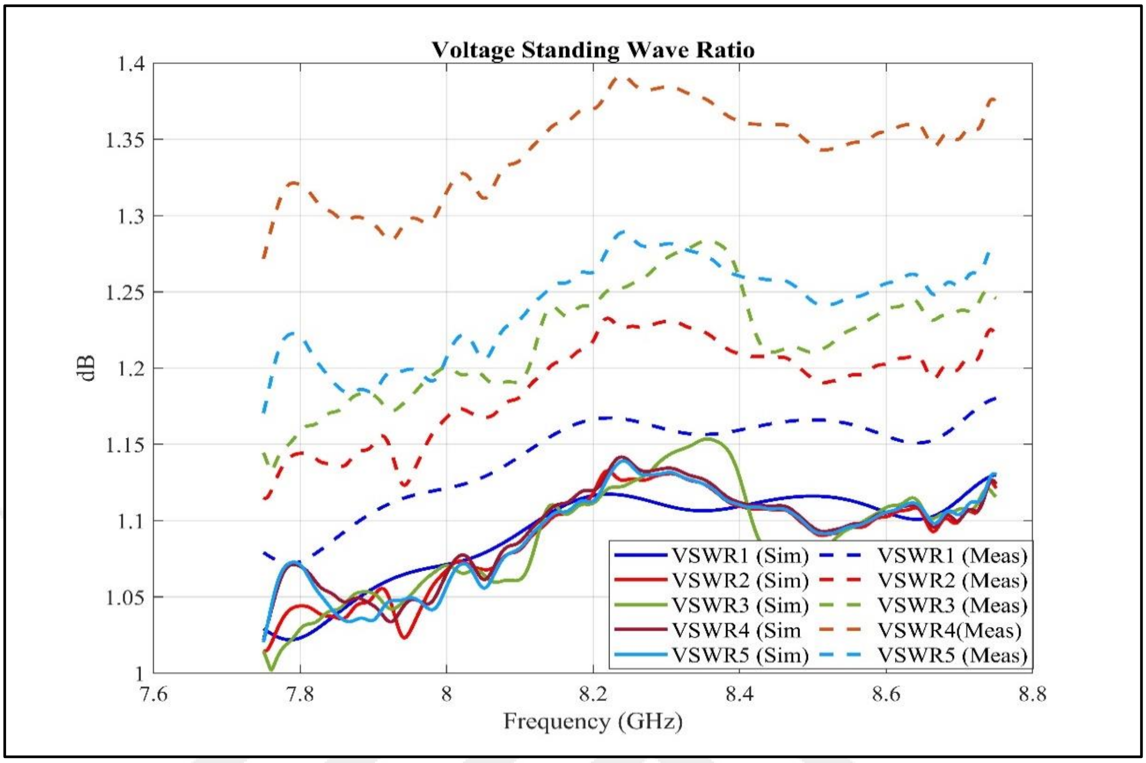

Figure 4.13.Measurement and simulation of the VSWR for all ports of the system

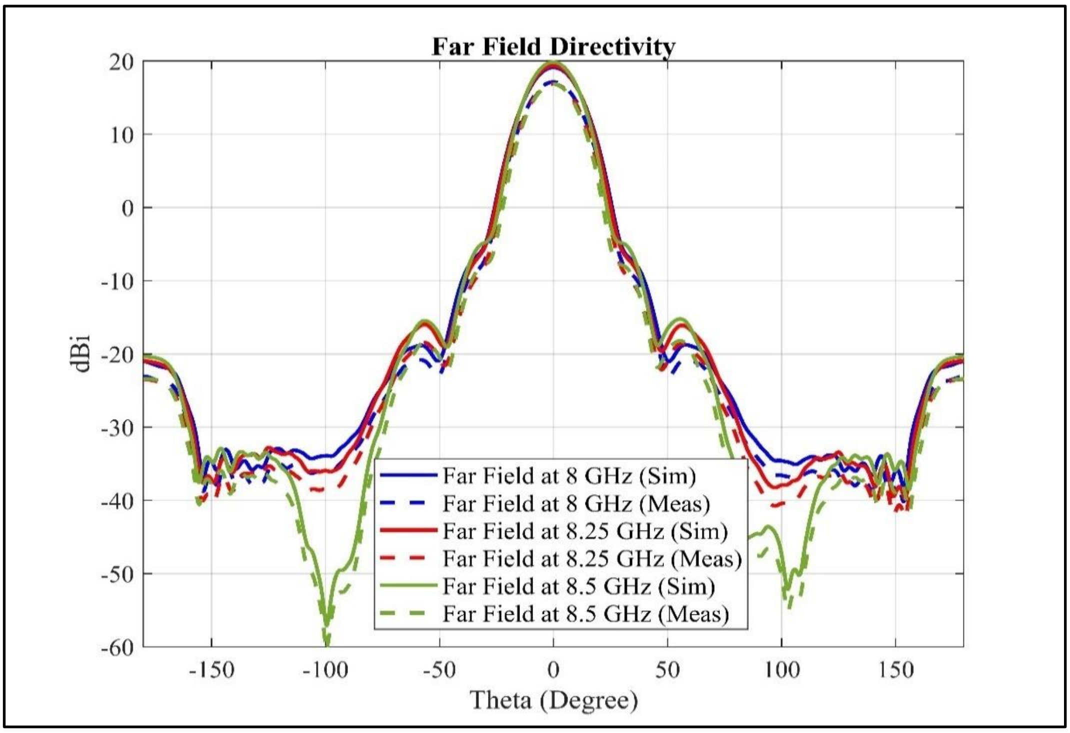

Figure 4.14. The radiation pattern measurement of the system at 8 GHz, 8.25 GHz, and 8.5 GHz for phi=0°

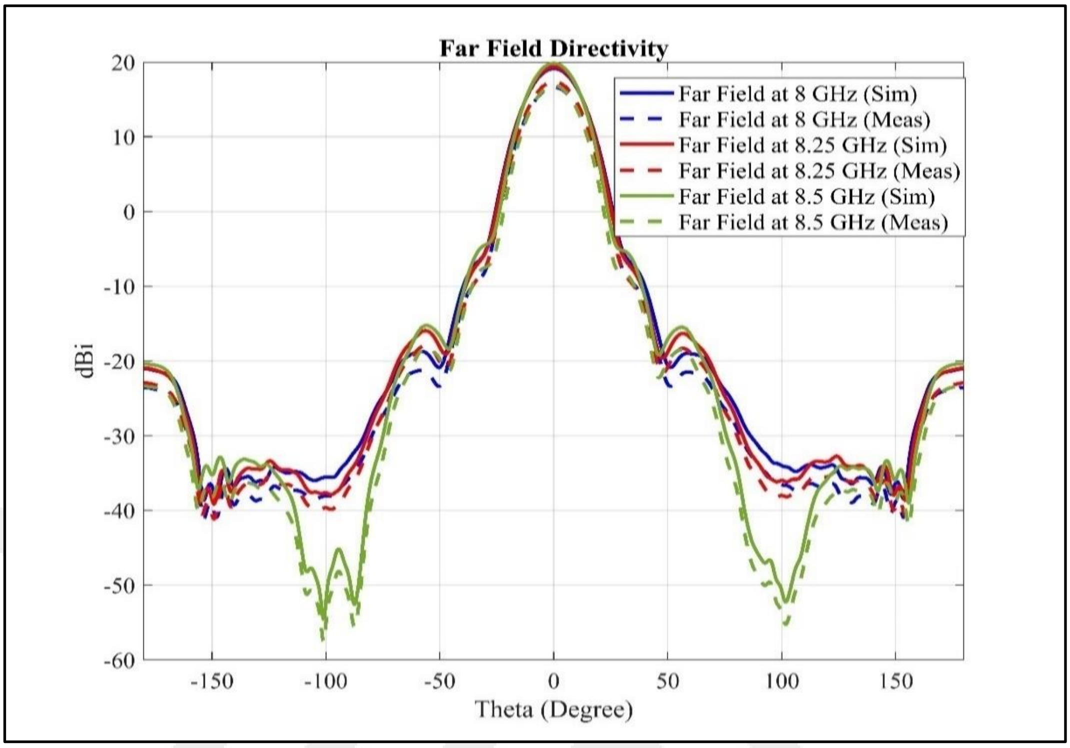

Figure 4.15. The radiation pattern measurement of the system at 8 GHz, 8.25 GHz, and 8.5 GHz for phi=90°

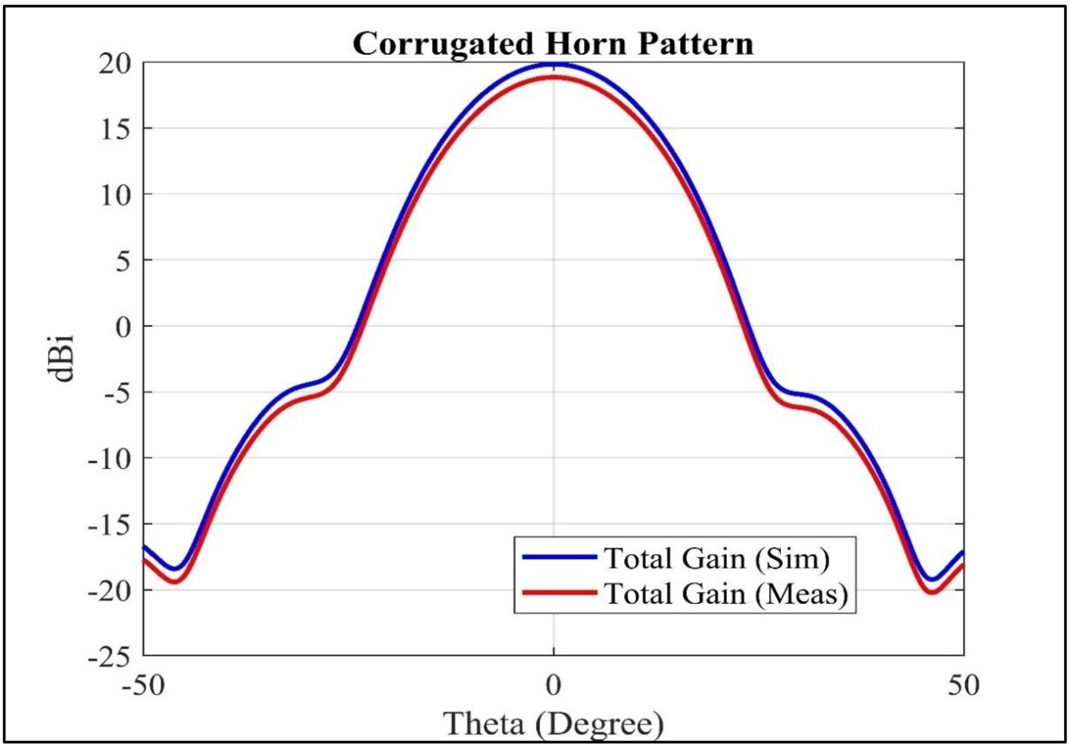

Figure 4.16. Measurement and simulation of the total gain of the corrugated horn

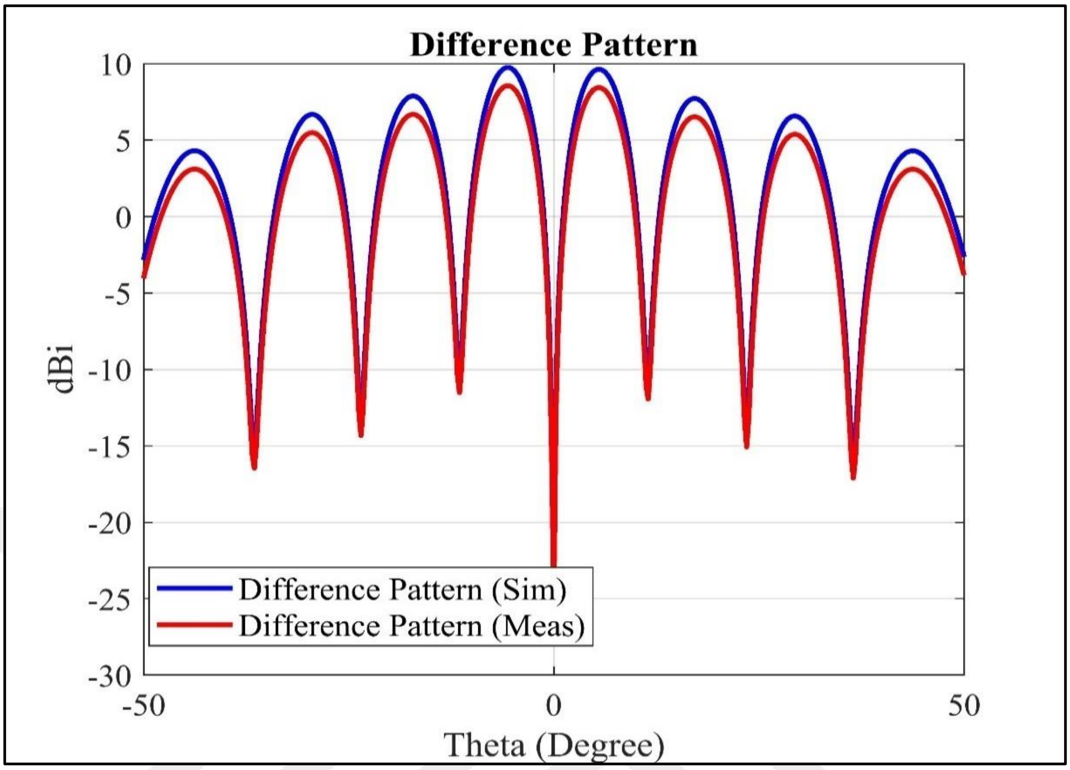

Figure 4.17. Measurement and simulation of the difference pattern

Figure 4.18. 7.3 m Cassegrain reflector antenna

The X-band feed antenna is placed on the reflector antenna with a diameter of 7.3 m, as shown in Figure 4.18. The gain of the sum signal is 54.6 dB, the communication signal in Figure 4.19. The antenna efficiency is approximately 72.52%, which is a good value for the proposed antenna. Additionally, the null level of the tracking signal has a pretty smooth pattern at 0°, as shown in Figure 4.19. For satellite tracking, the depth and form of this pattern is required to be smooth.

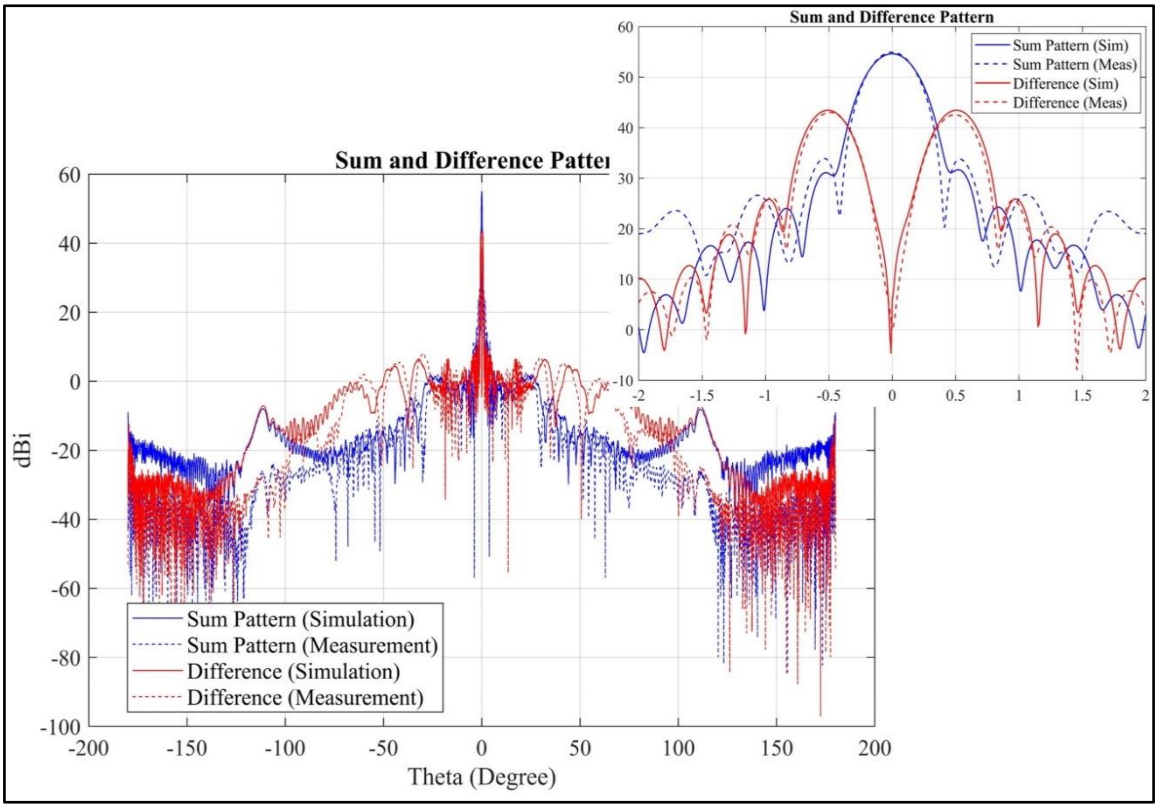

Figure 4.19. Measurement and simulation of the sum and difference pattern of the feed antenna

4.2 MEASUREMENT RESULT OF X-BAND LNA

Figure 4.20 shows the test measurement setup of the proposed X-band low-noise amplifier. The test setup includes a signal generator, DC power supply, spectrum analyzer, VNA, load, and noise source. An RF signal is applied to the LNA input, and measurement verification of all simulated requirements is performed. These are gain, P1dB, noise figure, and input-output back reflection values. The design steps above are considered to obtain high gain in the fabricated low-noise amplifier. The test environment shown in Figure 4.20 is set up for gain measurements.

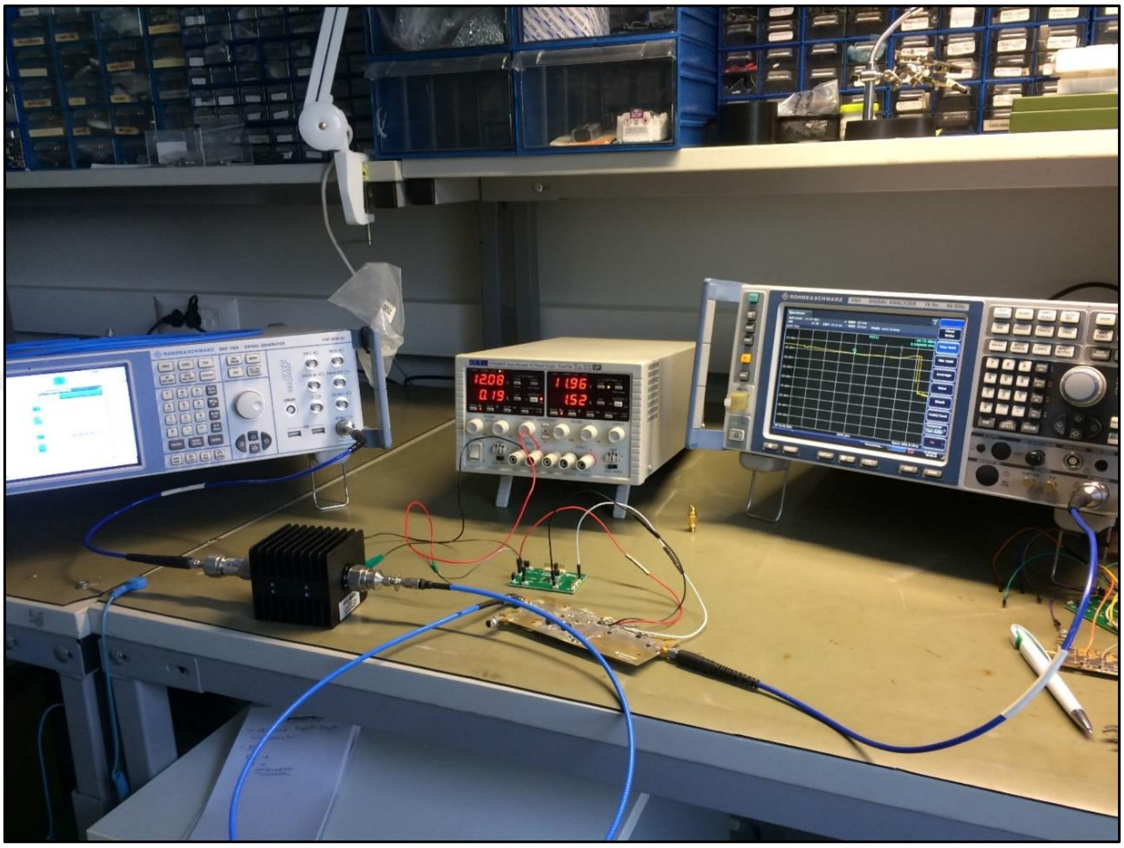

Figure 4.20. RF test setup for LNA

The total RF line loss caused by the 60 dB RF attenuator, RF cables, connector adapters, and DC choke can handle 200W of power connected to prevent damage to the spectrum analyzer in the LNA test, as shown in Figure 4.21. The RF line loss is -63.1 dBm, a 60 dB attenuator is used, and the cable connector loss is unknown. RF line loss showed that -60 - (-63.1) = 3.1 dB cable in the spectrum analyzer, and the connector loss is 3.1 dB. The measurement results are updated by adding 3.1 dB to the measurements.

The frequency sweep of the signal source is between 8 GHz and 8.5 GHz. In this case, a -20 dBm signal is given from the signal source. The connector and cable loss in the RF line is 3.1 dB in the frequency range of 8-8.5 GHz, and the RF attenuators are 60 dB. The total signal level given to the LNA becomes - 83.1 dB ((-20)+(-60) +(-3.1)).

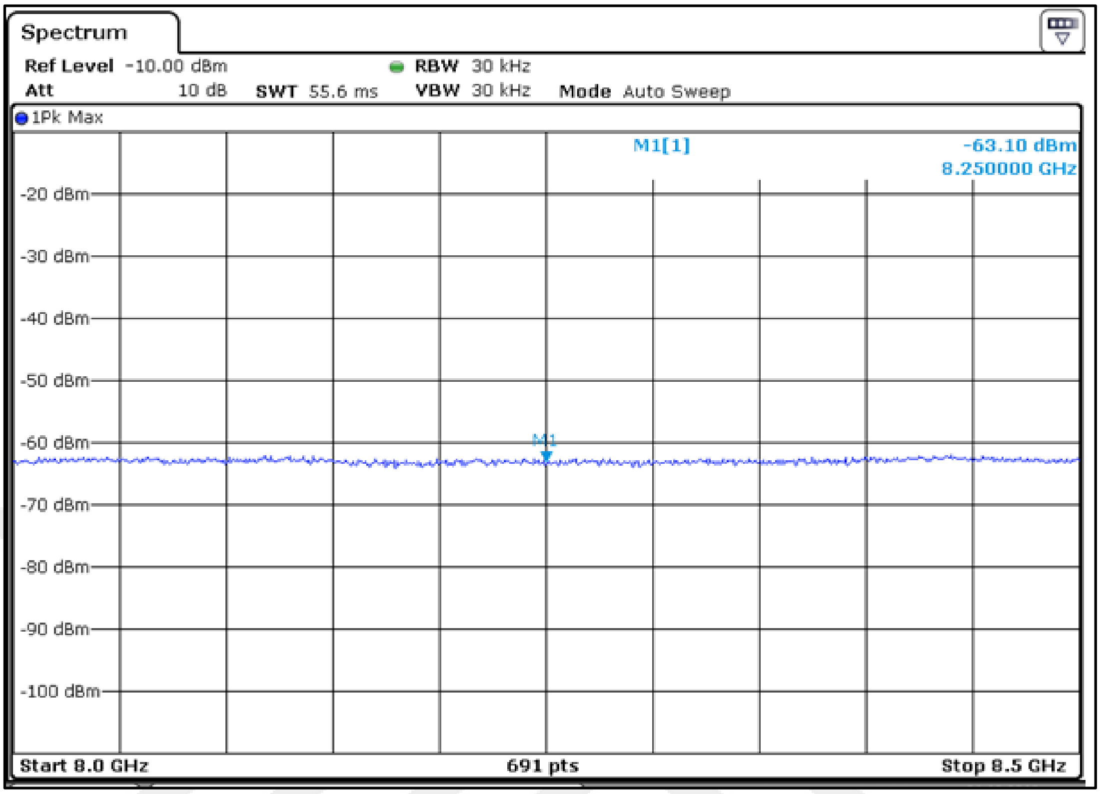

Figure 4.21. RF transmission line loss

Figure 4.22 shows the gain measurement result of the LNA. The values read from the spectrum analyzer are a maximum of - 25.68 dBm and a minimum of -30.73 dBm. In this case, the gain of the X-band LNA is minimum -30.73 - (-83.1) = 52.4 dB. Thus, the result satisfies the gain of the X-band low-noise amplifier is to be a minimum of 50 dB.

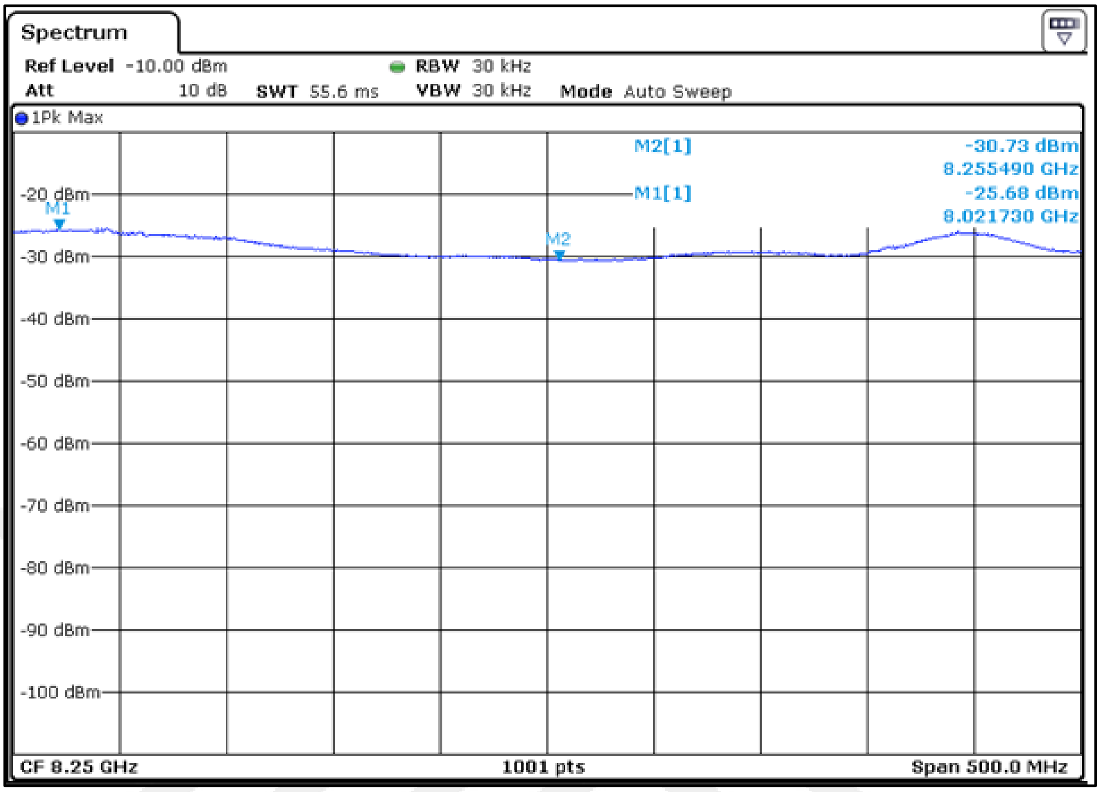

Figure 4.22. LNA gain measurement

The design steps, as mentioned earlier, are considered to obtain a low noise figure in the LNA. The test environment shown in Figure 4.23 is set up for noise figure measurements.

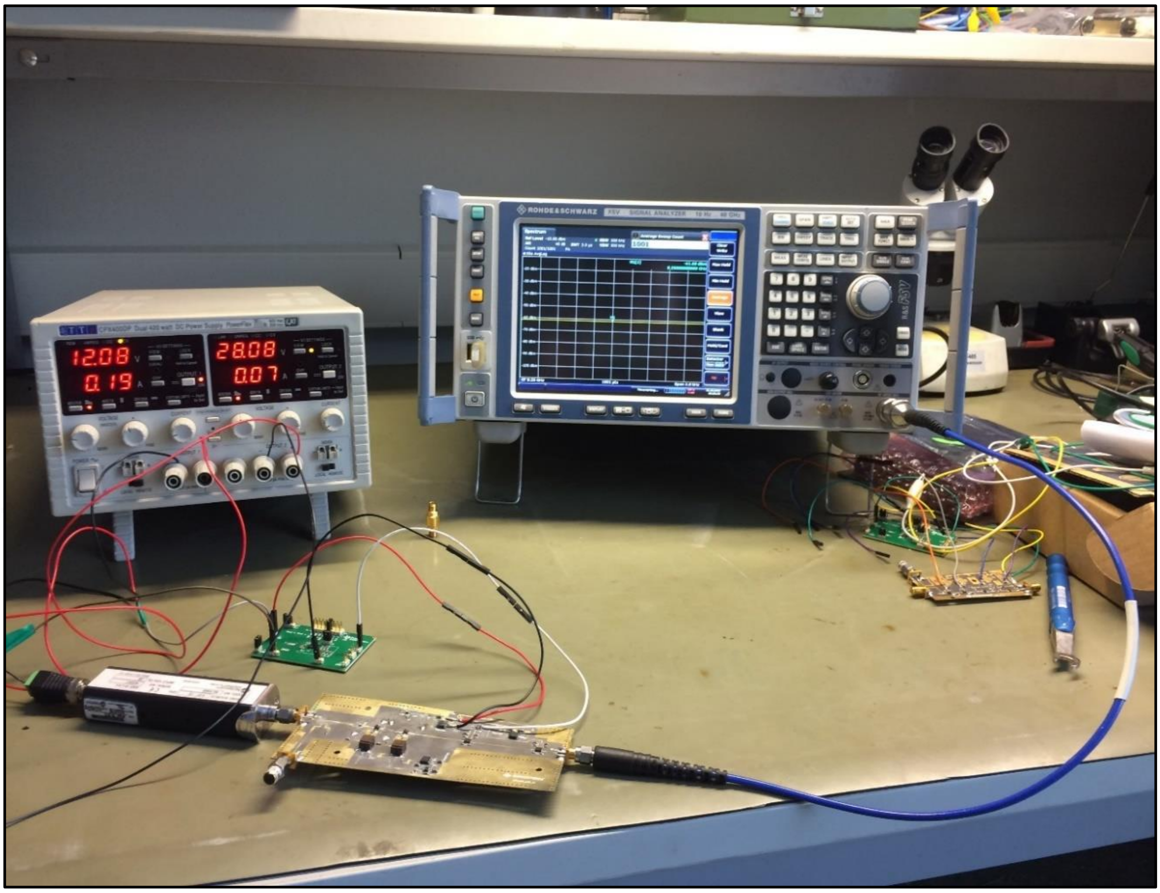

Figure 4.23. LNA noise figure RF test setup

The measured values in the test environment are calculated using the Y factor method, and the noise figure value of the X-band LNA is found. Voltage is applied to the LNA and the noise source, and the measurement result is given in Figure 4.24. At 8.25 GHz, this value is -50.82 dBm. In the measurement from the spectrum analyzer, the LNA is active, and the noise source is switched off, i.e., no voltage is applied (Figure 4.23). This value is -65.41 dBm at 8.25 GHz. The noise source ENR (Excess Noise Ratio) is 15.06, and the y value is 14.59 (-50.82-(-65.41)).

$$Noise\ Figure = 10 \times \log_{10} \frac{\left(10^{ENR/10}\right)}{\left(10^{Y/10} - 1\right)} \tag{4.1}$$

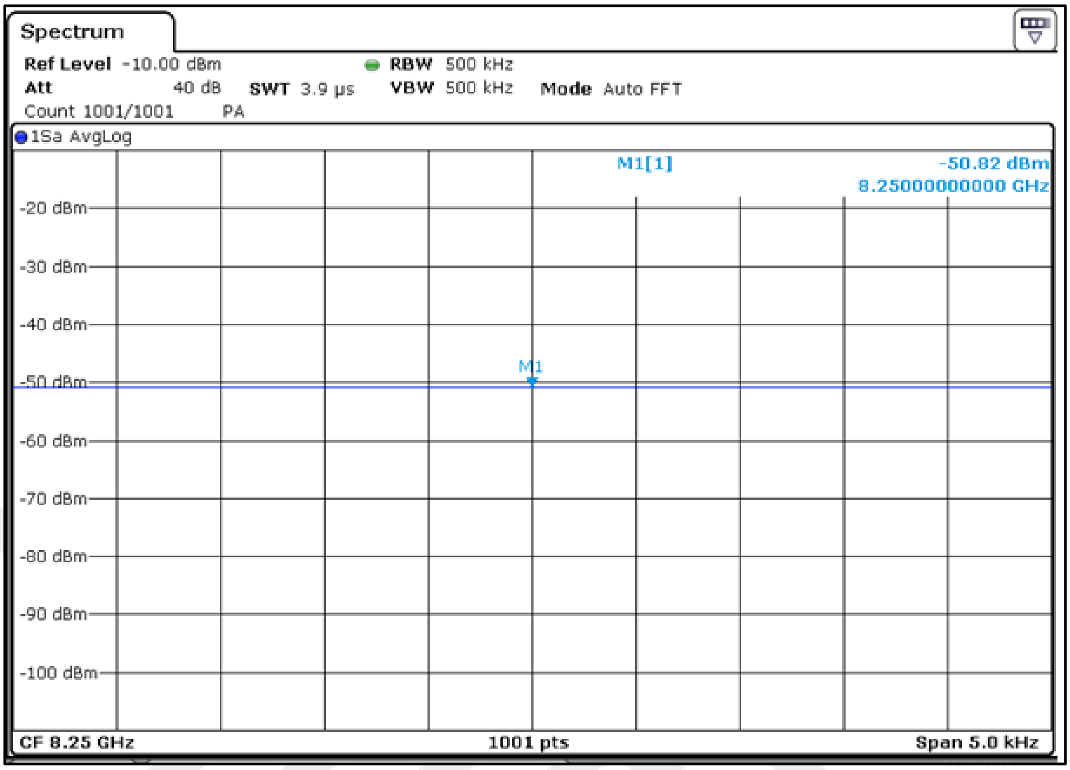

Figure 4.24. LNA noise figure (LNA+ Noise source active)

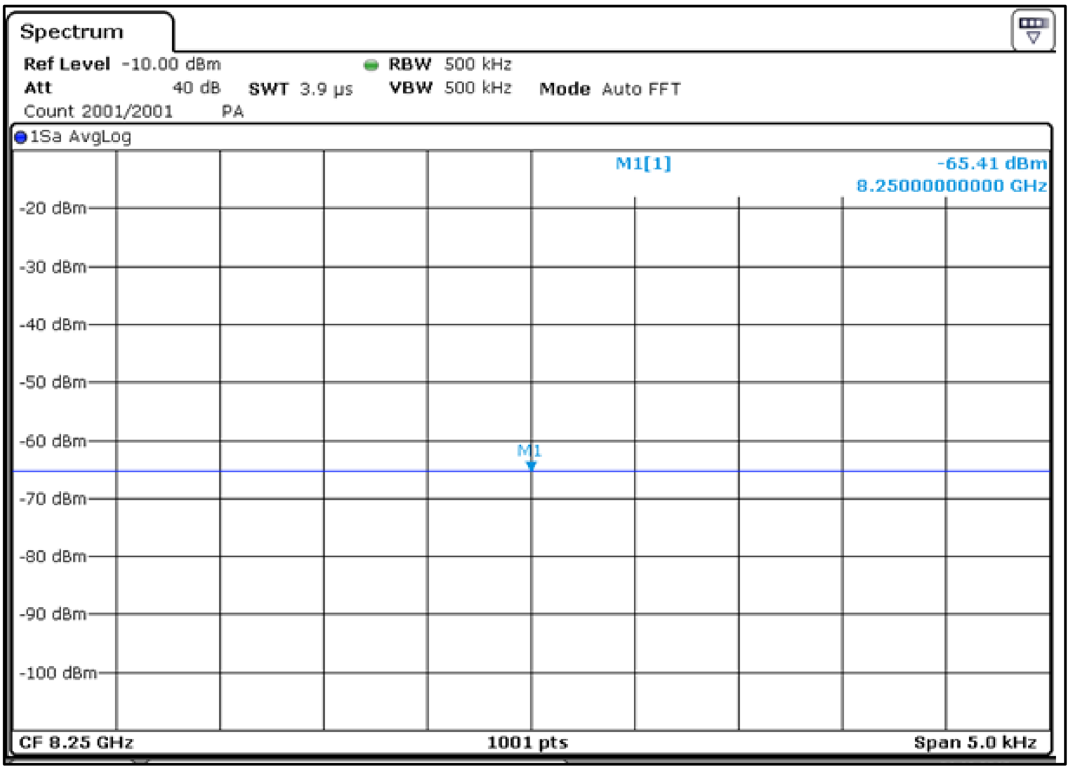

Figure 4.25.LNA noise figure (LNA active)

As a result of the calculation using the formula, this value is 0.623 dB. Thus, the noise figure of the X-band low-noise amplifier is at a maximum of 0.7 dB. The input and output impedances are obtained with 50Ω to obtain a VSWR of 1.5:1 in the LNA. For VSWR measurements, the test environment shown in Figure 4.20. The input and output reflection values for the X-band LNA are measured by VNA which are shown in Figure 4.26 and Figure 4.27.

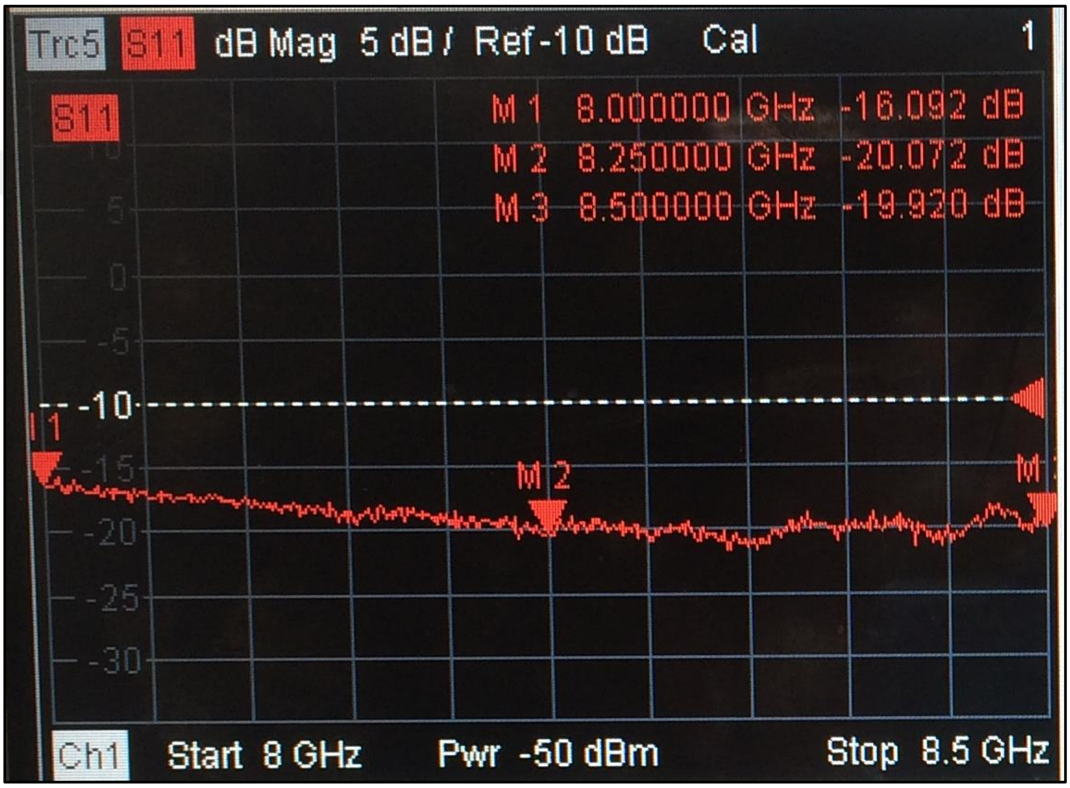

Figure 4.26. LNA input reflection

The input reflection scattering parameters of the X-band LNA are given in Figure 4.26. As a result of the measurement, it is observed that the VSWR value required in the technical specification is provided using the following equation.

$$VSWR = \frac{1+\Gamma}{1-\Gamma} = 1.37 \tag{4.2}$$

The output reflection scattering parameters of the LNA are given in Figure 4.27. It is observed that the VSWR value required in the technical specification is provided.

$$VSWR = \frac{1+\Gamma}{1-\Gamma} = 1.5 \qquad (4.3)$$

In this case, the VSWR ratio of the X-band low-noise amplifier is a minimum of 1.5:1. Thus, the results show that the input and output VSWR ratio of the X-band low-noise amplifier are at a minimum of 1.5:1 dB.

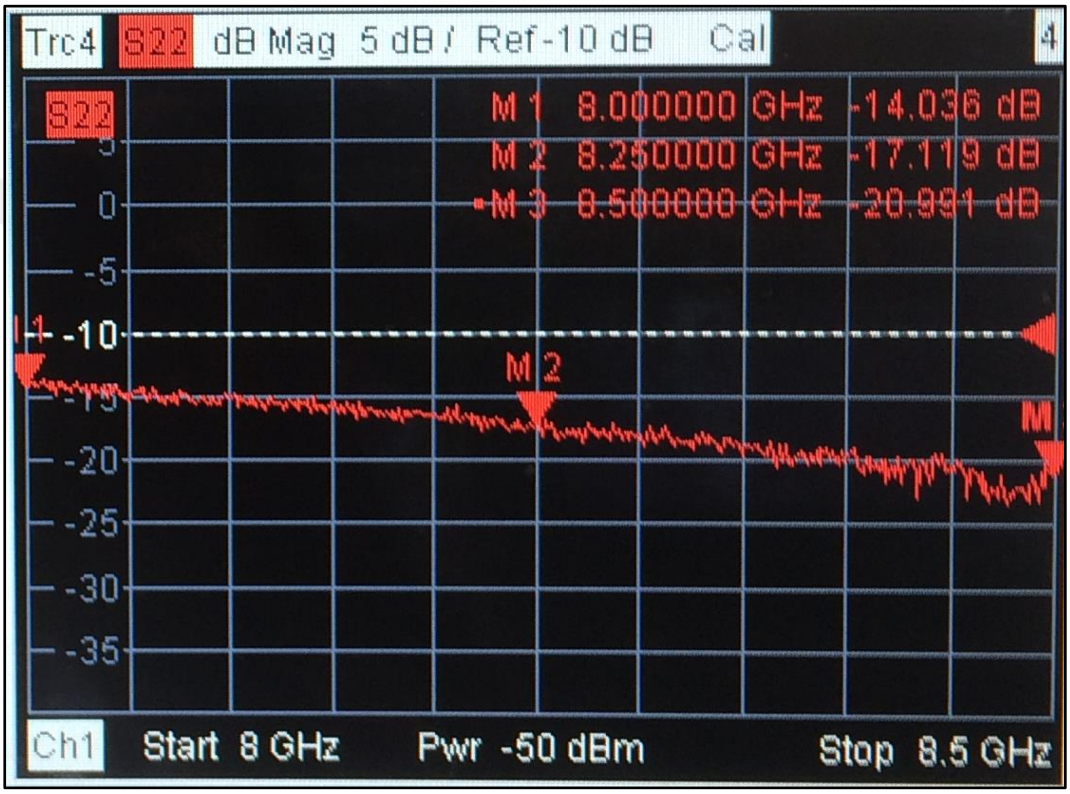

Figure 4.27. Output Reflection

MMIC amplifiers are used in the last stages of the cascade-designed LNA to obtain a minimum output 1 dB suppression power of 10 dBm in the LNA. A1 dB change is observed in the spectrum analyzer by changing the signal levels at the signal source to -20 dBm, -10 dBm, 0 dBm, 5 dBm, 10 dBm, 20 dBm, 23 dBm for the output 1 dB suppression power measurements. The P1dB for different power levels is shown from Figure 4.28 to Figure 4.34. As a result of the measurements, the output P1dB is 11.29 dBm. The X-band low-noise amplifier's output 1 dB compression power is shown to be at least 10 dBm.

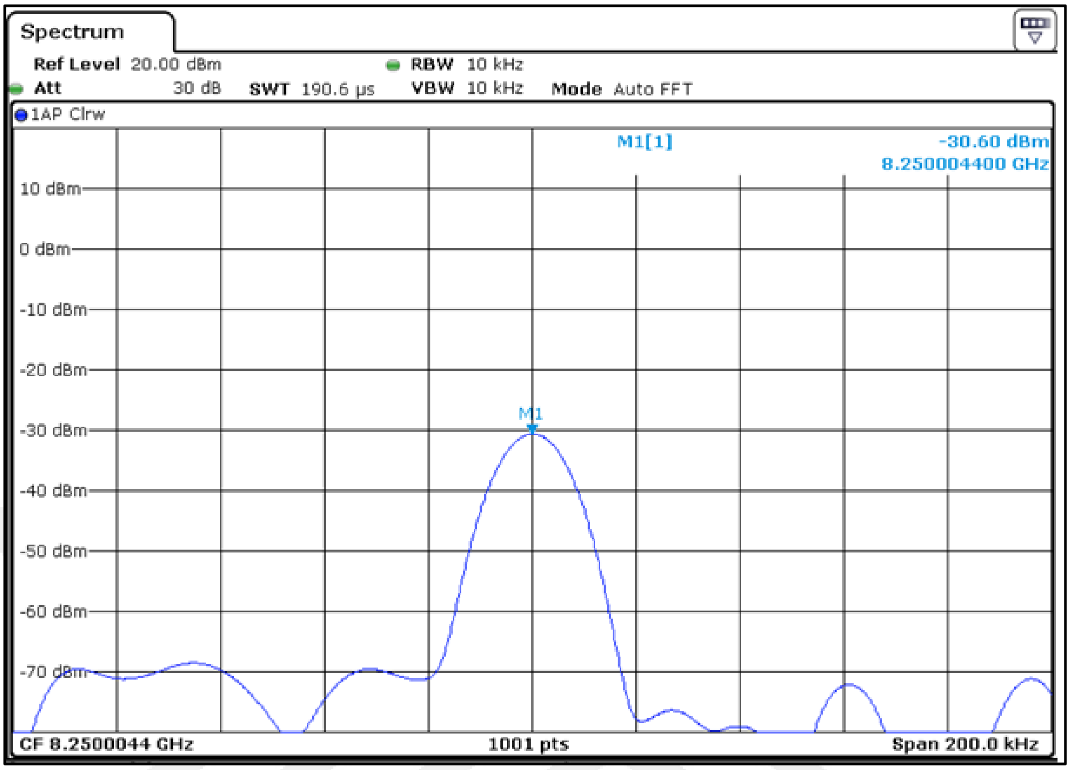

Figure 4.28. LNA P1dB (RF input= -20 dBm)

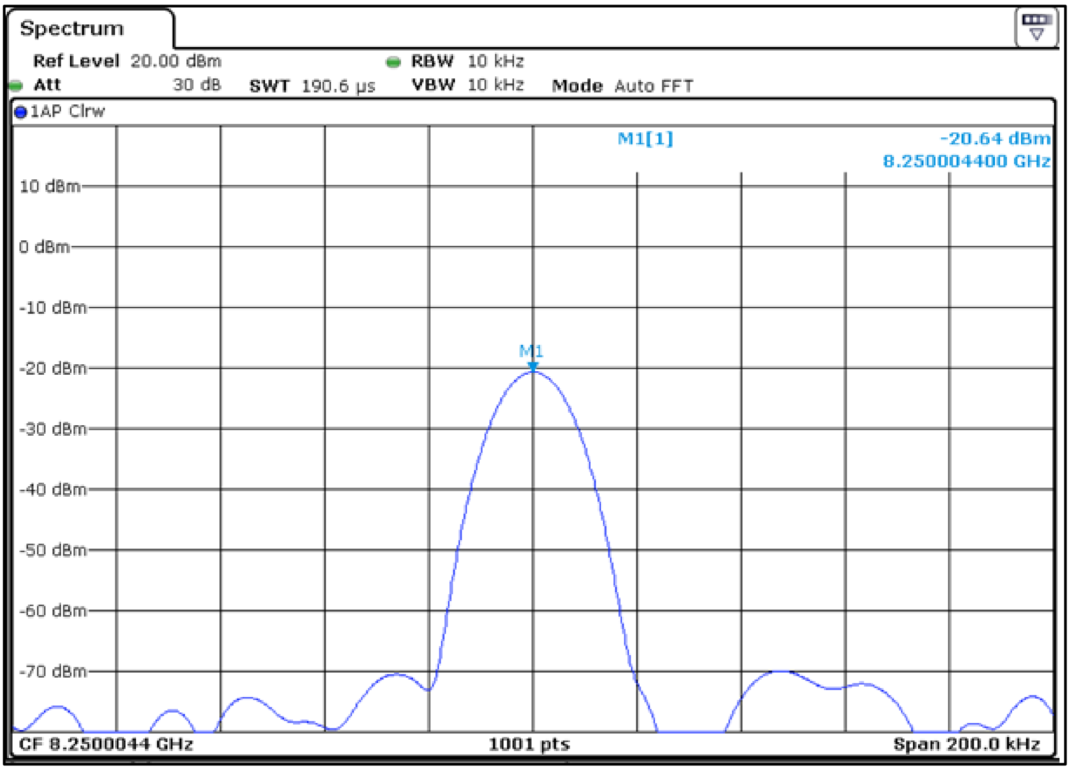

Figure 4.29. LNA P1dB (RF input= -10 dBm)

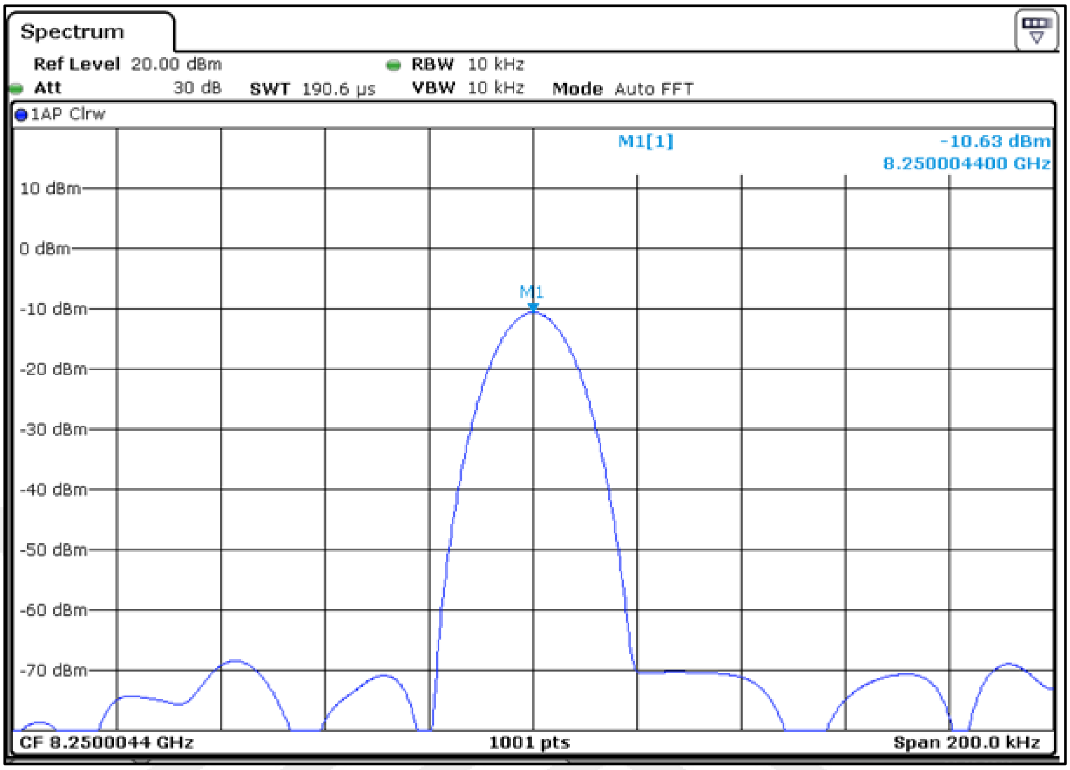

Figure 4.30. LNA P1dB (RF input= 0 dBm)

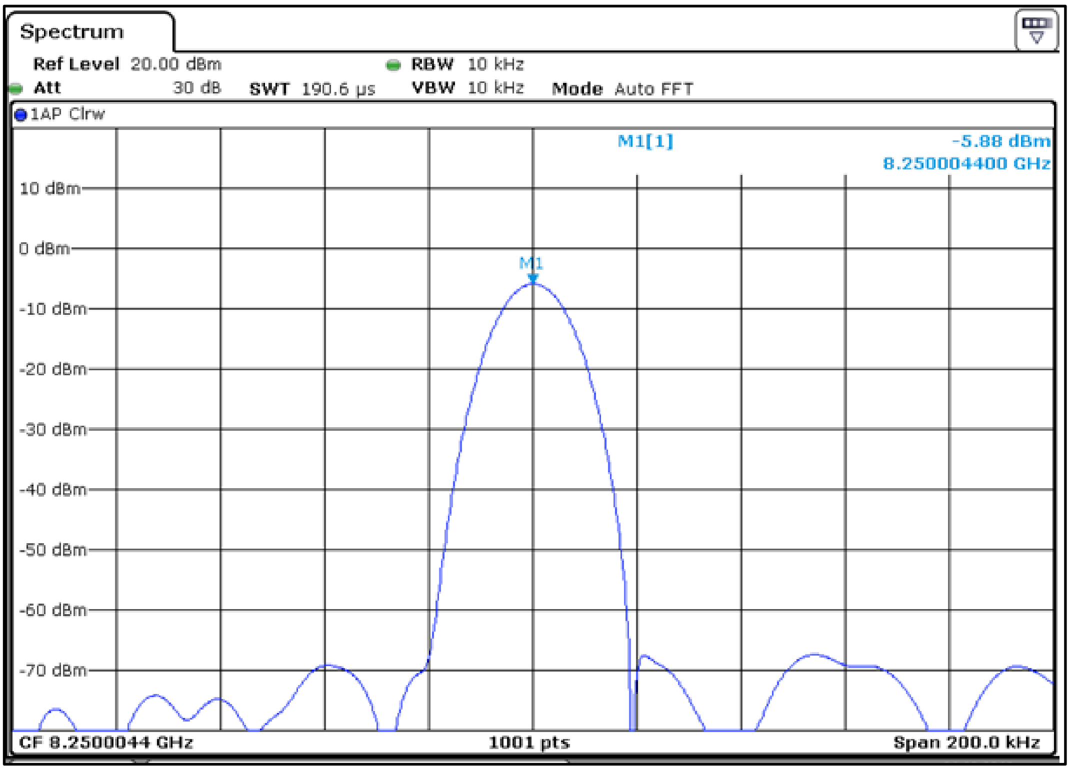

Figure 4.31. LNA P1dB (RF input= 5 dBm)

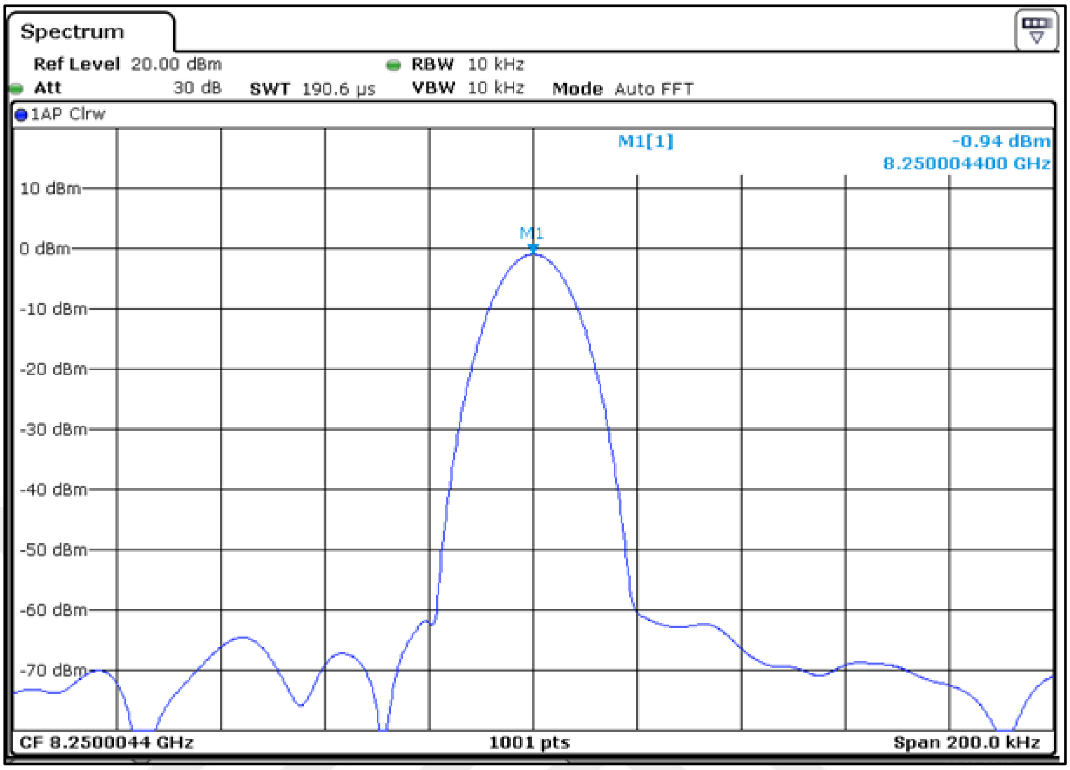

Figure 4.32. LNA P1dB (RF input= 10 dBm)

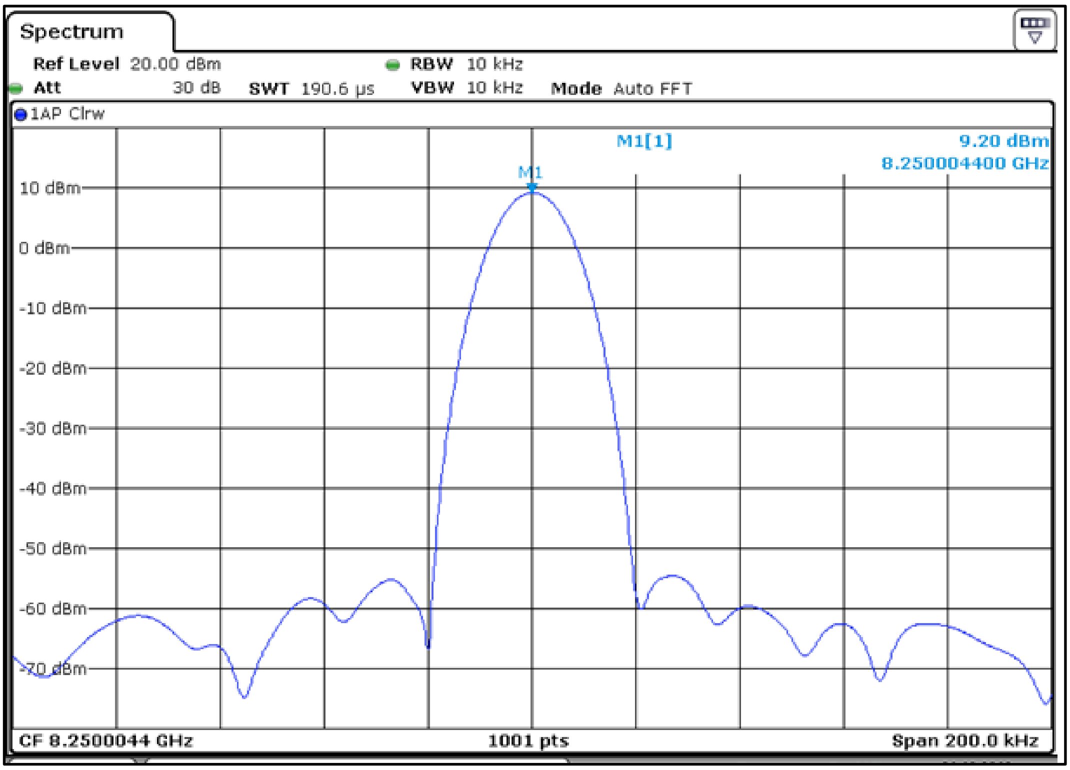

Figure 4.33. LNA P1dB (RF input= 20 dBm)

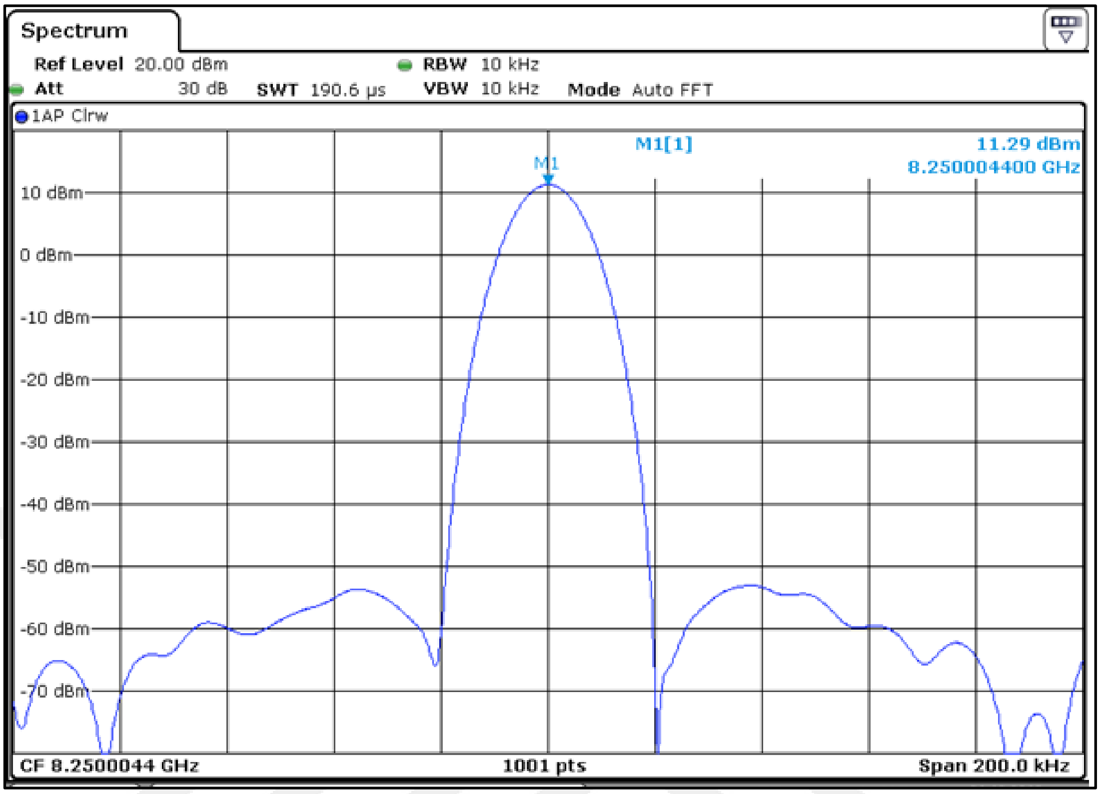

Figure 4.34. LNA P1dB (RF input= 23 dBm)

4.3 MEASUREMENT RESULTS OF THE X-BAND FREQUENCY DOWN CONVERTER

Figure 4.35 shows the measurement setup of the designed frequency down converter. There is a need for all of the subsystem units for this measurement. These are RF cards, regulator cards, PLL cards, interface control cards and control computers, signal generators, DC power supplies, and spectrum analyzers. A signal in the frequency range of 8-8.5 GHz is applied from the signal generator to the input of our RF card. This signal is required to generate a 720 MHz (±200 MHz) bandwidth signal at the IF output. For this, the regulator card makes the DC supply of all active components on the circuit. Our PLL card is connected to the signal input of the LO port of the mixer on the RF card. Since the input frequency is between 8 and 8.5 GHz, the frequency of the PLL card must change at each frequency signal. This is because the output IF frequency is 400 MHz bandwidth at 720 MHZ center. This change is made by the SPI communication pins on the PLL card with the Nucleo communication card. Measurement verification of all simulated requirements is performed by giving RF signal to the frequency down converter input. These are gain, P1dB, noise figure, input-output back reflection value, image rejection value, LO leakage, and spurious measurements. Figure 4.35 shows the test environment of the RF test of the frequency down converter. In Figure 4.36, the Nucleo card is the control card which controls the attenuator, SPI communication with the PLL card, control of the Power detector output, and Mute mode operation. This control card has been managed with an ethernet connection interface by performing the necessary software studies. Figure 4.37 shows the interface structure for the frequency down converter.

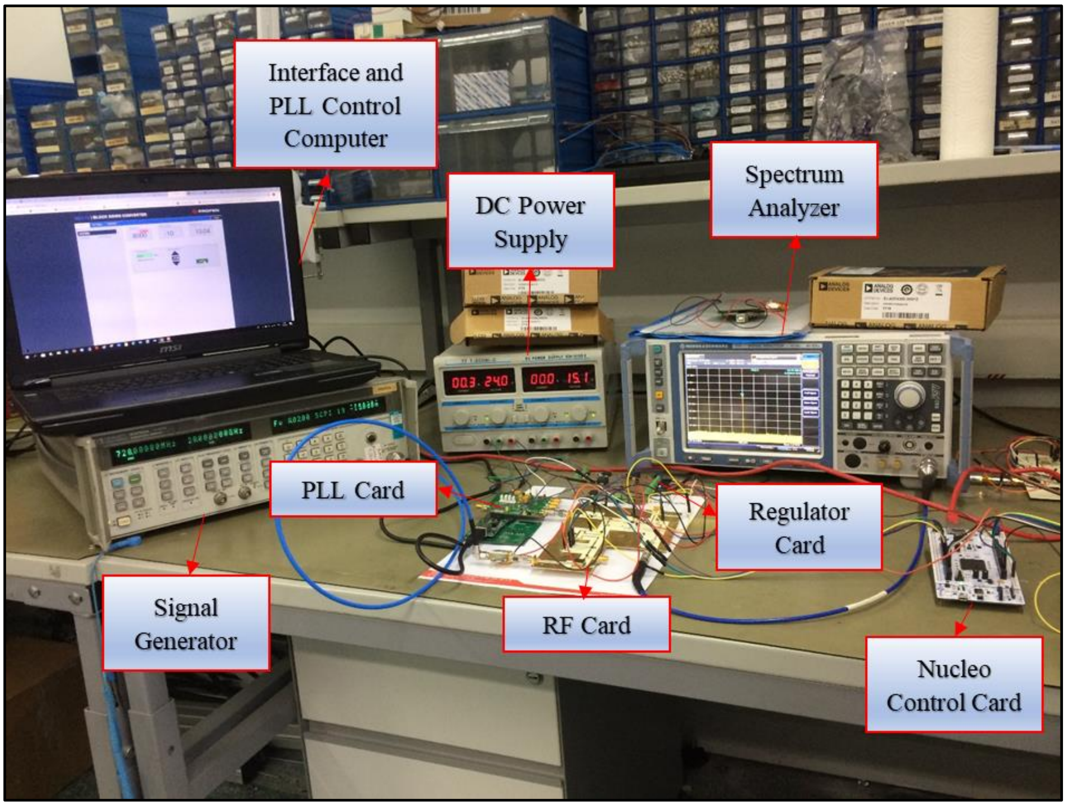

Figure 4.35. Frequency down converter RF test

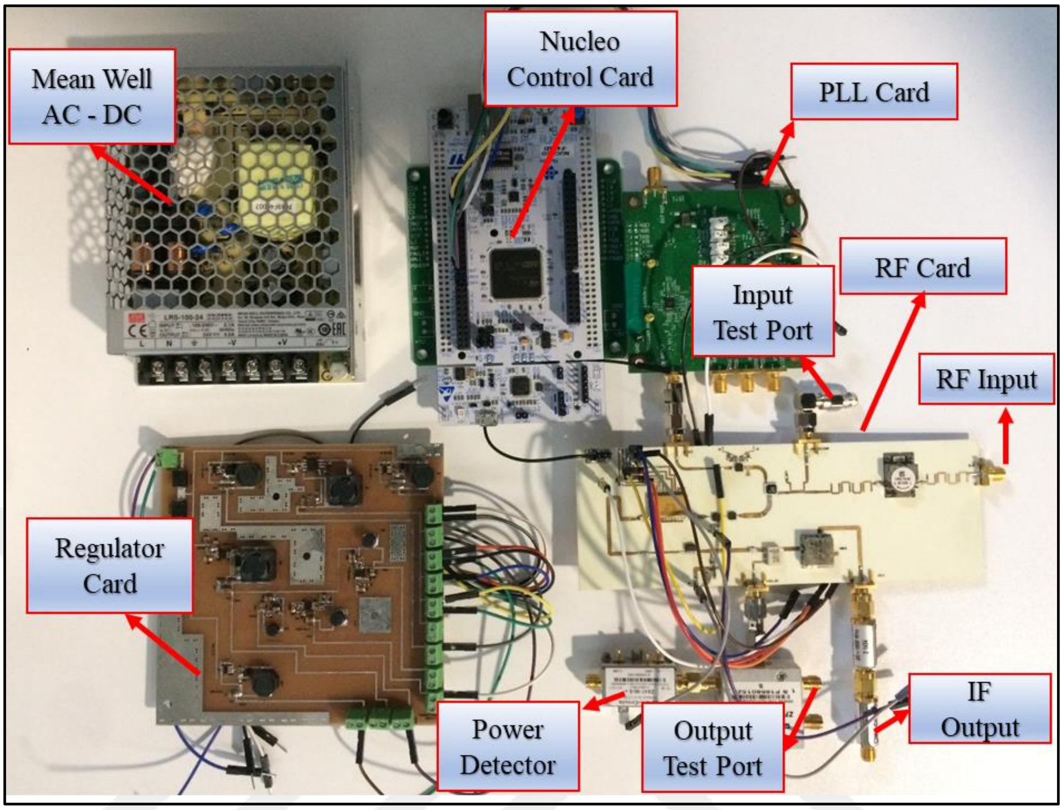

Figure 4.36. The circuit design of the frequency down converter

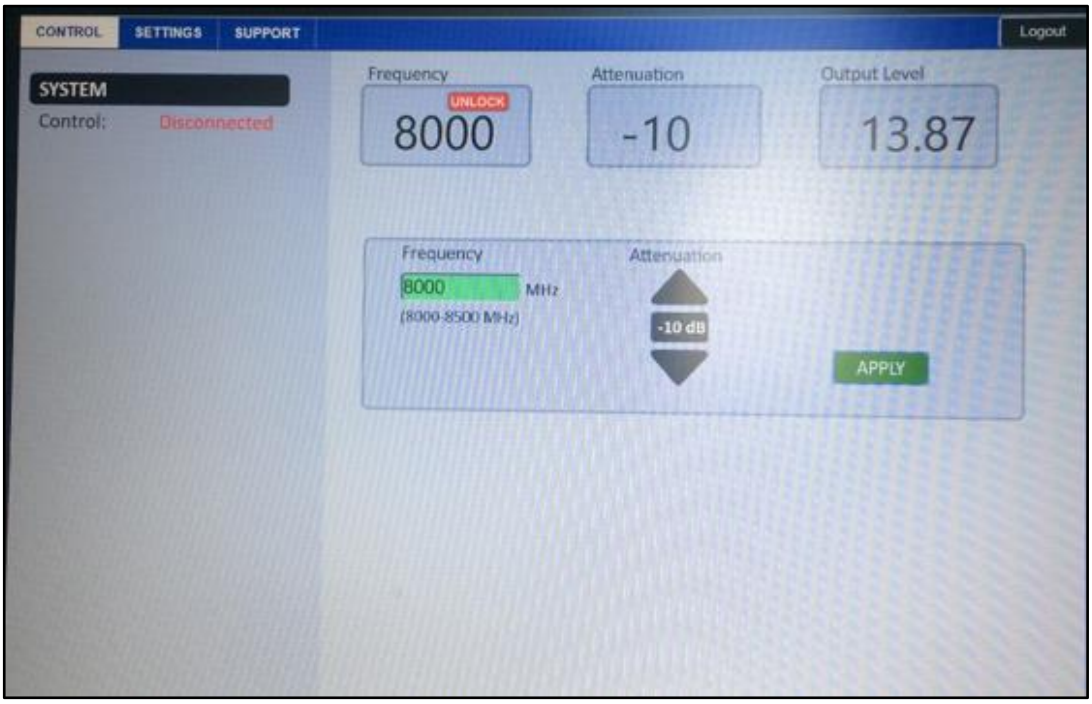

Figure 4.37. The interface of the frequency down converter control software

The 18 - 32 V DC input regulator card in the frequency down converter is fed with different DC voltage values. This card meets the DC supply requirement of the Frequency Down Converter (5V, 9V, -5 V, -2V, 15 V, 12 V, 5.5 V, 9 V, 3.3 V). The input of the Frequency Down Inverter is 220 V AC. 220 V AC voltage is reduced to AC 220 V, DC 24 V with LRS-100-24 of Mean Well.

The PLL board is the circuit in which the locking process in the frequency range of 7280 MHz and 7780 MHz for the LO input of the RF board is performed. This circuit uses a 10 MHz VCTCXO crystal oscillator, and frequency stability and depreciation year are ±1 ppm.

RF card is a circuit consisting of RF input, IF output, Input test port, Output test port, and Power detector output, as shown in Figure 4.36. At the IF output, two low-pass filters suitable for the output frequency are used. A 4-way splitter is used in the output test port. The purpose here is to give the test port output and power detector output.

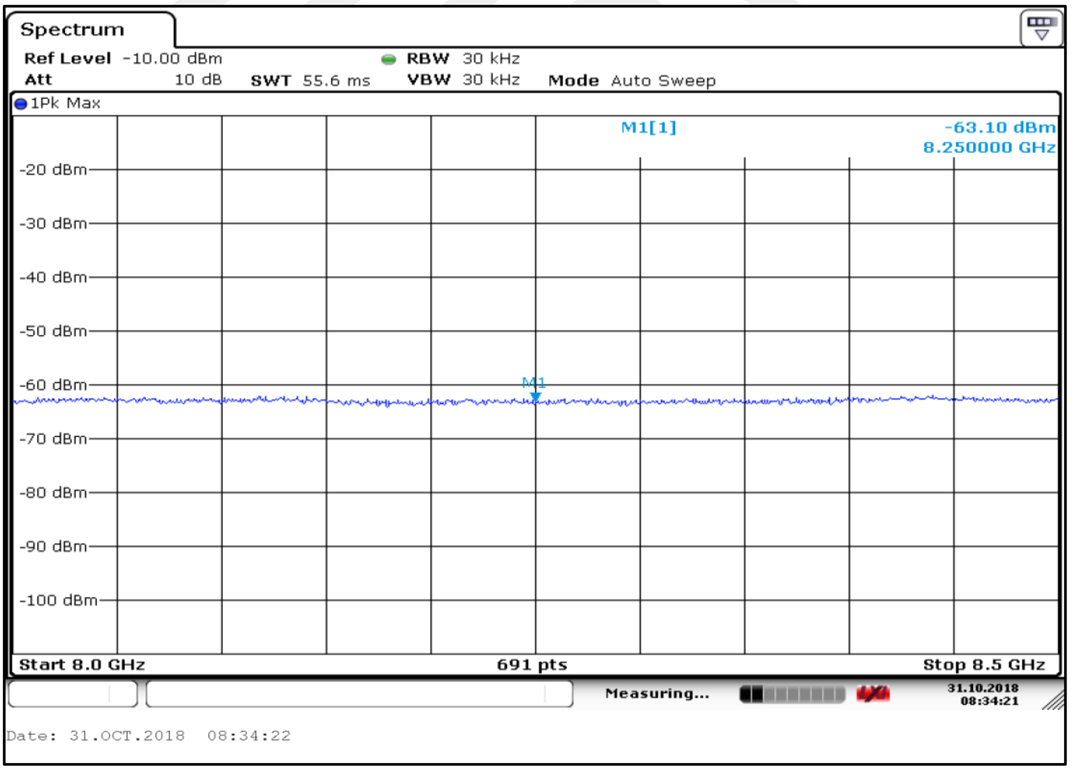

Figure 4.38. The measurement of the RF transmission line loss

For the RF test of the frequency down converter, RF line loss is given in Figure 4.38 when -60 dBm output power is provided from the signal source. In this case, the total loss is 3.1 dB. The measurement results are updated by adding 3.1 dB to the measurements made.

In the gain measurements, the measurement is performed at 0 - 1440 MHz bandwidth (Figure 4.39). RF input signal level is -10 dBm, input frequency is 8000 MHz, and PLL is 7280 MHz. Considering the frequency and PLL value, the output frequency is 720 MHz. As can be seen in Figure 4.39, the frequency value is shown with a marker. When these measurements are made, the attenuator level for the frequency down converter is - 20 dBm.

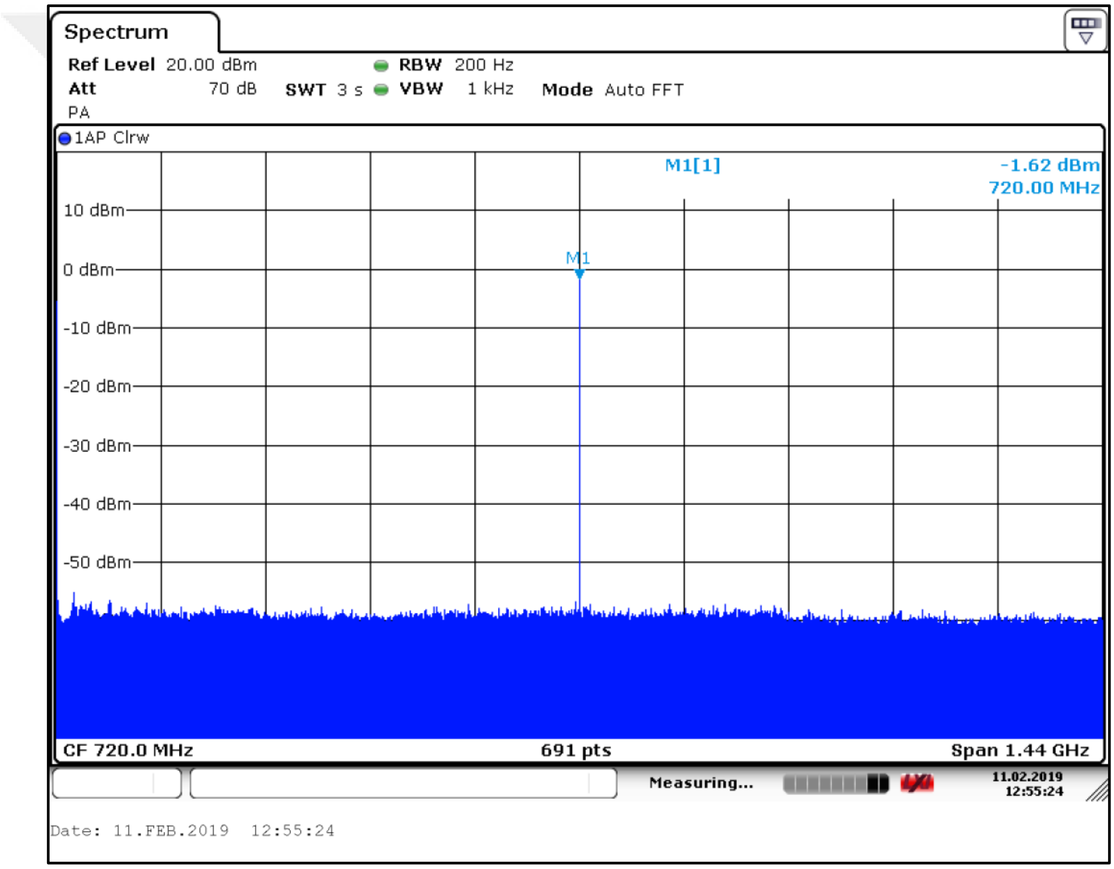

Figure 4.39. 720 MHz signal level for 8000 MHz input frequency

As shown in Figure 4.40, the measurement is performed at 0 – 1440 MHz bandwidth. The RF input signal level is -10 dBm, the input frequency is 8100 MHz, and the PLL is 7380 MHz. Considering the frequency and PLL value, the output frequency is 720 MHz. As can be seen in Figure 4.40, the frequency value is shown with a marker. During these measurements, the attenuator level for the frequency down converter is - 20 dBm.

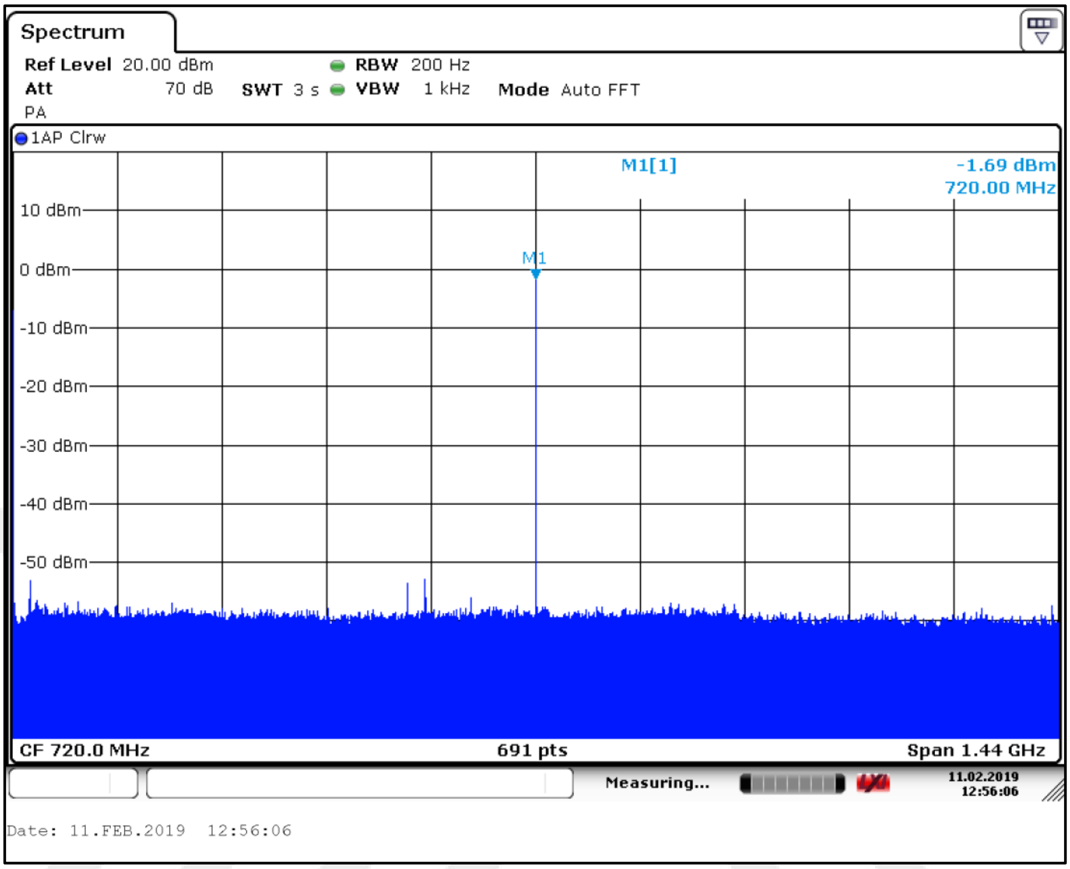

Figure 4.40. 720 MHz signal level for 8100 MHz input frequency

The input frequency is 8200 MHz, PLL is 7480 MHz, and the input power is -10 dBm. As shown in Figure 4.41, the measurement is performed at 0 - 1440 MHz bandwidth. RF input signal level is -10 dBm, input frequency is 8200 MHz, and PLL is 7480 MHz. Considering the frequency and PLL value, the output frequency should be 720 MHz. As can be seen in Figure 4.41, the frequency value is shown with a marker. During these measurements, the attenuator level for the frequency down converter is - 20 dBm.

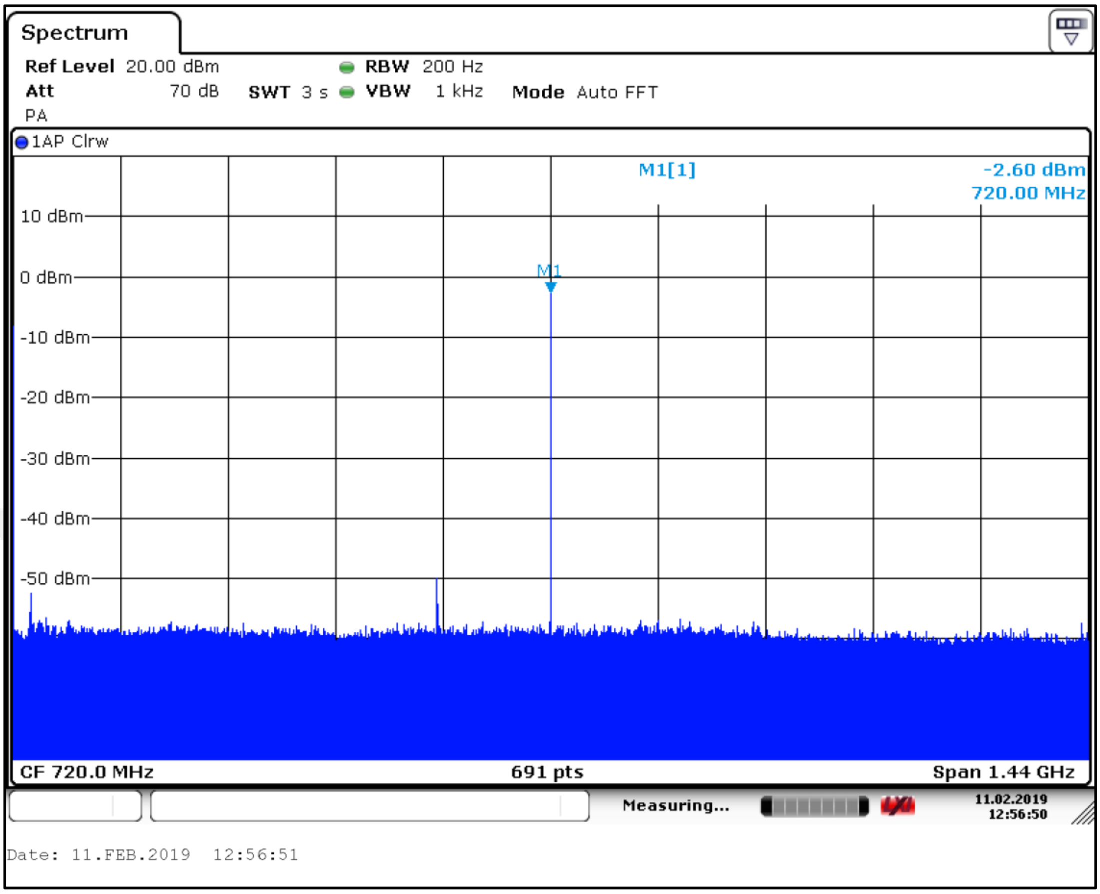

Figure 4.41. 720 MHz signal level for 8200 MHz input frequency

The input frequency is 8300 MHz, PLL is 7580 MHz, and the input power is -10 dBm. As shown in Figure 4.42, the measurement is performed at 0 - 1440 MHz bandwidth. When making this measurement, the RF input signal level is -10 dBm, the input frequency is 8300 MHz, and the PLL is 7580 MHz. Considering the frequency and PLL value, the output frequency should be 720 MHz. As can be seen in Figure 4.42, the frequency value is shown with a marker. During these measurements, the attenuator level for the frequency down converter is - 20 dBm.

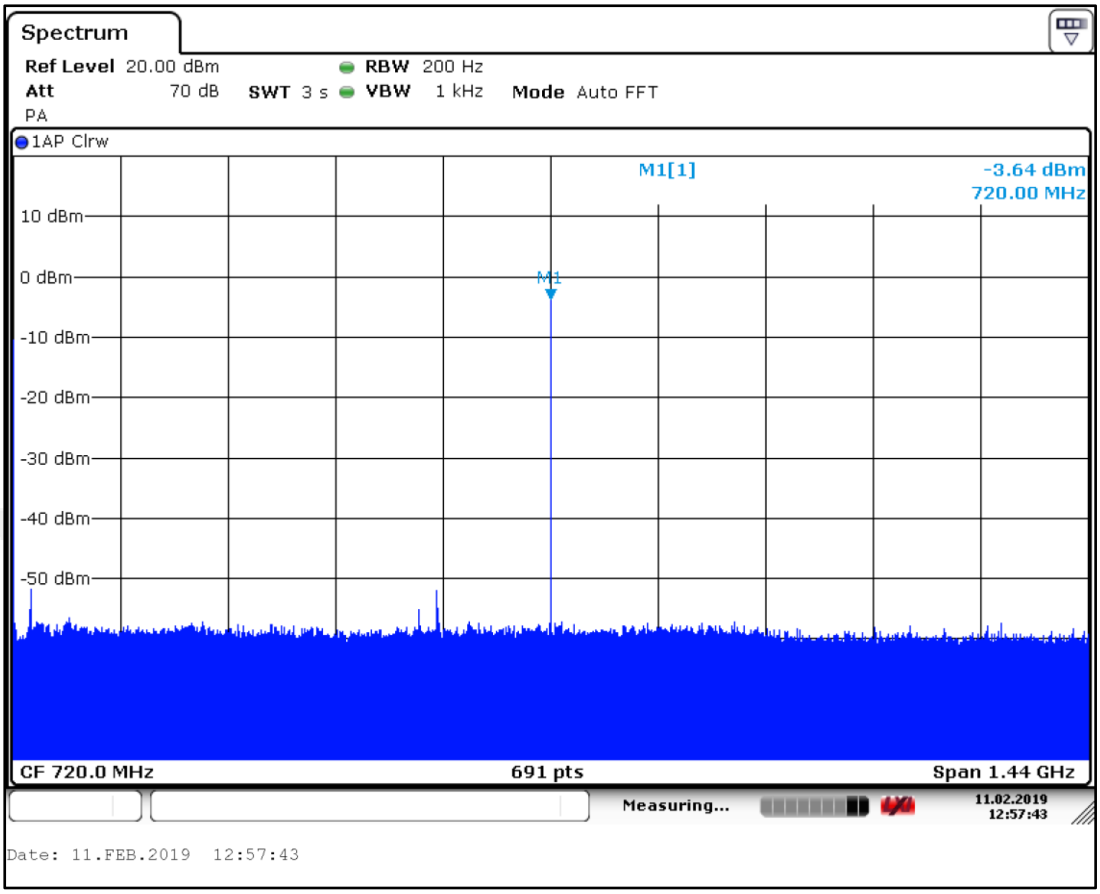

Figure 4.42. 720 MHz signal level for 8300 MHz input frequency

As shown in Figure 4.43, the measurement is performed at 0 - 1440 MHz bandwidth. When making this measurement, the RF input signal level is -10 dBm, the input frequency is 8400 MHz, and the PLL is 7680 MHz. Considering the frequency and PLL value, the output frequency should be 720 MHz. As can be seen in Figure 4.43, the frequency value is shown with a marker. When these measurements are made, the attenuator level for the frequency down converter is - 20 dBm.

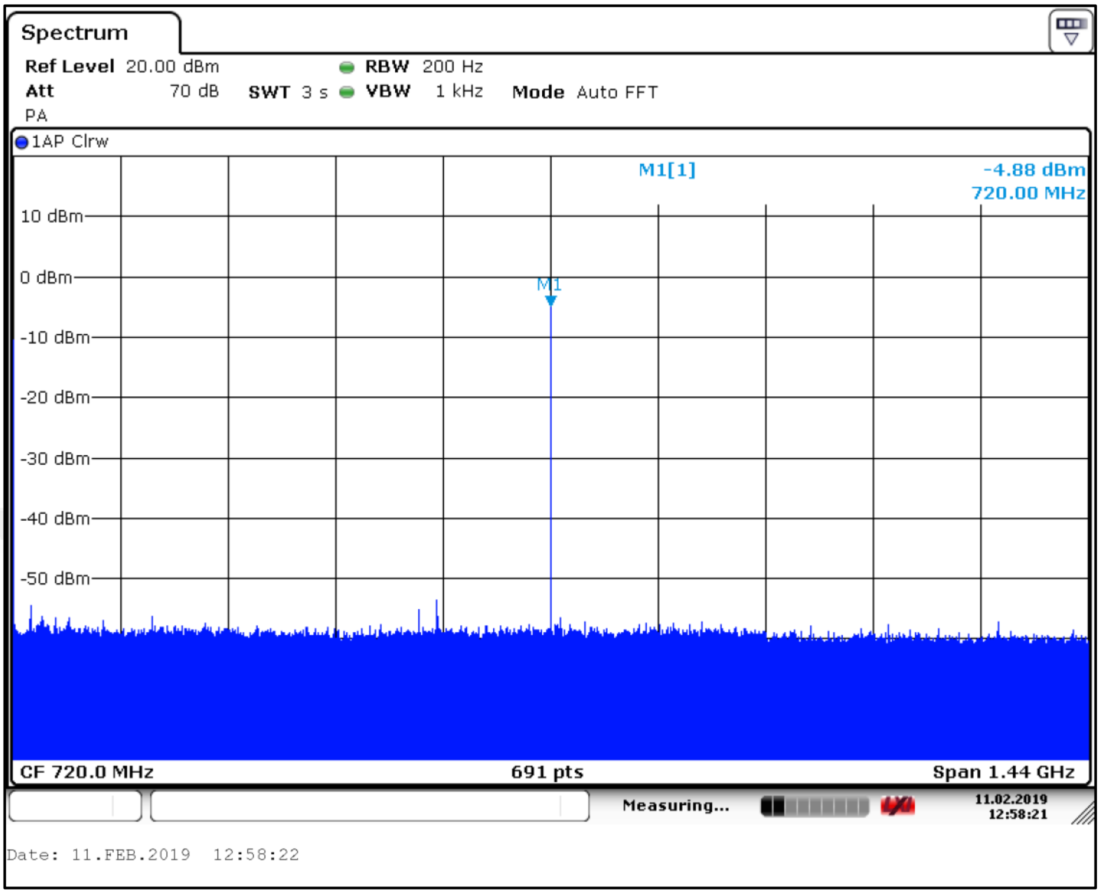

Figure 4.43. 720 MHz signal level for 8400 MHz input frequency

As shown in Figure 4.44, the measurement is made in the bandwidth of 0 - 1440 MHz. RF input signal level is -10 dBm, input frequency is 8500 MHz, and PLL is 7780 MHz. Considering the frequency and PLL value, the output frequency should be 720 MHz. As can be seen in Figure 4.44, the frequency value is shown with a marker. When these measurements are made, the attenuator level for the frequency down converter is - 20 dBm.

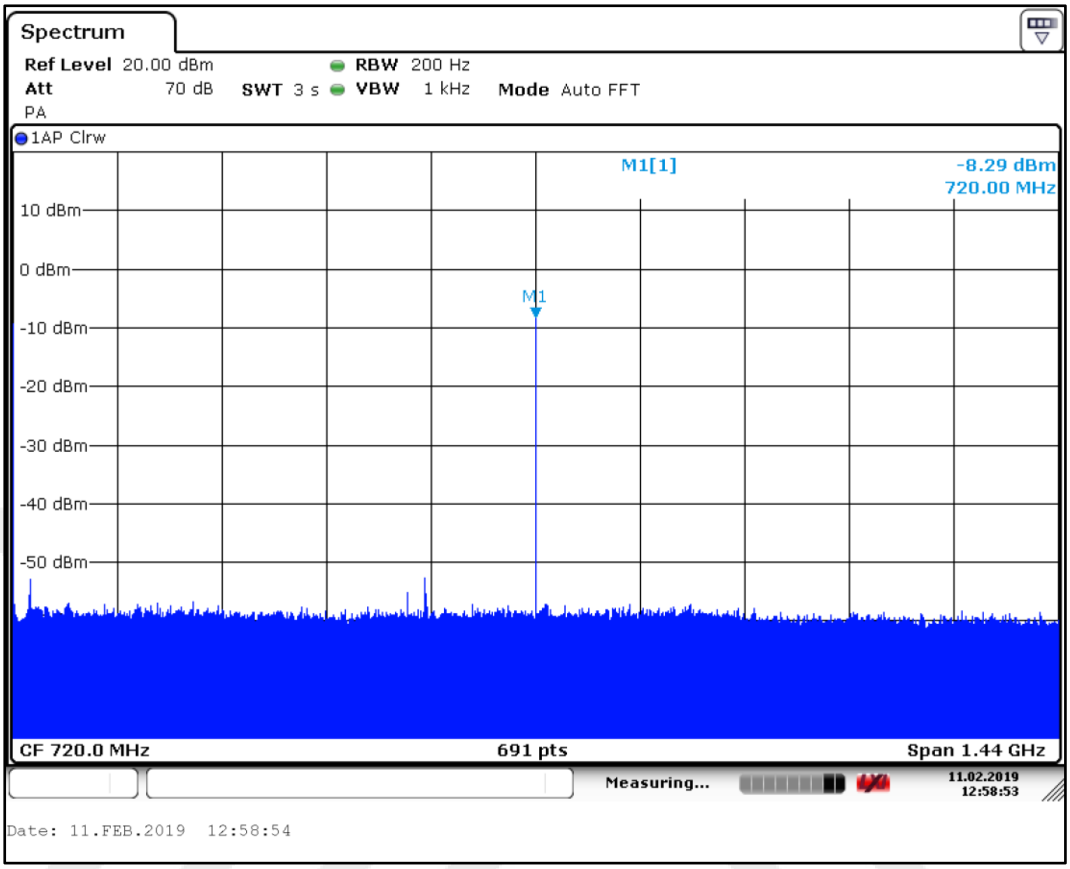

Figure 4.44. 720 MHz input signal level for 8500 MHz input frequency

For the output 1 dB compression power measurement, a 1 dB change is observed in the spectrum analyzer by changing the signal levels at the signal source to 0 dBm, 1 dBm, 2 dBm, 3 dBm, 4 dBm, 10 dBm, 11 dBm, 12 dBm, 13 dBm, 14 dBm, 15 dBm. The measurement results for different signal levels are shown between Figure 4.45 to Figure 4.55.

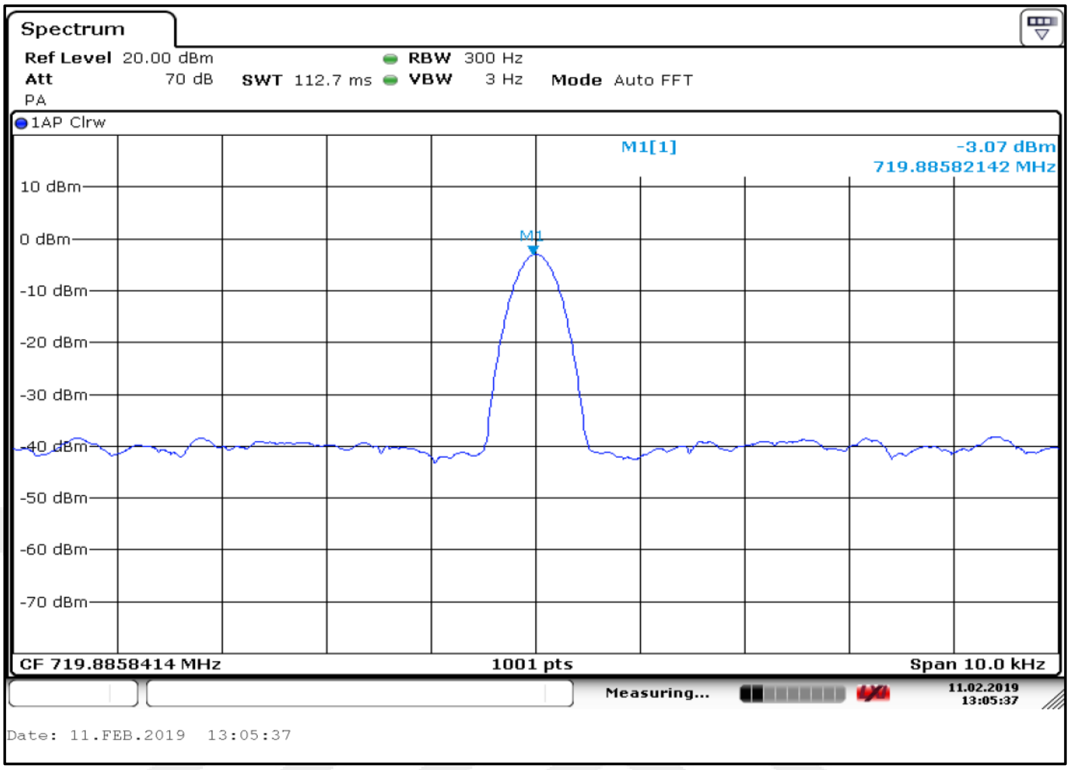

Figure 4.45. P1dB Measurement for 0 dBm input signal

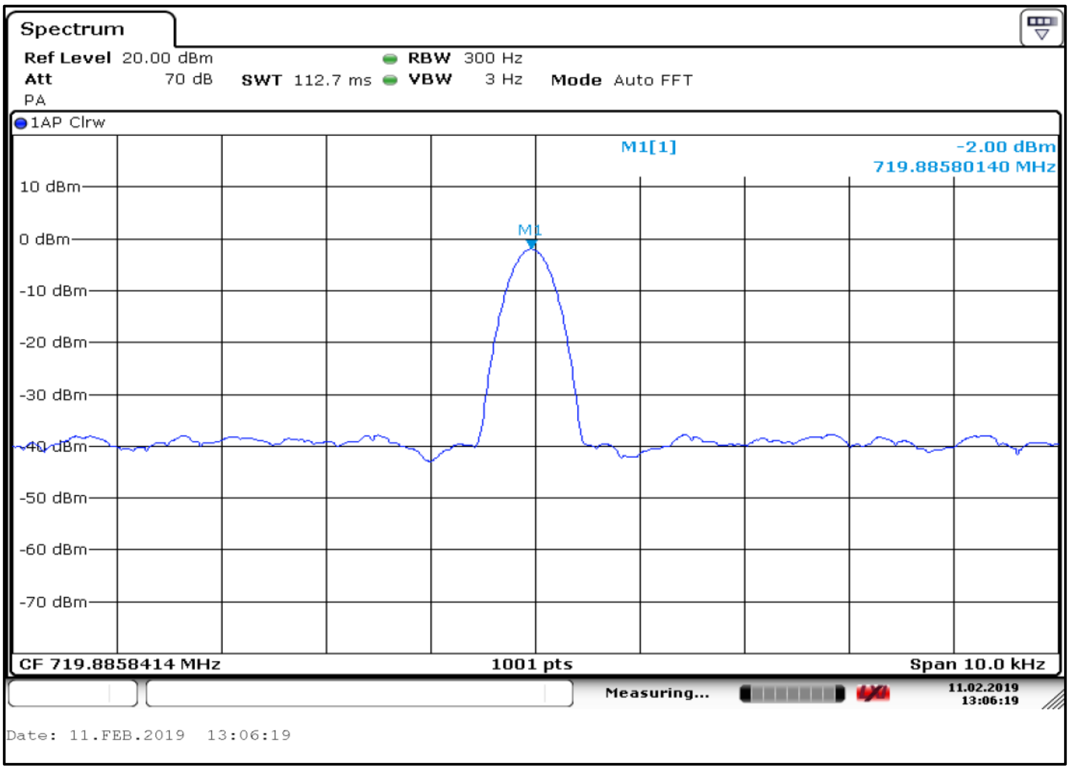

Figure 4.46. P1dB Measurement for 1dBm input signal

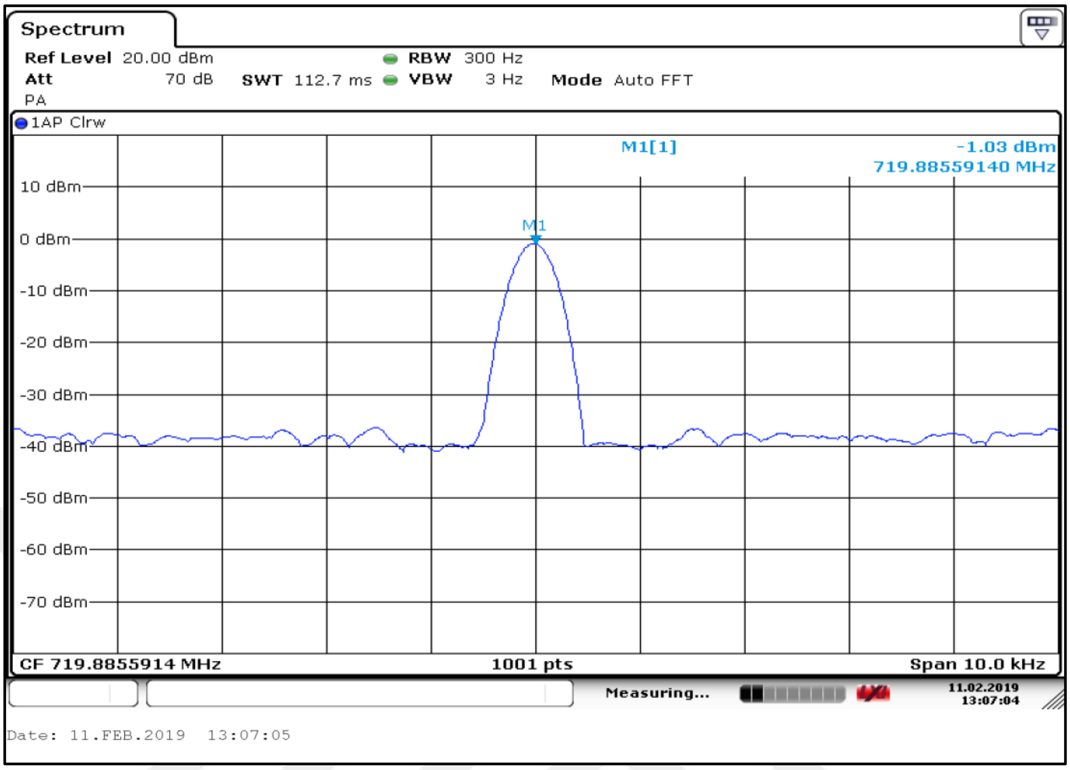

Figure 4.47. P1dB Measurement for 2dBm input signal

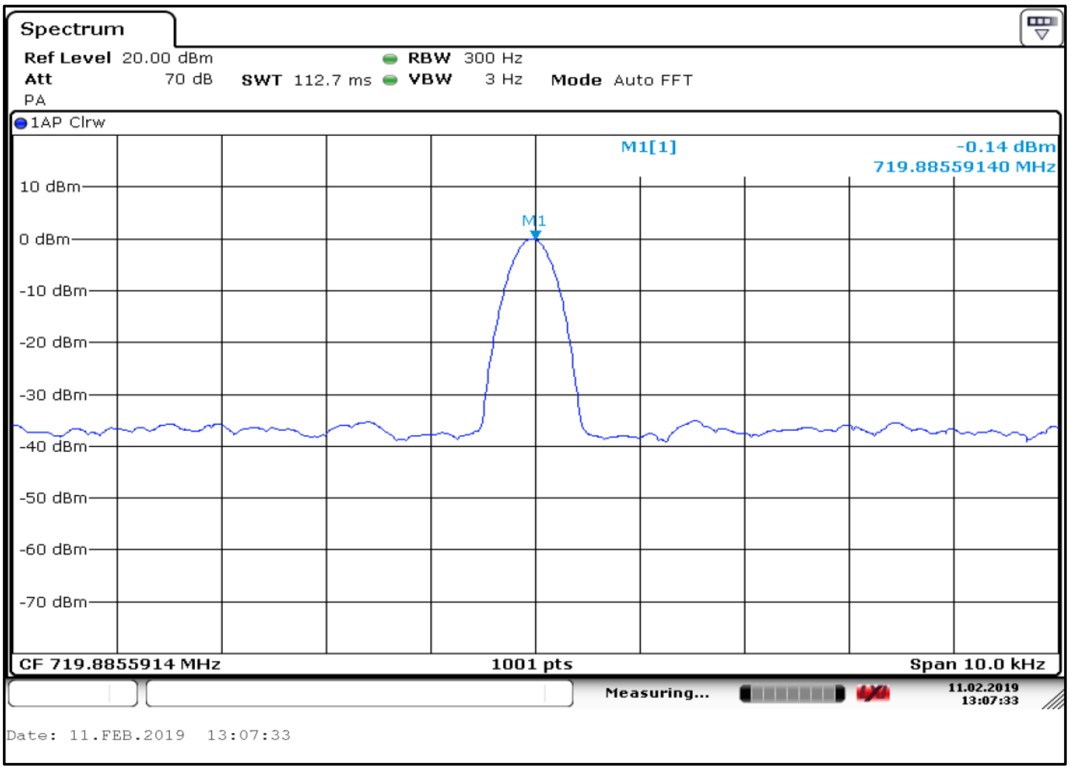

Figure 4.48. P1dB Measurement for 3dBm input signal

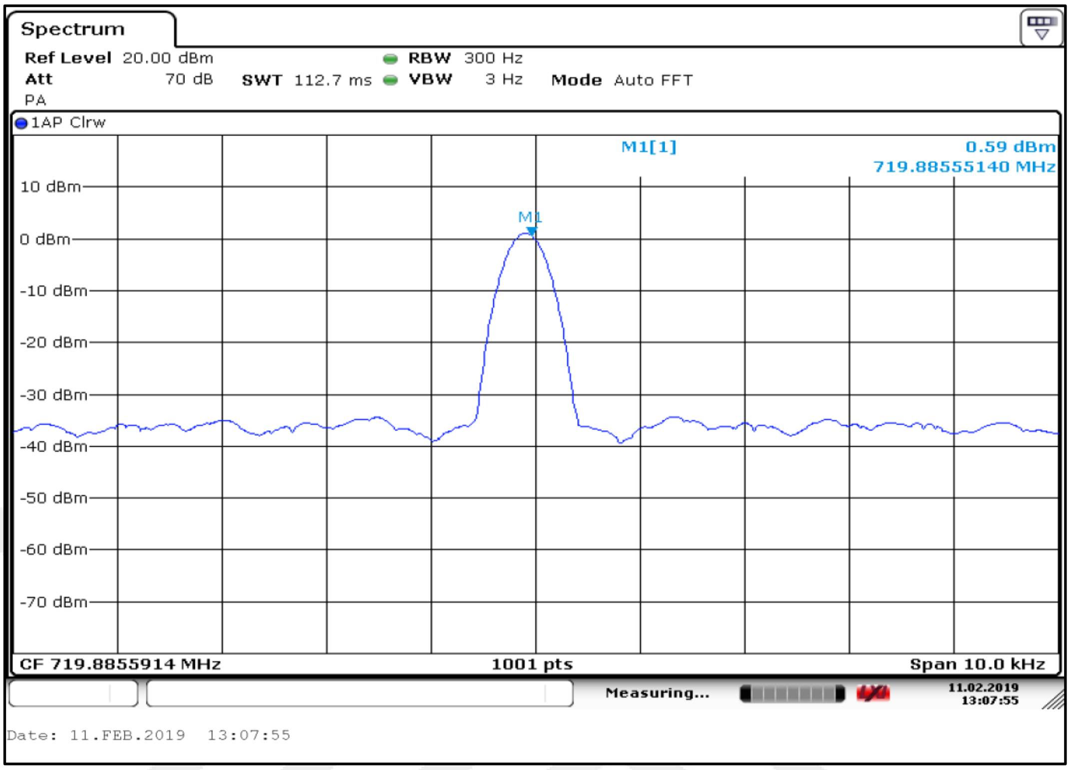

Figure 4.49. P1dB Measurement for 4dBm input signal

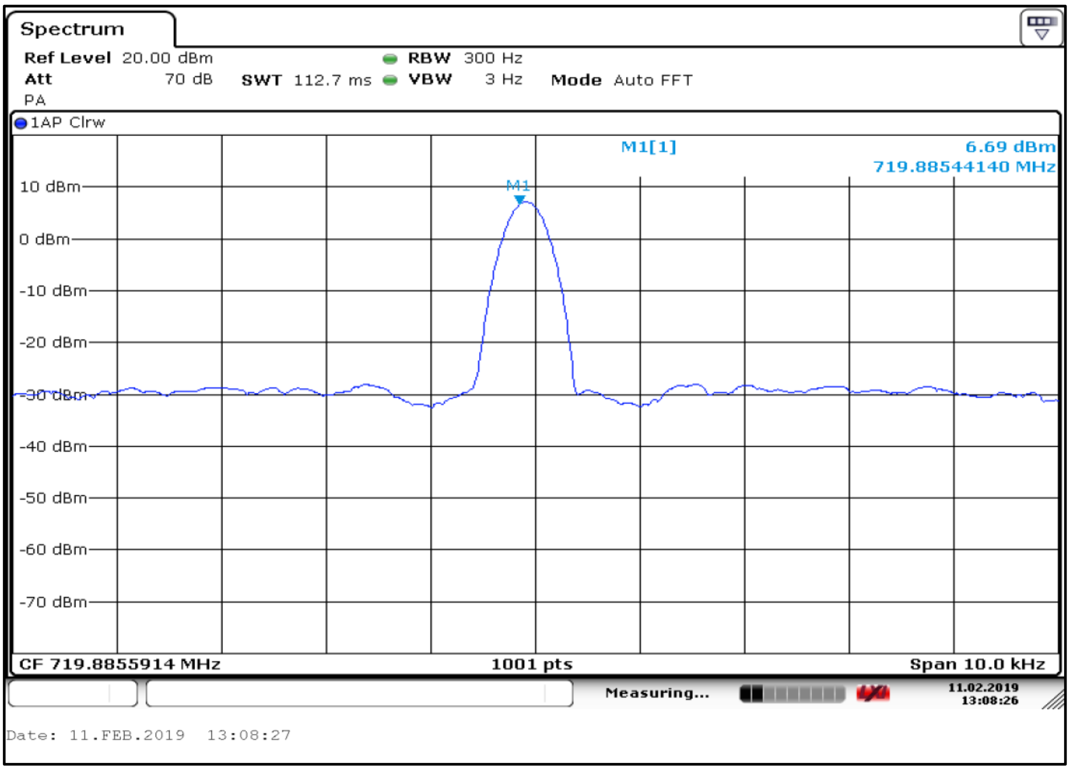

Figure 4.50. P1dB Measurement for 10dBm input signal

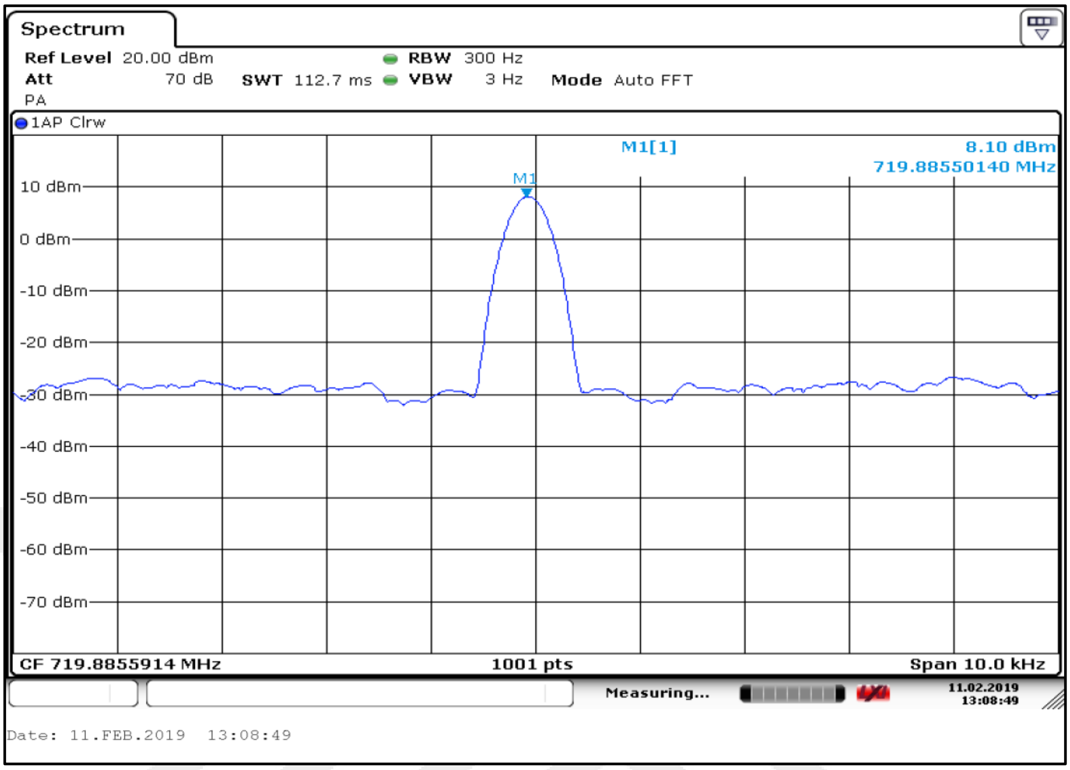

Figure 4.51. P1dB Measurement for 11dBm input signal

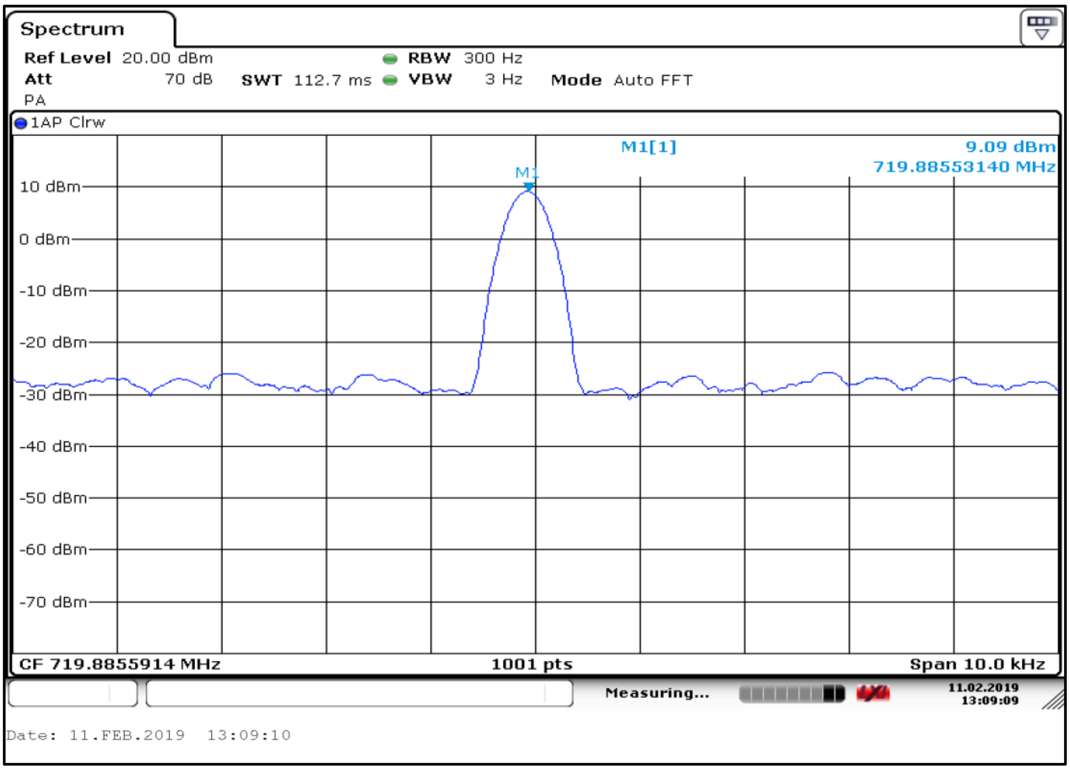

Figure 4.52. P1dB Measurement for 12dBm input signal

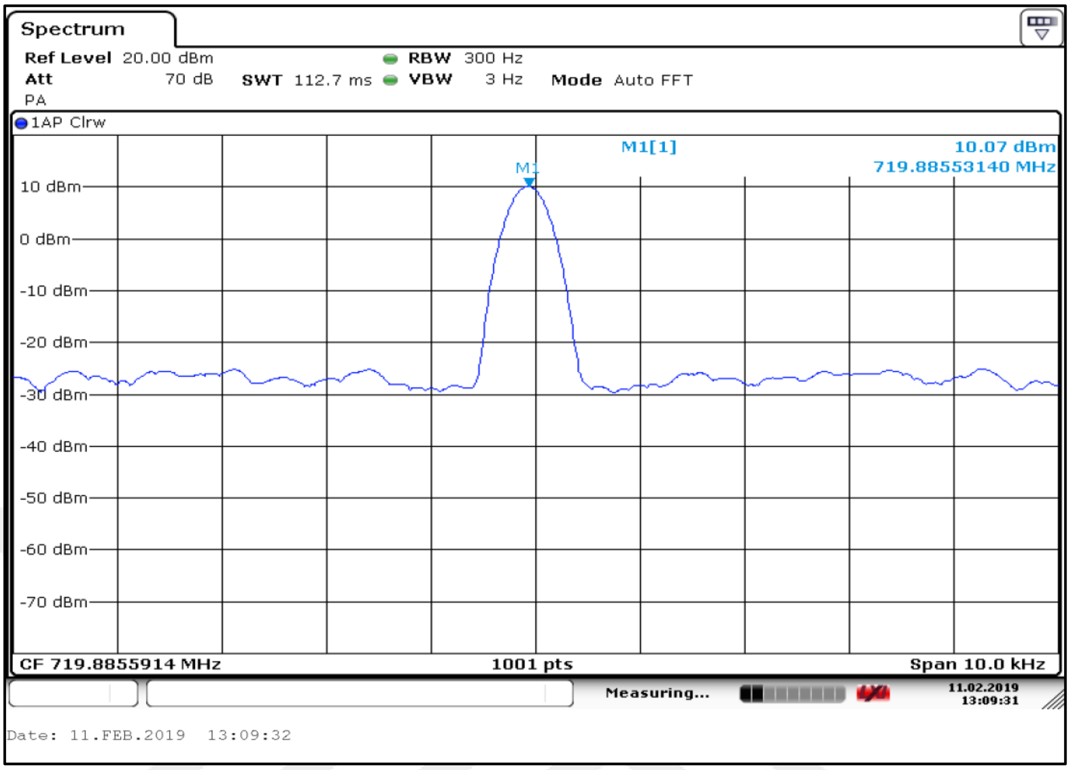

Figure 4.53. P1dB Measurement for 13 dBm input signal

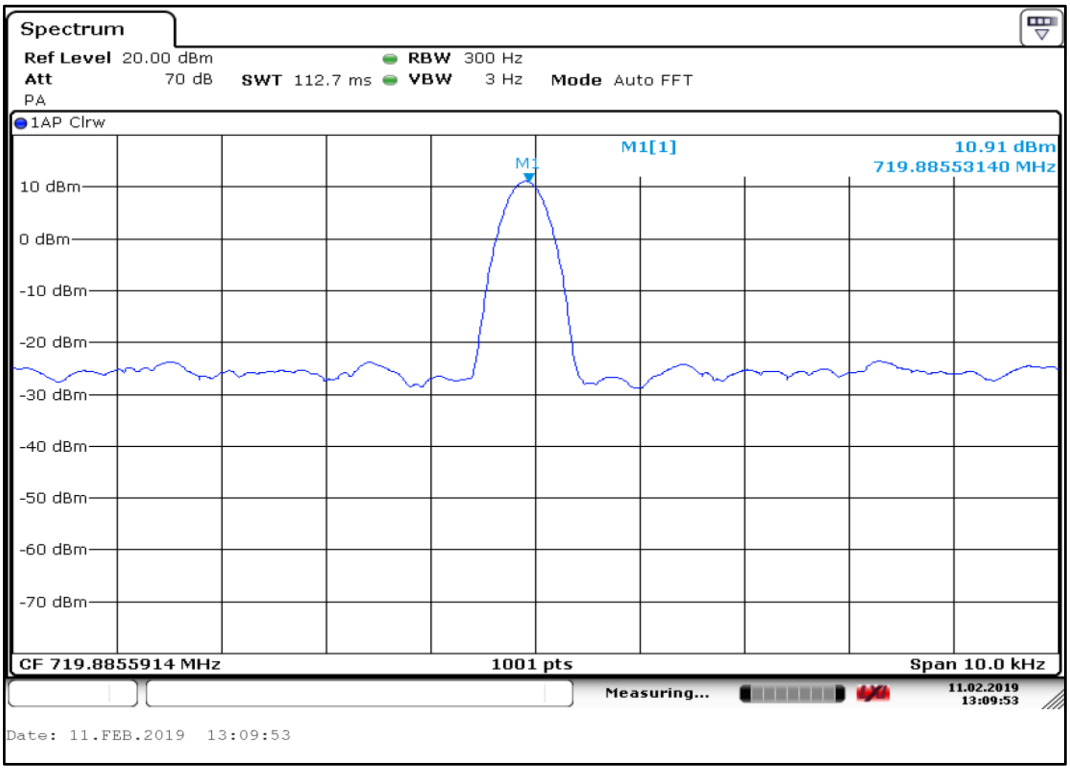

Figure 4.54. P1dB Measurement for 14dBm input signal

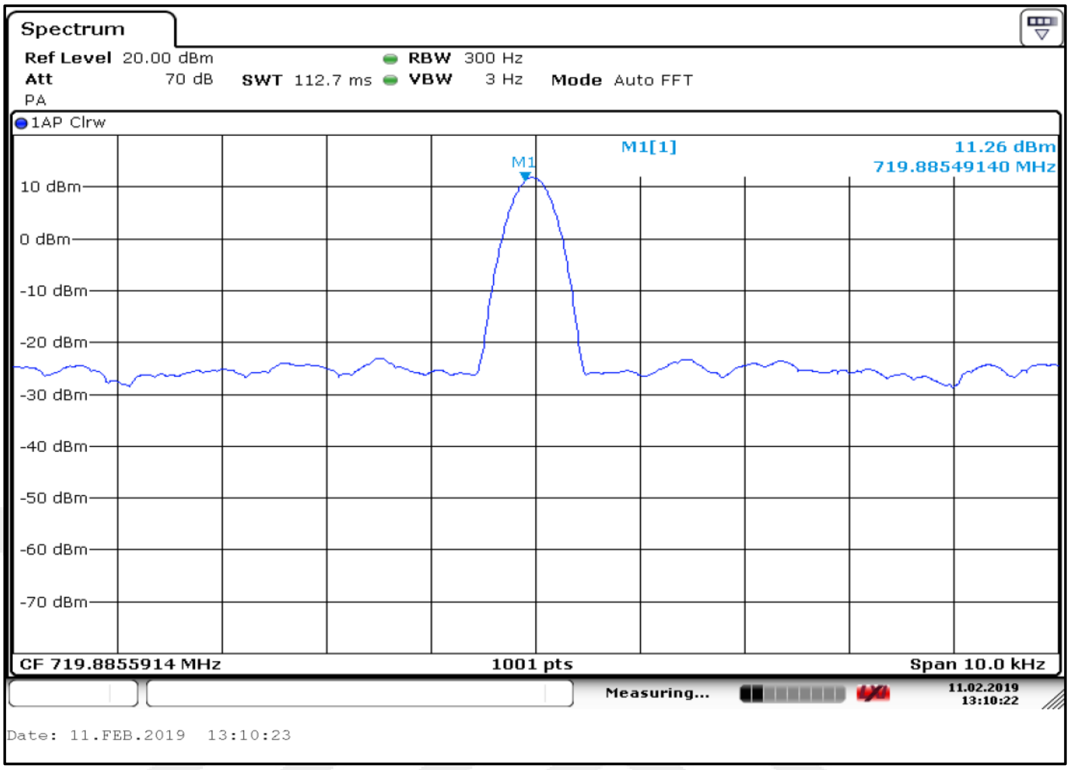

Figure 4.55. P1dB Measurement for 15dBm input signal

As a result of the measurements, the output P1dB is 11.26 dBm. The output P1dB in the technical specification is at a minimum of 10 dBm. The noise figure measurement's input frequency is 8300 MHz, and PLL is 7580 MHz. Note that the input power is -10 dB. Figure 4.56 shows the phase noise measurement of the frequency down converter. The M1 and M2 are -3 dBm and -44.79 dBm, respectively And the difference between these points is - 41.79 dBc. In the spectrum analyzer, RBW is 300 Hz, and VBW is 300 Hz. The phase noise value is -41.79 dBc + (-27.4 dBc): -69.2 dBc/Hz at 1KHz.

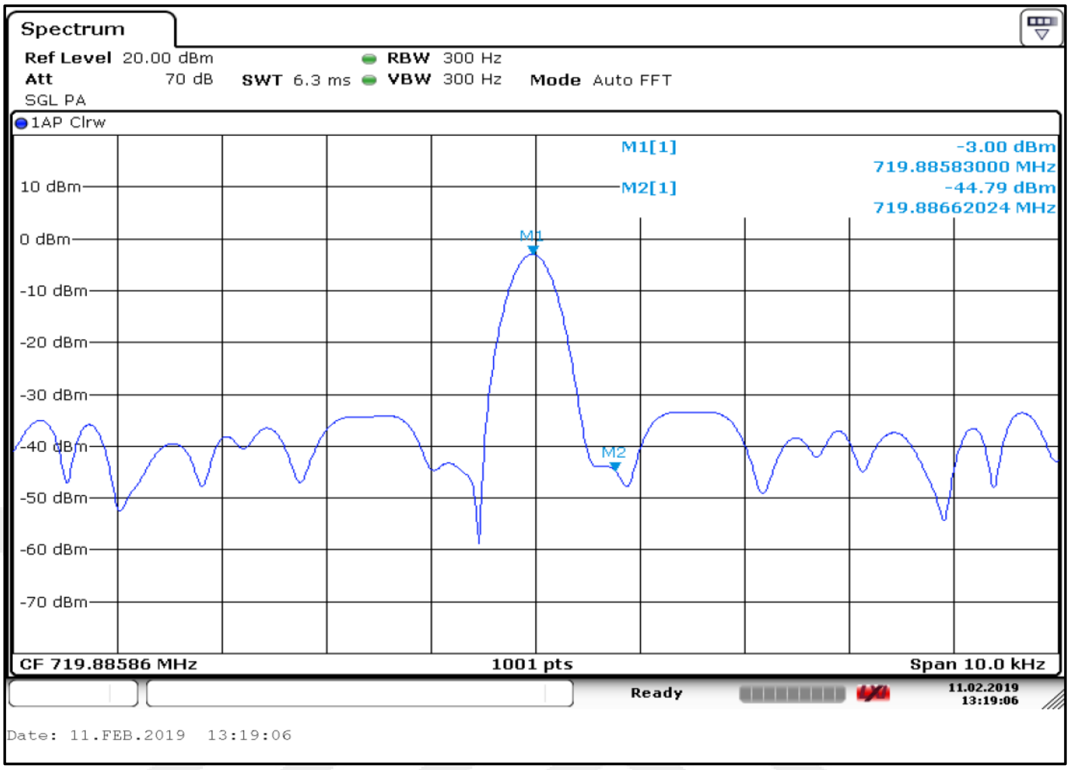

Figure 4.56. Phase noise measurement

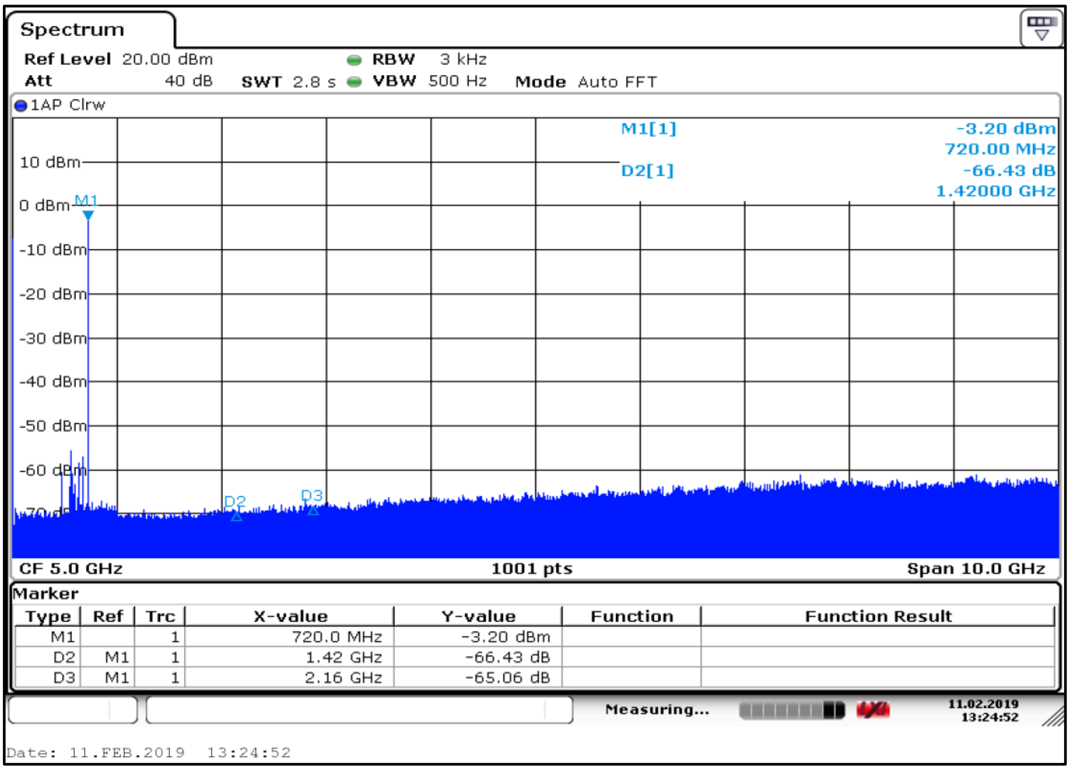

Figure 4.57. Second harmonic level

In the harmonic compression measurement, Figure 4.57 shows the harmonic compression value. This measurement has an input frequency of 8200 MHz, a PLL frequency of 7480 MHz, and an input signal level of 15 dBm. The second harmonic suppression value is below -65 dBm.

The input frequency in the image rejection measurement is 720 MHz, and PLL is 7380 GHz and the input power is -10 dBm. Figure 4.58 demonstrates the measurement result of the image rejection level for the frequency down converter. According to the calculation, the image rejection frequencies correspond to the range of 6560 MHz and 7060 MHz. In the technical requirements, the minimum image rejection value must be -50 dB, and the measurement result is below that in the frequency range.

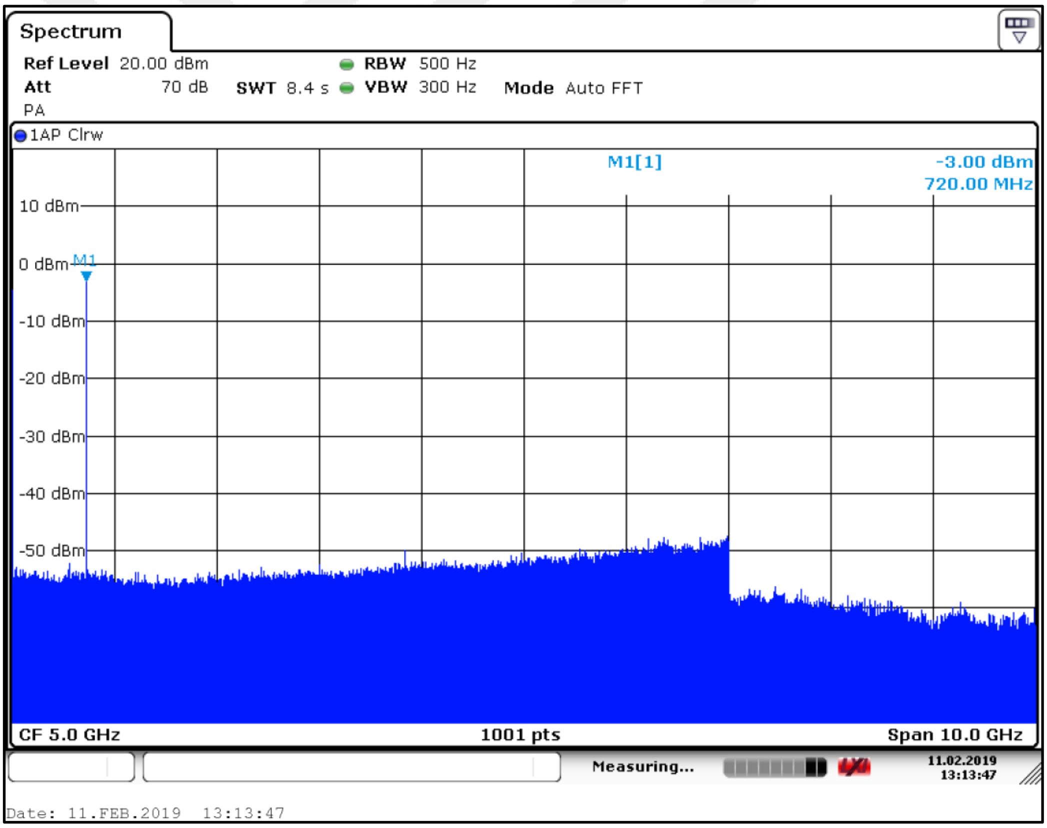

Figure 4.58. Image Rejection Level

In the input and output reflection loss measurements, the measurement of S parameters of X-band frequency down is realised in the 8000 MHz - 8500 MHz frequency range. X-band frequency down converter input and output reflection coefficient is given in Figure 4.59 and

Figure 4.60, respectively. As a result of the measurement, it is observed that the VSWR value required in the technical specification is provided.

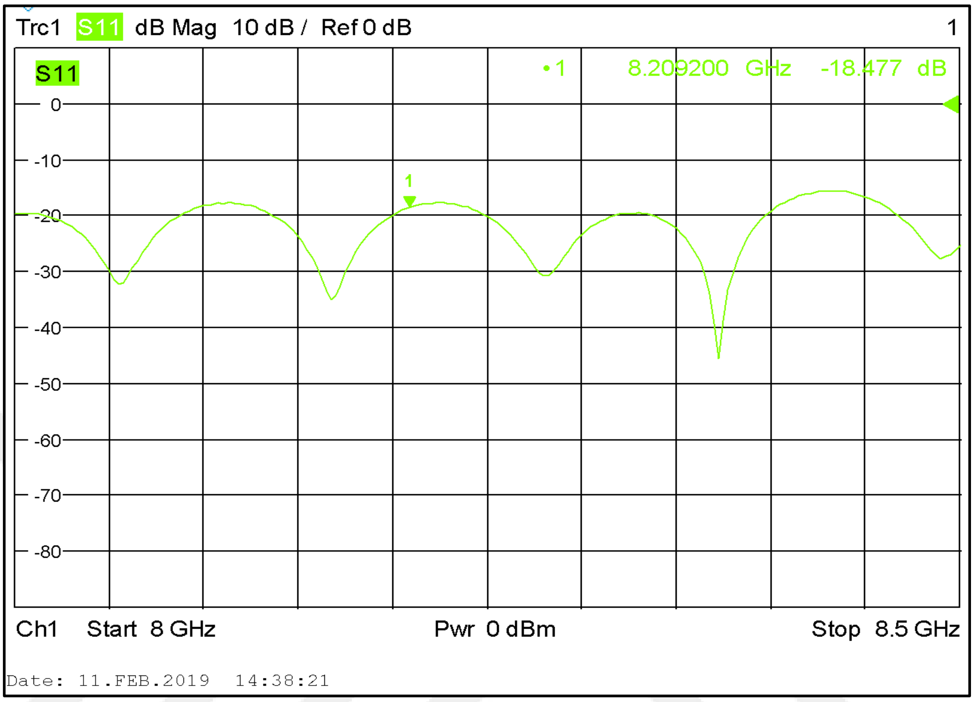

Figure 4.59. Input reflection of the frequency down converter

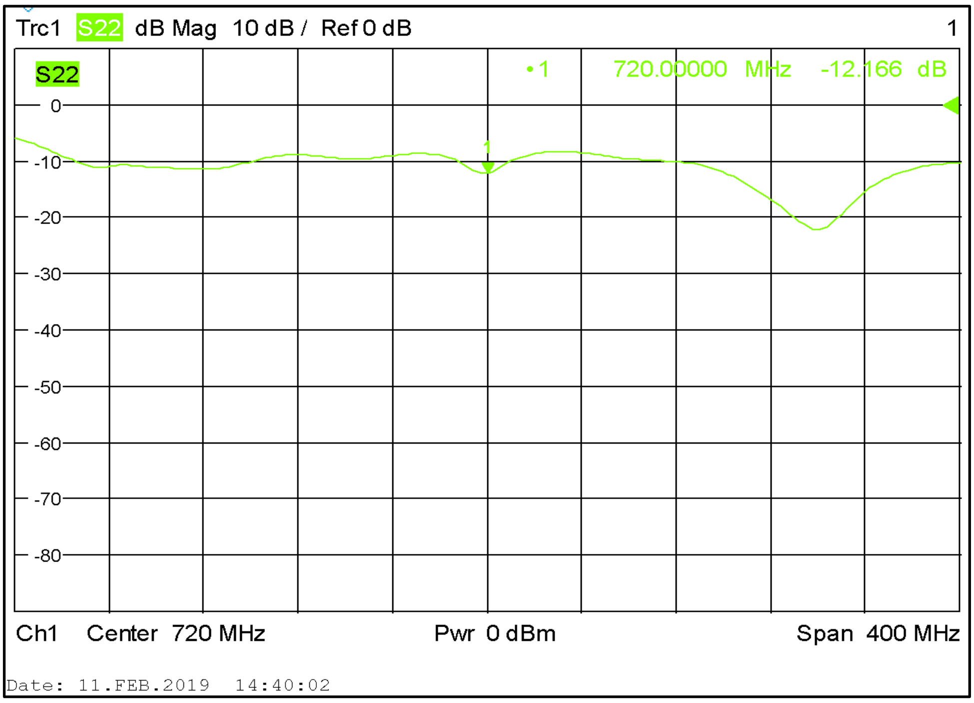

Figure 4.60. Output reflection of the frequency down converter

5. DISCUSSION

The system developed in this dissertation consists of a feed antenna, monopulse antenna, and septum polarizer. The X-band feed antenna used for communication and tracking is a corrugated horn and a monopulse unit is used for the tracking system. A septum polarizer separates RHCP and LHCP signals as linear signals in the feed antenna and waveguides.

The VSWR of the corrugated horn antenna is designed between 1.01 and 1.06. Additionally, the gain of the feed antenna is 19.40 and 19.48 dBi at phi=0 and phi=90, respectively. After the monopulse unit has been added to the feed antenna, the VSWR of the system for all ports is provided about 1.25 in the frequency range for the worst-case scenario. The radiation pattern of the system becomes 19.41 dBi and 19.41 dB at phi=0 and phi=90, respectively. In the septum polarizer part, the insertion loss lies between 3 and 3.14 in the X-band, and the phase difference is better than 94.5 degrees. All parts of the feed system are then combined. The VSWR of the system becomes 1.16, which is not good for the third port. Other ports have better values such as 1.14. It is also noticed that the gain of the feed system becomes 19.36 dBi after the combination process.

The measurement of cross polarization, an essential parameter for satellite operators in ground station systems, has been found as a value exceeding -35 dB. Cross polarization plays a crucial role in efficient bandwidth sharing, because it enables the use of the same frequency in two different polarization settings. However, if either or both systems are incorrectly polarized, the systems may interfere with each other, and the specified frequency cannot be used. A cross-polarization value above -25 dB is considered sufficient for satellite communication. In the proposed system, a value exceeding -35 dB is achieved through equal adjustment of the phase setting on the feed antenna.

The cross-polarization of the feed antenna is measured above -35 dB, which is very important for satellite operators in the ground station system. Because it plays an essential role in sharing and efficiently using bandwidth, the same frequency can be used in 2 different polarisation settings. However, if the polarisation setting of one or both systems is incorrect, the systems may affect each other, and the specified frequency cannot be used. Thus, cross polarization above -25 dB is sufficient for satellite communication. In the proposed system, this value is above -35 dB this which is realized with equal adjustment of the phase setting on the feed antenna.

Moreover, the port isolation value is measured as -23 dB, which is in line with the expected value above -20 dB, considering that the antenna design can receive both RHCP and LHCP. The performance of the feed antenna is consistent with the simulation results, and the crucial factor is the hybrid use of precision CNC fabrication mechanical production within the desired tolerances.

Subsequently, the feed antenna is placed on a reflector antenna with a diameter of 7.3 m, and its performance is measured at 8.25 GHz. A gain of 54.6 dB and an antenna radiation efficiency of 72.5% are achieved. These results demonstrate the designed feed antenna's effectiveness and compatibility with the reflector antenna, providing reliable and efficient communication between the LEO satellite and the ground station system.

In this dissertation, a LNA is designed for X-band communication systems. The LNA typically serves as the first component of a radio frequency receiver after the antenna. Its primary function is amplifying the signal power to the next stage while introducing minimal noise. A four-stage design is used to achieve the required gain, and microstrip technology is employed in the LNA design.

The circuit comprises 50 Ohm input and output ports and input, interstage, and output matching circuits. The S-parameters of the system are between -16 dB and -20 dB for S11, -14 dB, and -22 dB for S22, and 52 dB and 5.5 dB for S21. Moreover, the noise figure ranges from 0.5979 dB to 0.623 dB in the X-band frequency range. The P1dB is measured to be 11.244 dBm which satisfies the technical specification's minimum requirement of 10 dBm.

The frequency downconverter is the subsystem following the LNA in the ground station system. It converts the received high-frequency RF signal to the L band frequency level. This design's most critical performance parameters are gain, output P1dB, noise figure, phase noise, image rejection, LO leakage, and spurious levels. The frequency is converted from 8-8.5 GHz to 720 MHz (±200 MHz) using a single-stage mixer stage. Such broadband frequency attenuation with a single-stage mixer structure poses a challenge in terms of RF. The proposed design has overcome this challenge by testing and matching the filter, mixer, and PLL circuit at appropriate power levels. The resulting RF measurement performance, 11.26 dBm output P1dB, 69.2 dBc/kHz phase noise, 50 dB image rejection, and 42 dBc LO leakage values, is obtained.

The performance of these subsystems to be used in the ground station system directly affects the G/T value, which is the figure of the merit value of the ground station. a high G/T value with a 7.3 m diameter ground station can be achieved using the feed antenna structure, low-noise amplifier, and frequency down-converter.

Finally, the measurement process of the feed system, LNA, and frequency down converter for the X-band shows that the VSWR of all ports, the system's radiation pattern, and the ports' phases meet the simulation results with minor changes.

5.1 COMPARISON WITH EXISTING WORK

Monopulse tracking systems use multiple antennas to gather angular data in the azimuth and elevation axes. Satellite tracking uses a variety of configurations, including four-element, five-element, and monopulse feeds. The ideal monopulse feed has been sought after using various setups. The most popular and straightforward feed design for monopulse has been the four-element feed [27]. However, separate optimization of the sum and difference modes is not feasible in the four elements feed. A five-horn monopulse feed design has been provided with a sizable sum horn, and four rectangular tracking horns had a greater aspect ratio [25]. However, this design has been constrained by an unfavourable between the null and peak, which might result in misleading tracking conditions. A dual-band composite S/X-feed has been achieved utilizing a straightforward, cost-efficient configuration with desired system performance. A common cassegrain plane is where the proposed composite feed is located. A six-element feed is used to achieve X-band functioning, with a corrugated horn serving as the primary element and four circular septum polarizers (CSP) serving as tracking elements. Due to its linear aperture field, the corrugated horn performs better than other elements in terms of low cross polarization and the symmetric beam [9]. The design and implementation of a dual band, dual polarization composite monopulse tracking feed covers the S-band (2.0-2.3 GHz) and X-band (7.8-8.5 GHz). A corrugated horn serving as the primary or sum element is flanked by four circular septum polarizers that operate as tracking elements in an X-band, five-element monopulse feed. A square dielectric array constructed in 2 x 2 configurations makes up the four-element monopulse feed used in the S-band frequency range. The proposed composite feed's illumination efficiency, when placed in the same Cassegrain plane, is greater than the percentage of 90 for both bands [55].

In this dissertation provides an example of the design and effective implementation of a small dual-polarized five-element feed. A central corrugated horn is a primary component, while four rectangular waveguide septums are the tracking component. These tracking components feature waveguide outputs coupled with 180° hybrids to provide a different signal in the two axes. As a result, the design becomes more compact as the bulky waveguide comparator network is removed. The proposed feed is implemented and tested in an anechoic chamber, ensuring high agreement between the measured and simulated patterns. Gains of 54.6 dBi and 54.3 dBi, respectively, are produced by the simulated secondary sum and difference pattern after feeding the observed feed pattern data. After constructing the feed with the reflector antenna, G/T is confirmed using terrestrial sources. The antenna system is currently operating and built for single channel monopulse tracking.

In this dissertation, an LNA was designed to be used in X band LEO satellite applications. Using a transistor with an ideal NF of 0.5 dB, a four-stage amplifier might achieve a maximum NF of 0.623 dB. Gain, stability, and input and output impedance alignment met goal requirements. At this frequency range, the flatness of LNA gain is +/-0.5 dB, which is considered rather excellent. Comparing LNA's performance to that of its commercial competitors, it may be said to be good [60].

In this dissertation, the performance outputs of the design and commercially sold downconverter, this study difference in frequency sense is that all of them designed double conversion superheterodyne products, while we preferred the superheterodyne design. This showed that a product with this feature can perform better than its other counterparts. It is very difficult to achieve such high performance with superheterodyne designs. The new design we offer has reduced the design's complexity and provided higher performance compared to other products in this regard. In the performance comparison of commercially available products, 1st product [56] gives the best performance outputs compared to products [57][58][59]. However, compared to the product [56] of the new design we presented, our image rejection value, output P1dB value, phase noise, Spurious level, and Noise Figure value gave better performance output. These excellent performance outputs prevent the formation of unwanted harmonics in the carrier signal when decoding the broadcast from the satellite in modems, which are the latest terminal units in ground station systems. This is an important requirement in ground station systems.

6. CONCLUSION

In this dissertation, feed antenna, LNA, and frequency down-converter subsystems are designed for use in ground station systems operating in the 8-8.5 GHz frequency band. The need for communication with LEO satellites in ground station systems has been analysed, and the importance of having a high performance in the subsystem units needed for this purpose to the communication quality of the ground station has been examined. Furthermore, the diameter and type of the ground station antenna, the shape of the feed antenna to be used, and the critical performance inputs of the LNA and frequency down converter have been examined. The proposed design process can be categorized into four stages in detail. The first part is determining the diameter and type of the ground station antenna for the desired X-band frequency band communication quality. The second is the design of the appropriate feed antenna for this system, which has tracking capability and high performance. The third is the design of the LNA, and the last part is the design of the frequency down-converter.

Electromagnetic simulations of the designed antenna are performed using CST MWS. Electromagnetic simulations of the LNA and frequency down converter are performed using AWR. One of the feed antennas, LNA, and frequency downconverter are fabricated. Parameters such as radiation pattern, VSWR, gain, cross-polarization and port isolation variations of the antenna along the desired band, parameters such as gain, noise figure, output P1dB and input-output back reflection variations in the low-noise amplifier and parameters such as gain, output P1dB, phase noise, noise figure, image rejection, input-output back reflection and spurious level in the frequency downconverter are measured. It is observed that the measurement results of all sub-units are consistent with the results obtained in simulations. Radiation pattern measurements for the feed antenna are performed in the anechoic chamber of PROFEN using a near-field measurement system.

The most critical points of the designs of this dissertation are the determination of the horn type, septum polariser structure, and monopulse system structure in the feed antenna. The corrugated feed horn design structure affects the desired antenna gain and cross-polarization value. The septum polariser structure affects port isolation and cross-polarization. The tracking feature is a desired feature in the antenna. Here, the monopulse structure with the best tracking sensitivity is preferred, and an X-band feed antenna structure is formed. The best performance output of these units is obtained and integrated. In the LNA, noise figure and gain are essential parameters for subsystem integrity, thus passive components are not used on the RF line. Considering the bandwidth, the DC isolation between the stages is designed with coupling lines and radial stubs are used in the bias tees. These design techniques had direct effects on the best performance. The best performance in the frequency down converter is achieved using a single LO mixer stage. Compared to the literature, providing such high performance at close LO and RF frequencies in terms of frequency is challenging, and this challenge has been achieved in the proposed design. The performance outputs obtained from all these studies directly affect G/T, which is the figure of merit value in the proposed ground station system. With these proposed designs, the maximum G/T value that can be provided in the ground station with an antenna diameter of 7.3 m will be increased by 1.5 dB.

7. FUTURE WORK

In the proposed system, which is used in the communication of satellite ground stations, the following studies are to design a dual-band feed antenna with high gain and high cross-polarisation value, capable of communicating and tracking in both X-band and Ka-band. It is planned to develop low-noise amplifiers and frequency down-converters for utilization in ground stations designed in this way.

REFERENCES

1. Elbert BR. Introduction to Satellite Communications. 2nd ed. Norwood, MA: Artech House; 2008.

2. Elbert BR. The Satellite Communication Applications Handbook. 2nd ed. Norwood, MA: Artech House; 2003.

3. Cakaj S, Malaric K. Isolation measurement between uplink and downlink antennas at low earth orbiting satellite ground station. In: 2007 19th International Conference on Applied Electromagnetics and Communications. IEEE; 2007. p. 1–4.

4. Gadelrab M, Shams SI, Sebak AR. Dual Linear Polarized Antenna Feed for LEO Satellites. In: 2022 International Telecommunications Conference (ITC-Egypt). IEEE; 2022. p. 1–4.

5. Kildal PS. Gaussian beam model for aperture-controlled and flareangle-controlled corrugated horn antennas. IEE Proceedings H Microwaves, Antennas and Propagation. 1988;135(4):237.

6. Wang H, Lu Z, Liu Y, Yu J, Yao Y, Liu X, et al. Design of a tanh profiled compact Gaussian corrugated horn for Cassegrain antenna application. In: 2015 Asia-Pacific Microwave Conference (APMC). IEEE; 2015. p. 1–3.

7. Arora S, Sitaraman P V., Reddy B S, Kraanthi VS, Sriharsha C, V SK. Ka-Band Broad Beam Choke Horn Antenna for LEO Satellite Data Transceiver Application. In: 2019 IEEE Indian Conference on Antennas and Propogation (InCAP). IEEE; 2019. p. 1–4.

8. Roy SS, Sekhar TN, Padmavathy CS, Bhattachariya K, Kumar MN, Saha C. Design of double layers dichroic subreflector for S and X-Band Cassegrain antenna. In: 2016 IEEE Indian Antenna Week (IAW 2016). IEEE; 2016. p. 47–50.

9. James GL. Analysis and Design of TE/sub 11/-to-HE/sub 11/ Corrugated Cylindrical Waveguide Mode Converters. IEEE Trans Microw Theory Tech. 1981 Oct;29(10):1059–66.

10. Barton D, Sherman S. Monopulse Principles and Techniques. 2011.

11. Hannan P. Optimum feeds for all three modes of a monopulse antenna I: Theory. IRE Transactions on Antennas and Propagation. 1961 Sep;9(5):444–54.

12. Bartlett H, Smith E, Gutwein T. Five-horn Cassegrain feed with sidelobe crossover. In: 1977 Antennas and Propagation Society International Symposium. Institute of Electrical and Electronics Engineers; p. 332–5.

13. He G, Gao X, Sun L, Zhang R. A Review of Multibeam Phased Array Antennas as LEO Satellite Constellation Ground Station. IEEE Access. 2021;9:147142–54.

14. Fulton C, Yeary M, Thompson D, Lake J, Mitchell A. Digital Phased Arrays: Challenges and Opportunities. Proceedings of the IEEE. 2016 Mar;104(3):487–503.

15. Herd JS, Conway MD. The Evolution to Modern Phased Array Architectures. Proceedings of the IEEE. 2016 Mar;104(3):519–29.

16. Liu X, Zeng X, Hao C, Zhang H, Yu Z, Lv T, et al. Design of Ka-Band Phased Array Antenna with Calibration Function. Computers, Materials & Continua. 2023;74(3):6251–61.

17. Wu TK. Phased array antenna for tracking and communication with LEO satellites. In: Proceedings of International Symposium on Phased Array Systems and Technology. IEEE; p. 293–6.

18. Zhang Y, Zhu L, Li C, Deng X, Feng H. Store-Load Phased Array Antenna for Tracking and Communication with LEO Satellites. In: 2021 International Symposium on Networks, Computers and Communications (ISNCC). IEEE; 2021. p. 1–6.

19. Kurek K, Yashchyshyn Y, Kondrak G, Modelski J. Investigation of 2D Phased Smart Antenna Array for LEO Satellite System. In: The European Conference on Wireless Technology, 2005. IEEE; p. 77–80.

20. Sanad M, Hassan N. A Multibeam Antenna for Multi-Orbit LEO Satellites and Terminals with a Very Simple Tracking Technique. In: 2022 5th International Conference on Communications, Signal Processing, and their Applications (ICCSPA). IEEE; 2022. p. 1–5.

21. Zheng P, Zhao GQ, Xu SH, Yang F, Sun HJ. Design of a W-Band Full-Polarization Monopulse Cassegrain Antenna. IEEE Antennas Wirel Propag Lett. 2017;16:99–103.

22. Zhao J, Li H, Yang X, Mao W, Hu B, Li T, et al. A Compact Ka-Band Monopulse Cassegrain Antenna Based on Reflectarray Elements. IEEE Antennas Wirel Propag Lett. 2018 Feb;17(2):193–6.

23. Qian S song, Li X guo, Wang B qing. Ka band Cassegrain monopulse antenna fed by tapered rod antennas. In: 2008 8th International Symposium on Antennas, Propagation and EM Theory. IEEE; 2008. p. 39–41.

24. Wang H, Fang DG, Chen XG. A Compact Single Layer Monopulse Microstrip Antenna Array. IEEE Trans Antennas Propag. 2006 Feb;54(2):503–9.

25. Bartlett H. Five-horn Cassegrain Antenna. United States; US4283728A, 1978.

26. Roy SS, Nagasekhar T, Saha C, Mane SB, M. MS, Padmavathy CS, et al. Dual Band (S-X) Ground Station Antenna for Low Earth Orbit (LEO) Satellite Tracking Application. IEEE Access. 2022;10:80910–7.

27. Evans M, Louza S, Audeh NF. Feed for a four-horn monopulse tracking radar. In: 1991 IEEE Aerospace Applications Conference Digest. IEEE; p. 2/1-210.

28. Nawaz W, Ali AKMS. Improvement of gain in dual fed X-Band isoflux Choke horn antenna for use in LEO satellite mission. In: 2015 Fourth International Conference on Aerospace Science and Engineering (ICASE). IEEE; 2015. p. 1–4.

29. Mothe AT, Saha C, Roy SS. Dual Band (X-Ka) Smooth-Wall Multimode Monopulse Feed for LEO Satellite Tracking. In: 2021 IEEE Indian Conference on Antennas and Propagation (InCAP). IEEE; 2021. p. 953–6.

30. Arnaud E, Dugenet J, Elis K, Girardot A, Guihard D, Menudier C, et al. Compact Isoflux X-Band Payload Telemetry Antenna With Simultaneous Dual Circular Polarization for LEO Satellite Applications. IEEE Antennas Wirel Propag Lett. 2020 Oct;19(10):1679–83.

31. Granet C, Davis I, Kot J, Pope G. A simultaneous S/X feed-system for a LEO-satellite-tracking reflector antenna. In: 3rd European Conference on Antennas and Propagation. Berlin; 2009.

32. Chang W, Jeon GI, Park YR, Lee S, Mun JK. X-band LNA MMIC using AlGaN/GaN HEMT technology on SiC substrate. In: 2013 Asia-Pacific Microwave Conference Proceedings (APMC). IEEE; 2013. p. 681–4.

33. Nawaz MI, Aras YE, Zafar S, Akoglu BC, Tendurus G, Ozbay E. X-band Cascode LNA with Bias-invariant Noise Figure using 0.15 µm GaN-on-SiC Technology. In: 2022 Microwave Mediterranean Symposium (MMS). IEEE; 2022. p. 1–4.

34. Kanar T, Rebeiz GM. X- and K-Band SiGe HBT LNAs With 1.2- and 2.2-dB Mean Noise Figures. IEEE Trans Microw Theory Tech. 2014 Oct;62(10):2381–9.

35. Lehmann RE, Heston DD. X-Band Monolithic Series Feedback LNA. IEEE Trans Microw Theory Tech. 1985 Dec;33(12):1560–6.

36. Vittori M, Colangeli S, Ciccognani W, Salvucci A, Polli G, Limiti E. High performance X-band LNAs using a 0.25 µm GaN technology. In: 2017 13th Conference on PhD Research in Microelectronics and Electronics (PRIME). IEEE; 2017. p. 157–60.

37. Cao C, Li X, Li Y, Zeng H, Wang Z, Yasir U. A Triple-Cascode X-Band LNA Design with Modified Post-Distortion Network. Electronics (Basel). 2021 Feb 26;10(5):546.

38. Tsai JH, Huang WL, Lin CY, Chang RA. An X-band low-power CMOS LNA with transformer inter-stage matching networks. In: 2014 9th European Microwave Integrated Circuit Conference. IEEE; 2014. p. 524–7.

39. Wang C, Chen KY, Lee YL, Li CH. A X-Ku-Band QFN-Packaged GaAs LNA Supporting Dual-Polarization Signal Reception. In: 2019 IEEE Asia-Pacific Microwave Conference (APMC). IEEE; 2019. p. 1521–3.

40. Kobayashi KW, Campbell C, Lee C, Gallagher J, Shust J, Botelho A. A reconfigurable S-/X-band GaN cascode LNA MMIC. In: 2017 IEEE Compound Semiconductor Integrated Circuit Symposium (CSICS). IEEE; 2017. p. 1–4.

41. Kuo WML, Krithivasan R, Li X, Lu Y, Cressler JD, Gustat H, et al. A Low-Power,X-Band SiGe HBT Low-Noise Amplifier for Near-Space Radar Applications. IEEE Microwave and Wireless Components Letters. 2006 Sep;16(9):520–2.

42. Thrivikraman TK, Kuo WML, Comeau JP, Sutton AK, Cressler JD, Marshall PW, et al. A 2 mW, Sub-2 dB Noise Figure, SiGe Low-Noise Amplifier For X-band High-Altitude or Space-based Radar Applications. In: 2007 IEEE Radio Frequency Integrated Circuits (RFIC) Symposium. IEEE; 2007. p. 629–32.

43. Qiu C, Zhang S. Design of a X-band down converter module. In: 2019 International Conference on Microwave and Millimeter Wave Technology (ICMMT). IEEE; 2019. p. 1–3.

44. Eppe B, Soniya N, Sivaprasad PVL. Analysis and design of x-band down converter for data acquisition system of satellite ground station. In: 2017 International Conference on Computing Methodologies and Communication (ICCMC). IEEE; 2017. p. 635–40.

45. Tu Z, Xu J, Chen K, Lei O, Zhang X. Design of a X -band Frequency-Conversion Front-End T/R Module. In: 2018 China International SAR Symposium (CISS). IEEE; 2018. p. 1–3.

46. Yoshimasu T, Sakuno K, Matsumoto N, Suematsu E, Tsukao T, Tomita T. A low current GaAs monolithic image rejection downconverter for X-band broadcast satellite applications. IEEE Trans Microw Theory Tech. 1992;40(12):2433–8.

47. Kumar A, Pai P, Kavitha V, Prashanth S. Design of X-Band Pulsed Power Amplifier & Downconverter. In: 2021 IEEE MTT-S International Microwave and RF Conference (IMARC). IEEE; 2021. p. 1–4.

48. Roy SS, Saha C, Nagasekhar T, Mane SB, Padmavathy CS, Umadevi G, et al. Design of a Compact Multielement Monopulse Feed for Ground-Station Satellite Tracking Applications. IEEE Antennas Wirel Propag Lett. 2019 Sep;18(9):1721–5.

49. Sherman SM. Monopulse Principles and Techniques. Norwood, MA: Artech House; 1984.

50. Nateghi J, Mohammadi L, Solat GR. Analysis of the four-horn monopulse for LEO satellite tracking using the exact model. In: 11th International Conference on Advanced Communication Technology. 2009.

51. Evans M, Louza S, Audeh NF. Feed for a four-horn monopulse tracking radar. In: 1991 IEEE Aerospace Applications Conference Digest. IEEE; p. 2/1-210.

52. Bornemann J, Labay VA. Ridge waveguide polarizer with finite and stepped-thickness septum. IEEE Trans Microw Theory Tech. 1995;43(8):1782–7.

53. Zhong W, Li B, Fan Q, Shen Z. X-band compact septum polarizer design. In: 2011 IEEE International Conference on Microwave Technology & Computational Electromagnetics. IEEE; 2011. p. 167–70.

54. Jeeheung Kim, Seongsik Yoon, Eunyoung Jung, Lee JW, Lee TK, Lee WK. Triangular-shaped stepped septum polarizer for satellite communication. In: 2011 IEEE International Symposium on Antennas and Propagation (APSURSI). IEEE; 2011. p. 854–7.

55. James GL. Dual Band (S-X) Ground Station Antenna for Low Earth Orbit (LEO) Satellite Tracking Application," IEEE Access vol. 10, no. 10, pp. 80910-80917, 2022.

56. https://bhe-mw.eu/wp-content/uploads/2023/03/BMCD127-LM-K10992-V01.pdf.

57. https://www.crosstechnologies.com/data_sheets/2016-8085720_DATA_SHEET.pdf.

58. http://www.novella.co.uk/PDF/Downconverter_Specs_X_band_720MHz.pdf.

59. https://teldatasystem.de/wp-content/uploads/2013/09/Media126.pdf.

60. https://www.kuhne-electronic.com/funk/en/shop/industrial/prof-low-noise-ampli/prof-lna-x-band/.

APPENDIX

The datasheet of the CE3512K2 is below:

CEL

RF Low Noise FET

CE3512K2

12 GHz Super Low Noise FET in Hollow Plastic PKG

DESCRIPTION

- Super Low Noise and High Gain
- Hollow (Air Cavity) Plastic package

FEATURES

- Super Low noise figure and high associated gain:
  NF = 0.30 dB TYP., Ga = 13.7 dB TYP.
  @V_{DS} = 2 V, I_D = 10 mA, f = 12 GHz

PACKAGE

- Micro-X plastic package

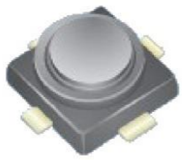

APPLICATIONS

- KU Band LNB (Low Noise Block)
  Suitable for 1st Stage

ORDERING INFORMATION

Part Number	Order Number	Package	Marking	Description
CE3512K2	CE3512K2-C1	Micro-X plastic package	C5	• Embossed tape 8 mm wide • Pin 4 (Gate) faces the perforation side of the tape • MOQ 10 kpcs/reel

This document is subject to change without notice.
Date Published: Nov 2018
CDS-0018-05 (Issue B)

1

The datasheet of the MGF4935AM is below:

May/2008

MITSUBISHI SEMICONDUTOR <GaAs FET>

MGF4935AM

SUPER LOW NOISE InGaAs HEMT (4pin flat lead package)

DESCRIPTION

The MGF4935AM super-low noise HEMT (High Electron Mobility Transistor) is designed for use in S to Ku band amplifiers.

The 4pin flat lead package is small-thin size, and offers high cost performance.

Outline Drawing

Fig.1

FEATURES

Low noise figure @ f=12GHz
NFmin. = 0.45dB (Typ.)

High associated gain @ f=12GHz
Gs = 12.0dB (Typ.)

MITSUBISHI Proprietary
Not to be reproduced or disclosed
without permission by Mitsubishi Electric

APPLICATION

S to Ku band low noise amplifiers

QUALITY GRADE

GG

RECOMMENDED BIAS CONDITIONS

V_{DS}=2V , I_D=10mA

ORDERING INFORMATION

Tape & reel 3000pcs/reel

Keep Safety first in your circuit designs!

Mitsubishi Electric Corporation puts the maximum effort into making semiconductor products better and more reliable , but there is always the possibility that trouble may occur with them. Trouble with semiconductors may lead to personal injury , fire or property damage. Remember to give due consideration to safety when making your circuit designs , with appropriate measure such as (I) placement of substitutive , auxiliary circuits , (ii) use of non-flammable material or (iii) prevention against any malfunction or mishap.

ABSOLUTE MAXIMUM RATINGS (Ta=25°C)

Symbol	Parameter	Ratings	Unit
V_{GDO}	Gate to drain voltage	-3	V
V_{GSO}	Gate to source voltage	-3	V
I_D	Drain current	IDSS	mA
PT	Total power dissipation	50	mW
T_{ch}	Channel temperature	125	°C
T_{stg}	Storage temperature	-55 to +125	°C

ELECTRICAL CHARACTERISTICS (Ta=25°C)

Symbol	Parameter	Test conditions	Limits			Unit
			MIN.	TYP.	MAX	
$V_{(BR)GDO}$	Gate to drain breakdown voltage	I_G=-10μA	-3.5	--	--	V
I_{GSS}	Gate to source leakage current	V_{GS}=-2V,V_{DS}=0V	--	--	50	μA
I_{DSS}	Saturated drain current	V_{GS}=0V,V_{DS}=2V	12	--	60	mA
$V_{GS(off)}$	Gate to source cut-off voltage	V_{DS}=2V,I_D=500μA	-0.1	--	-1.5	V
Gs	Associated gain	V_{DS}=2V,	11.0	12.0	--	dB
NFmin.	Minimum noise figure	I_D=10mA,f=12GHz	--	0.45	0.65	dB

MITSUBISHI

The datasheet of the ADM7160 is below:

ANALOG DEVICES

Ultralow Noise, 200 mA Linear Regulator

Data Sheet **ADM7160**

FEATURES

PSRR performance of 54 dB at 100 kHz
Ultralow noise independent of V_{OUT}
- **3 µV rms, 0.1 Hz to 10 Hz**
- **9.5 µV rms, 0.1 Hz to 100 kHz**
- **9 µV rms, 10 Hz to 100 kHz**
- **17 µV rms, 10 Hz to 1 MHz**

Low dropout voltage: 150 mV at 200 mA load
Maximum output current: 200 mA
Input voltage range: 2.2 V to 5.5 V
Low quiescent and shutdown current
Initial accuracy: ±1%
Accuracy over line, load, and temperature: −2.5%/+1.5%
5-lead TSOT package and 6-lead LFCSP package

APPLICATIONS

ADC/DAC power supplies
RF, VCO, and PLL power supplies
Post dc-to-dc regulation

APPLICATION CIRCUIT

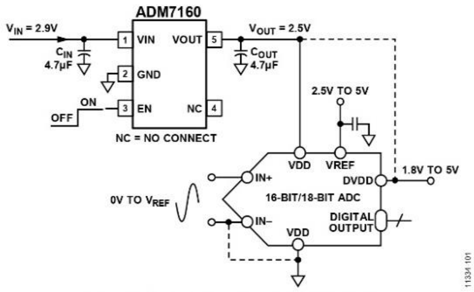

Figure 1. ADM7160 Powering a 16-Bit/18-Bit ADC

GENERAL DESCRIPTION

The ADM7160 is an ultralow noise, low dropout linear regulator that operates from 2.2 V to 5.5 V and provides up to 200 mA of output current. The low 150 mV dropout voltage at 200 mA load improves efficiency and allows operation over a wide input voltage range.

Using an innovative circuit topology, the ADM7160 achieves ultralow noise performance without the need for a bypass capacitor, making the device ideal for noise-sensitive analog front-end and RF applications. The ADM7160 also achieves ultralow noise performance without compromising PSRR or transient line and load performance.

Current-limit and thermal overload protection circuits prevent damage under adverse conditions. The ADM7160 also includes an internal pull-down resistor on the EN input.

The ADM7160 is specifically designed for stable operation with tiny 1 µF, ±30% ceramic input and output capacitors to meet the requirements of high performance, space constrained applications.

The ADM7160 is available in tiny 5-lead TSOT and 6-lead LFCSP packages with 16 fixed output voltage options, ranging from 1.1 V to 3.3 V. The LFCSP offers a very compact solution that provides excellent thermal performance for applications that require up to 200 mA of output current in a small, low profile footprint.

One Technology Way, P.O. Box 9106, Norwood, MA 02062-9106, U.S.A.
Tel: 781.329.4700

The datasheet of the TPS72325 is below:

Product Folder | Order Now | Technical Documents | Tools & Software | Support & Community

TEXAS INSTRUMENTS

TPS723

SLVS346D – SEPTEMBER 2003 – REVISED DECEMBER 2019

TPS723 200-mA, Low-Noise, High-PSRR, Negative Output Low-Dropout Linear Regulators

1 Features

- Ultralow noise: 60 μV_{RMS} typical
- High PSRR: 65 dB typical at 1 kHz
- Low dropout voltage: 280 mV typical at 200 mA, 2.5 V
- Available in –2.5-V and adjustable (–1.2 V to –10 V) versions
- Stable with a 2.2-μF ceramic output capacitor
- Less than 2-μA typical quiescent current in shutdown mode
- 2% overall accuracy (line, load, temperature)
- Thermal and over-current protection
- Packages:
  - SOT23-5 (DBV)
  - SOT23-5 (DDC)
  - WSON-6 (DRV)
- Operating junction temperature range: –40°C to 125°C

2 Applications

- Optical modules
- Semiconductor manufacturing
- Medical accessories
- Oscilloscopes
- Active antenna system mMIMO (AAS)

3 Description

The TPS723 low-dropout (LDO) negative voltage regulator offers an ideal combination of features to support low noise applications. This device is capable of operating with input voltages from –10 V to –2.7 V, and support outputs from –10 V to –1.2 V. This regulator is stable with small, low-cost ceramic capacitors, and include enable (EN) and noise reduction (NR) functions. Thermal short-circuit and over-current protections are provided by internal detection and shutdown logic. High PSRR (65 dB at 1 kHz) and low noise (60 μV_{RMS}) make the TPS723 ideal for low-noise applications.

The TPS723 uses a precision voltage reference to achieve 2% overall accuracy over load, line, and temperature variations. Available in a small SOT23-5 package, the TPS723 is fully specified over a temperature range of –40°C to 125°C.

Device Information(1)

PART NUMBER	PACKAGE(2)	BODY SIZE (NOM)
TPS723	SOT-23 (5)	2.90 mm x 1.60 mm
	SOT (5)	2.90 mm x 1.60 mm
	WSON (6)	2.00 mm x 2.00 mm

(1) For all available packages, see the orderable addendum at the end of the data sheet.

(2) The two SOT23 packages are identical in size, but the SOT package is thinner.

Typical Application Circuit

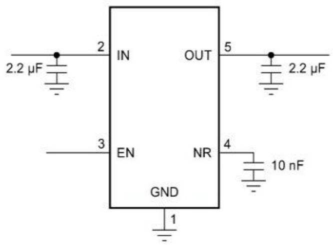

The datasheet of the LM2931AMX is below:

TEXAS INSTRUMENTS

LM2931-N

www.ti.com SNOSBE5G – MARCH 2000 – REVISED APRIL 2013

LM2931-N Series Low Dropout Regulators

Check for Samples: LM2931-N

FEATURES

- **Very Low Quiescent Current**
- **Output Current in Excess of 100 mA**
- **Input-output Differential Less than 0.6V**
- **Reverse Battery Protection**
- **60V Load Dump Protection**
- **−50V Reverse Transient Protection**
- **Short Circuit Protection**
- **Internal Thermal Overload Protection**
- **Mirror-image Insertion Protection**
- **Available in TO-220, TO-92, TO-263, or SOIC-8 Packages**
- **Available as Adjustable with TTL Compatible Switch**

DESCRIPTION

The LM2931-N positive voltage regulator features a very low quiescent current of 1mA or less when supplying 10mA loads. This unique characteristic and the extremely low input-output differential required for proper regulation (0.2V for output currents of 10mA) make the LM2931-N the ideal regulator for standby power systems. Applications include memory standby circuits, CMOS and other low power processor power supplies as well as systems demanding as much as 100mA of output current.

Designed originally for automotive applications, the LM2931-N and all regulated circuitry are protected from reverse battery installations or 2 battery jumps. During line transients, such as a load dump (60V) when the input voltage to the regulator can momentarily exceed the specified maximum operating voltage, the regulator will automatically shut down to protect both internal circuits and the load. The LM2931-N cannot be harmed by temporary mirror-image insertion. Familiar regulator features such as short circuit and thermal overload protection are also provided.

The LM2931-N family includes a fixed 5V output (±3.8% tolerance for A grade) or an adjustable output with ON/OFF pin. Both versions are available in a TO-220 power package, DDPAK/TO-263 surface mount package, and an 8-lead SOIC package. The fixed output version is also available in the TO-92 plastic package.

Connection Diagrams

FIXED VOLTAGE OUTPUT

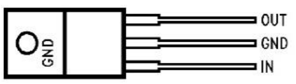

Figure 1. TO-220 3-Lead Power Package Front View

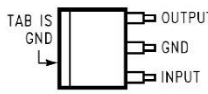

Figure 2. DDPAK/TO-263 Surface-Mount Package Top View

Figure 3. Side View

The datasheet of the TC7660 is below:

MICROCHIP

TC7660

Charge Pump DC-to-DC Voltage Converter

Features

- Wide Input Voltage Range: +1.5V to +10V
- Efficient Voltage Conversion (99.9%, typ)
- Excellent Power Efficiency (98%, typ)
- Low Power Consumption: 80 µA (typ) @ V_{IN} = 5V
- Low Cost and Easy to Use
  - Only Two External Capacitors Required
- Available in 8-Pin Small Outline (SOIC), 8-Pin PDIP and 8-Pin CERDIP Packages
- Improved ESD Protection (3 kV HBM)
- No External Diode Required for High-Voltage Operation

Applications

- RS-232 Negative Power Supply
- Simple Conversion of +5V to ±5V Supplies
- Voltage Multiplication $V_{OUT} = \pm n V^+$
- Negative Supplies for Data Acquisition Systems and Instrumentation

Package Types

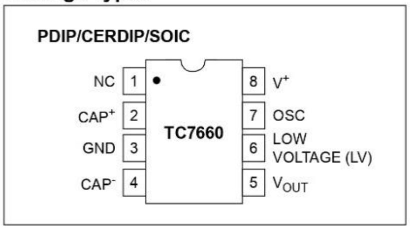

General Description

The TC7660 device is a pin-compatible replacement for the industry standard 7660 charge pump voltage converter. It converts a +1.5V to +10V input to a corresponding -1.5V to -10V output using only two low-cost capacitors, eliminating inductors and their associated cost, size and electromagnetic interference (EMI).

The on-board oscillator operates at a nominal frequency of 10 kHz. Operation below 10 kHz (for lower supply current applications) is possible by connecting an external capacitor from OSC to ground.

The TC7660 is available in 8-Pin PDIP, 8-Pin Small Outline (SOIC) and 8-Pin CERDIP packages in commercial and extended temperature ranges.

Functional Block Diagram

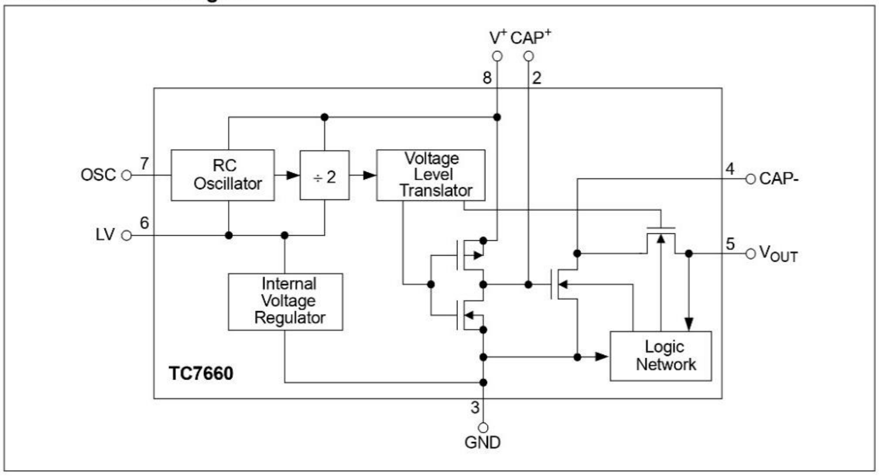

The datasheet of the HMC902LP3E is below:

ANALOG DEVICES

HMC902LP3E

v00.0210

GaAs pHEMT MMIC LOW NOISE AMPLIFIER, 5 - 10 GHz

RoHS✓
EARTH FRIENDLY

Application Circuit - Standard (Self-Biased) Operation

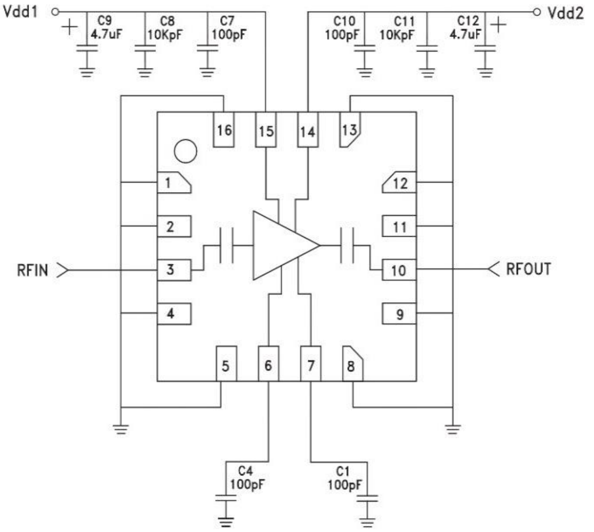

Application Circuit - Gate Control, Reduced Current Operation

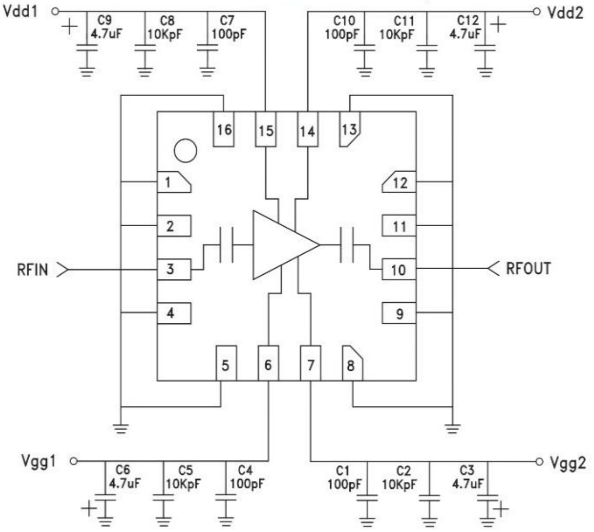

For price, delivery, and to place orders: Analog Devices, Inc., One Technology Way, P.O. Box 9106, Norwood, MA 02062-9106
Phone: 781-329-4700 • Order online at www.analog.com
Application Support: Phone: 1-800-ANALOG-D

The datasheet of the RFSL2950 is below:

COMMUNICATION NARROW BAND

FLANGE MOUNT DROP-IN ISOLATORS 7.0 GHZ TO 18.0 GHZ

PRODUCT DESCRIPTION

RFCI Miniature Drop-in Isolators designed for Narrow X and Ku-Bands Radar applications in high performance linear power amplifiers and utilize the latest technology in miniaturization to assure a fit into the most compact assemblies

KEY FEATURES

- Miniature drop-in package size.
- Robust Construction for High Reliability performance
- RoHS compliant
- Low typical Insertion loss, High Isolation
- Magnetically Shielded.

- Products available with alternative configuration such as high power termination and reverse rotation direction.
- Special Tab is offset available.
- S-parameters are available upon request.

RoHS

FUNCTION DIAGRAM

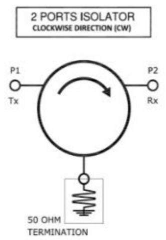

ISOLATOR OUTLINE DRAWING

Figure DI-31 **(8.9mm Package Outline)**

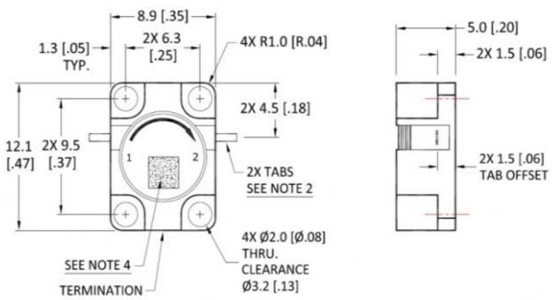

UNLESS OTHERWISE SPECIFIED
ALL DIMENSIONS ARE IN MILLIMETERS [INCHES]:
TOLERANCES ARE:

1 PLACE DECIMAL	±.2 [±.01]	ANGULAR:	±1.0°
2 PLACE DECIMAL	±.10 [±.004]	SURFACE ROUGHNESS	16

Notes:
1. Typical Values Represent Performance @ +23 °C.
2. Tab Dimensions: 0.62 [.024]W x 2.0 [.08]L x 0.20 [.008]T
3. Isolator Flange held to +85°C; 30 Minute Maximum Duration
4. MATRIX BAR CODE: Part Number, Serial Number and Date Code

Drop in Flange Mount Isolators Communication Band 7.0GHz to 18GHz BR-0017 Revision 01

RF Circulator Isolator Inc. ■ Phone +1 408 977 1526 Fax +1 408 977 1534 ■ sales@rf-ci.com

Visit www.rf-ci.com for addition data sheets and information

Products and product Information are Subject to Change Without Notice.

The datasheet of the ADC-10-4 is below:

NON-CATALOG

Surface Mount
Directional Coupler

ADC-10-4

50Ω 5 to 1000 MHz

Generic photo used for illustration purposes only

CASE STYLE: CD542

Maximum Ratings

Operating Temperature	-40°C to 85°C
Storage Temperature	-55°C to 100°C

Permanent damage may occur if any of these limits are exceeded.

Pin Connections

INPUT	1
OUTPUT	6
COUPLED	3
GROUND	2
50Ω TERM EXTERNAL	4
ISOLATE (DO NOT USE)	5

Features

- wideband, 5-1000 MHz
- low mainline loss, 0.8 dB typ.
- high directivity, 40 dB typ.
- aqueous washable
- protected by U.S Patents 6,133,525 & 6,140,887

Applications

- communications
- cable tv

Directional Coupler Electrical Specifications

FREQ. (MHz)	COUPLING (dB)		MAINLINE LOSS[1] (dB)			DIRECTIVITY (dB)			VSWR (:1)	POWER INPUT, W	
f_L-f_U	Nom.	Flatness	L Typ. Max.	M Typ. Max.	U Typ. Max.	L Typ. Min.	M Typ. Min.	U Typ. Min.	Typ.	L Max.	MU Max.
5-1000	10.5±0.5	±1.0	0.8 1.3	0.8 1.2	1.0 1.5	40 23	40 20	25 13	1.2	1	1

L= 5-50 MHz M= 50-500 MHz U= 500-1000 MHz

1. Mainline loss includes theoretical power loss at coupled port.

Outline Drawing

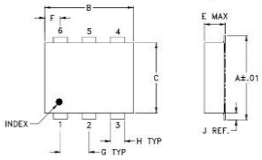

PCB Land Pattern

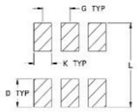

Suggested Layout,
Tolerance to be within ±.002

Typical Performance Data

Frequency (MHz)	Mainline Loss (dB) In-Out	Coupling (dB) In-Cpl	Directivity (dB)	Return Loss (dB) In	Return Loss (dB) Out	Return Loss (dB) Cpl
5.00	0.73	10.45	39.49	22.96	30.01	20.21
10.00	0.72	10.44	41.58	23.49	31.11	20.71
50.00	0.73	10.47	46.29	23.98	31.76	20.95
200.00	0.79	10.62	43.84	22.59	26.52	18.33
300.00	0.82	10.73	34.95	21.24	24.15	16.40
500.00	0.89	10.94	25.53	19.19	20.98	13.59
700.00	0.97	11.12	19.79	18.06	19.06	11.89
800.00	1.02	11.18	17.70	17.82	18.42	11.33
900.00	1.08	11.22	15.83	17.78	17.99	10.91
1000.00	1.17	11.24	14.27	17.91	17.72	10.60

Outline Dimensions (inch/mm)

A	B	C	D	E	F	G
.272	.310	.220	.100	.112	.055	.100
6.91	7.87	5.59	2.54	2.84	1.40	2.54

H	J	K	L	wt
.030	.026	.065	.300	grams
0.76	0.66	1.65	7.62	0.20

Demo Board MCL P/N: TB-05
Suggested PCB Layout (PL-095)

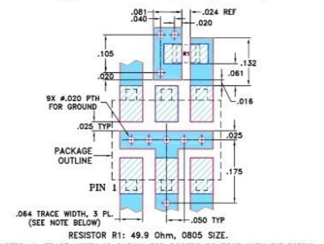

RESISTOR R1: 49.9 Ohm, 0805 SIZE.

NOTES: 1. TRACE WIDTH IS SHOWN FOR ROGERS RO4350B WITH DIELECTRIC THICKNESS .030" ± .002"; COPPER: 1/2 OZ. EACH SIDE. FOR OTHER MATERIALS TRACE WIDTH MAY NEED TO BE MODIFIED.
2. BOTTOM SIDE OF THE PCB IS CONTINUOUS GROUND PLANE.

DENOTES PCB COPPER LAYOUT WITH SMOBC (SOLDER MASK OVER BARE COPPER)

DENOTES COPPER LAND PATTERN FREE OF SOLDER MASK

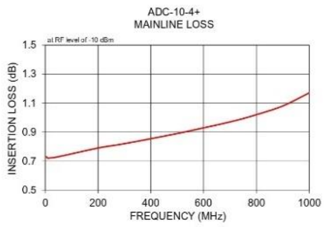

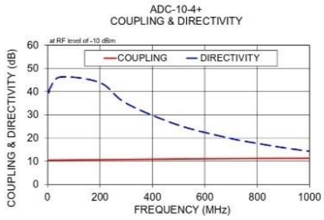

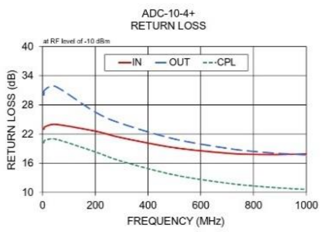

Electrical Schematic

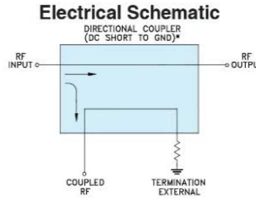

* ELECTRICAL SCHEMATIC IS FOR DIRECTIONAL COUPLER WITH INTERNAL TRANSFORMER(S) AND EXTERNAL TERMINATION.

Notes

A. Performance and quality attributes and conditions not expressly stated in this specification document are intended to be excluded and do not form a part of this specification document.
B. Electrical specifications and performance data contained in this specification document are based on Mini-Circuit's applicable established test performance criteria and measurement instructions.
C. The parts covered by this specification document are subject to Mini-Circuits standard limited warranty and terms and conditions (collectively, "Standard Terms"); Purchasers of this part are entitled to the rights and benefits contained therein. For a full statement of the Standard Terms and the exclusive rights and remedies thereunder, please visit Mini-Circuits' website at www.minicircuits.com/MCLStore/terms.jsp

REV. L
ECO-005915
ED-6560/2
ADC-10-4
WZ/TD/CP/AM
210125
Page 1 of 1

Mini-Circuits®

www.minicircuits.com P.O. Box 350166, Brooklyn, NY 11235-0003 (718) 934-4500 sales@minicircuits.com

The datasheet of the SIM-14H+ is below:

Ceramic Surface Mount

Frequency Mixer WIDE BAND

SIM-14H+

Level 17 (LO Power +17 dBm) 3700 to 10000 MHz

Generic photo used for illustration purposes only

CASE STYLE: HV1195

+RoHS Compliant
The +Suffix identifies RoHS Compliance. See our web site for RoHS Compliance methodologies and qualifications

Available Tape and Reel at no extra cost

Reel Size	Devices/Reel
7"	10, 20, 50, 100, 200, 500

Maximum Ratings

Operating Temperature	-40°C to 85°C
Storage Temperature	-55°C to 100°C
RF Power	100mW

For extended temperature range, consult factory.
Permanent damage may occur if any of these limits are exceeded.

Pin Connections

LO	8
RF	4
IF	2
GROUND	1,3,5,6,7

Features

- wide bandwidth, 3700 to 10000 MHz
- low conversion loss, 7.0 dB typ.
- high L-R isolation, 38 dB typ.
- excellent IF BW, DC to 4000 MHz
- LTCC double balanced mixer
- tiny size, low profile, 0.08"
- useable as up and down converter
- aqueous washable
- protected by US patent 7,027,795

Applications

- satellite up and down converters
- defense radar and communications
- line of sight links
- federal fixed service
- WIFI
- blue tooth
- VSAT
- ISM

Outline Drawing

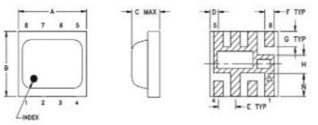

PCB Metal Land Pattern

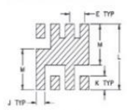

Suggested Layout,
Tolerance to be within±.002

Electrical Specifications

FREQUENCY (MHz) LO/RF f_L-f_U	FREQUENCY (MHz) IF	CONVERSION LOSS* (dB) Typ.	CONVERSION LOSS* (dB) σ	CONVERSION LOSS* (dB) Max.	LO-RF ISOLATION (dB) Typ.	LO-RF ISOLATION (dB) Min.	LO-IF ISOLATION (dB) Typ.	LO-IF ISOLATION (dB) Min.	IP3 (dBm) Typ.
3700-10000	**DC-4000**								
3700-6200		7.0	0.3	9.3	38	29	16	9	25
6200-10000		7.0	0.3	10.5	35	24	17	8	25

1 dB Compression: +14 dBm typ.
* Conversion loss at 30 MHz IF. σ is a measure of repeatability from unit to unit.

Typical Performance Data

Frequency (MHz) RF	Frequency (MHz) LO	Conversion Loss (dB) LO +17dBm	Isolation L-R (dB) LO +17dBm	Isolation L-I (dB) LO +17dBm	VSWR RF Port (:1) LO +17dBm	VSWR LO Port (:1) LO +17dBm
3560.00	3590.00	7.51	37.51	16.92	2.55	7.97
3720.00	3750.00	8.17	42.81	18.98	3.05	3.95
3880.00	3910.00	7.17	40.82	17.17	3.17	6.58
4040.00	4070.00	7.62	43.86	18.91	3.51	7.34
4200.00	4230.00	7.48	38.33	16.97	3.29	4.29
4520.00	4550.00	7.00	37.71	16.17	3.56	1.94
4840.00	4870.00	6.57	37.94	16.15	3.28	2.16
5100.00	5130.00	7.10	39.65	16.32	3.40	1.59
5880.00	5910.00	7.55	39.57	13.91	5.48	1.36
6270.00	6300.00	7.79	35.34	13.12	4.81	2.46
6660.00	6690.00	7.56	29.49	12.32	3.01	2.34
7050.00	7080.00	6.71	31.34	12.85	2.24	3.16
7830.00	7860.00	6.80	33.03	14.74	1.54	3.97
8220.00	8250.00	6.99	32.05	15.28	1.90	3.32
8610.00	8640.00	7.19	39.29	15.05	2.77	2.30
9000.00	9030.00	7.96	37.33	15.47	3.79	1.54
9100.00	9130.00	7.93	37.82	16.00	3.99	1.45
9450.00	9480.00	8.29	41.23	18.02	4.17	1.54
9800.00	9830.00	8.39	42.86	19.43	4.83	2.02
10150.00	10180.00	8.92	42.41	21.36	5.20	2.60

Outline Dimensions (inch / mm)

A	B	C	D	E	F	G
.200	.180	.087	.025	.050	.028	.043
5.08	4.57	2.2098	0.64	1.27	0.71	1.09

H	J	K	L	M	N	wt
.050	.030	.043	.204	.127	0.065	grams
1.27	0.76	1.09	5.18	3.23	1.65	0.08

Demo Board MCL P/N: TB-382
Suggested PCB Layout (PL-239)

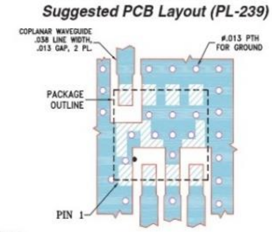

NOTES:
1. TRACE WIDTH AND GAP ARE SHOWN FOR ROGERS RO4350B WITH DIELECTRIC THICKNESS .020"±.0015"; COPPER: 1/2 OZ. EACH SIDE.
FOR OTHER MATERIALS TRACE WIDTH AND GAP MAY NEED TO BE MODIFIED.
2. BOTTOM SIDE OF THE PCB IS CONTINUOUS GROUND PLANE.

DENOTES PCB COPPER LAYOUT WITH SMOBC (SOLDER MASK OVER BARE COPPER).
DENOTES COPPER LAND PATTERN FREE OF SOLDER MASK.

Electrical Schematic

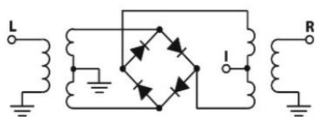

Notes
A. Performance and quality attributes and conditions not expressly stated in this specification document are intended to be excluded and do not form a part of this specification document.
B. Electrical specifications and performance data contained in this specification document are based on Mini-Circuit's applicable established test performance criteria and measurement instructions.
C. The parts covered by this specification document are subject to Mini-Circuits standard limited warranty and terms and conditions (collectively, "Standard Terms"); Purchasers of this part are entitled to the rights and benefits contained therein. For a full statement of the Standard Terms and the exclusive rights and remedies thereunder, please visit Mini-Circuits' website at www.minicircuits.com/MCLStore/terms.jsp

Mini-Circuits®
www.minicircuits.com P.O. Box 350166, Brooklyn, NY 11235-0003 (718) 934-4500 sales@minicircuits.com

REV. B
ECO-000060
SIM-14H+
ED-12399/6
DJ/RS/CP/AM
200821
Page 1 of 2

The datasheet of the XLF-861 is below:

NEW!

MMIC

REFLECTIONLESS FILTERS

50Ω DC to 21 GHz

The Big Deal

- Patented design eliminates in band spurs
- Pass band cut-off up to 21 GHz
- Stop band up to 35 GHz
- Excellent repeatability through IPD* process

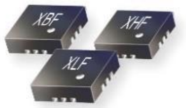

X-Series

Available in Low Pass, High Pass and Band Pass designs

Product Overview

Mini-Circuits' *X-Series* reflectionless filters employs a novel filter topology which absorbs and terminates stop band signals internally rather than reflecting them back to the source. This new capability enables unique applications for filter circuits beyond those suited to traditional approaches. Traditional filters are reflective in the stop band, sending signals back to the source at 100% of the power level which interact with neighboring components and often result in intermodulation and other interferences. Reflectionless filters eliminate stop band reflections, allowing them to be paired with sensitive devices and used in applications that otherwise require circuits such as isolation amplifiers or attenuators.

Key Features	Advantages
Easy integration with sensitive reflective components, e.g. mixers, multipliers	Reflectionless filters absorb unwanted signals, preventing reflections back to the source. This reduces generation of additional unwanted signals without the need for extra components like attenuators, improving system dynamic range and saving board space.
Enables stable integration of wideband amplifiers	Because reflectionless filters maintain good impedance in the stop band; they can be integrated with high gain, wideband amplifiers without the risk of creating instabilities in these out of band regions.
Cascadable	Reflectionless filters can be cascaded in multiple sections to provide sharper and higher attenuation, while also preventing any standing waves that could affect pass band signals.
Excellent power handling in a tiny surface mount device	High power handling extends the usability of these filters to the transmit path for inter-stage filtering.
Small size, 3x3mm QFN	Allows replacement of filter/attenuator pairs with a single reflectionless filter, saving board space.
Excellent repeatability of RF performance	Through semiconductor IPD process, X-series filters are inherently repeatable for large volume production.
Excellent stability over temperature	With ±0.3 dB variation over temperature ideal for use in wide temperature range applications without the need for additional temperature compensation.
Operating temperature up to 105˚C	Suitable for operation close to high power components.

*IPD – Integrated Passive Device, is a GaAs semiconductor process

Mini-Circuits®

www.minicircuits.com P.O. Box 350166, Brooklyn, NY 11235-0003 (718) 934-4500 sales@minicircuits.com

Page 1 of 5

The datasheet of the MNA-2W is below:

HIGH DIRECTIVITY

Monolithic Amplifier MNA-2W+

Mini-Circuits

50Ω 0.5 to 4.5 GHz

THE BIG DEAL

- Integrated matching, DC Blocks and bias circuits
- Excellent Active Directivity, +21 dB typ. at 2.5 GHz and 5V
- Choice of supply voltage, +2.8V to +5V
- Micro-miniature size .120"X.120"
- Output power, +17.5 dBm typ. at 2.5 GHz and 5V
- Aqueous washable

Generic photo used for illustration purposes only

CASE STYLE: DQ849

+RoHS Compliant
The +Suffix identifies RoHS Compliance.
See our website for methodologies and qualifications

APPLICATIONS

- Buffer amplifier
- Cellular infrastructure
- Communications satellite
- Defense

PRODUCT OVERVIEW

MNA-2W+ is a wideband PHEMT based MMIC amplifier with high active Directivity. MNA integrates the entire matching network and majority of the bias circuit inside the package, reducing the need for complicated external circuits. This approach makes the MNA amplifier extremely straightforward to use. This design operates on a single 2.8 to 5V supply, is well matched for 50Ω and comes in a tiny, low profile 3x3mm 8-lead MCLP package accommodating dense circuit board layouts. MNA-2W+ belongs to MNA series of models available in Die and packaged form.

KEY FEATURES

Feature	Advantages
Excellent Active Directivity (Isolation- Gain) 21-36 dB	Ideal for use as a buffer amplifier minimizing interaction of adjacent circuits
Integrates DC blocks and RF choke	Minimizes external components, component count and circuit area.
Single +2.8 to +5V operation	Amplifier can be used at low voltage such as +3V or standard +5V. +5V operation results in higher P1dB and OIP3.
3 x 3mm 8-lead MCLP package	Tiny footprint saves space in dense layouts while providing low inductance, repeatable transitions, and excellent thermal contact to the PCB.

The datasheet of the LFCN-1400 is below:

NON-CATALOG

Ceramic

Low Pass Filter

LFCN-1400

50Ω DC(1) to 1400 MHz

Generic photo used for illustration purposes only

CASE STYLE: FV1206

Maximum Ratings

Operating Temperature	-55°C to 100°C
Storage Temperature	-55°C to 100°C
RF Power Input*	10W max. at 25°C

* Passband rating, derate linearly to 3.5W at 100°C ambient.
Permanent damage may occur if any of these limits are exceeded.

Pin Connections

RF IN	1
RF OUT	3
GROUND	2,4

Features

- excellent power handling, 10W
- small size
- 7 sections
- temperature stable
- LTCC construction
- protected by U.S Patent 6,943,646

Applications

- harmonic rejection
- VHF/UHF transmitters/receivers
- lab use

Outline Drawing

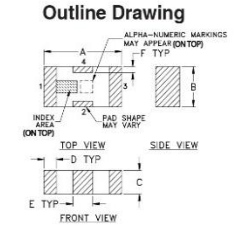

Outline Dimensions (inch / mm)

A	B	C	D	E	F	G
.126	.063	.037	.020	.032	.009	.169
3.20	1.60	0.94	0.51	0.81	0.23	4.29

H	J	K	L	M	N	P	wt
.087	.024	.122	.024	.087	.012	.071	grams
2.21	0.61	3.10	0.61	2.21	0.30	1.80	.020

Electrical Specifications(1,2) at 25°C

Parameter		F#	Frequency (MHz)	Min.	Typ.	Max.	Unit
Pass Band	Insertion Loss	DC-F1	DC-1400	—	—	1.0	dB
	Freq. Cut-Off	F2	1700	—	3.0	—	dB
	VSWR	DC-F1	DC-1400	—	1.2	—	:1
Stop Band	Rejection Loss	F3	2015	20	—	—	dB
		F4-F5	2100-6600	—	30	—	dB
		F6	6800	—	20	—	dB
	VSWR	F3-F6	2015-6800	—	20	—	:1

(1) In Applications where DC isolation to ground is required, coupling capacitors are recommended to avoid DC leakage. Alternatively, if DC pass IN-OUT is required, Mini-Circuits' "D" suffix version of this model will support DC IN-OUT, and provide>100 MOhm isolation to ground.
(2) Measured on Mini-Circuits Characterization Test Board TB-270.

Typical Frequency Response

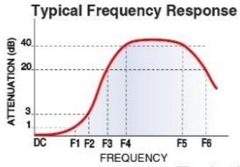

Electrical Schematic

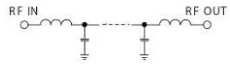

Demo Board MCL P/N: TB-270
Suggested PCB Layout (PL-137)

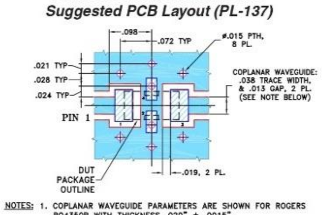

NOTES: 1. COPLANAR WAVEGUIDE PARAMETERS ARE SHOWN FOR ROGERS RO4350B WITH THICKNESS .020" ± .0015". COPPER: 1/2 OZ. EACH SIDE. FOR OTHER MATERIALS TRACE WIDTH & GAP MAY NEED TO BE MODIFIED.
2. BOTTOM SIDE OF THE PCB IS CONTINUOUS GROUND PLANE.
DENOTES PCB COPPER LAYOUT WITH SMOBC (SOLDER MASK OVER BARE COPPER)
DENOTES COPPER LAND PATTERN FREE OF SOLDER MASK

Typical Performance Data at 25°C

Frequency (MHz)	Insertion Loss (dB)	VSWR (:1)
100.00	0.11	1.02
500.00	0.24	1.08
1000.00	0.41	1.11
1400.00	0.72	1.22
1700.00	3.20	3.20
1975.00	24.77	16.89
2000.00	28.65	17.39
2050.00	38.72	17.75
2500.00	34.93	17.75
3000.00	37.62	24.14
4000.00	50.70	39.49
5000.00	45.47	30.49
6600.00	34.00	18.70
6800.00	26.51	16.56
7000.00	16.88	10.89

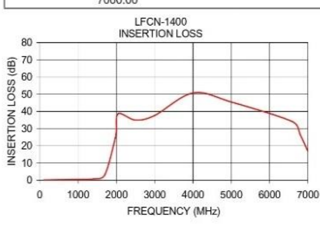

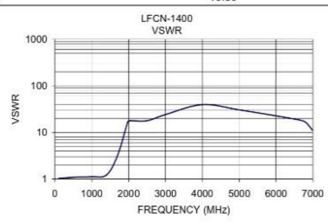

Notes
A. Performance and quality attributes and conditions not expressly stated in this specification document are intended to be excluded and do not form a part of this specification document.
B. Electrical specifications and performance data contained in this specification document are based on Mini-Circuit's applicable established test performance criteria and measurement instructions.
C. The parts covered by this specification document are subject to Mini-Circuits standard limited warranty and terms and conditions (collectively, "Standard Terms"); Purchasers of this part are entitled to the rights and benefits contained therein. For a full statement of the Standard Terms and the exclusive rights and remedies thereunder, please visit Mini-Circuits' website at www.minicircuits.com/MCLStore/terms.jsp

REV. L
ECO-006038
LFCN-1400
ED-11690/4
AD/CP/AM
210202

Mini-Circuits®

www.minicircuits.com P.O. Box 350166, Brooklyn, NY 11235-0003 (718) 934-4500 sales@minicircuits.com

The datasheet of the AT-106-PIN is below:

AT-106-PIN

Digital Attenuator
50.0 dB, 6-Bit, TTL Driver, DC-2.0 GHz **Rev. V10**

Features

- Attenuation: 1 dB steps to 50 dB
- Temperature Stability: ± 0.18 dB from –55°C to +85°C Typical
- Low DC Power Consumption
- Hermetic Surface Mount Package
- Integral TTL Driver
- 50 Ohm Nominal Impedance
- Lead-Free CR-13 Package
- 260°C Reflow Compatible
- RoHS* Compliant

Description

M/A-COM's AT-106-PIN is a GaAs FET 6-bit digital attenuator with a 1 dB minimum step size and 50 dB total attenuation. This attenuator and integral TTL driver is in a hermetically sealed ceramic 24-lead surface mount package. The AT-106-PIN is ideally suited for use where accuracy, fast switching, very low power consumption and low intermodulation products are required. Typical applications include dynamic range setting in precision receiver circuits and other gain/leveling control circuits. Environmental screening is available. Contact the factory for information.

Functional Schematic

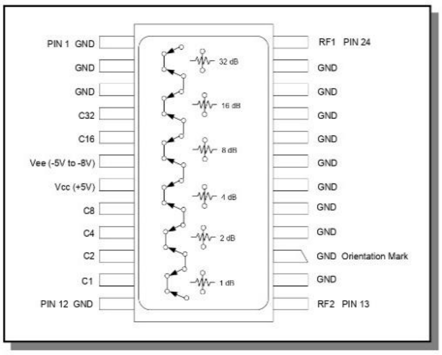

Pin Configuration

Pin No.	Function	Pin No.	Function
1	GND	13	RF2
2	GND	14	GND
3	GND	15	GND
4	C32	16	GND
5	C16	17	GND
6	Vee (-5V to -8V)	18	GND
7	Vcc (+5V)	19	GND
8	C8	20	GND
9	C4	21	GND
10	C2	22	GND
11	C1	23	GND
12	GND	24	RF1

The metal bottom of the case must be connected to RF and DC ground.

Ordering Information

Part Number	Package
AT-106-PIN	Bulk Packaging
AT-106-TR	1000 piece reel
AT-106-TB	Sample Test Board

Note: Reference Application Note M513 for reel size information.

* Restrictions on Hazardous Substances, European Union Directive 2002/95/EC.

The datasheet of the LFCN-1200 is below:

NON-CATALOG

Ceramic

Low Pass Filter

LFCN-1200

50Ω   DC(1) to 1200 MHz

Generic photo used for illustration purposes only

CASE STYLE: FV1206

Maximum Ratings

Operating Temperature	-55°C to 100°C
Storage Temperature	-55°C to 100°C
RF Power Input*	10W max. at 25°C

* Passband ratiing, derate linearly to 3.5W at 100°C ambient.
Permanent damage may occur if any of these limits are exceeded.

Pin Connections

RF IN	1
RF OUT	3
GROUND	2,4

Features

- excellent power handling, 10W
- small size
- 7 sections
- temperature stable
- LTCC construction
- protected by U.S Patent 6,943,646

Applications

- harmonic rejection
- VHF/UHF transmitters/receivers
- lab use

Outline Drawing

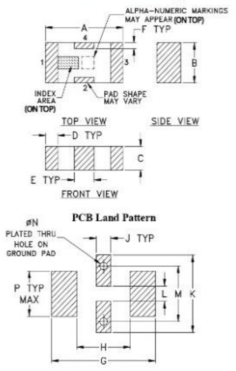

Suggested Layout,
Tolerance to be within ±.002

Electrical Specifications(1,2) at 25°C

Parameter		F#	Frequency (MHz)	Min.	Typ.	Max.	Unit
Pass Band	Insertion Loss	DC-F1	DC-1200	—	—	1.0	dB
	Freq. Cut-Off	F2	1530	—	3.0	—	dB
	VSWR	DC-F1	DC-1200	—	1.2	—	:1
Stop Band	Rejection Loss	F3	1865	20	—	—	dB
		F4-F5	2000-5000	—	30	—	dB
		F6	6200	—	20	—	dB
	VSWR	F3-F6	1865-6200	—	20	—	:1

(1) In Applications where DC isolation to ground is required, coupling capacitors are recommended to avoid DC leakage. Alternatively, if DC pass IN-OUT is required, Mini-Circuits' "D" suffix version of this model will support DC IN-OUT, and provide>100 MOhm isolation to ground.
(2) Measured on Mini-Circuits Characterization Test Board TB-270.

Typical Frequency Response

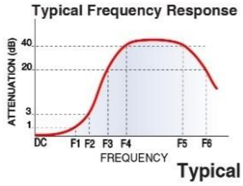

Electrical Schematic

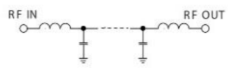

Outline Dimensions (inch / mm)

A	B	C	D	E	F	G
.126	.063	.037	.020	.032	.009	.169
3.20	1.60	0.94	0.51	0.81	0.23	4.29

H	J	K	L	M	N	P	wt
.087	.024	.122	.024	.087	.012	.071	grams
2.21	0.61	3.10	0.61	2.21	0.30	1.80	.020

Typical Performance Data at 25°C

Frequency (MHz)	Insertion Loss (dB)	VSWR (:1)
50.00	0.04	1.02
500.00	0.30	1.18
750.00	0.34	1.20
1200.00	0.73	1.16
1480.00	2.79	2.15
1750.00	24.69	9.43
2000.00	31.88	16.56
2375.00	40.40	25.19
3000.00	39.23	31.60
3500.00	37.97	36.20
4500.00	36.37	39.49
5000.00	36.23	34.07
6050.00	22.99	26.74
6500.00	12.01	15.00
7000.00	16.10	37.77

Demo Board MCL P/N: TB-270
Suggested PCB Layout (PL-137)

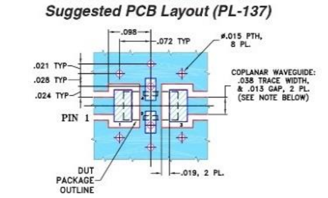

NOTES: 1. COPLANAR WAVEGUIDE PARAMETERS ARE SHOWN FOR ROGERS RO4350B WITH THICKNESS .020" ± .0015". COPPER: 1/2 OZ. EACH SIDE. FOR OTHER MATERIALS TRACE WIDTH & GAP MAY NEED TO BE MODIFIED.
2. BOTTOM SIDE OF THE PCB IS CONTINUOUS GROUND PLANE.
DENOTES PCB COPPER LAYOUT WITH SMOBC (SOLDER MASK OVER BARE COPPER)
DENOTES COPPER LAND PATTERN FREE OF SOLDER MASK

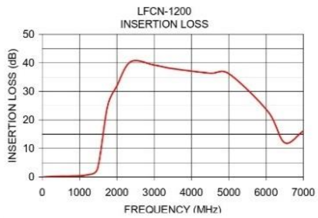

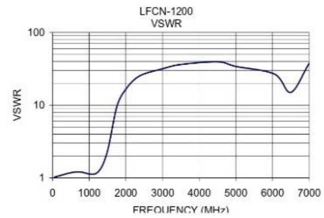

Notes
A. Performance and quality attributes and conditions not expressly stated in this specification document are intended to be excluded and do not form a part of this specification document.
B. Electrical specifications and performance data contained in this specification document are based on Mini-Circuit's applicable established test performance criteria and measurement instructions.
C. The parts covered by this specification document are subject to Mini-Circuits standard limited warranty and terms and conditions (collectively, "Standard Terms"); Purchasers of this part are entitled to the rights and benefits contained therein. For a full statement of the Standard Terms and the exclusive rights and remedies thereunder, please visit Mini-Circuits' website at www.minicircuits.com/MCLStore/terms.jsp

REV. P
ECO-006038
LFCN-1200
EDR-6469/3
RVN/AD/CP/AM
210202

Mini-Circuits®

www.minicircuits.com P.O. Box 350166, Brooklyn, NY 11235-0003 (718) 934-4500 sales@minicircuits.com

The datasheet of the PHA-101 is below:

ULTRA HIGH DYNAMIC RANGE

Monolithic Amplifier

PHA-101+

50Ω 0.05 to 1.5GHz

THE BIG DEAL

- Ultra High IP3
- Broadband High Dynamic Range without External Matching Components
- May be used as a replacement to WJ AH101[a,b]

Generic photo used for illustration purposes only

CASE STYLE: DF782

+RoHS Compliant
The +Suffix identifies RoHS Compliance. See our web site for RoHS Compliance methodologies and qualifications

APPLICATIONS

- Base station infrastructure
- CATV
- LTE

PRODUCT OVERVIEW

PHA-101+ (RoHS compliant) is an advanced wideband amplifier fabricated using E-PHEMT technology and offers extremely high dynamic range over a broad frequency range and with low noise figure. In addition, the PHA-101+ has good input and output return loss over a broad frequency range without the need for external matching components and has demonstrated excellent reliability. It has repeatable performance from lot to lot and is enclosed in a SOT-89 package for very good thermal performance.

KEY FEATURES

Feature	Advantages
Broad Band: 0.05 to 1.5 GHz	Broadband covering primary wireless communications bands: Cellular, PCS, LTE
Extremely High IP3 Versus DC power Consumption 45 dBm typical at 0.9 GHz	The PHA-101+ matches industry leading IP3 performance relative to device size and power consumption. The combination of the design and E-PHEMT Structure provides enhanced linearity over a broad frequency range as evidence in the IP3 being typically 20 dB above the P 1dB point. This feature makes this amplifier ideal for use in: • Driver amplifiers for complex waveform up converter paths • Drivers in linearized transmit systems • Secondary amplifiers in ultra High Dynamic range receivers
No External Matching Components Required	Unlike competing products, Mini-Circuits PHA-101+ provides Input and Output Return Loss of 9.9-12.5 dB up to 1.5 GHz without the need for any external matching components

a. Suitability for model replacement within a particular system must be determined by and is solely the responsibility of the customer based on, among other things, electrical performance criteria, stimulus conditions, application, compatibility with other components and environmental conditions and stresses.
b. The WJ AH1 part number is used for identification and comparison purposes only.

REV. B
ECO-010399
M156908
PHA-101+
TH/RS/CP/AM
211027

Mini-Circuits

www.minicircuits.com P.O. Box 350166, Brooklyn, NY 11235-0003 (718) 934-4500 sales@minicircuits.com

PAGE 1 OF 5

The datasheet of the LFCN-1000 is below:

NON-CATALOG

Ceramic

Low Pass Filter

LFCN-1000

50Ω DC(1) to 1000 MHz

Generic photo used for illustration purposes only

CASE STYLE: FV1206

Maximum Ratings

Operating Temperature	-55°C to 100°C
Storage Temperature	-55°C to 100°C
RF Power Input*	10W max. at 25°C

* Passband rating, derate linearly to 3.5W at 100°C ambient.
Permanent damage may occur if any of these limits are exceeded.

Pin Connections

RF IN	1
RF OUT	3
GROUND	2,4

Features

- excellent power handling, 10W
- small size
- 7 sections
- temperature stable
- LTCC construction
- protected by U.S Patent 6,943,646

Applications

- harmonic rejection
- VHF/UHF transmitters/receivers
- lab use

Outline Drawing

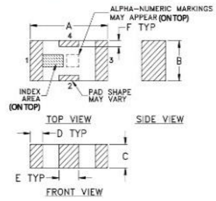

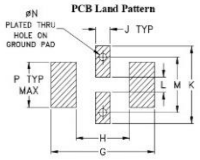

Suggested Layout,
Tolerance to be within ±.002

Outline Dimensions (inch / mm)

A	B	C	D	E	F	G
.126	.063	.037	.020	.032	.009	.169
3.20	1.60	0.94	0.51	0.81	0.23	4.29

H	J	K	L	M	N	P	wt
.087	.024	.122	.024	.087	.012	.071	grams
2.21	0.61	3.10	0.61	2.21	0.30	1.80	.020

Demo Board MCL P/N: TB-270
Suggested PCB Layout (PL-137)

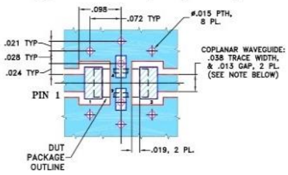

NOTES: 1. COPLANAR WAVEGUIDE PARAMETERS ARE SHOWN FOR ROGERS RO4350B WITH THICKNESS .020" ± .0015". COPPER: 1/2 OZ. EACH SIDE. FOR OTHER MATERIALS TRACE WIDTH & GAP MAY NEED TO BE MODIFIED.
2. BOTTOM SIDE OF THE PCB IS CONTINUOUS GROUND PLANE.
DENOTES PCB COPPER LAYOUT WITH SMOBC (SOLDER MASK OVER BARE COPPER)
DENOTES COPPER LAND PATTERN FREE OF SOLDER MASK

Electrical Specifications(1,2) at 25°C

Parameter		F#	Frequency (MHz)	Min.	Typ.	Max.	Unit
Pass Band	Insertion Loss	DC-F1	DC-1000	—	—	1.0	dB
	Freq. Cut-Off	F2	1300	—	3.0	—	dB
	VSWR	DC-F1	DC-1000	—	1.3	—	:1
Stop Band	Rejection Loss	F3	1550	20	—	—	dB
		F4-F5	1900-5000	—	30	—	dB
		F6	5500	—	20	—	dB
	VSWR	F3-F6	1550-5500	—	20	—	:1

(1) In Applications where DC isolation to ground is required, coupling capacitors are recommended to avoid DC leakage. Alternatively, if DC pass IN-OUT is required, Mini-Circuits' "D" suffix version of this model will support DC IN-OUT, and provide>100 MOhm isolation to ground.
(2) Measured on Mini-Circuits Characterization Test Board TB-270.

Typical Frequency Response

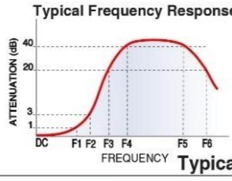

Electrical Schematic

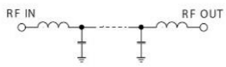

Typical Performance Data at 25°C

Frequency (MHz)	Insertion Loss (dB)	VSWR (:1)
50.00	0.01	1.01
500.00	0.30	1.05
1000.00	0.80	1.21
1275.00	3.33	2.23
1500.00	25.87	17.57
2000.00	49.50	34.75
2750.00	39.80	59.91
3250.00	43.45	51.10
4000.00	43.25	52.65
4600.00	43.25	59.91
5125.00	43.11	41.37
5500.00	22.76	34.75
6000.00	15.24	29.46
6500.00	19.30	62.05
7000.00	18.56	69.49

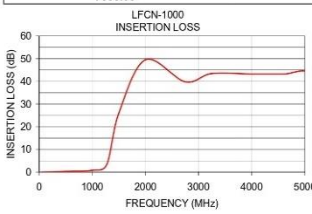

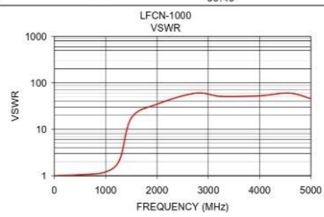

Notes
A. Performance and quality attributes and conditions not expressly stated in this specification document are intended to be excluded and do not form a part of this specification document.
B. Electrical specifications and performance data contained in this specification document are based on Mini-Circuit's applicable established test performance criteria and measurement instructions.
C. The parts covered by this specification document are subject to Mini-Circuits standard limited warranty and terms and conditions (collectively, "Standard Terms"); Purchasers of this part are entitled to the rights and benefits contained therein. For a full statement of the Standard Terms and the exclusive rights and remedies thereunder, please visit Mini-Circuits' website at www.minicircuits.com/MCLStore/terms.jsp

REV. Q
ECO-006038
LFCN-1000
EDR-6469/2
RVN
210202

Mini-Circuits®

www.minicircuits.com P.O. Box 350166, Brooklyn, NY 11235-0003 (718) 934-4500 sales@minicircuits.com

The datasheet of the RDP-2R15+ is below:

Surface Mount

Diplexer

RDP-2R15+

50Ω DC to 2150 MHz
(DC-20, 950-2150 MHz)

CASE STYLE: CK605

The Big Deal

- Low insertion loss
- High stopband insertion loss
- Miniature shielded package

Product Overview

RDP-2R15+ is a low-pass + high-pass combination device. Low pass port is designed for DC to 20 MHz and high pass port is designed for 950 to 2150 MHz. This diplexer can be used to pass, IF, pilot carrier or clock synchronizing signal, SATCOM modems, air-traffic control and other multiband radio systems.

Key Features

Feature	Advantages
Low passband insertion loss	Suitable for high performance application.
Extended stopband rejection	Spurious rejection and avoids using additional filters.
Shielded case.	Reduced interference with the surrounding components.

The datasheet of the HMC3653LP3BE is below:

ANALOG DEVICES

HMC3653LP3BE

v02.0917

HBT GAIN BLOCK MMIC AMPLIFIER, 7 - 15 GHz

Typical Applications

The HMC3653LP3BE is ideal for:

- Point-to-Point Radios
- Point-to-Multipoint Radios
- VSAT
- LO Driver for HMC Mixers
- Military EW & ECM

Features

High Output IP3: +28 dBm

Single Positive Supply: +5V

Low Noise Figure: 4.0 dB [1]

12 Lead 3x3 mm SMT Package: $9mm^2$

Functional Diagram

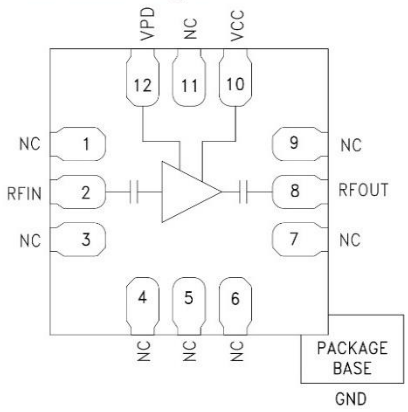

General Description

The HMC3653LP3BE is a HBT Gain Block MMIC amplifier covering 7 GHz to 15 GHz and packaged in a 3x3 mm plastic QFN SMT package. This versatile amplifier can be used as a cascadable IF or RF gain stage in 50 Ohm applications. The HMC3653LP3BE delivers 15 dB gain, and +15 dBm output P1dB with only 4 dB noise figure.

Electrical Specifications, T_A = +25° C, Vcc =5V, Vpd = 5V

Parameter	Min.	Typ.	Max.	Min.	Typ.	Max.	Min.	Typ.	Max	Units
Frequency Range		7 - 9			9 - 14			14 - 15		GHz
Gain [1]	10.5	14		12	15		12	15		dB
Gain Variation Over Temperature		0.016			0.016			0.022		dB / °C
Input Return Loss		14			15			11		dB
Output Return Loss		8			8			7		dB
Output Power for 1 dB Compression (P1dB) [1]	13	16		12	15		10.5	13.5		dBm
Output Third Order Intercept (IP3) (Pout = 0 dBm per tone, 1 MHz spacing)		26			28			26		dBm
Noise Figure [1]		6			4			4		dB
Icc (Vpd = 5V)		40	55		40	55		40	55	mA
Icc (Vpd = 0V)		4	6		4	6		4	6	mA

[1] Board loss subtracted out

For price, delivery, and to place orders: Analog Devices, Inc., One Technology Way, P.O. Box 9106, Norwood, MA 02062-9106
Phone: 781-329-4700 • Order online at www.analog.com
Application Support: Phone: 1-800-ANALOG-D

The datasheet of the VLF-1500+ is below:

Coaxial

Low Pass Filter

VLF-1500+

50Ω *DC to 1500 MHz

Generic photo used for illustration purposes only

CASE STYLE: FF704

Connectors	Model
SMA	VLF-1500+

+RoHS Compliant
The +Suffix identifies RoHS Compliance. See our web site for RoHS Compliance methodologies and qualifications

Maximum Ratings

Operating Temperature	-55°C to 100°C
Storage Temperature	-55°C to 100°C
RF Power Input*	10W max. at 25°C
DC Current Input to Output	0.5A max. at 25°C

** Passband rating, derate linearly to 3.5W at 100°C ambient.*
Permanent damage may occur if any of these limits are exceeded.

Features
- rugged uni-body construction, small size
- 7 sections
- excellent power handling, 10W
- temperature stable
- low cost
- protected by U.S. Patent 6,943,646

Applications
- harmonic rejection
- transmitters/receivers
- lab use

Outline Drawing

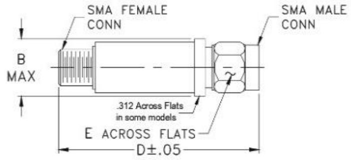

Outline Dimensions (inch/mm)

B	D	E	wt
.410	1.43	.312	grams
10.41	36.32	7.92	10.0

Electrical Specifications at 25°C

PASSBAND (MHz)	fco, MHz Nom.	STOP BAND (MHz) (loss, dB)			VSWR (:1)		NO. OF SECTIONS
(loss < 1 dB)	(loss 3 dB)	f 20	30	fr 20	Stopband	Passband	
Max.	Typ.	Min.	Typ.	Typ.	Typ.	Typ.	
*DC-1500	1825	2100	2150-6600	6800	20	1.2	7

** Not for use with DC voltage at input and output ports*

typical frequency response

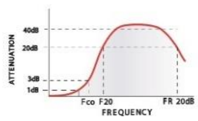

electrical schematic

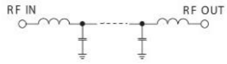

Typical Performance Data at 25°C

Frequency (MHz)	Insertion Loss (dB)	VSWR (:1)
50	0.07	1.04
500	0.18	1.04
1500	0.67	1.27
1700	1.16	1.38
1825	2.84	2.46
1900	6.24	4.93
2000	16.20	12.80
2100	36.11	20.22
2150	34.78	23.49
3000	31.36	45.72
4000	42.21	51.10
5000	45.73	62.05
6600	31.36	38.61
6800	34.26	41.37
7000	24.02	31.03

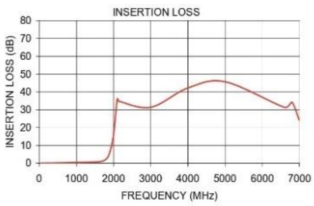

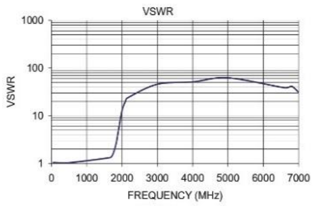

Notes
A. Performance and quality attributes and conditions not expressly stated in this specification document are intended to be excluded and do not form a part of this specification document.
B. Electrical specifications and performance data contained in this specification document are based on Mini-Circuit's applicable established test performance criteria and measurement instructions.
C. The parts covered by this specification document are subject to Mini-Circuits standard limited warranty and terms and conditions (collectively, "Standard Terms"); Purchasers of this part are entitled to the rights and benefits contained therein. For a full statement of the Standard Terms and the exclusive rights and remedies thereunder, please visit Mini-Circuits' website at www.minicircuits.com/MCLStore/terms.jsp

Mini-Circuits®

www.minicircuits.com P.O. Box 350166, Brooklyn, NY 11235-0003 (718) 934-4500 sales@minicircuits.com

REV. E
M151107
VLF-1500+
ED-11960/3
AD/TD/CP/AM
200522
Page 1 of 1

The datasheet of the VLF-1575+ is below:

Coaxial

Low Pass Filter

VLF-1575+

50Ω *DC to 1575 MHz

Generic photo used for illustration purposes only

CASE STYLE: FF704

Connectors	Model
SMA	VLF-1575+

+RoHS Compliant
The +Suffix identifies RoHS Compliance. See our web site for RoHS Compliance methodologies and qualifications

Maximum Ratings

Operating Temperature	-55°C to 100°C
Storage Temperature	-55°C to 100°C
RF Power Input*	10W max. at 25°C
DC Current Input to Output	0.5A max. at 25°C

** Passband rating, derate linearly to 3.5W at 100°C ambient.*
Permanent damage may occur if any of these limits are exceeded.

Features

- rugged uni-body construction, small size
- 7 sections
- excellent power handling, 10W
- temperature stable
- low cost
- protected by U.S. Patent 6,943,646

Applications

- harmonic rejection
- transmitters/receivers
- lab use

Outline Drawing

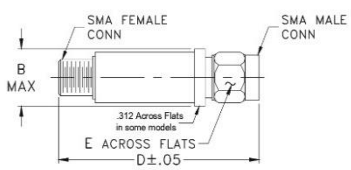

Outline Dimensions (Inch / mm)

B	D	E	wt
.410	1.43	.312	grams
10.41	36.32	7.92	10.0

Electrical Specifications at 25°C

PASSBAND (MHz) (loss < 1 dB) Max.	fco, MHz Nom. (loss 3 dB) Typ.	STOP BAND (MHz) (loss, dB) f 20 Min.	30 Typ.	fr 20 Typ.	VSWR (:1) Stopband Typ.	Passband Typ.	NO. OF SECTIONS
*DC-1575	1875	2175	2225-6800	7100	20	1.2	7

** Not for use with DC voltage at input and output ports*

typical frequency response

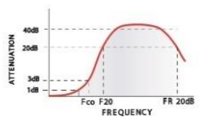

electrical schematic

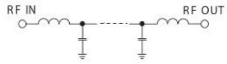

Typical Performance Data

Frequency (MHz)	Insertion Loss (dB)	VSWR (:1)
50	0.06	1.03
500	0.19	1.05
1575	0.73	1.29
1800	1.51	1.56
1875	2.71	2.29
1950	5.83	4.40
2020	11.60	8.81
2100	22.31	15.26
2175	38.03	20.22
2225	33.68	22.58
4000	41.86	44.55
5000	42.91	59.91
6800	33.43	34.07
7100	30.89	32.18
9000	19.27	52.65

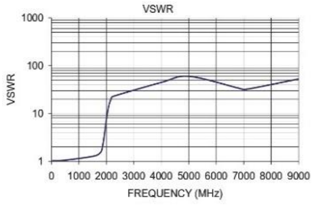

Notes
A. Performance and quality attributes and conditions not expressly stated in this specification document are intended to be excluded and do not form a part of this specification document.
B. Electrical specifications and performance data contained in this specification document are based on Mini-Circuit's applicable established test performance criteria and measurement instructions.
C. The parts covered by this specification document are subject to Mini-Circuits standard limited warranty and terms and conditions (collectively, "Standard Terms"); Purchasers of this part are entitled to the rights and benefits contained therein. For a full statement of the Standard Terms and the exclusive rights and remedies thereunder, please visit Mini-Circuits' website at www.minicircuits.com/MCLStore/terms.jsp

REV. D
M151107
VLF-1575+
ED-11960/5
AD/TD/CP/AM
200522
Page 1 of 1

Mini-Circuits®

www.minicircuits.com P.O. Box 350166, Brooklyn, NY 11235-0003 (718) 934-4500 sales@minicircuits.com

The datasheet of the HMC508LP5 is below:

ANALOG DEVICES

HMC508LP5 / 508LP5E

v04.0811

MMIC VCO w/ HALF FREQUENCY OUTPUT 7.3 - 8.2 GHz

RoHS✓ EARTH FRIENDLY

Typical Applications

Low noise MMIC VCO w/Half Frequency, for:

- VSAT Radio
- Point to Point/Multi-Point Radio
- Test Equipment & Industrial Controls
- Military End-Use

Features

Dual Output: Fo = 7.3 - 8.2 GHz
Fo/2 = 3.65 - 4.1 GHz

Pout: +15.0 dBm

Phase Noise: -116 dBc/Hz @100 kHz Typ.

No External Resonator Needed

32 Lead 5x5mm SMT Package: 25mm²

Functional Diagram

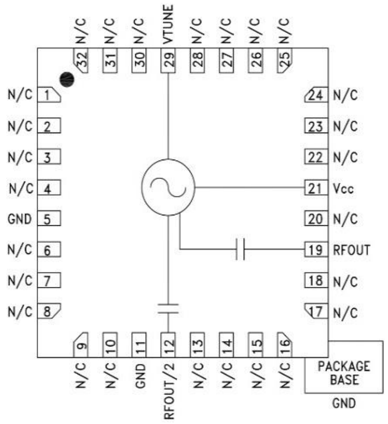

General Description

The HMC508LP5 & HMC508LP5E are GaAs InGaP Heterojunction Bipolar Transistor (HBT) MMIC VCOs. The HMC508LP5 & HMC508LP5E integrate resonators, negative resistance devices, varactor diodes and feature a half frequency output. The VCO's phase noise performance is excellent over temperature, shock, and process due to the oscillator's monolithic structure. Power output is +15 dBm typical from a +5V supply. The voltage controlled oscillator is packaged in a leadless QFN 5x5 mm surface mount package, and requires no external matching components.

Electrical Specifications, T_A = +25° C, Vcc = +5V

Parameter		Min.	Typ.	Max.	Units
Frequency Range	Fo Fo/2		7.3 - 8.2 3.65 - 4.1		GHz GHz
Power Output	RFOUT RFOUT/2	+12 +4		+17 +10	dBm dBm
SSB Phase Noise @ 100 kHz Offset, Vtune= +5V @ RFOUT			-116		dBc/Hz
Tune Voltage	Vtune	2		13	V
Supply Current (Icc) (Vcc = +5.0V)		200	240	280	mA
Tune Port Leakage Current (Vtune= 13V)				10	µA
Output Return Loss			2		dB
Harmonics/Subharmonics	1/2 2nd 3rd		40 20 35		dBc dBc dBc
Pulling (into a 2.0:1 VSWR)			8		MHz pp
Pushing @ Vtune= 5V			10		MHz/V
Frequency Drift Rate			1.0		MHz/°C

For price, delivery, and to place orders: Analog Devices, Inc., One Technology Way, P.O. Box 9106, Norwood, MA 02062-9106
Phone: 781-329-4700 • Order online at www.analog.com
Application Support: Phone: 1-800-ANALOG-D

The datasheet of the HMC703LP4E is below:

ANALOG DEVICES

HMC703LP4E

v02.0813

8 GHz FRACTIONAL SYNTHESIZER

RoHS ✓ EARTH FRIENDLY

Typical Applications

The HMC703LP4E is ideal for:

- Microwave Point-to-Point Radios
- Base Stations for Mobile Radio (GSM, PCS, DCS, CDMA, WCDMA)
- Wireless LANs, WiMAX
- Communications Test Equipment
- CATV Equipment
- Automotive Sensors
- AESA - Phased Arrays
- FMCW Radar Systems

Features

Wide band: DC - 8 GHz RF Input

Best Phase Noise and Spurious in the Industry:
-112 dBc/Hz @ 8 GHz Fractional, 50 kHz Offset

Figure of Merit

-230 dBc/Hz Fractional Mode

-233 dBc/Hz Integer Mode

High PFD rate: 100 MHz

< 50 fs RMS jitter

Frequency and Phase Modulation

Integrated Frequency Sweeper

Triggered Frequency Hopping

External Triggering

24 Lead 4x4 mm SMT Package: 16 mm^2

PLLS - SMT

Functional Diagram

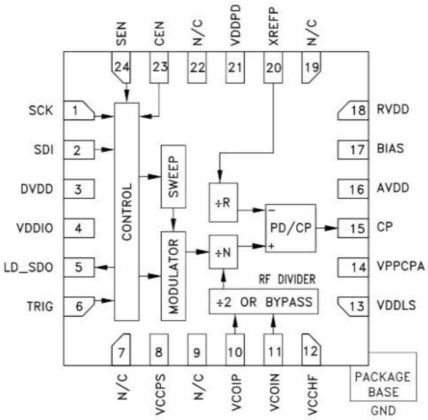

General Description

The HMC703LP4E fractional synthesizer is built upon the high performance PLL platform also contained in the HMC704LP4E and Hittite's latest generation of PLL+VCO products. This platform has the best phase-noise and spurious performance in the industry - enabling higher order modulation schemes while minimizing blocker effects in high performance radios.

In addition, the HMC703LP4E offers frequency sweep and modulation features, external triggering, double-buffering, exact frequency control, phase modulation and more - while maintaining pin compatibility with the HMC700LP4E PLL.

Exact frequency mode with a 24-bit fractional modulator provides the ability to generate fractional frequencies with zero frequency error and very low channel spurious, an important feature for Digital Pre-Distortion systems.

The serial interface offers read back capability and is compatible with a wide variety of protocols.

The datasheet of the HMC860LP3E is below:

ANALOG DEVICES

HMC860LP3E

v01.0811

QUAD LOW NOISE HIGH PSRR LINEAR VOLTAGE REGULATOR

RoHS✓ EARTH FRIENDLY

Typical Applications

The HMC860LP3E is ideal for:

- Test Instrumentation
- Military Radios, Radar and ECM
- Basestation Infrastructure
- Ultra Low Noise Frequency Generation
- Fractional-N Synthesizer Supply
- Mixed-Signal Circuit Supply

Features

Ultra Low Noise:
3nV/√Hz at 10 kHz, 7nV/√Hz at 1 kHz

High Power Supply Rejection Ratio (PSRR)
80 dB at 1 kHz, 60 dB at 1 MHz

Four Voltage Outputs:
VR1 @ 3V / 80 mA
VR2, VR3 @ 3V / 20 mA
VR4 @ 4.5V / 120 mA

Adjustable Outputs: 2.5V to 5.2V

Low Power-Down Current: <1 µA

16 Lead 3x3 mm SMT Package: 9mm²

Functional Diagram

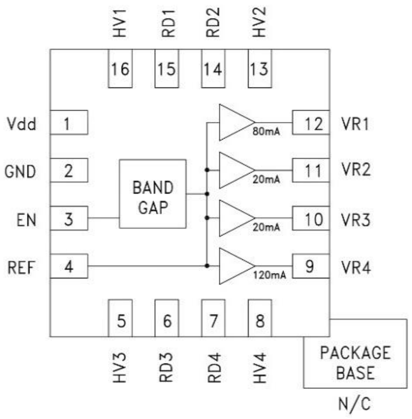

General Description

The HMC860LP3E is a BiCMOS ultra low noise quad-output voltage regulator. It features a low noise band-gap reference externally decoupled for best in-close noise performance. High Power Supply Rejection Ratio (PSRR) in the 0.1 MHz to 10 MHz range provides excellent rejection of preceding switching regulator noise. The four voltage outputs are ideal for frequency generation subsystems including Hittite's broad line of PLLs with Integrated VCOs.

Each output voltage can be adjusted higher or lower than the default value by using one external resistor. Each output can be set to 5V by grounding the corresponding HV pin. The regulator can be powered down by the TTL-compatible Enable input. The HMC860LP3E is housed in a 3x3mm QFN SMT package.

Electrical Specifications, T_A = +25 °C

Parameter	Conditions	Min	Typ	Max	Units
Default Output Voltage VR1, VR2, VR3	Vdd = 5.5V; Maximum load current	3	3.05	3.1	V
Default Output Voltage VR4	Vdd = 5.5V; Maximum load current	4.4	4.5	4.6	V
Output Voltage Tolerance	Vdd = 5.5V; Maximum load current			2	%
Input Voltage Range (Default)	Default output voltage configuration	4.8		5.6	V
Input Voltage Range	E.g.: VR1 = VR2 = VR3 = VR4 = 3.05V; Vdd, min = 3.35V	Max (VRx) + 0.3V		5.6	V
Output Voltage Range VR1 to VR4	Set by external resistors. Vdd = Max(VRx)+0.3V	2.5		5.2	V

For price, delivery, and to place orders: Analog Devices, Inc., One Technology Way, P.O. Box 9106, Norwood, MA 02062-9106
Phone: 781-329-4700 • Order online at www.analog.com
Application Support: Phone: 1-800-ANALOG-D

9

POWER CONDITIONING - SMT

The datasheet of the HMC976LP3E is below:

ANALOG DEVICES

HMC976LP3E

v02.1112

400mA LOW NOISE, HIGH PSRR LINEAR VOLTAGE REGULATOR

RoHS✓ EARTH FRIENDLY

Typical Applications

The HMC976LP3E is ideal for:

- Test Instrumentation
- Military Radios, Radar and ECM
- Basestation Infrastructure
- Ultra Low Noise Frequency Generation
- Fractional-N Synthesizer Supply
- Microwave VCO Supply
- Mixed-Signal Circuit Supply
- Low Noise Baseband Circuit Supply

Features

High Output Current: 400mA

Low Dropout: 300mV at 400mA Output and VR>3V

Ultra Low Noise: 3nV/√Hz at 10 kHz, 6nV/√Hz at 1 kHz

High Power Supply Rejection Ratio (PSRR):

<-60 dB at 1 kHz, <-30 dB at 1 MHz

Adjustable Voltage Output: VR 1.8 to 5V at 400mA

Designed to work with low ESR ceramic capacitors

Low Power-Down Current: <1 µA

Thermal Protection

16 Lead 3x3 mm SMT Package: 9mm²

Functional Diagram

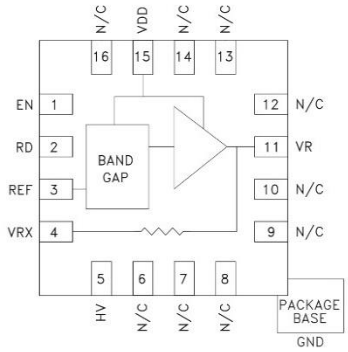

General Description

The HMC976LP3E is a BiCMOS ultra low noise linear voltage regulator. The high Power Supply Rejection Ratio (PSRR) in the 0.1 MHz to 10 MHz range provides excellent rejection of any preceding switching regulator or other power supply noise. The voltage output is ideal for frequency generation subsystems including Hittite's broad line of PLLs with integrated VCOs.

The output voltage can be adjusted lower than the default value by using one external resistor. The output can be set to 5V by grounding the HV pin. The regulator can be powered down by the TTL-compatible Enable input. The HMC976LP3E is housed in a 3x3mm QFN SMT package.

Table 1. Electrical Specifications, $T_A = +25$ °C

Parameter	Conditions	Min	Typ	Max	Units
Output Voltage VR (Default)	Vdd = 5.5V; Maximum load current	4.7	4.8	4.9	V
Output Voltage VR (5V setting)	Vdd = 5.5V; Maximum load current	4.9	5	5.1	V
Output Voltage Tolerance	Vdd = 5.5V; Maximum load current; Default and 5V setting			2	%
Input Voltage Range (Default)	Default output voltage configuration	5.1		5.5	V
Input Voltage Range	For VR>3V[1] VDD>VR+0.3V	3.3		5.5	V
Output Voltage Range VR	Set by external resistors.	1.8		5.1	V

[1] See Absolute Maximum Ratings Table "Absolute Maximum Ratings"

For price, delivery, and to place orders: Analog Devices, Inc., One Technology Way, P.O. Box 9106, Norwood, MA 02062-9106
Phone: 781-329-4700 • Order online at www.analog.com
Application Support: Phone: 1-800-ANALOG-D

The datasheet of the CFPT-9301 is below:

IQD

TCXO Specification

CFPT-9301

ISSUE 7; February 2022

Description

- Surface mount temperature compensated voltage controlled crystal oscillators for medium to high volume applications where small size and high performance are prerequisites. Capable of sub 0.3ppm performance over an extended temperature range. Its ability to function down to a supply voltage of 2.4V and low power consumption makes it particularly suitable for mobile applications.
- -A Freq Adj option
- Option A (standard):
  Ageing adjustment by means of external Control Voltage applied to pad 1
  Range (frequency ≤ 20MHz) ≥ ±5ppm
  Range (frequency > 20MHz) ≥ ±7ppm
  Linearity ≤2%
  Slope Positive
  Input resistance ≥100kΩ
  Modulation bandwidth ≥2kHz
  Standard control voltage range 1.5V±1V
- -B No Freq Adj
- Option B:
  No frequency adjustment
  Initial Calibration ≤ ±1.0ppm

Outline (mm) -B = No Freq Adj

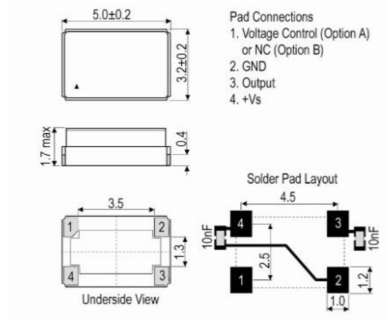

Frequency Parameters

- Frequency 1.5MHz to 52.0MHz
- Frequency Tolerance ±1.00ppm
- Frequency Stability ±0.20ppm to ±2.00ppm
- Ageing ±1ppm max in 1st year (see Note 1)
- Supply Voltage Variation (@ ±5% change):
  Frequency <20MHz: ±0.1ppm typ
  Frequency 20MHz to <35MHz: ±0.3ppm typ
  Frequency 35MHz to 52MHz: ±0.5ppm typ
- Load Variation (@ ±5pF change):
  Frequency <20MHz: ±0.2ppm typ
  Frequency 20MHz to <35MHz: ±0.3ppm typ
  Frequency 35MHz to 52MHz: ±0.5ppm typ
- Note 1 Ageing:
  Frequency ≤20MHz: ±1ppm max in 1st year
  Frequency ≤20MHz: ±3ppm max for 10 years (including the 1st year)
  Frequency >20MHz: ±2ppm max in 1st year
  Frequency >20MHz: ±5ppm max for 10 years (including the 1st year)

Electrical Parameters

- Supply Voltage 3.3V ±10%
- Supply Current (typical):
  HCMOS: 1+Frequency(MHz)*Supply(V)*{Load(pF)+15}*1E–3mA
  i.e @ 20MHz, 3.3V, 15pF ≈ 3mA
  Calculation: 1 + (20 x 3.3 x (15+15) x 0.001) = 2.98mA
- Supply Voltage Tolerance: Parts will operate correctly with ±10% supply voltage variation but supply coefficient is measured with ±5% variation
- Frequency Adjustment - option B
  No frequency adjustment
  Initial calibration: ≤ ±1.0ppm

Sales Office Contact Details:
UK: +44 (0)1460 270200
USA: +1.760.318.2824
Email: info@iqdfrequencyproducts.com
Web: www.iqdfrequencyproducts.com